

**THIS REPORT HAS BEEN DECLASSIFIED  
AND CLEARED FOR PUBLIC RELEASE.**

**DISTRIBUTION A  
APPROVED FOR PUBLIC RELEASE;  
DISTRIBUTION UNLIMITED.**

**UNCLASSIFIED**

**AD \_\_\_\_\_**

**DEFENSE DOCUMENTATION CENTER  
FOR  
SCIENTIFIC AND TECHNICAL INFORMATION**

**CAMERON STATION ALEXANDRIA, VIRGINIA**

**DOWNGRADED AT 3 YEAR INTERVALS:  
DECLASSIFIED AFTER 12 YEARS  
DOD DIR 5200.10**



**UNCLASSIFIED**

Semi-Annual Progress Report

REPORT PREPARED BY: Dr. Gilbert F. Otto

Date: January 31, 1953

D NO 5881  
COPY

For Period: Jan. 1, 1952

To: December 31, 1952

NLR: 130-059/6-6-50 Biological Sciences Division

CONTRACT: N - cnr-248(23) (N M - 005-062)

ANNUAL RATE: \$6,325.00

PRINCIPAL INVESTIGATOR: Dr. Gilbert F. Otto

COLLABORATORS: Lt. Leo A. Jachowski, Jr., M S C, U.S.N.

Dr. Lloyd E. Rozeboom

ASSISTANTS: Mr. Robert Ingram

Mr. Robert Wallis

TITLE OF PROJECT: Studies on the epidemiology and control of filariasis, with particular reference to the biology of the vector, Aedes pseudoscutellaris in the South Pacific.

Objectives: To determine detailed effects of climatic factors on the biology, including oviposition, movement, and survival of, upon Aedes pseudoscutellaris and to compare it with such closely related forms as the ubiquitous Aedes aegypti.

To complete the statistical analysis of the mass of data accumulated from Samoa bearing on the epidemiology of filariasis in the Pacific.

SUMMARY OF RESULTS:

A. SINCE START OF CONTRACT: The basic biology of the mosquito vector of filariasis in Samoa has been studied by the use of the colony established in 1950. The following points appear to have been established:

Eggs are laid by preference just above the water line or just above a water soaked material on the bottom. Rarely are the eggs laid more than one inch above the water and almost never on the water itself. Above the water, eggs are laid almost entirely in crevices, crinkles, or cracks.

The females will, for instance, pass up a container lined with smooth filter paper and deposit all their eggs in an adjacent container lined with wrinkled filter paper. This alone may account for the preference in nature for small natural water collections in the bush rather than similar collections in artificial containers around human dwellings.

The eggs die if dried immediately after being laid. However, if they are kept moist for 24 hours so that embryonation can be initiated, they will withstand drying for months and continue developing normally when thereafter remoistened. Optimum temperatures for survival and development are 75-80° F. Adults require an atmosphere almost completely saturated with moisture.

Mating takes place primarily in the early morning hours but egg-laying and feeding in the air-conditioned laboratory takes place during any of the day light hours. There is little activity and no feeding in the dark.

These studies have supplemented and substantiated field observations. These have shown that the mosquitoes feed primarily in the dense bush in the day time. There is very little excursion into the open and mosquitoes are found in houses only rarely and then only on overcast days.

B. DURING CURRENT REPORT PERIOD: The mosquito vector in Samoa has been known as Aedes pseudoscutellaris and although we have been concerned about certain variations we have seen, we have used that name. Recently, Mark in London has concluded that A. pseudoscutellaris is restricted to Fiji and that a new species, A. polynesiensis, occurs in Samoa and other islands where this complex has been known. We have recently established a colony of the Fijian mosquito from eggs provided by Marks from her London colony. Dr. L. E. Rozeboom has been comparing the two forms. A number of doubts exist as to the adequacy of the reported distinctions.

Analysis of the microfilaria prevalence in various elements of the population have revealed that the highest infection rates (35 to 55 %)

are found in the adult males whose activities take them recurrently into the plantation areas and into the bush areas regardless of the type of habitation in which they live. On the contrary, the adult females who live primarily in the village and have less occasion to work or travel in the plantations or bush areas have less infection than the males. Those females who live in the large open villages have 11 to 30 per cent infection and those who live in small villages closely surrounded by the dense bush have 20 to 50 per cent infection. There is no sex difference in the infection rates of children but those 5-9 years of age, both males and females, who live in the large open villages have about seven per cent infection while the same groups in the small bush villages have 15-16 per cent infection. Thus the analyses of the microfilaria prevalence in the several elements of the population, together with a study of the human habits, appears to confirm the earlier impression, gained from a study of the mosquito habits and infection rates, that transmission is not domestic but occurs in a wild ecological niche.

Analysis of our post-treatment data suggests that sodium thiocetarsamide (arsenamide, caparsolate sodium) in fifteen daily intravenous doses has a good chance of eliminating the infection. However, diethylcarbamazine (Hetrazan, Banocide) which is rapidly microfilaricidal appears to have comparatively little effect upon the adult worms. Microfilaria begin to reappear in the blood in a few months. Furthermore, the rapid destruction of large numbers of microfilariae may be associated with clinical evidence of protein shock.

#### PLANS FOR THE FUTURE:

Plans for the future focus on the completion of the analyses of the field data from Samoa and the preparation of the data for publications. Lt. Jachowski and a corpsman will make the final rocheck during March and April 1953 of the villages under study in Samoa. Analysis of these data and their publication will complete this phase of the study.

In the laboratory studies are continuing on the response of the vector mosquitos to different environmental factors. A variant of the mosquito, not hitherto studied in the laboratory has stimulated increasing interest. This variant is conspicuous because it has a fuzzy larvae. Attempts will be made by Lt. Jachowski to bring eggs of this species to Baltimore. Dr. L. E. Rozeboom plans cross-breeding experiments between the common Samoan forms (Mark's A. polynesiensis) and the Fijian form (Mark's A. pseudoscutellaris) and, if we can get it established, the Samoan "fuzzy larval form" in an attempt to establish the taxonomy and biological relationships of the three forms.

SPECIAL NOTE - AWARD: It seems appropriate to record here that the Bailey K. Ashford Award was made to Lt. Leo A. Jachowski by the American Society of Tropical Medicine and Hygiene at its annual meeting in Galveston, Texas, November, 1952. This award is given every two years to an American under 35 years of age who has made an outstanding contribution to our knowledge in the field of Tropical Medicine and Hygiene. The award was made to Lt. Jachowski for his contributions in the Studies on Filariasis in American Samoa.

PAPERS PUBLISHED OR IN PRESS:

1. Jachowski, L. A., Jr. G. F. Otto and J. D. Wharton.  
1950 Filariasis in American Samoa. J. Parasit. 36 (6, Sect. 2):34.
2. Jachowski, L. A., Jr., G. F. Otto and J. D. Wharton.  
1951 Filariasis in American Samoa. I. Loss of microfilaria in absence of continued reinfection. Proc. Helm. Soc. Wash. 18 (1): 25-28. (NM 005 048.08.01).
3. Jachowski, L. A., Jr. and G. F. Otto.  
1952 Filariasis in American Samoa. II. Evidence of transmission outside of villages. Amer. J. Trop. Med. and Hyg. 1 (4):662-670.
4. Otto, G. F. and L. A. Jachowski, Jr.  
1952 New Facts on an Old Disease. Research Reviews, pp. 20-26.

5. Jachowski, L. A., Jr.

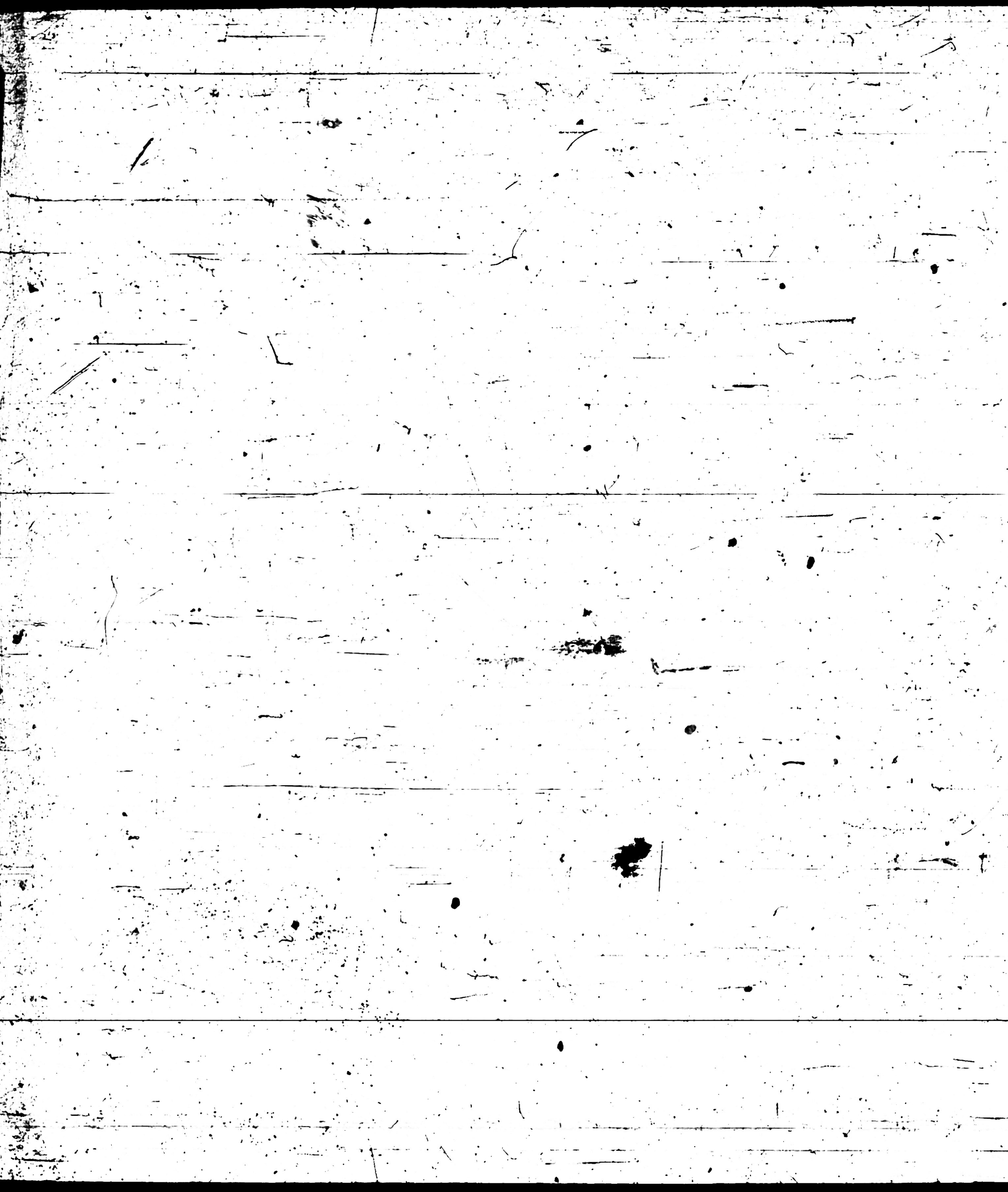
1953 Transmission of non-periodic filariasis in the South Pacific.  
Trop. Med. and Hyg. News, in press (March).

6. Otto, O. F., L. A. Jachowski, Jr. and J. D. Wharton.

1953 Filariasis in American Samoa. III. Studies on chemotherapy  
against the non-periodic form of Wuchereria bancrofti. Amer.  
J. Trop. Med. and Hyg., in press (March or May).

7. Wallis, Robert Charles

1953 Observations on oviposition activities of two Aedes mosquitoes.  
Ann. Entom. Soc. Amer., in press.



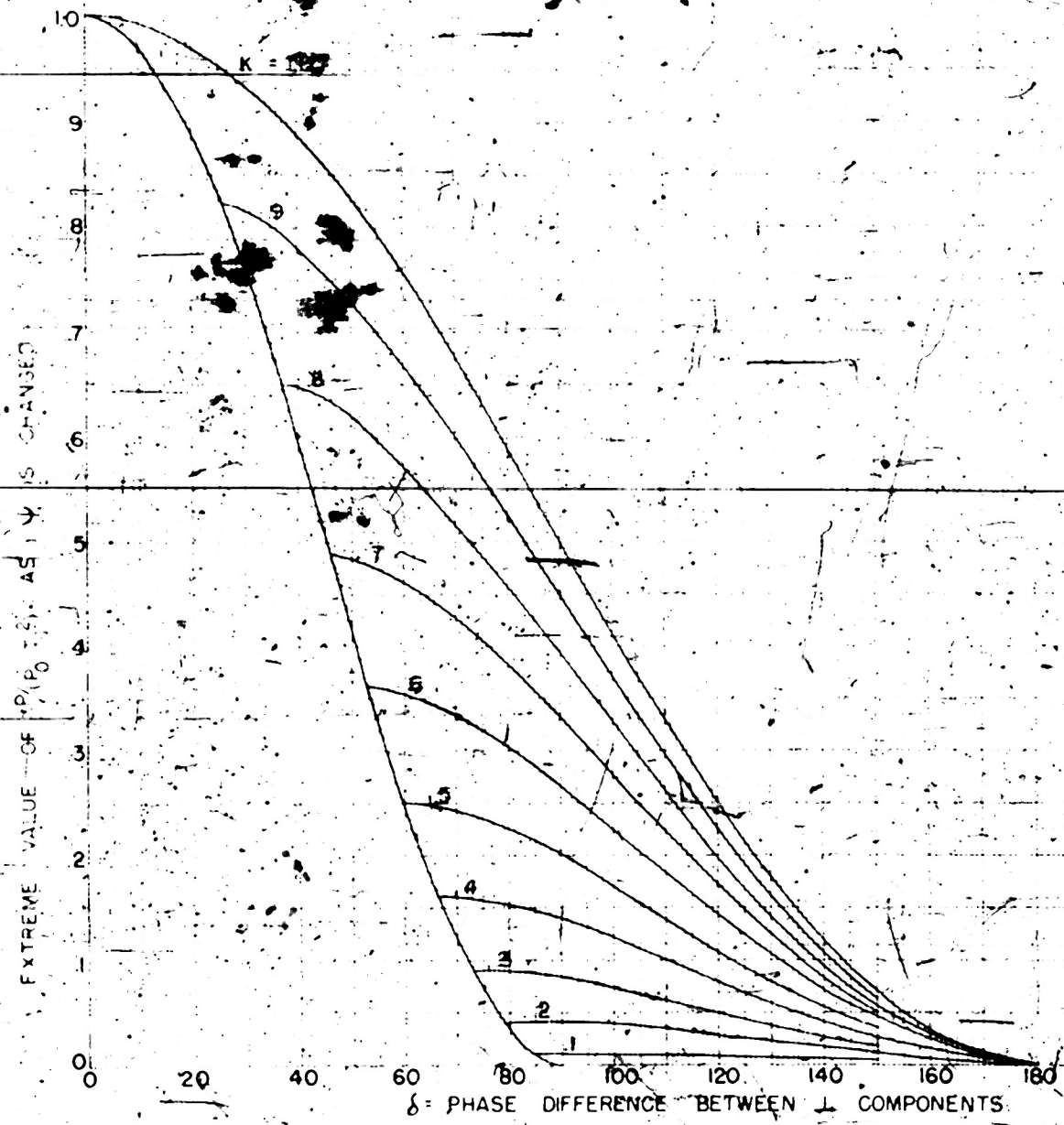


FIG. 274-MAXIMUM OR MINIMUM VALUE FOR TRANSMISSION AS A FUNCTION OF POLARIZATION ANGLE, WHEN THIS MAXIMUM OR MINIMUM OCCURS AT A POLARIZATION INTERBAND IN BETWEEN P-SIMILAR AND P-HORIZONTAL.

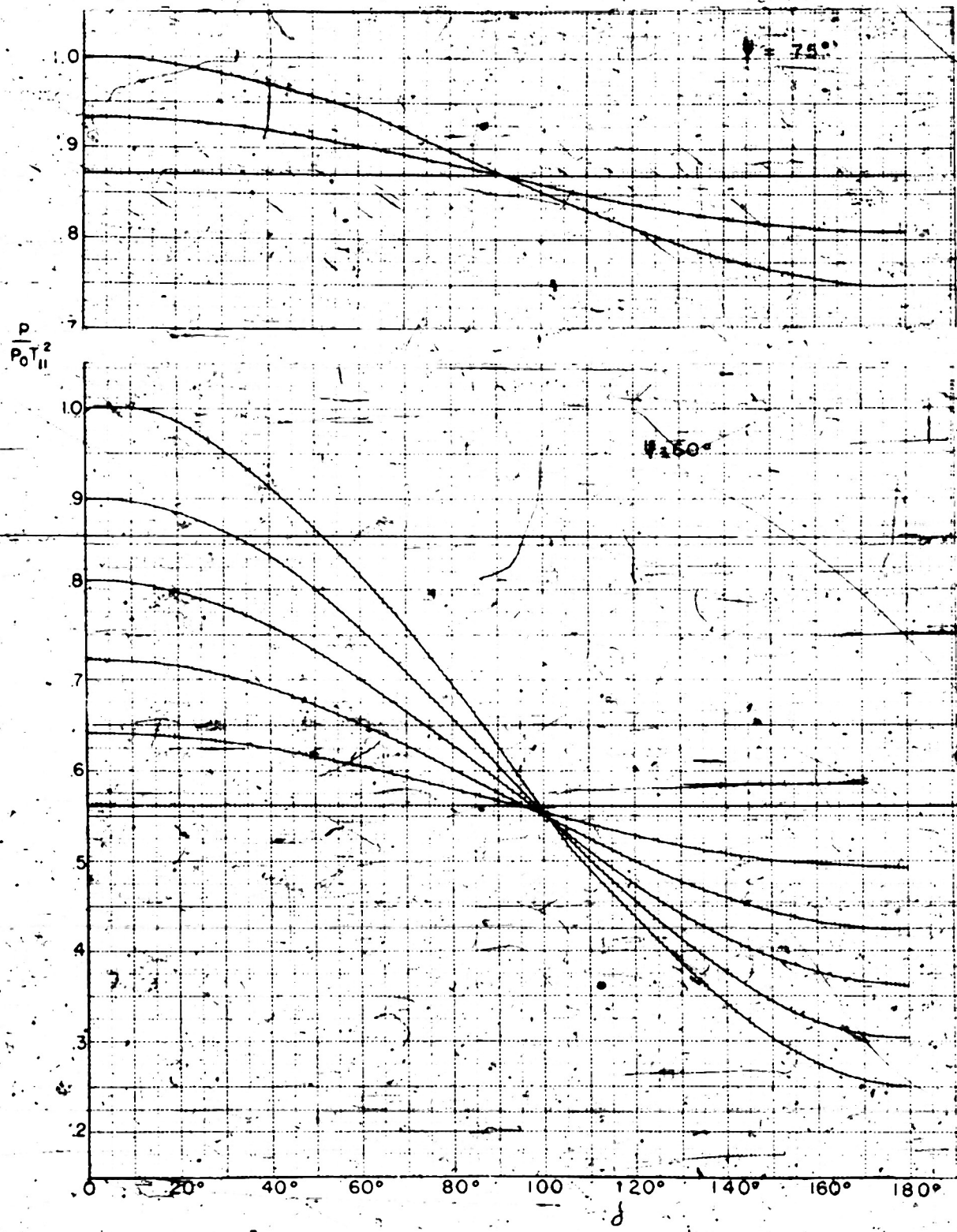


FIG. 96 - SAME

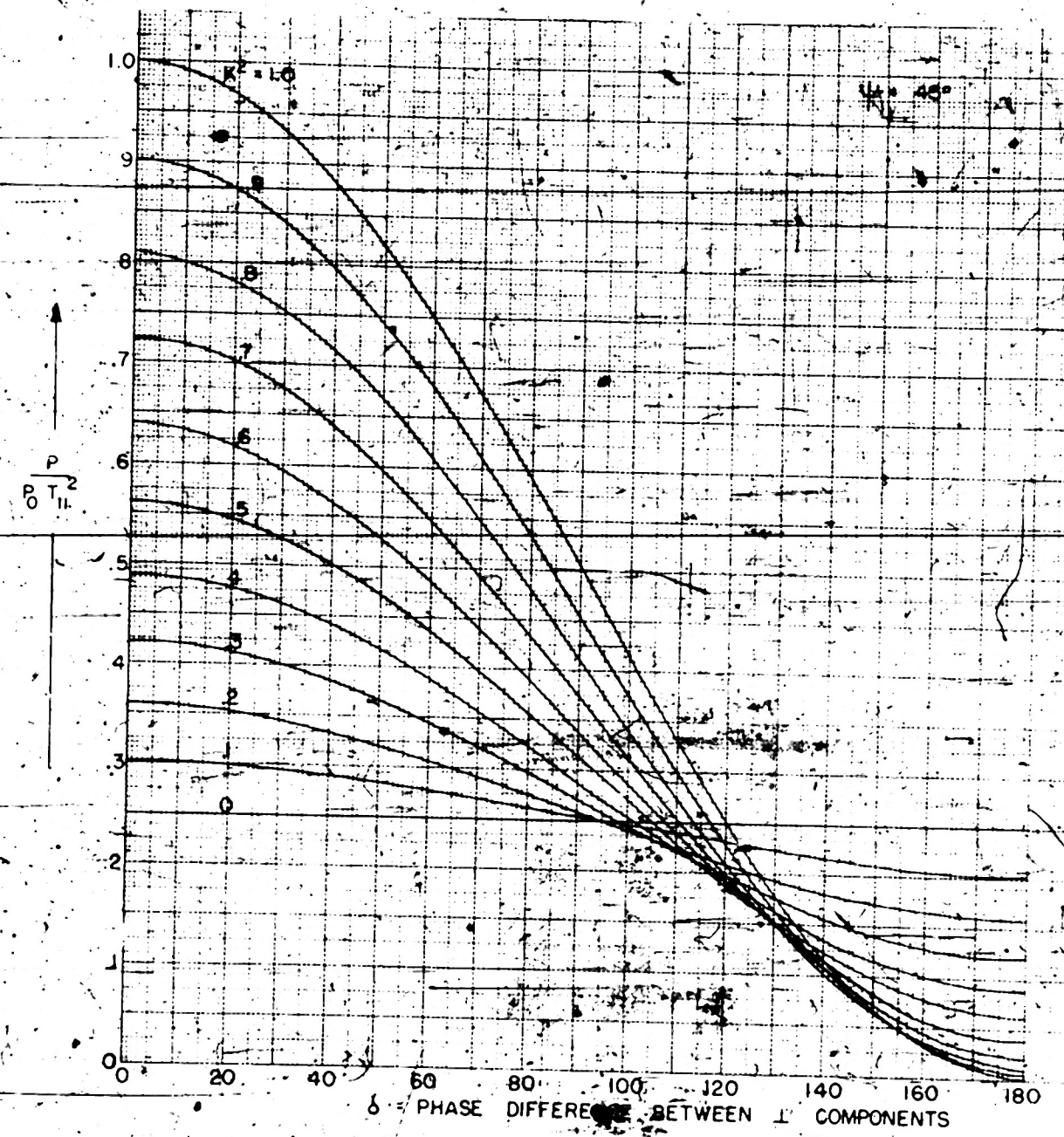


FIG. 95-3 ME

483-18

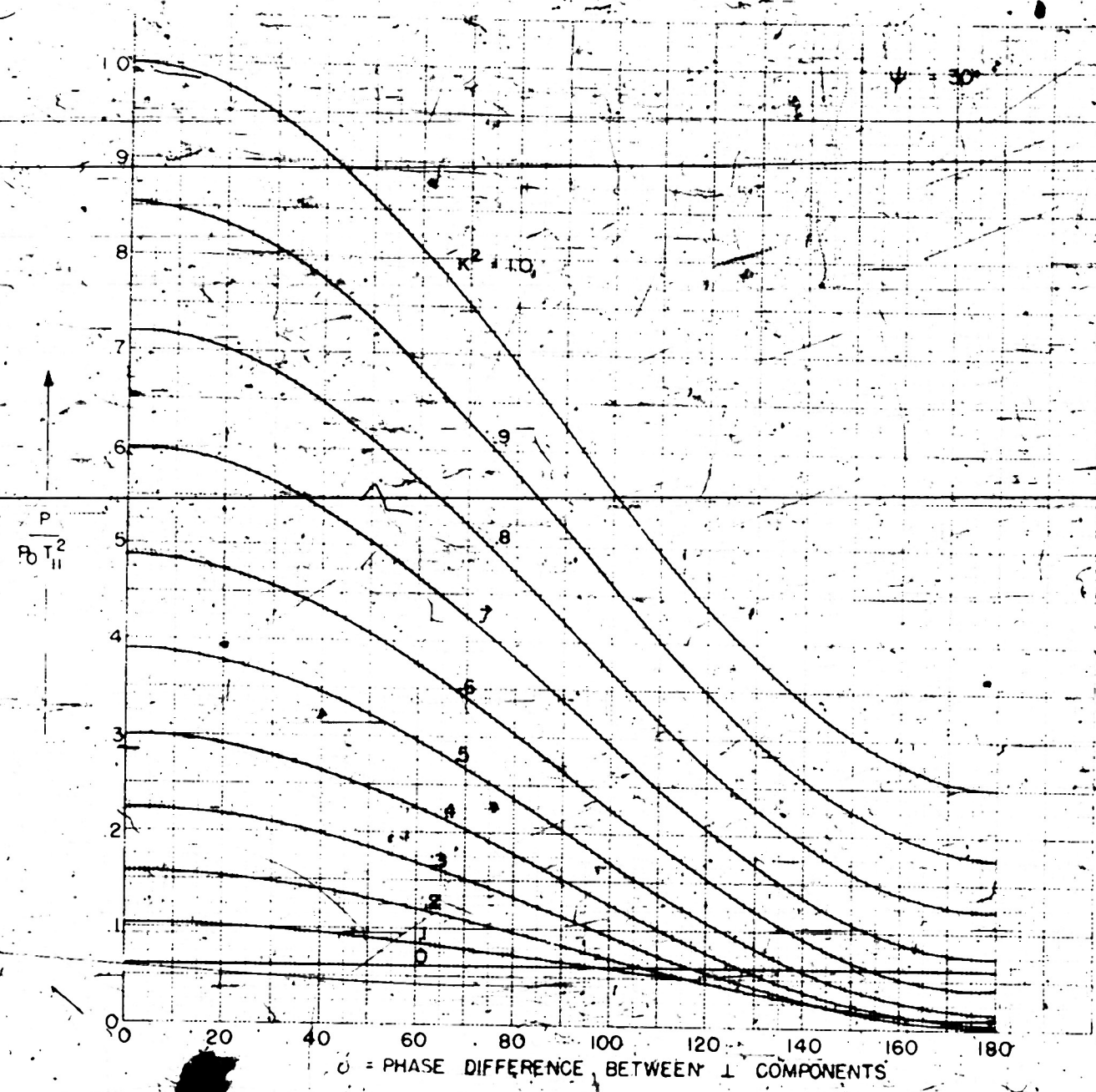
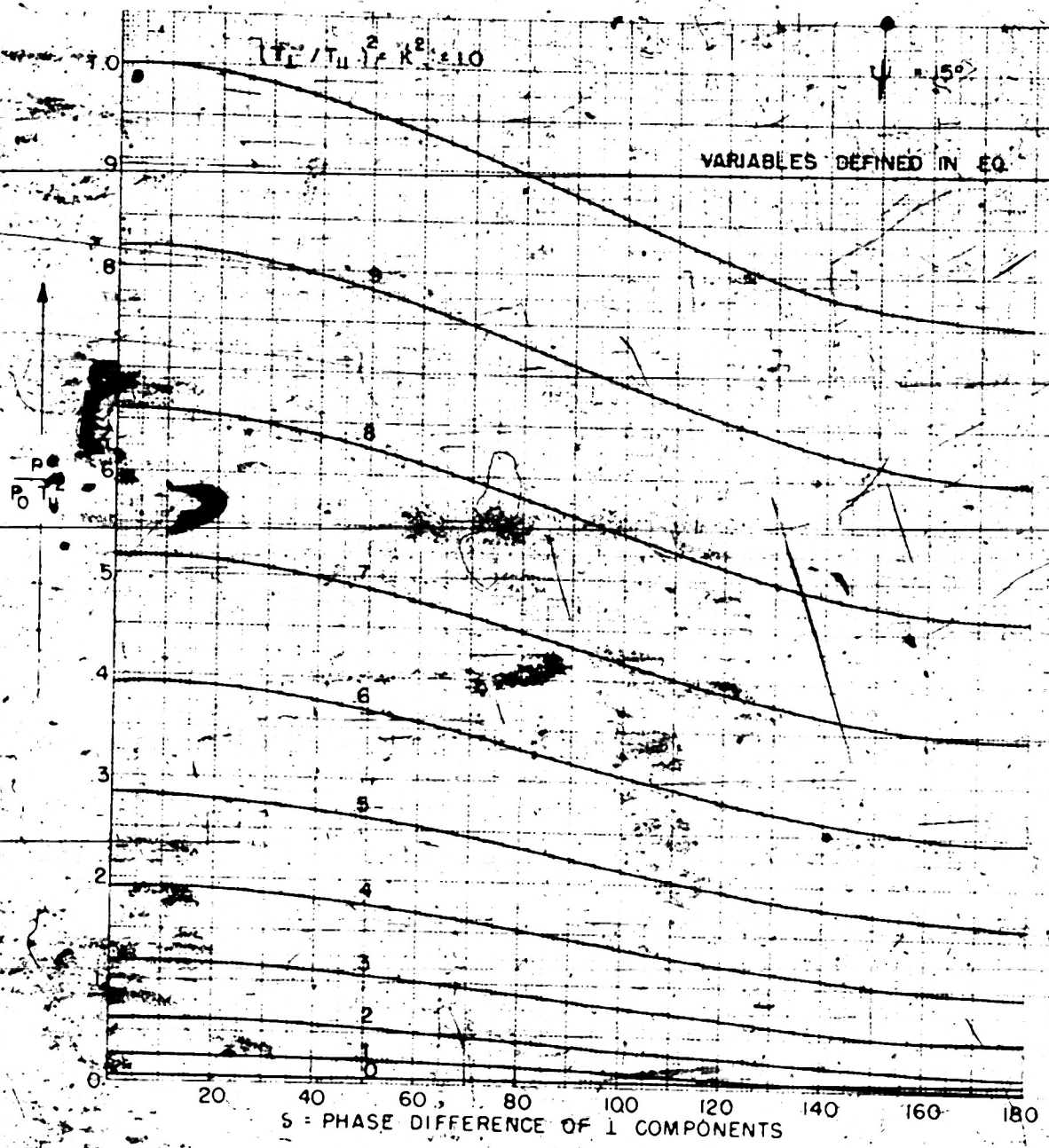


FIG. 94

483-18



OPTICAL TRANSMISSION COEFFICIENT FOR QUADRATIC POLARIZATION  
IN THE PLANE PERPENDICULAR TO THE PLANE OF POLARIZATION

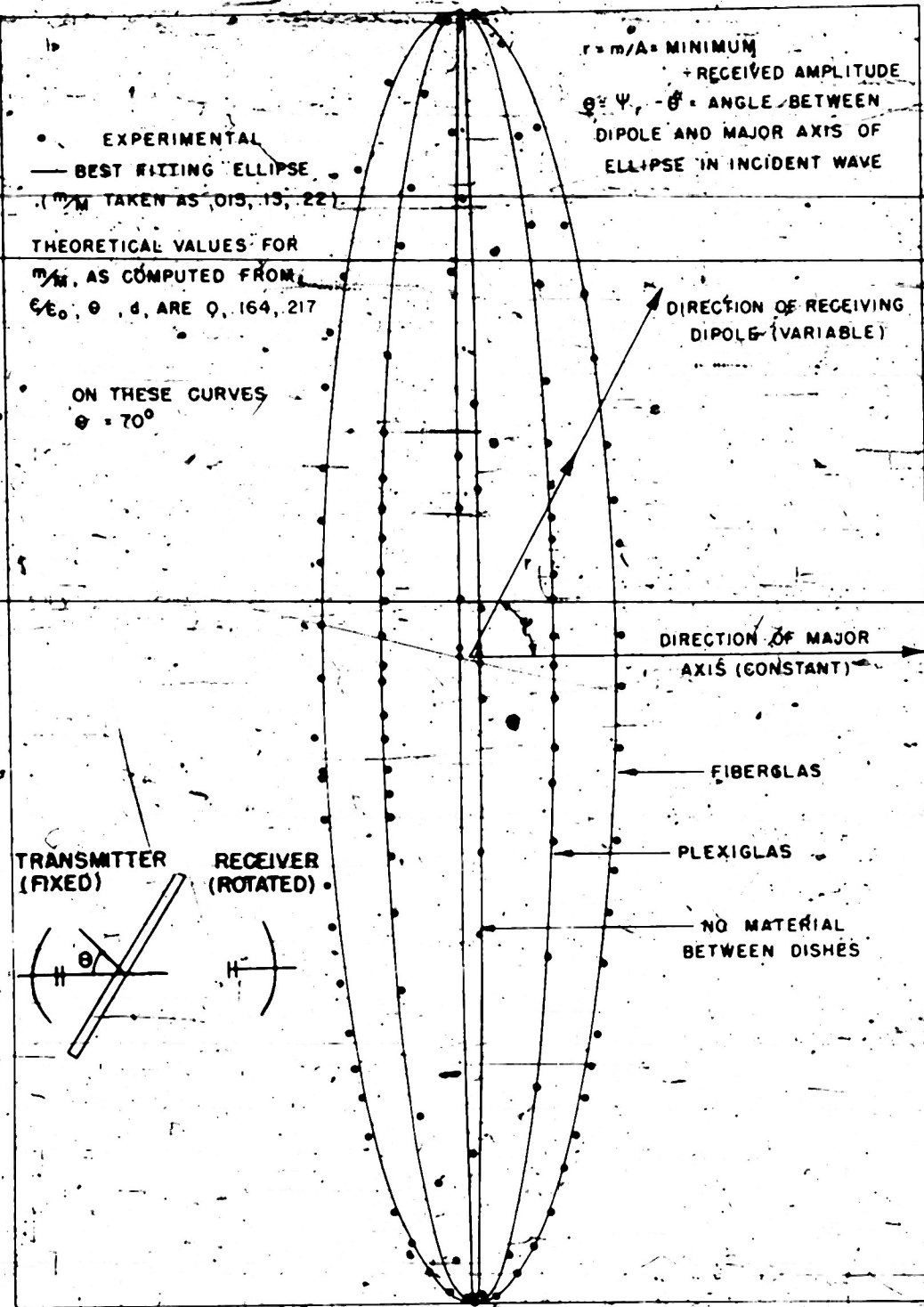


FIG. 92.—VERIFICATION THAT RECIPROCAL OF RECEIVED AMPLITUDE VERSUS POLARIZATION ANGLE IS IN ELLIPSE, WHEN AN ELIPTICALLY POLARIZED WAVE IS INCIDENT ON A LINEARLY POLARIZED ANTENNA

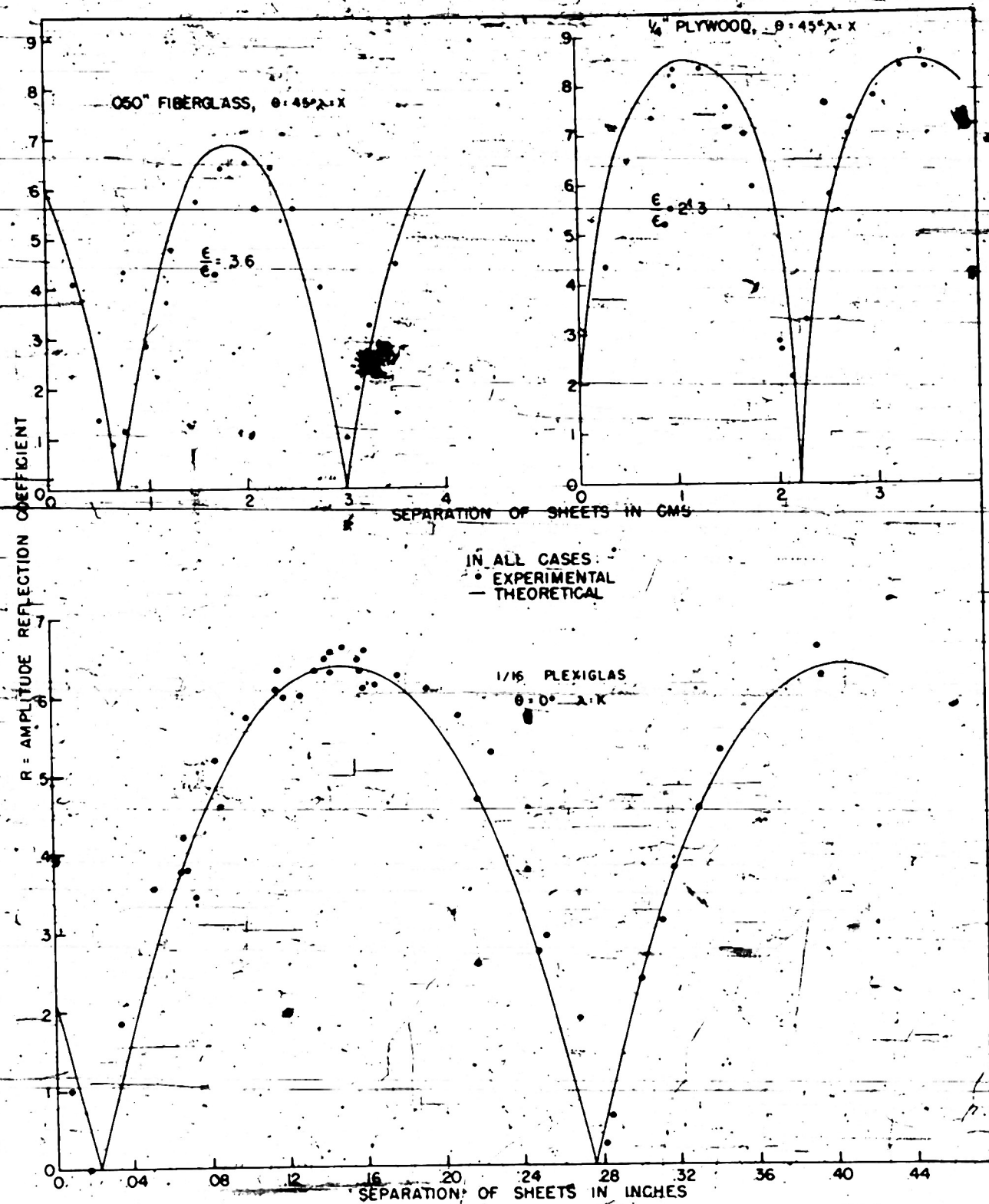


FIG. 91--SAME AT  $45^\circ$  INCIDENCE, AND FOR NORMAL INCIDENCE AT K-BAND

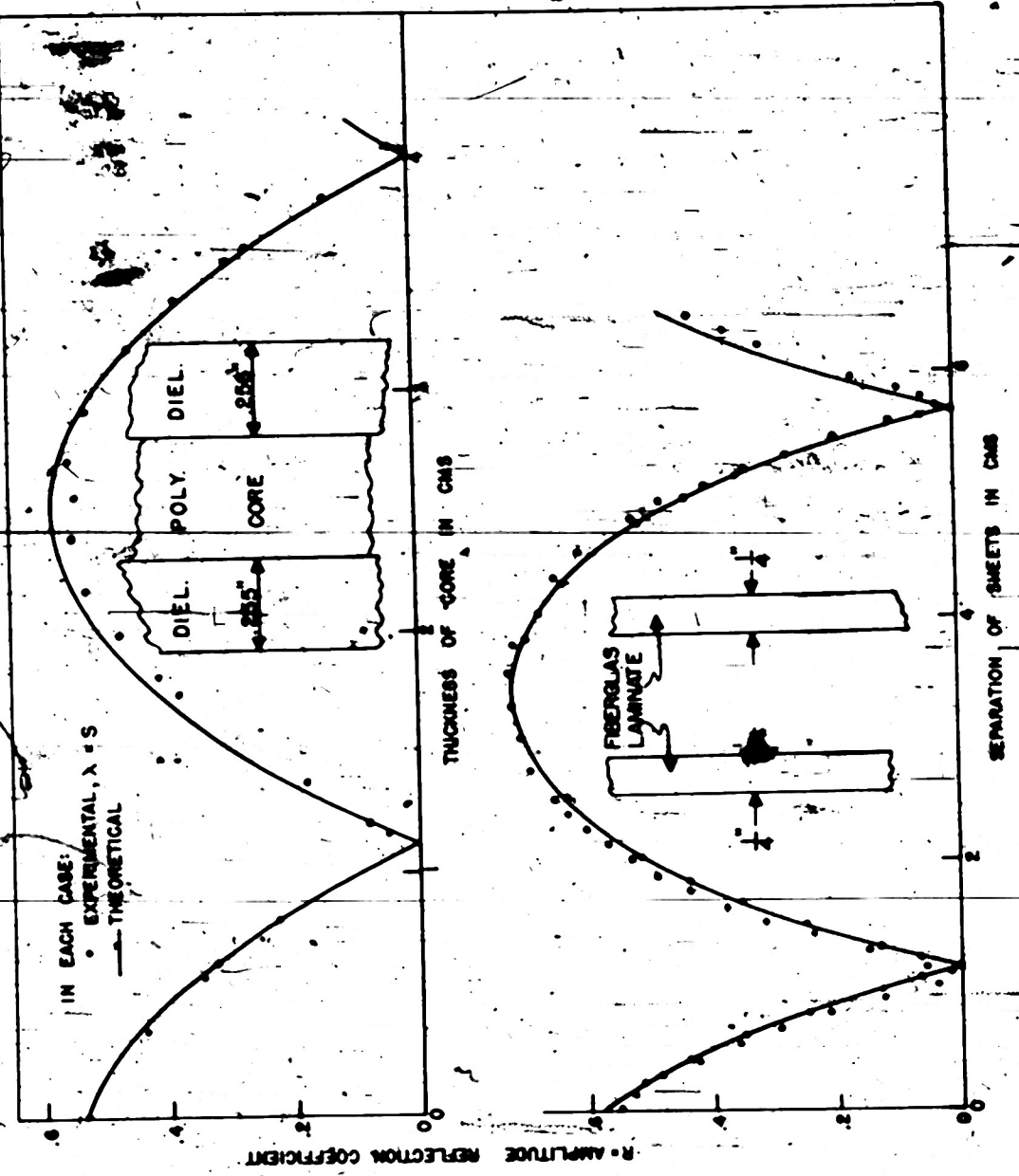


FIG. 90--COMPARISON OF THEORETICAL AND MEASURED REFLECTION VERSUS SPACING FOR TWO SHEETS AND FOR A SANDWICH AT NORMAL INCIDENCE

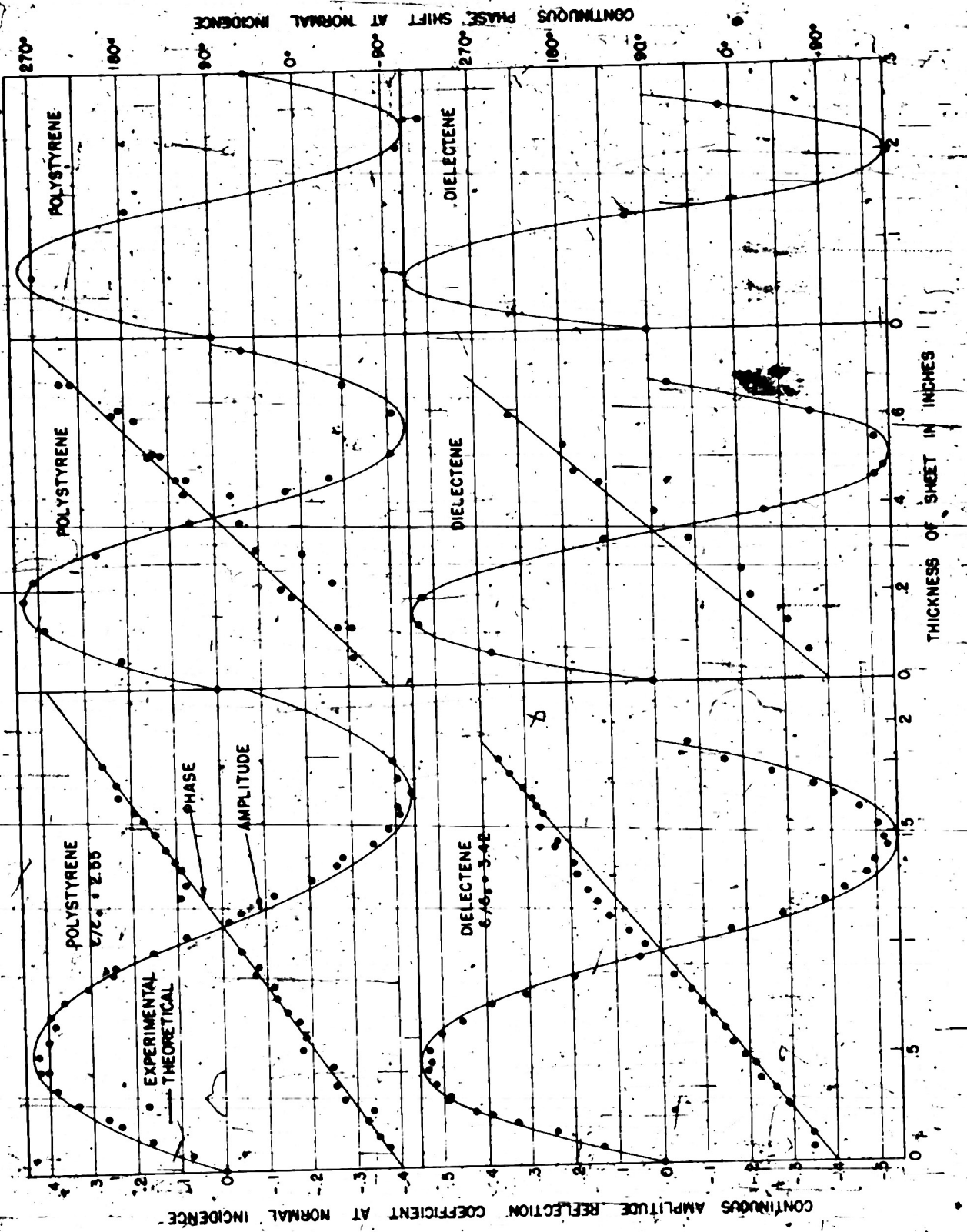
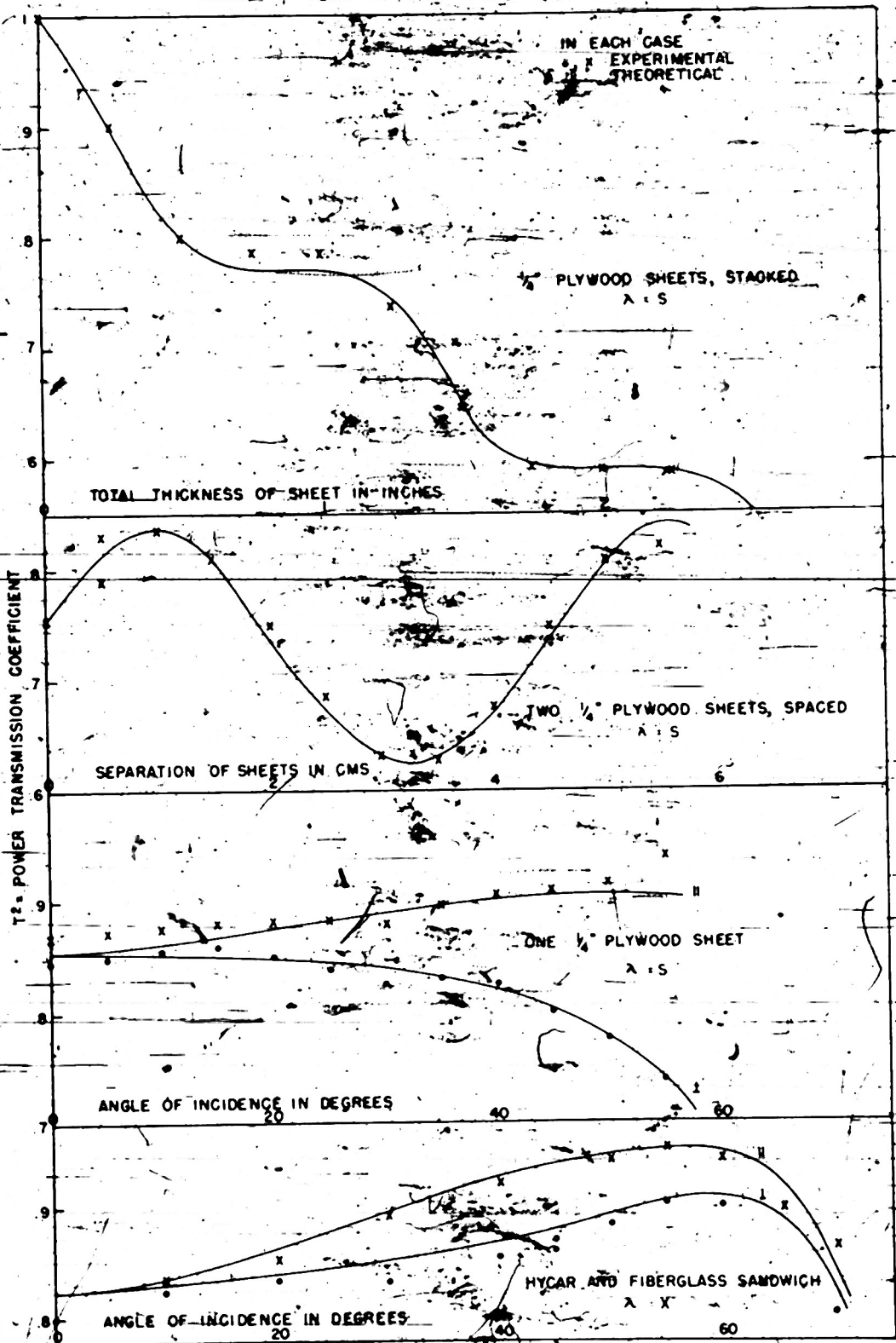


FIG. P9--COMPARISON OF THEORETICAL AND MEASURED REFLECTION OF A SINGLE SHEET VERSUS ITS THICKNESS AT S, X, AND K BANDS



88. COMPARISON OF THEORETICAL AND MEASURED TRANSMISSION OF LOSSY SHEETS, GIVING TRANSMISSION VERSUS THICKNESS, TRANSMISSION VERSUS SEPARATION, AND TRANSMISSION VERSUS ANGLE FOR A SINGLE SHEET AND FOR A SANDWICH

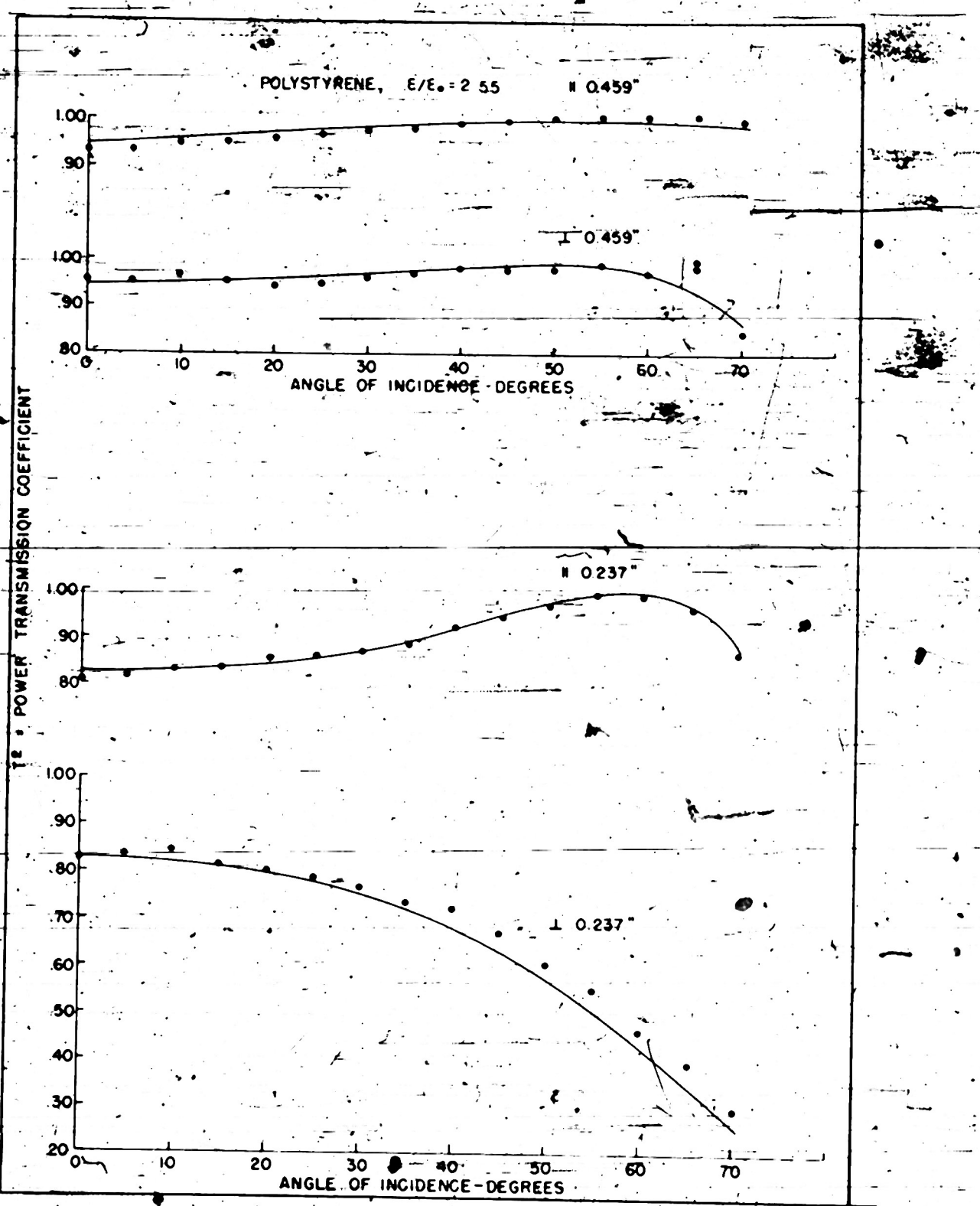


FIG. 87--SAME

483-18

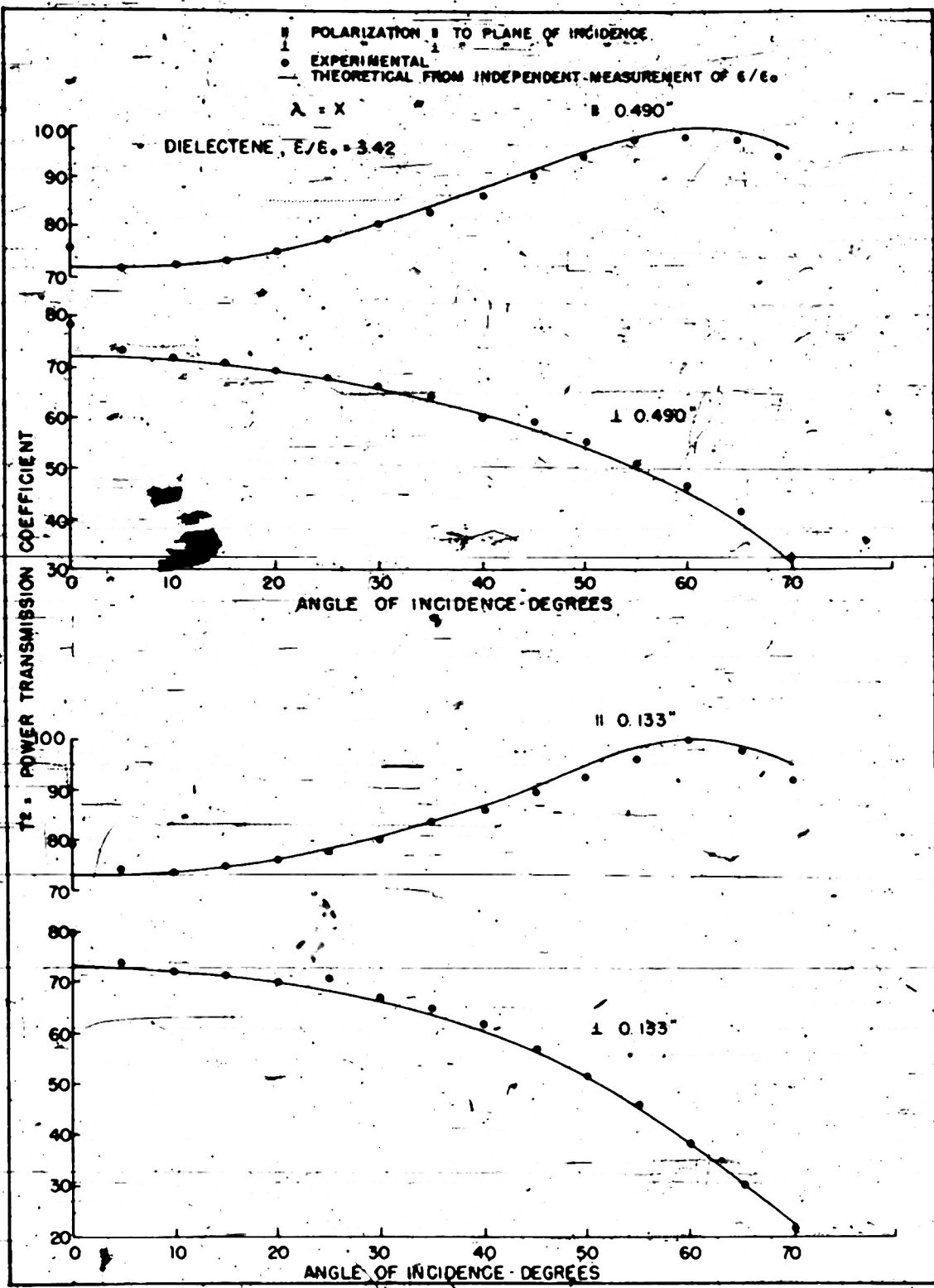


FIG. 86.—COMPARISON OF EXPERIMENTAL AND THEORETICAL TRANSMISSION VERSUS ANGLE FOR SINGLE SHEET

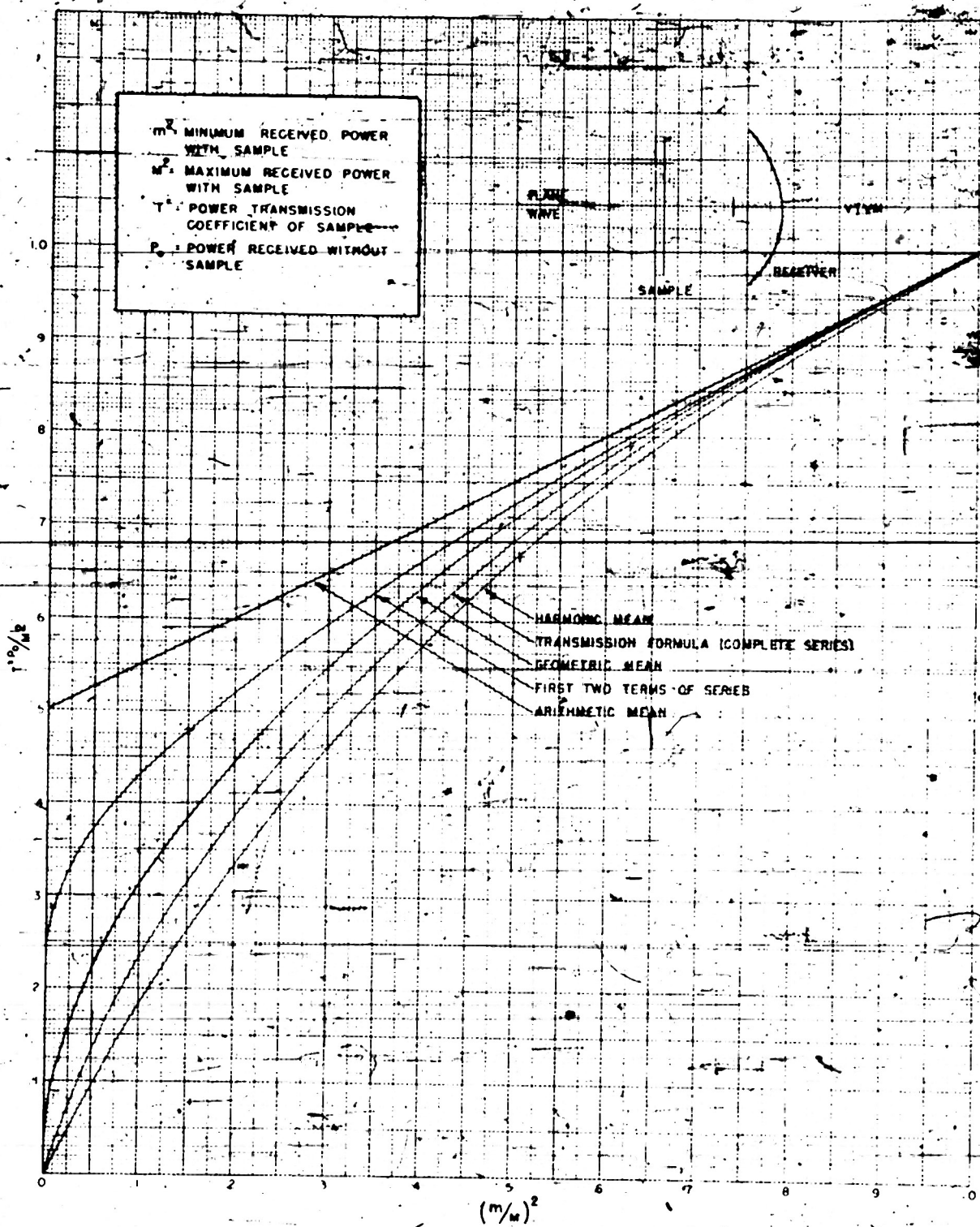
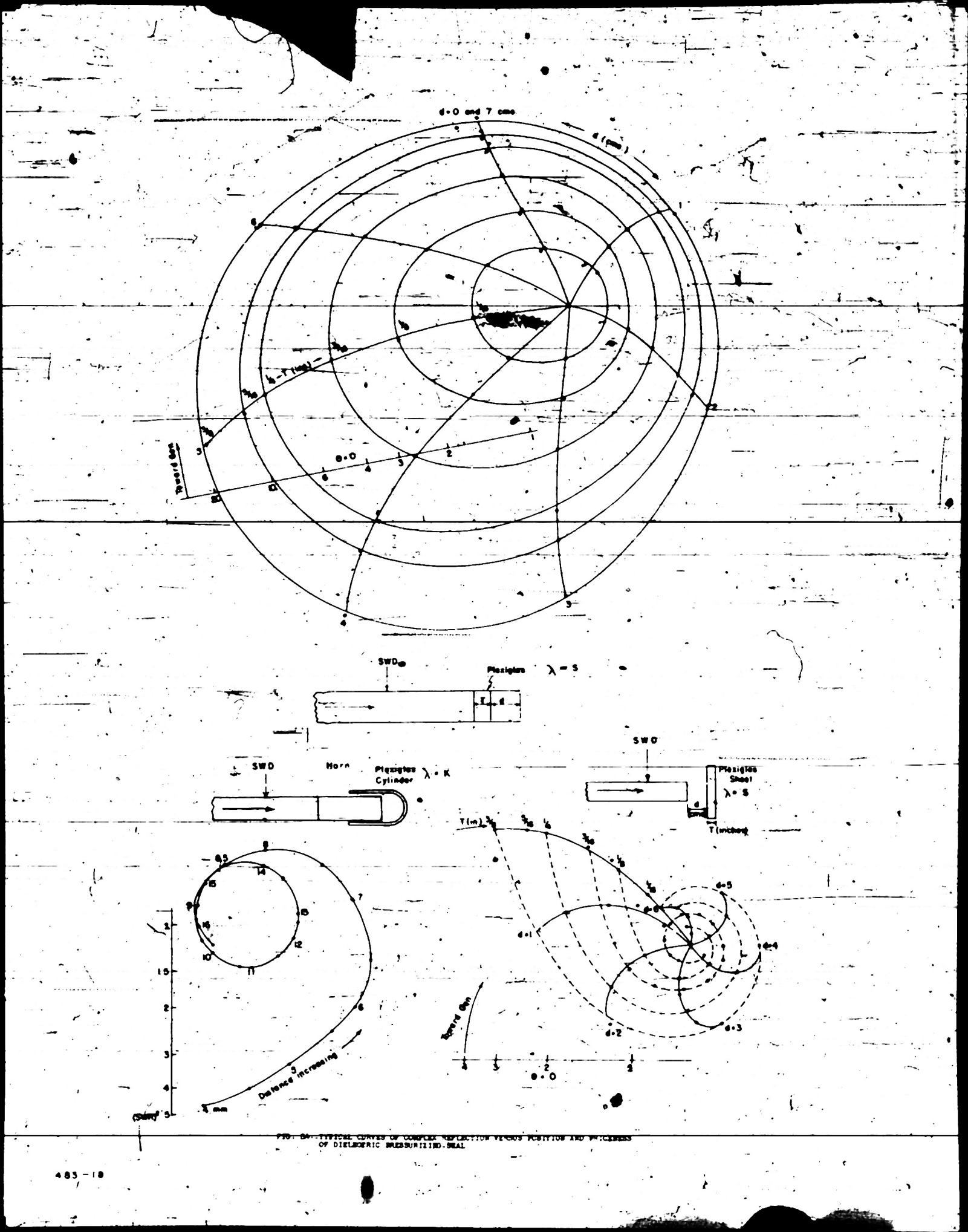


FIG. 58 - COMPARISON OF FORMULAS FOR TRANSMISSION WITH SIMPLER AVERAGES OF MAXIMUM AND MINIMUM RECEIVED POWER.



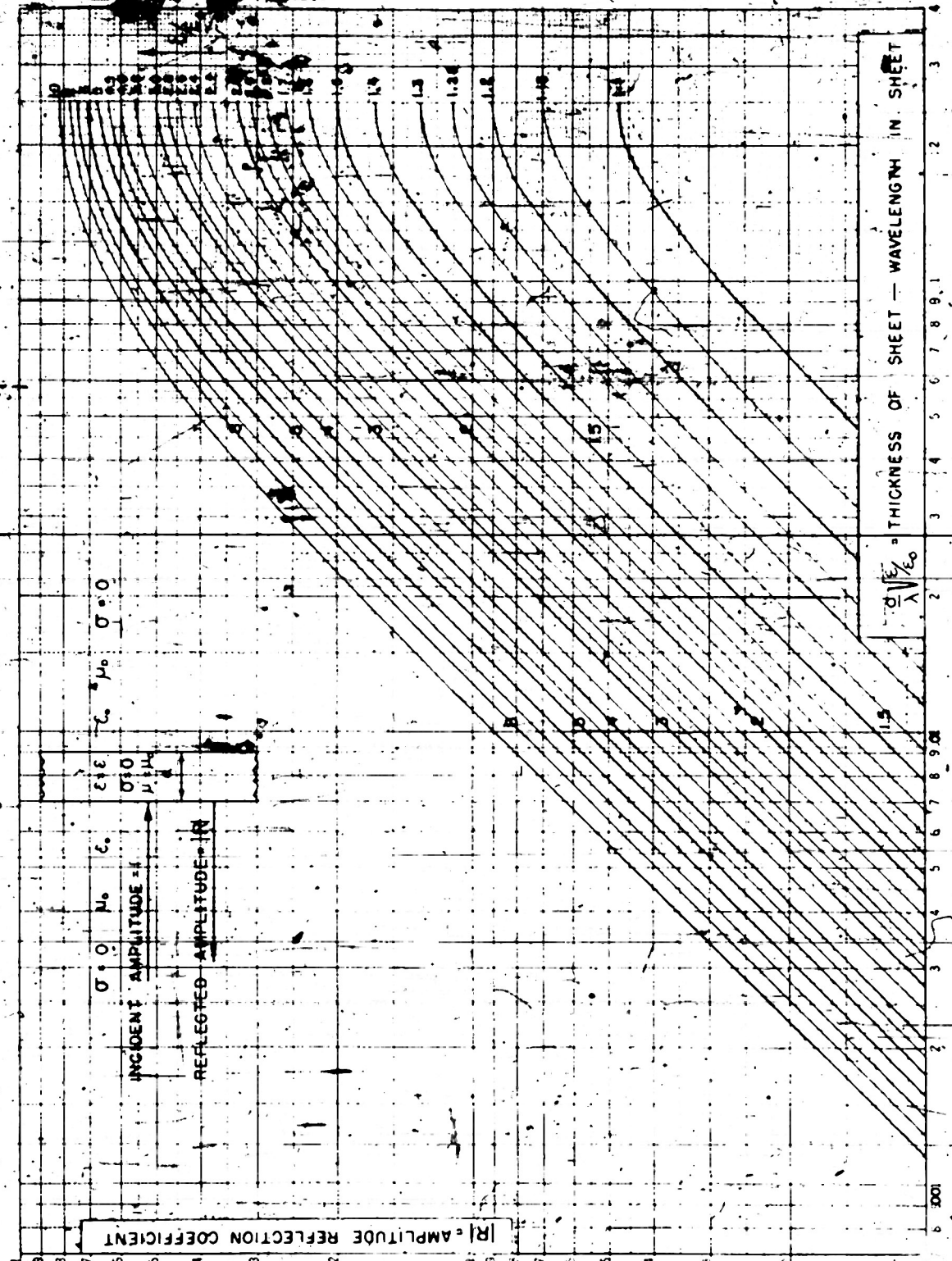


FIG. 83--THEORETICAL REFLECTION COEFFICIENT VERSUS THICKNESS OF DIELECTRIC SHEET AT NORMAL INCIDENCE

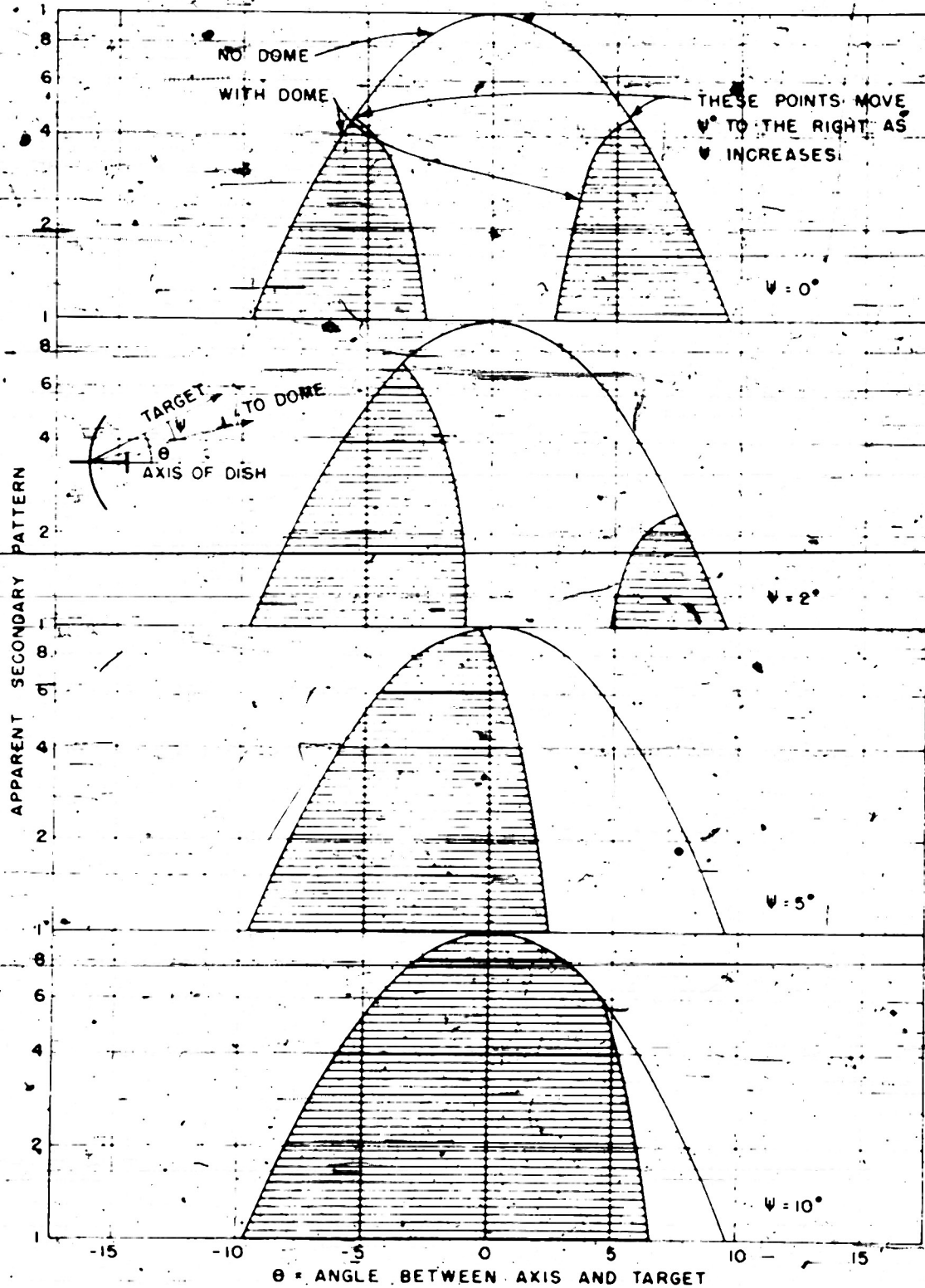


FIG. APPARENT BEAM SHIFT PRODUCED BY REFLECTION FROM RADOME

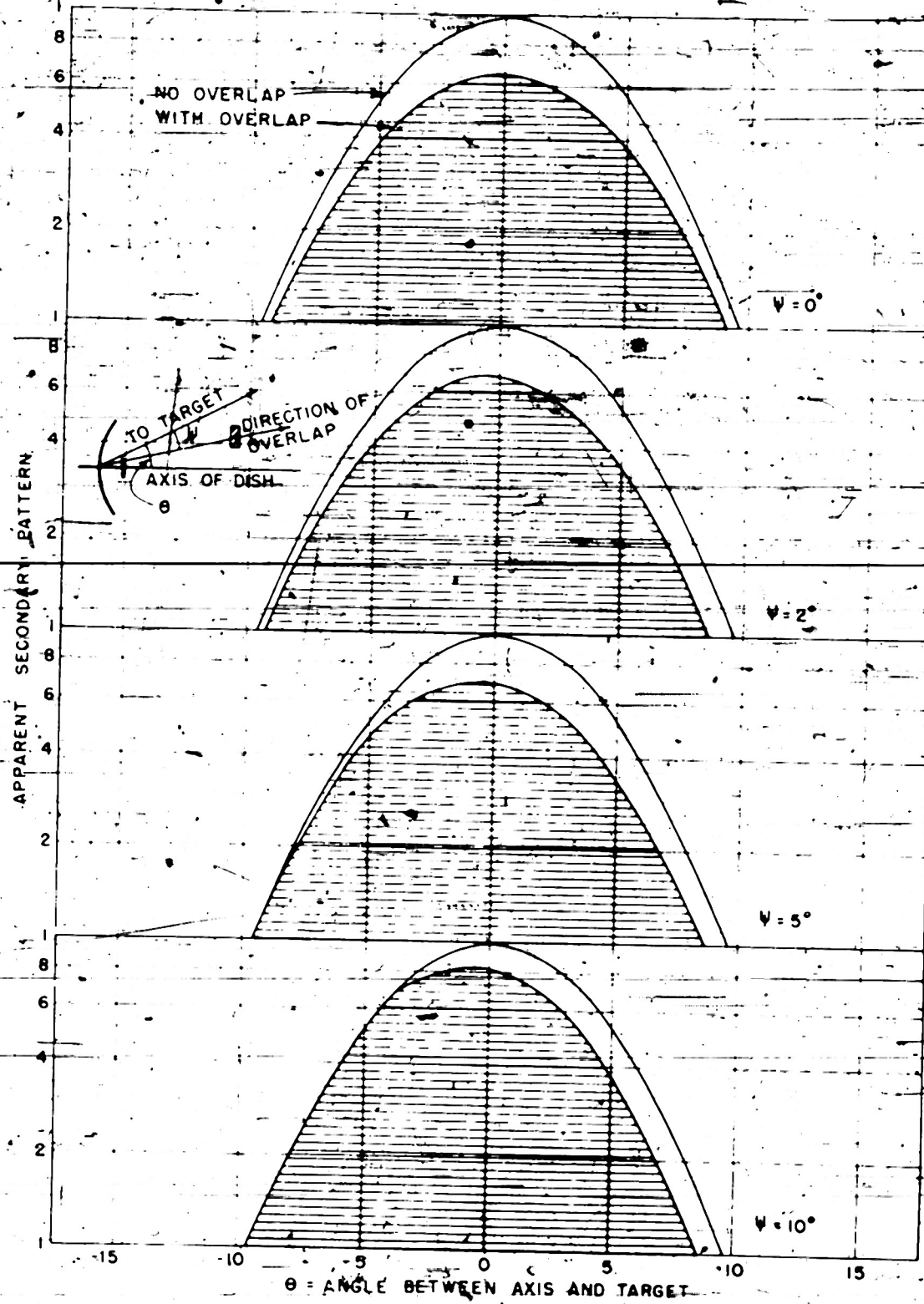


FIG. 1 APPARENT BEAM SHIFT PRODUCED BY REFLECTION FROM OVERLAP

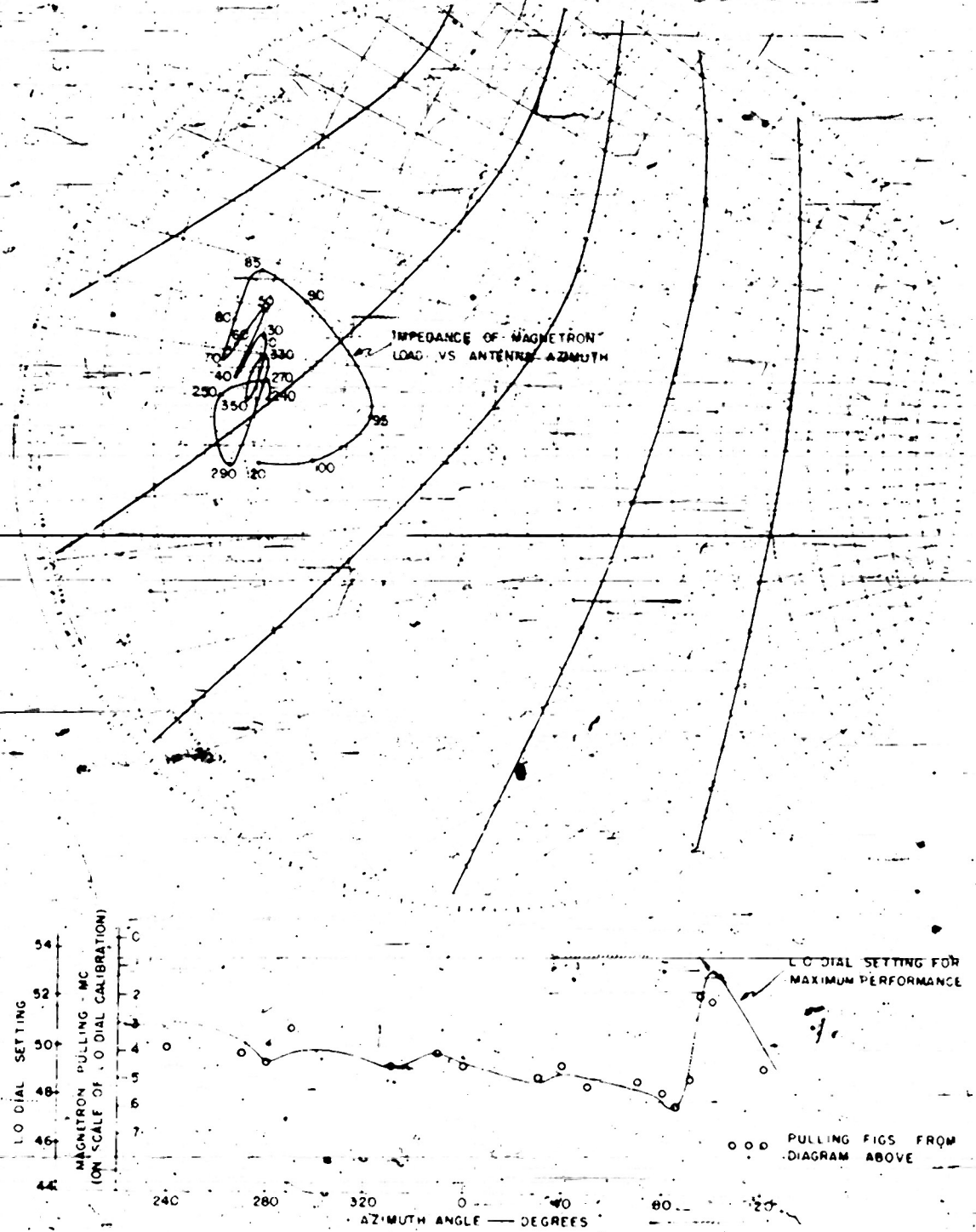


FIG. 50 CORRELATION OF FIELD AND LABORATORY MEASUREMENTS OF PULLING

ABOVE - IMPEDANCE VS AZIMUTH, AND RIEKE DIAGRAM

BETWEEN - PREDICTED AND ACTUAL LO DIAL SETTINGS VS AZIMUTH

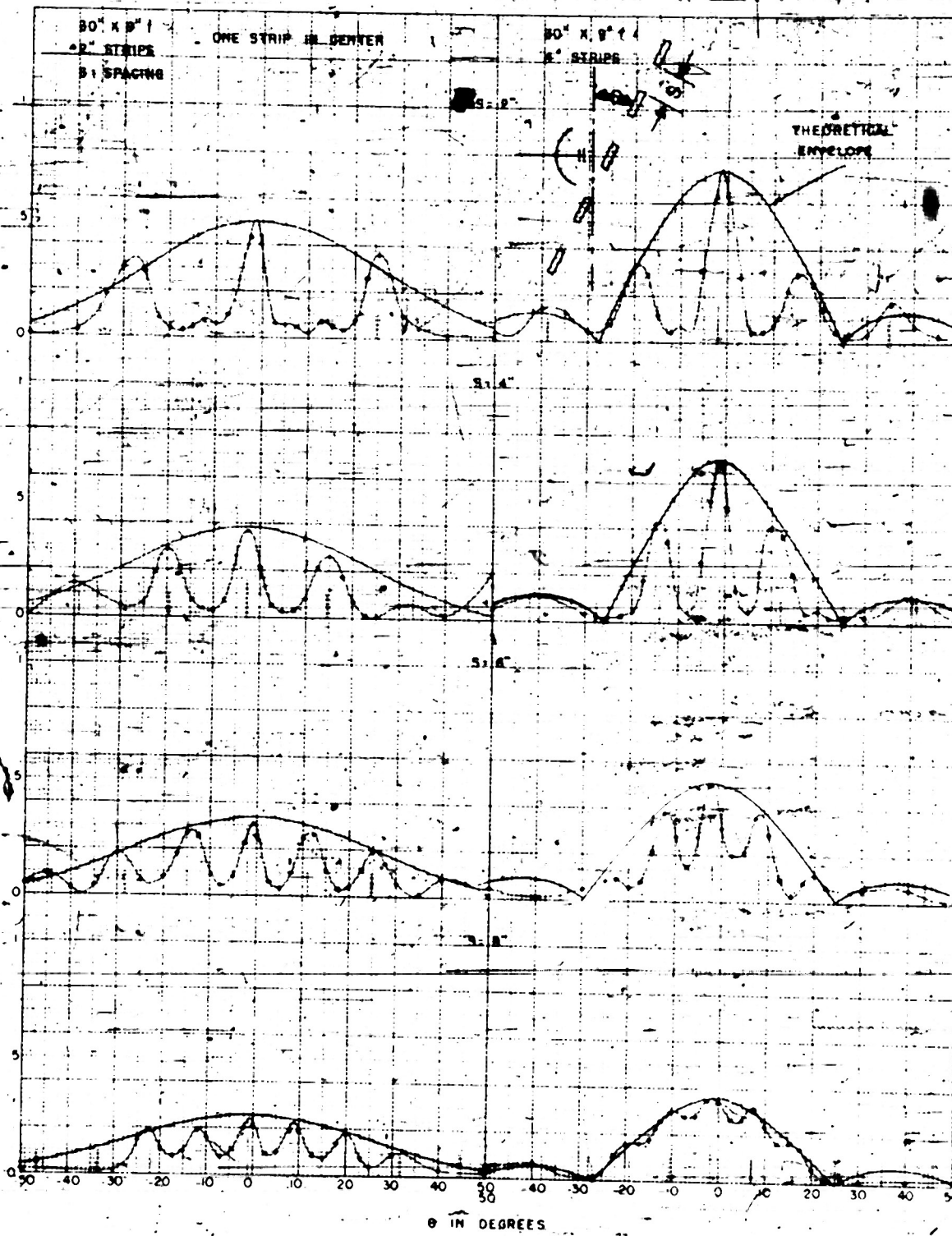


FIG. 79a--REFLECTION VERSUS ANGLE FOR A SERIES OF STRIPS, AND COMPARISON WITH THEORY

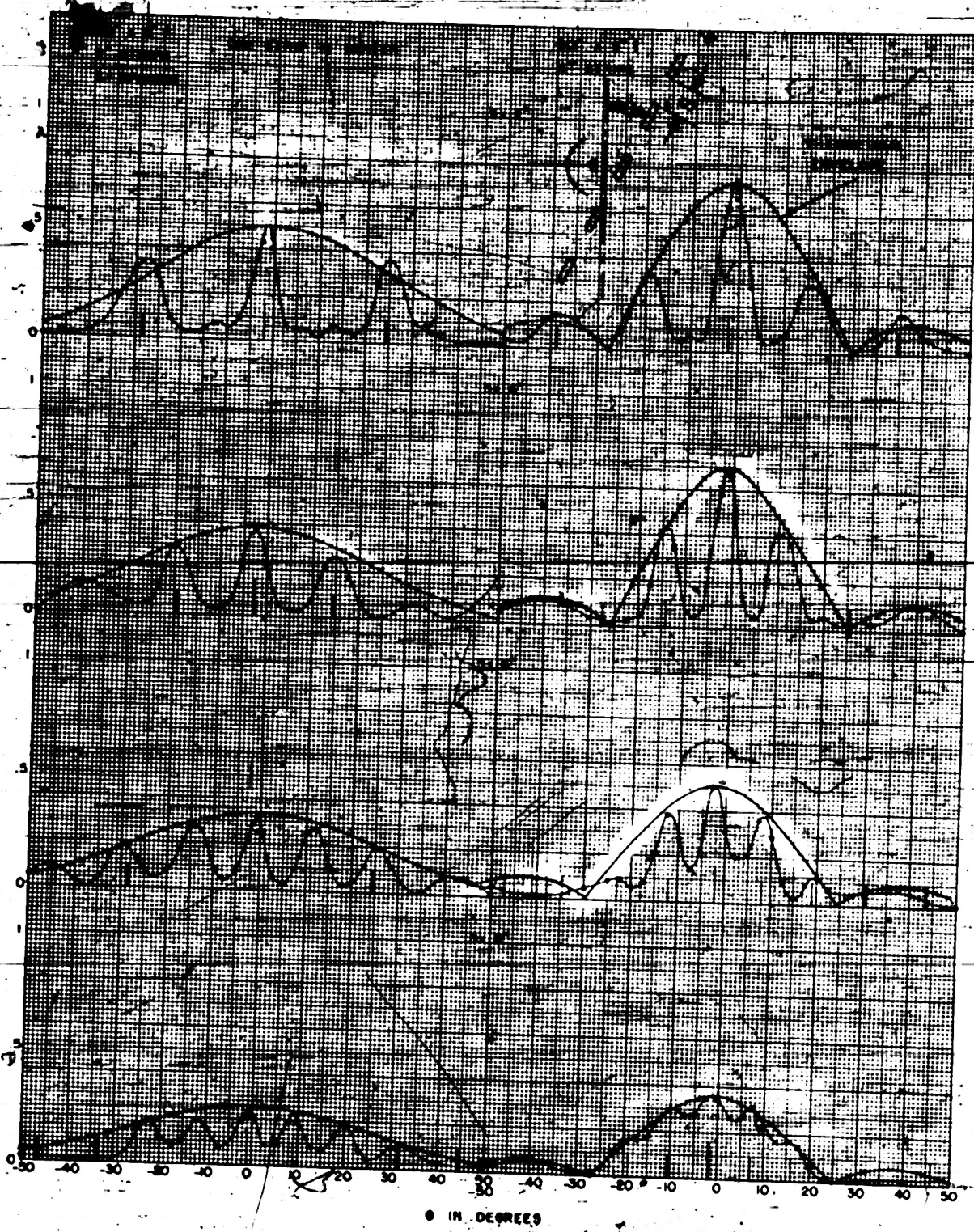


FIG. 79a--REFLECTION VERSUS ANGLE FOR A SERIES OF STRIPS, AND COMPARISON WITH THEORY

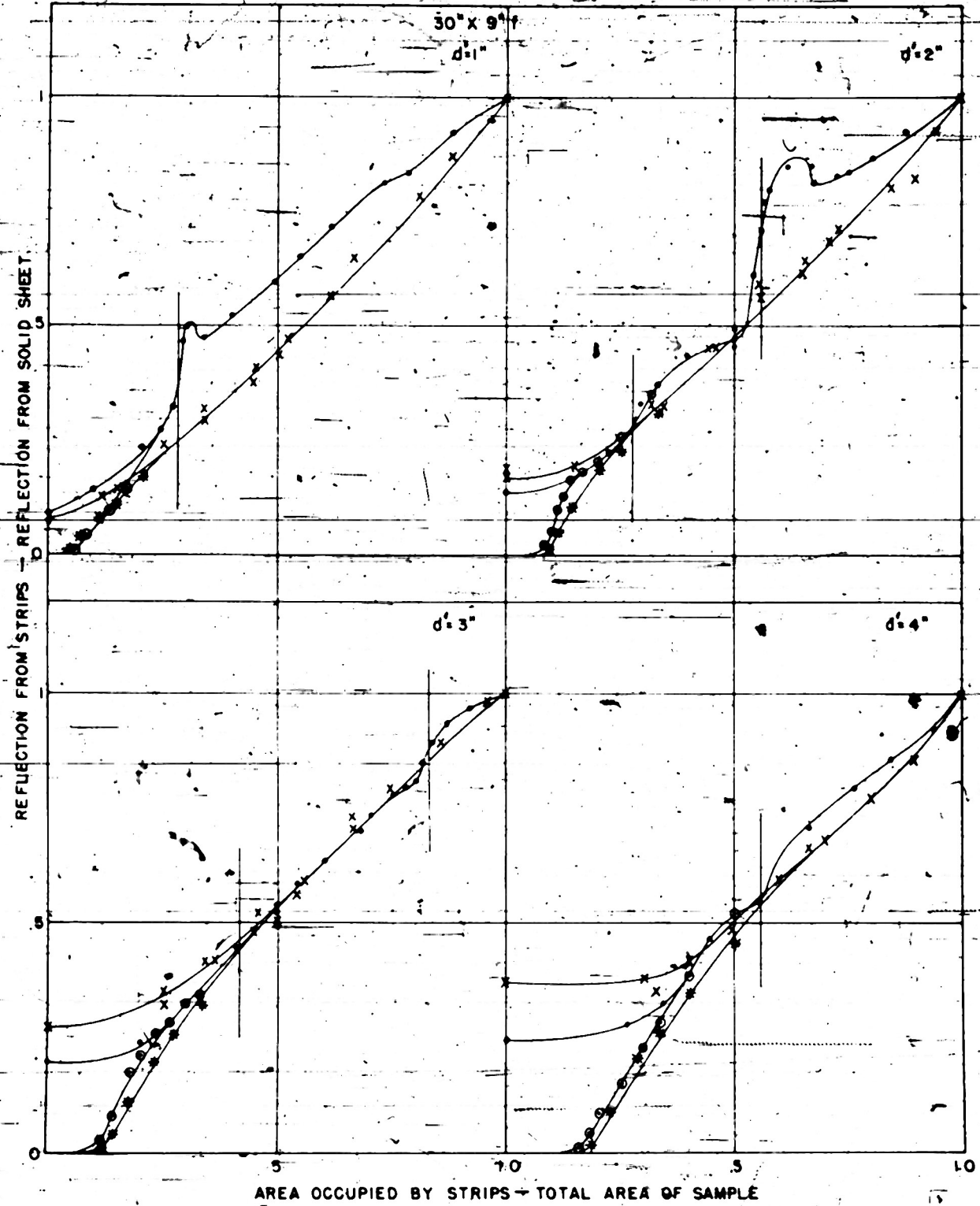


FIG. 79--SANE

483-18

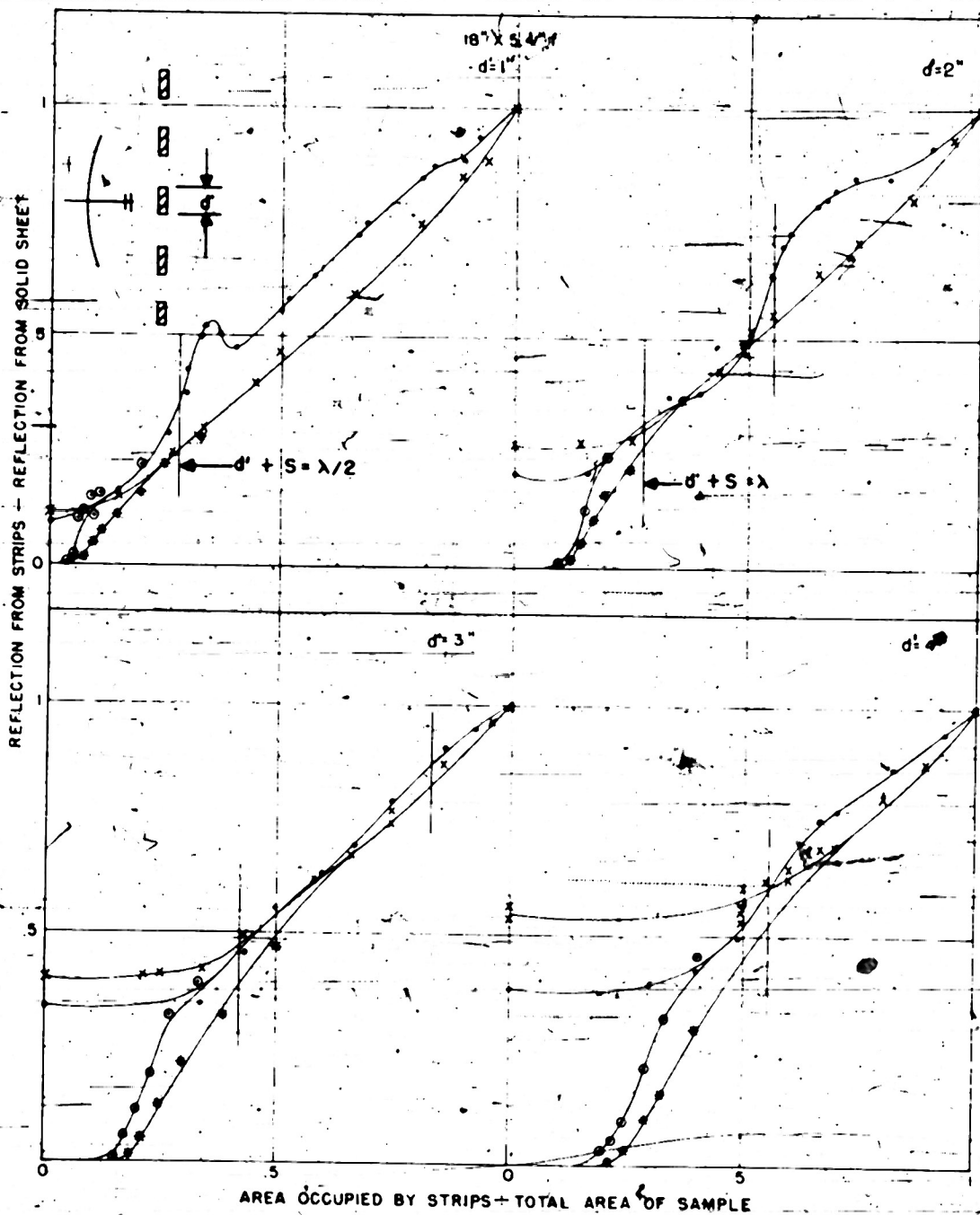


FIG. 78-REFLECTION OF STRIPS AS A FUNCTION OF SPACING AT NORMAL INCIDENCE

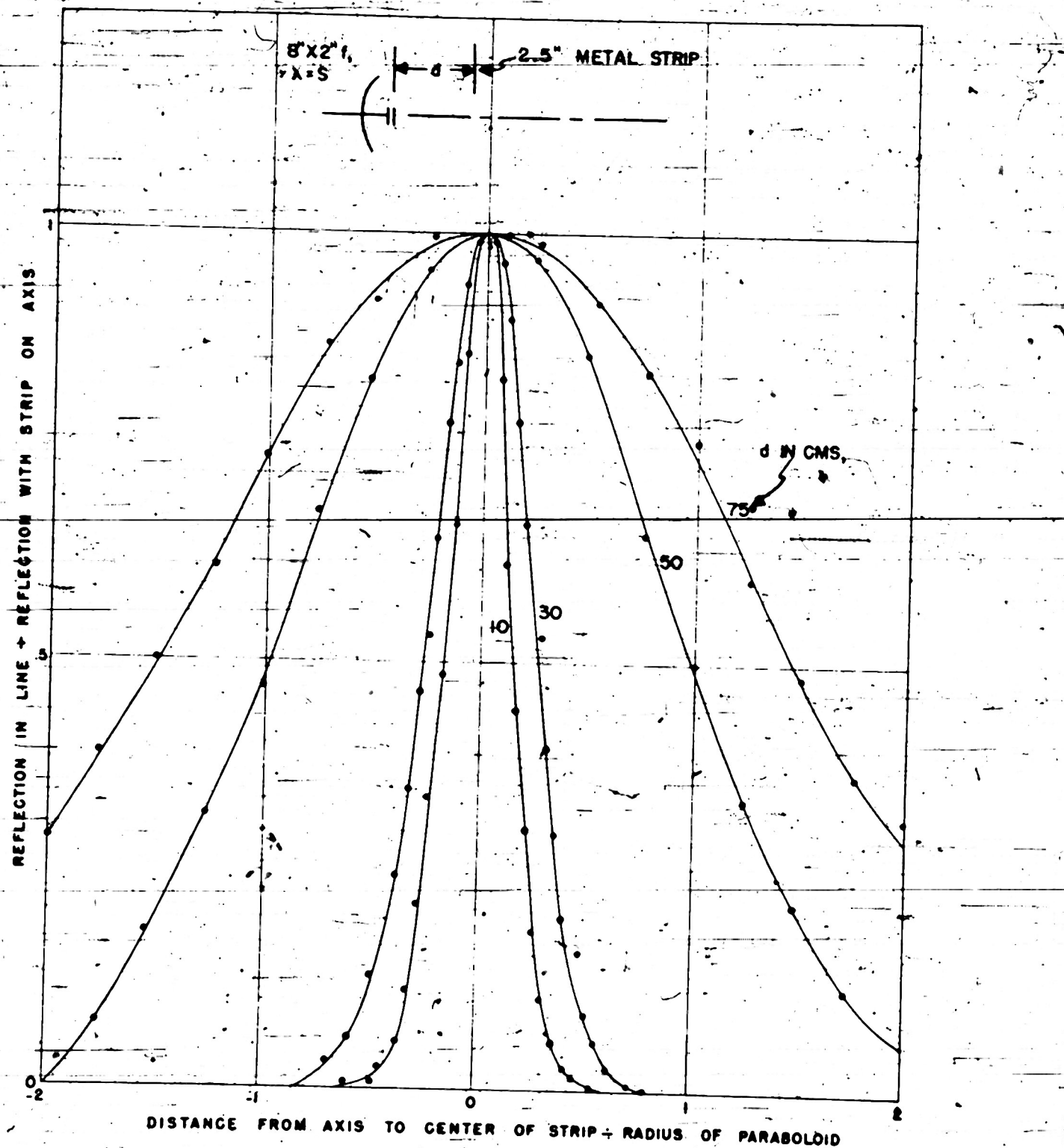


FIG. 77--EXPERIMENTAL REFLECTION VERSUS DISTANCE FROM STRIP TO ANTENNA  
AXIS, SHOWING TRANSITION FROM FRESNEL TO FRAUNHOFER REGION

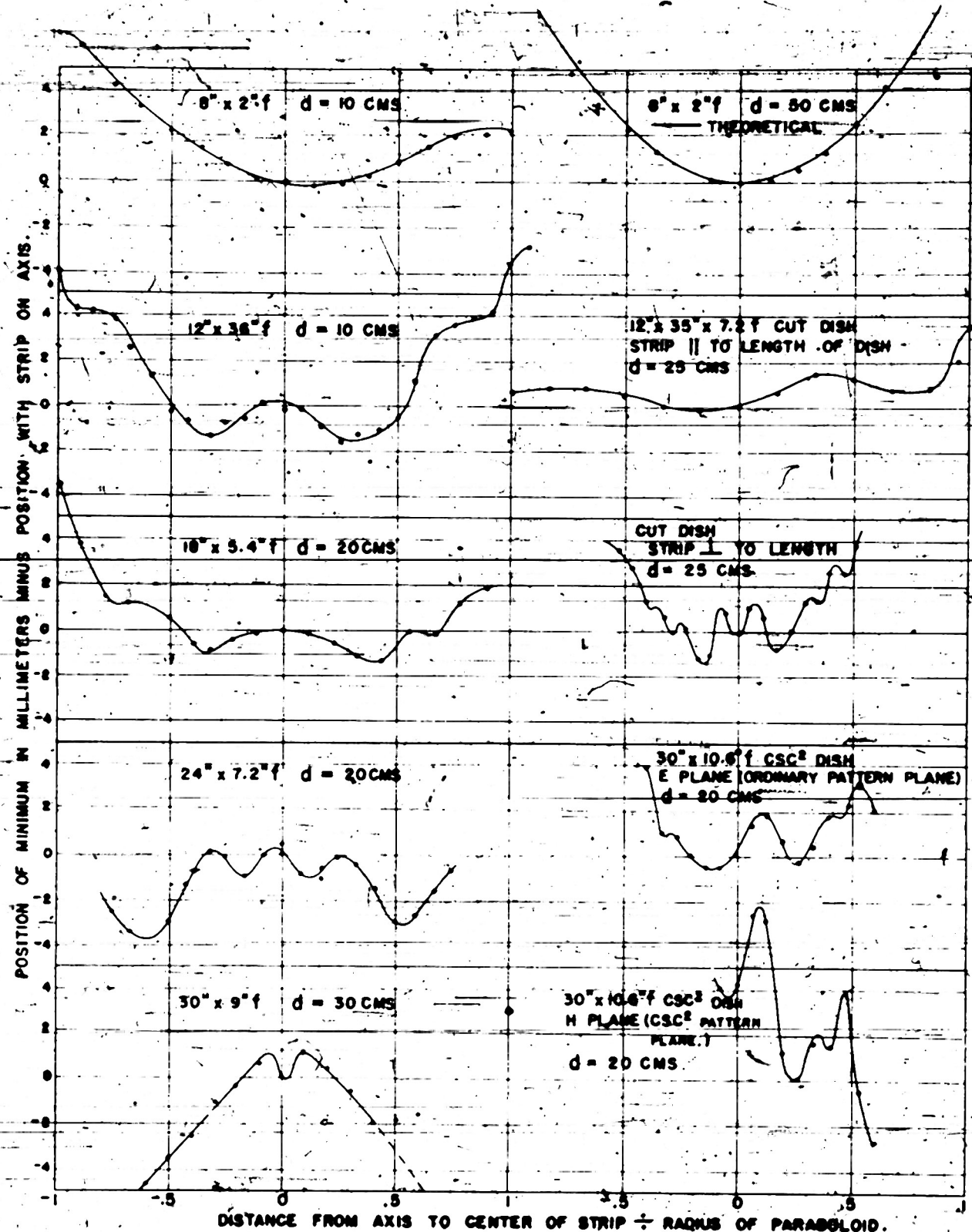


FIG. 76--VERIFICATION THAT PHASE VERSUS DISTANCE FROM STRIP TO AXIS IS PRACTICALLY CONSTANT IN FRESNEL REGION, AND COMPARISON WITH THEORY IN FRAUNHOFER REGION.

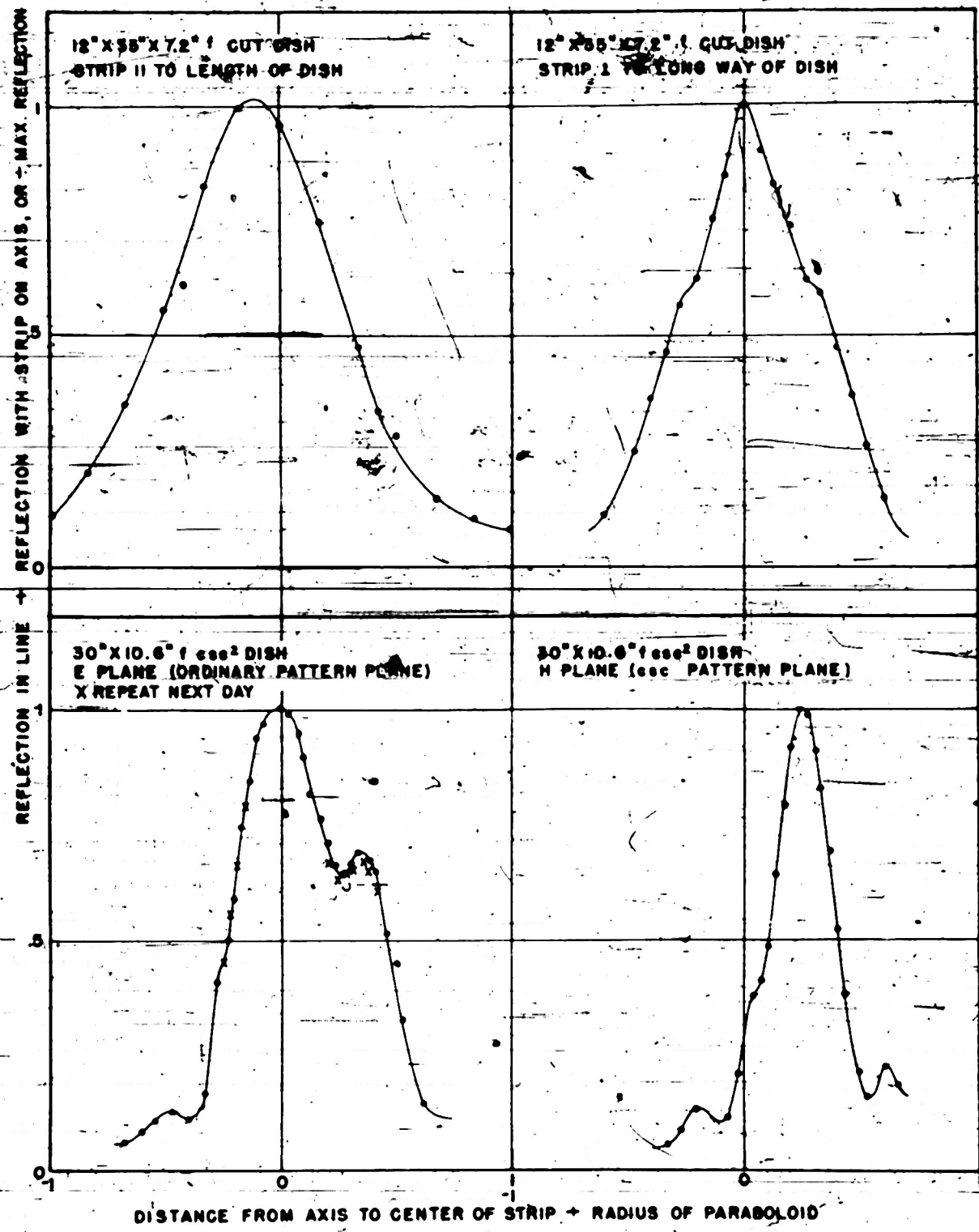


FIG. 75--EXPERIMENTAL REFLECTION FROM A DIELECTRIC STRIP VERSUS ITS DISTANCE TO THE AXIS FOR MISCELLANEOUS ANTENNAS

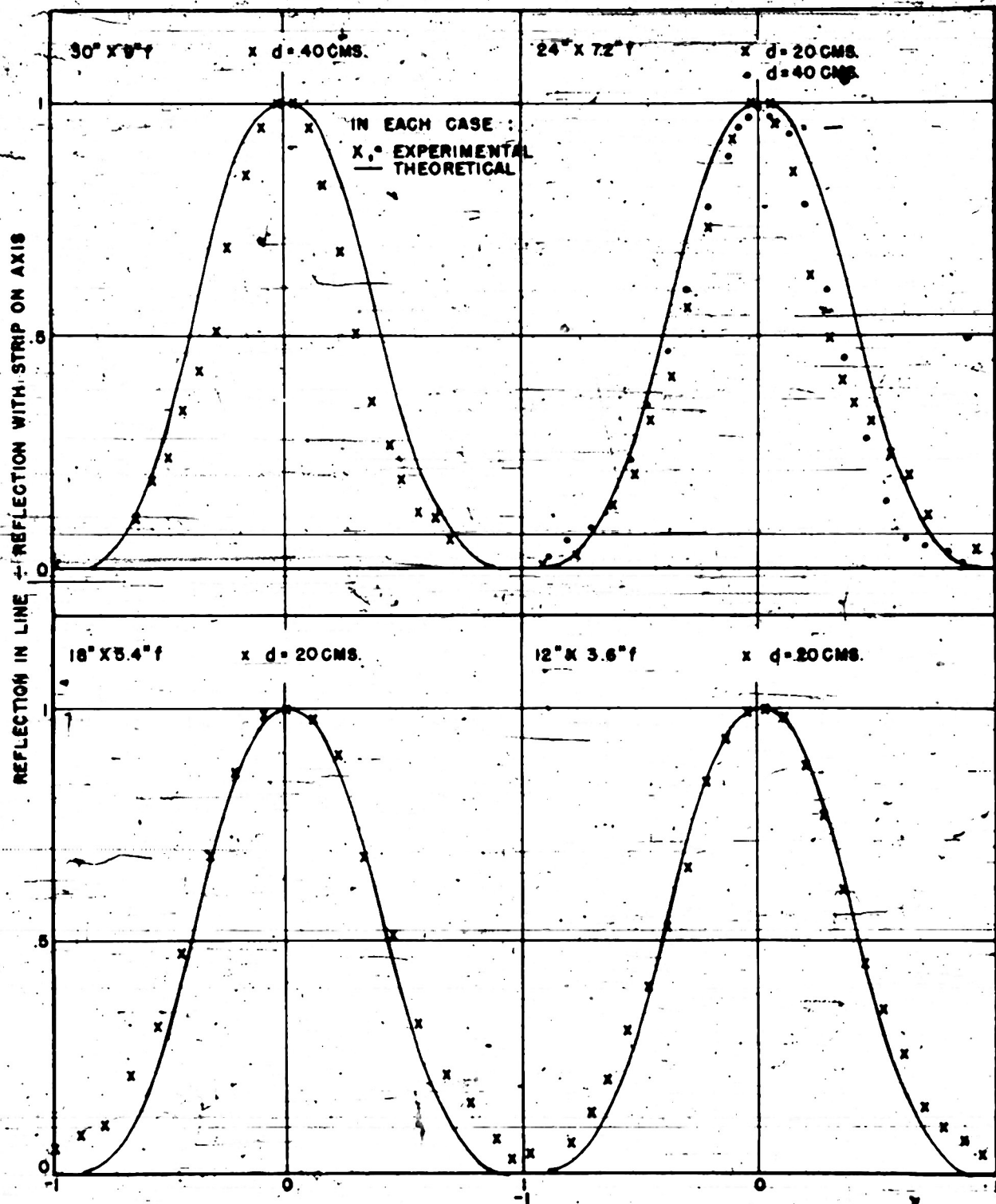
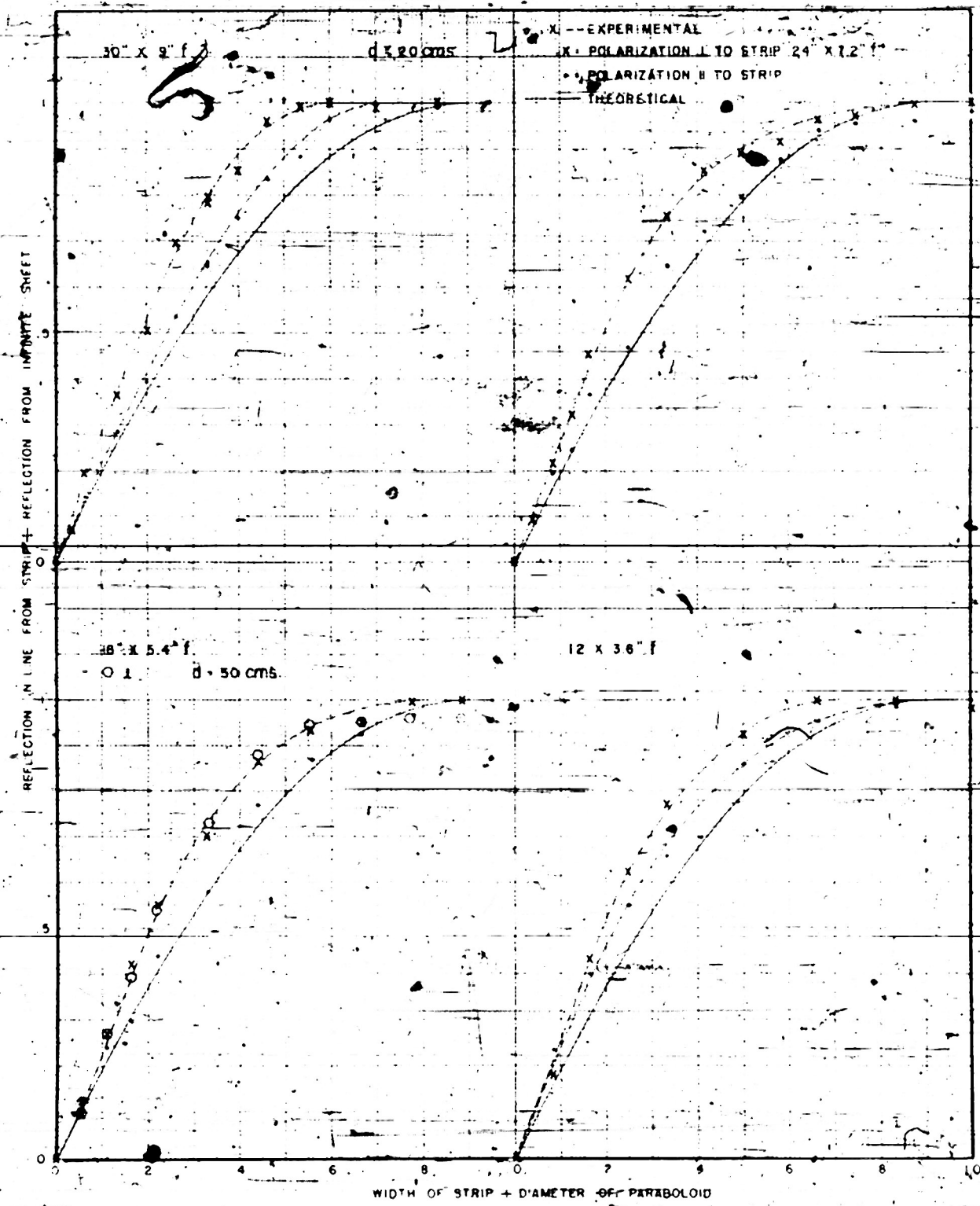


FIG. 74--THEORETICAL AND EXPERIMENTAL REFLECTION FROM A DIELECTRIC STRIP  
AS A FUNCTION OF ITS DISTANCE FROM THE AXIS OF A PARABOLOID ANTENNA



THEORETICAL AND EXPERIMENTAL REFLECTION VERSUS WIDTH FOR A  
PARABOLOID STRIP CENTERED ON THE SURFACE OF PARABOLIC ANTENNA

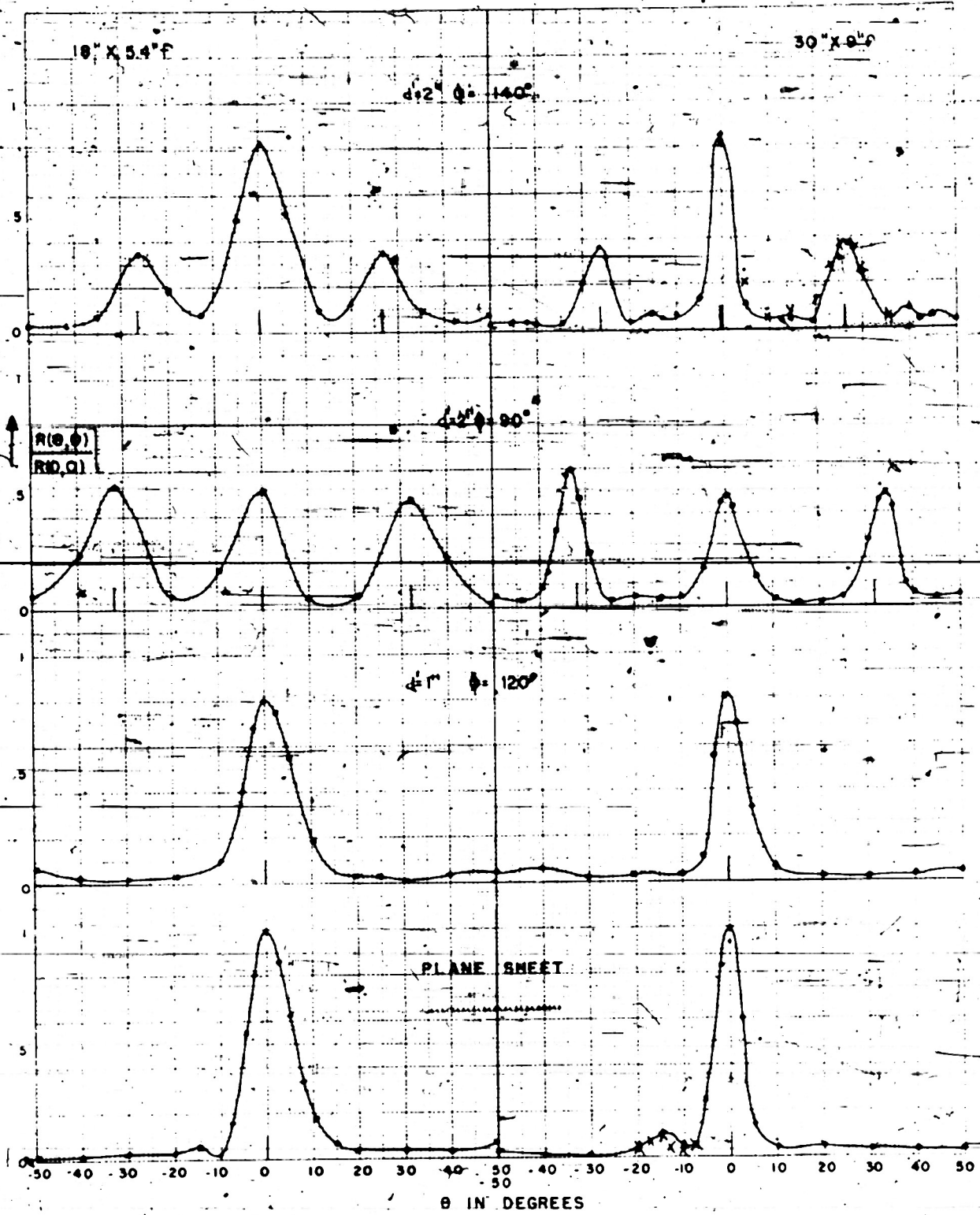
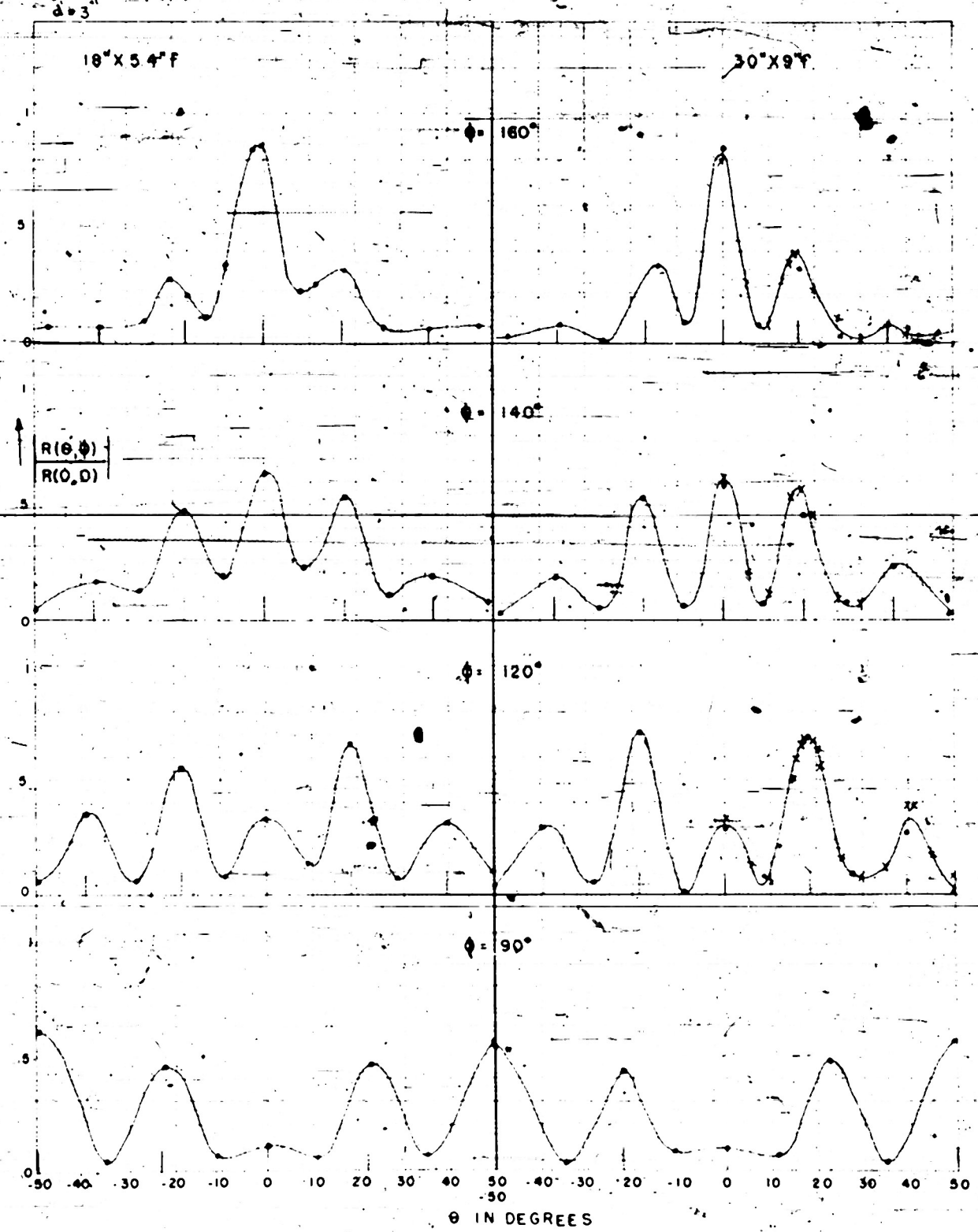


FIG. 72--6748

483-18



18" X 5.4" F

30" X 9" F

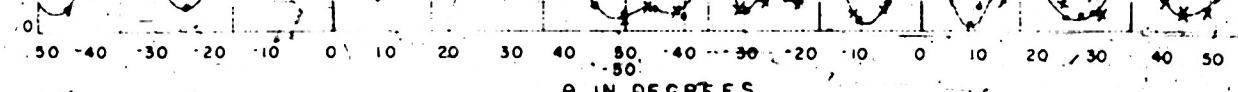
θ = 160°

θ = 140°

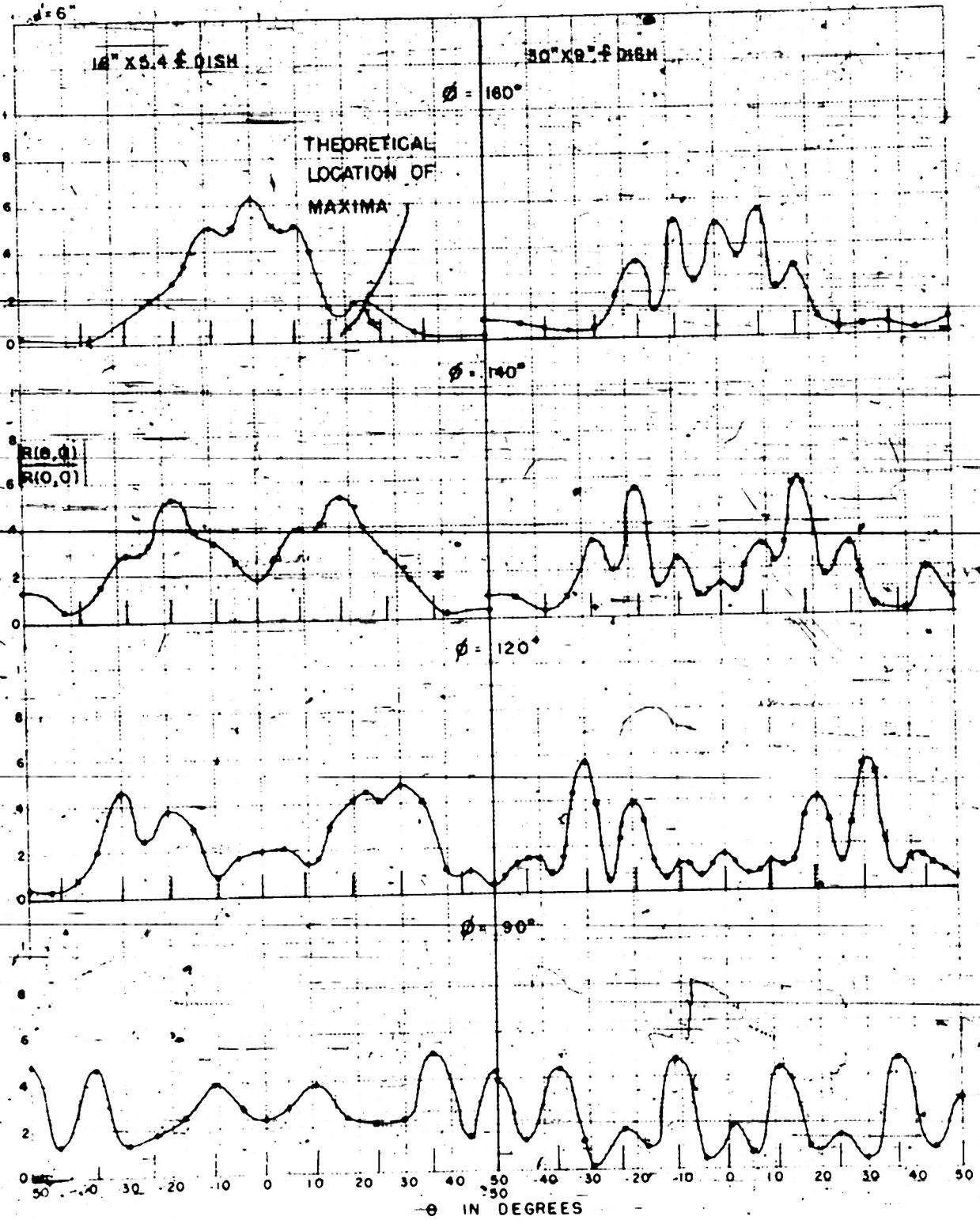
θ = 120°

θ = 90°

X SAMPLE BACKWARDS 18x9 + 180°



483-18



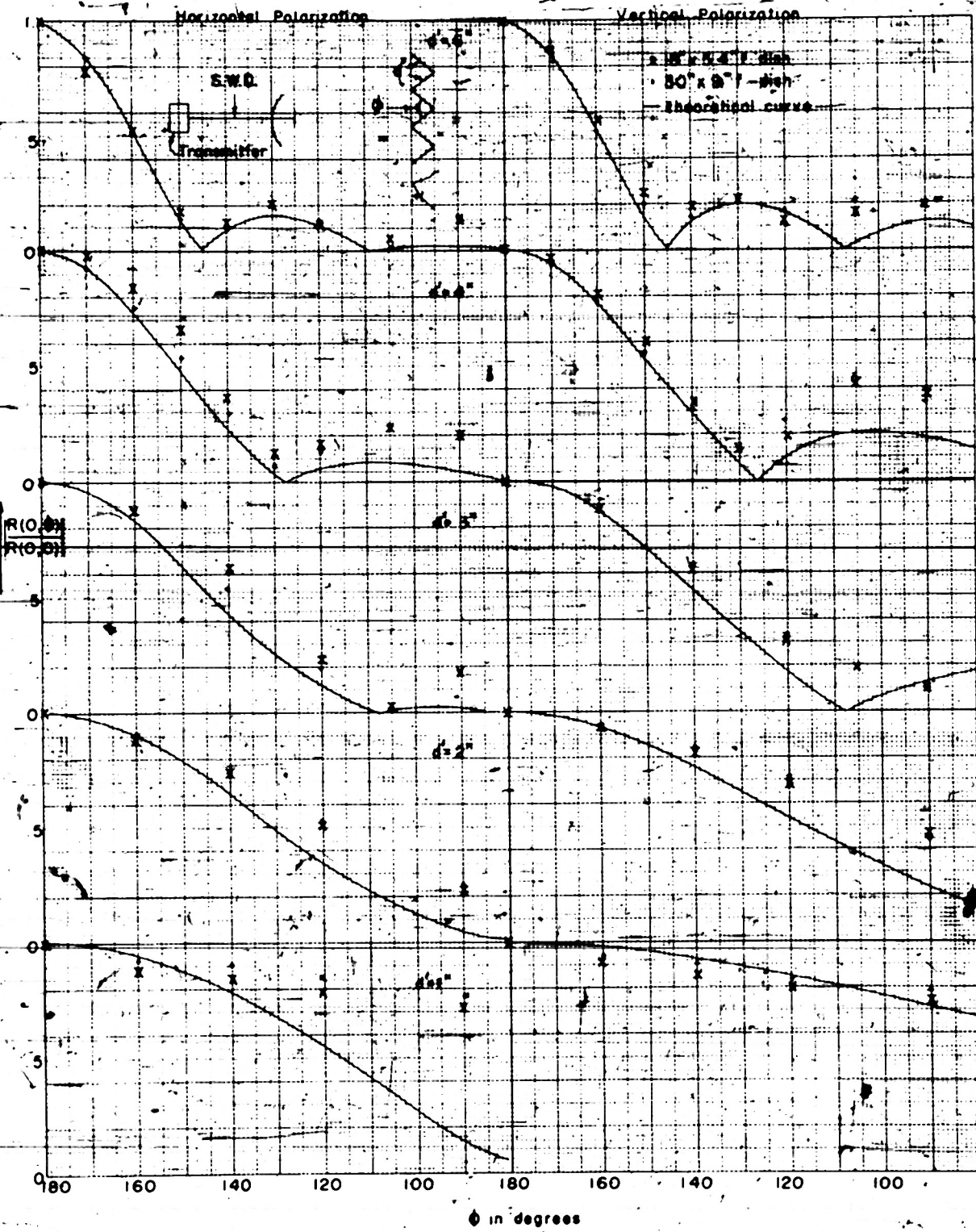


FIG. 62--SAME, COMPARED WITH EXPERIMENTAL VALUES

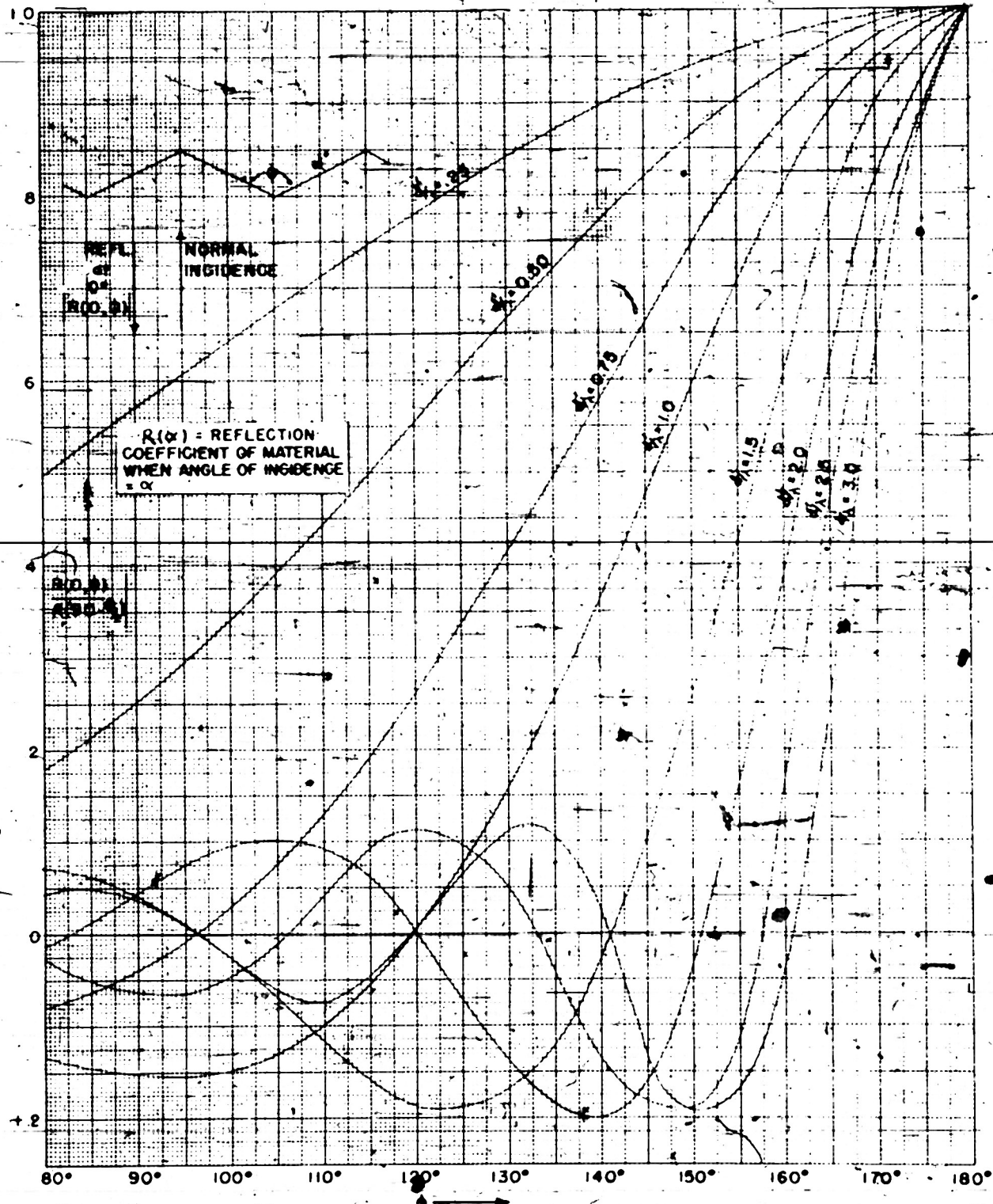


FIG. 67--THEORETICAL REFLECTION FROM CRITICAL CORRUGATED SURFACES  
AT NORMAL INCIDENCE

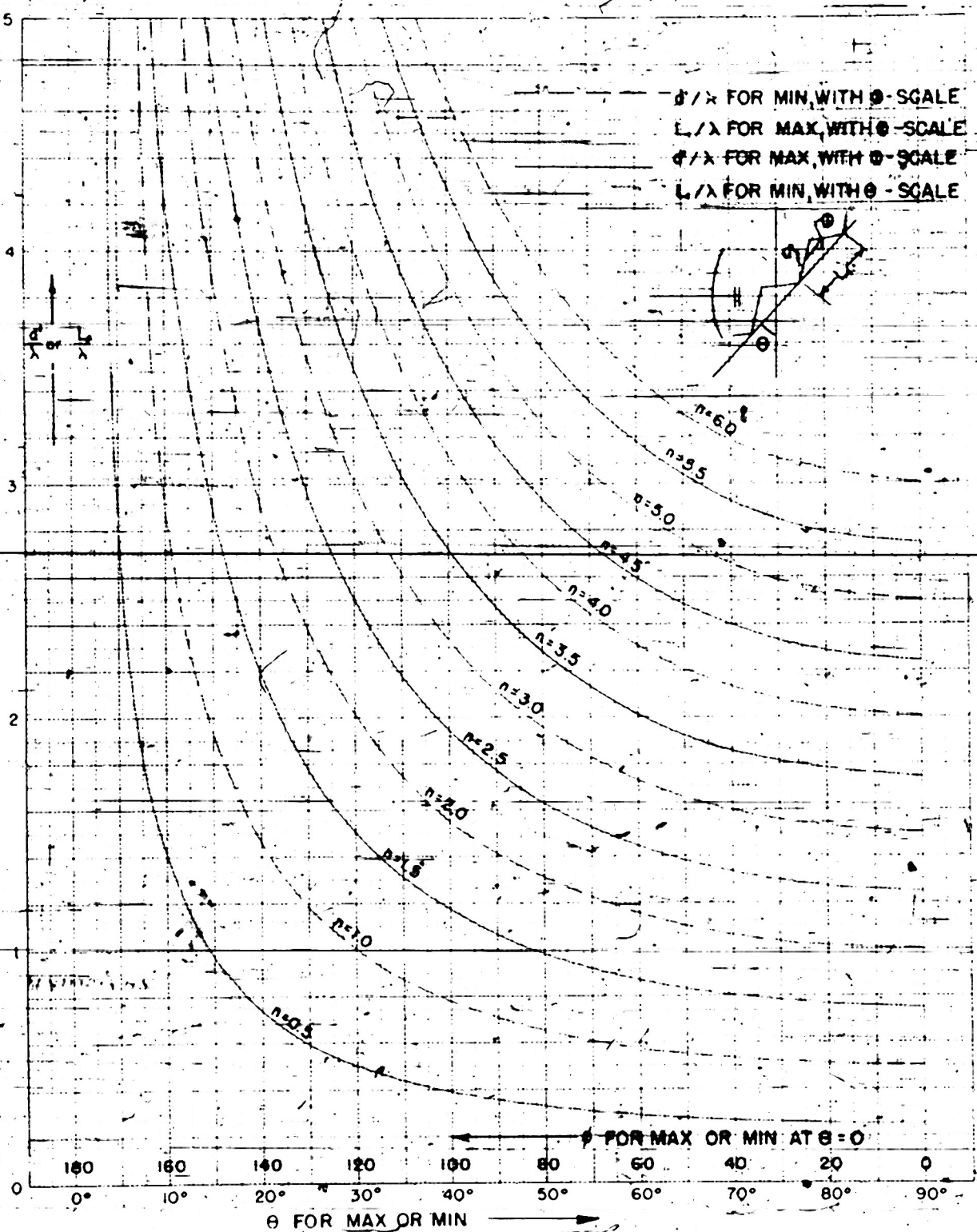
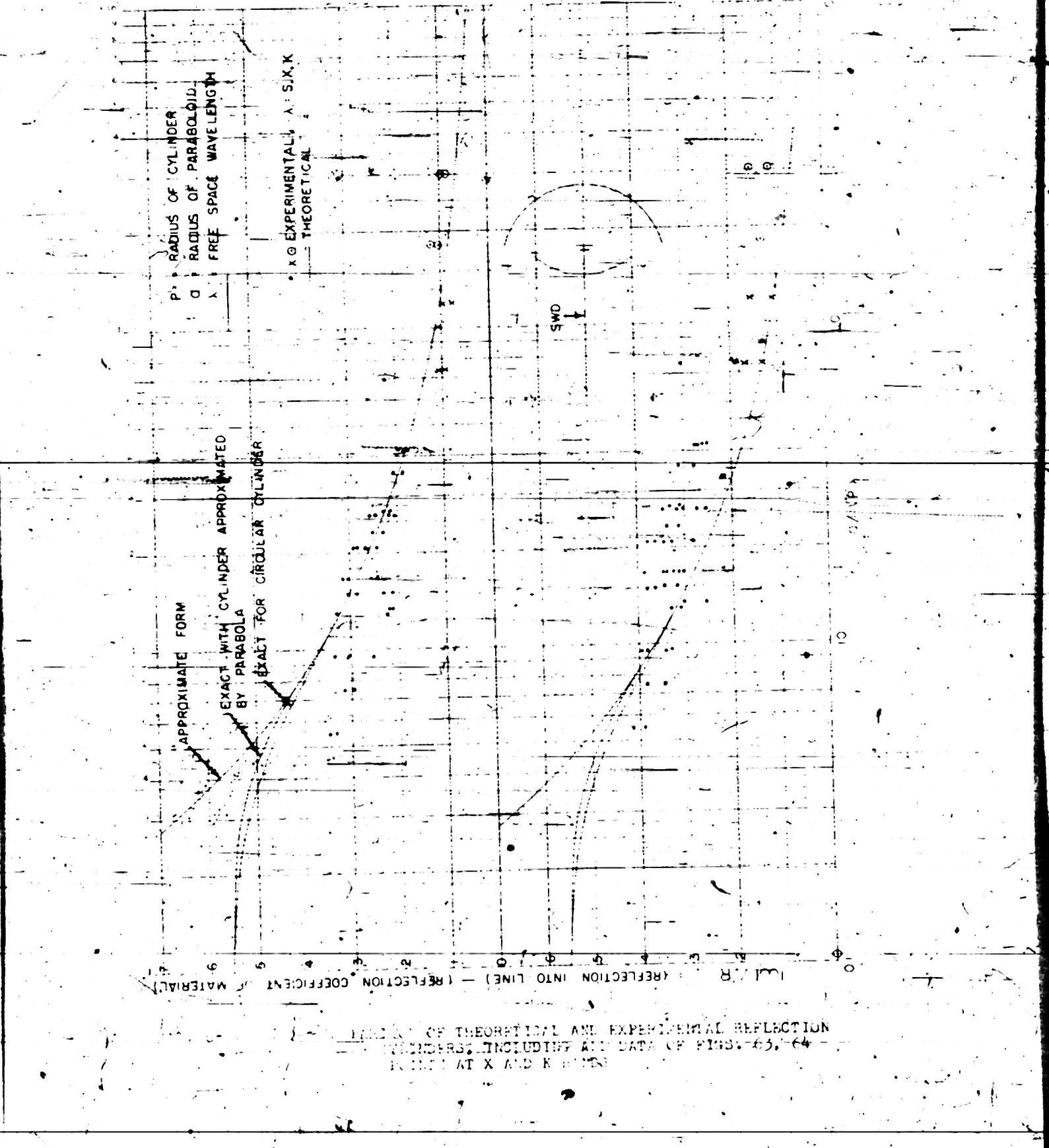
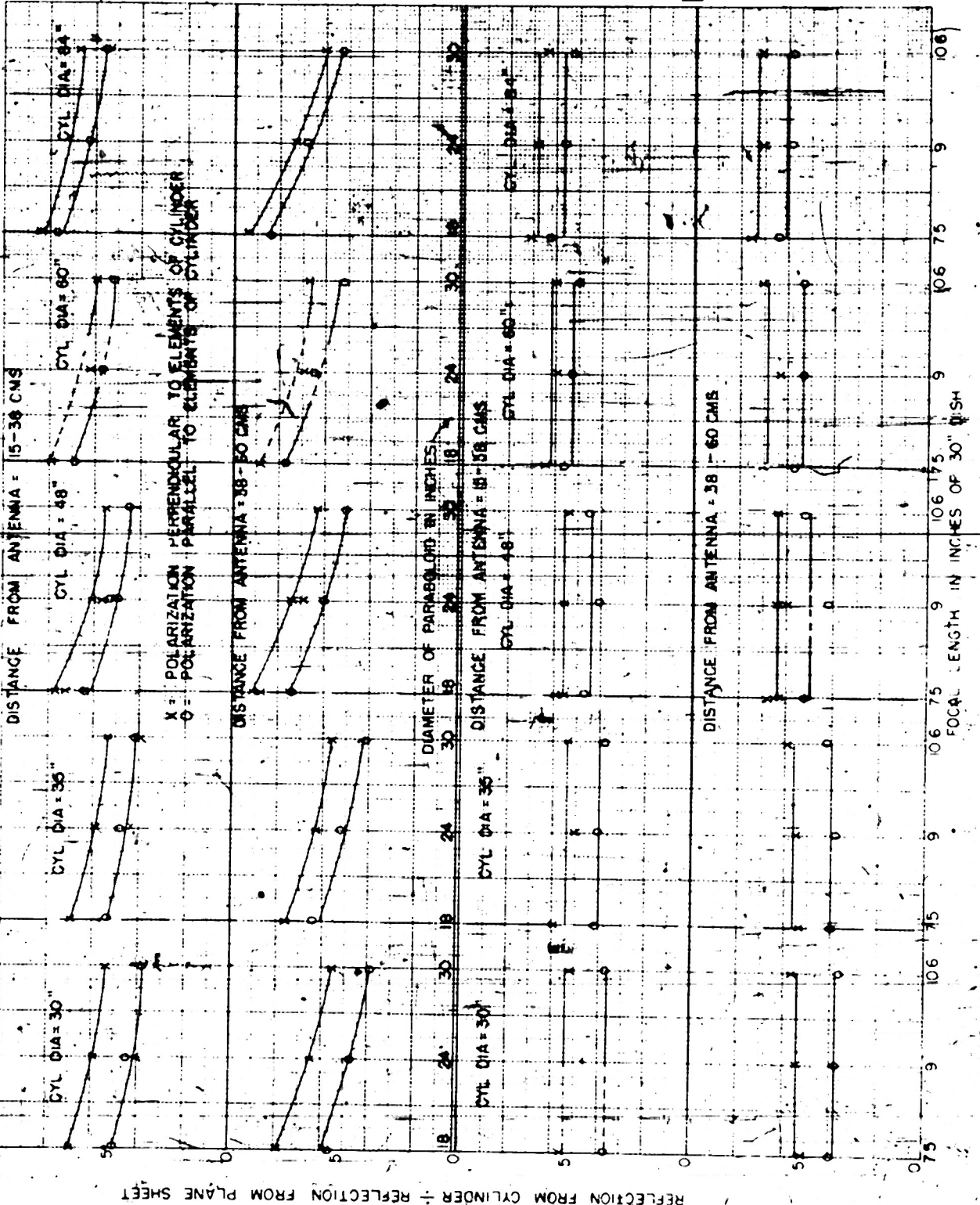


FIG. 66--THEORETICAL ANGLE OF INCIDENCE FOR MINIMUM REFLECTION FROM A RIGID SURFACE; OR DIMENSIONS OF CORRUGATED SURFACE FOR MINIMUM REFLECTION AT NORMAL INCIDENCE.

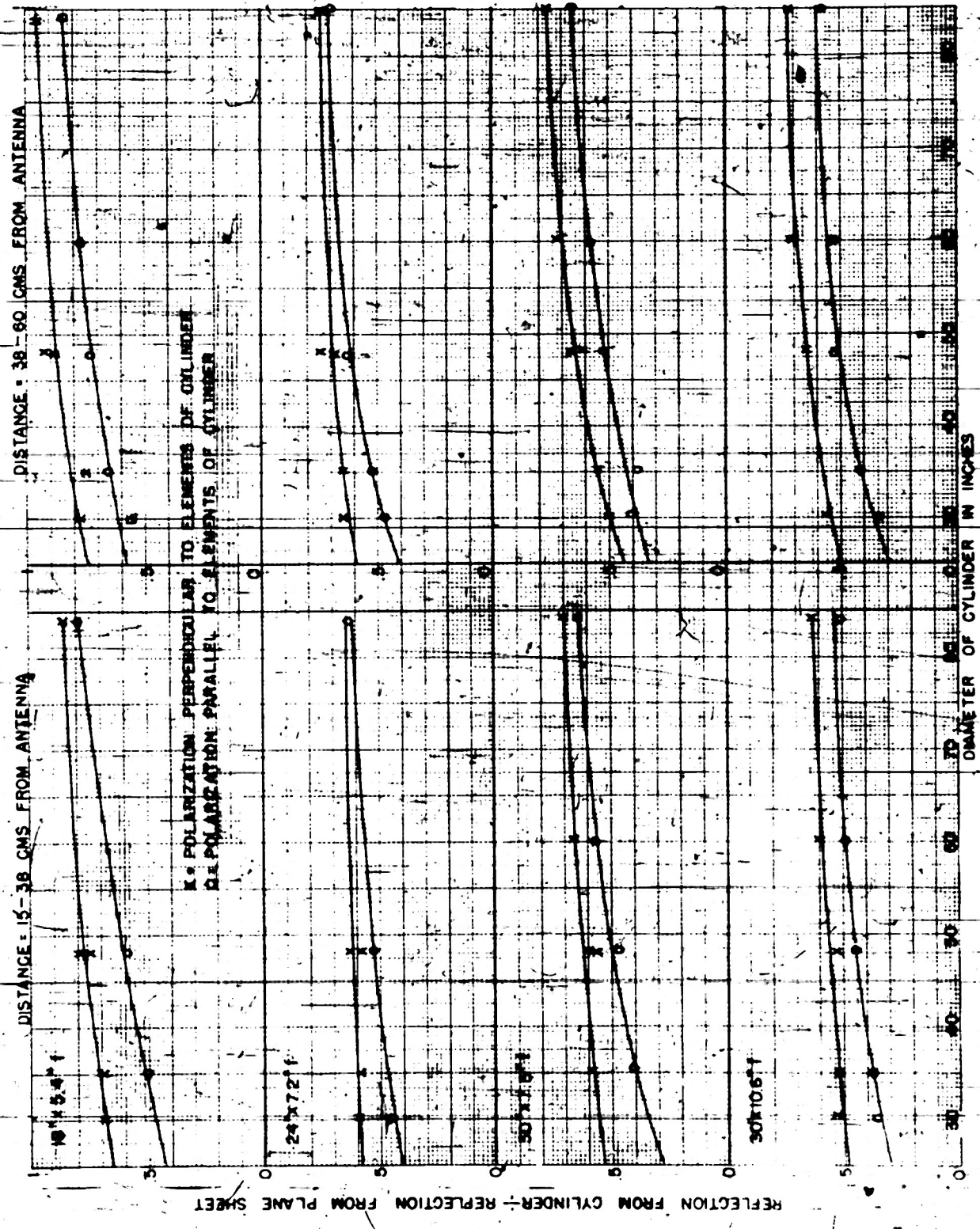


483-1



REFLECTION FROM CYLINDER + REFLECTION FROM PLANE SHEET

Fig. 64--3. REFLECTION VERSUS ANTENNA SIZE OR FOCAL LENGTH FOR VARIOUS CYLINDER DIAMETERS.



13-63-R-121 PLEASE RETURN THIS FORM TO THE LIBRARY  
AND USE IT AGAIN

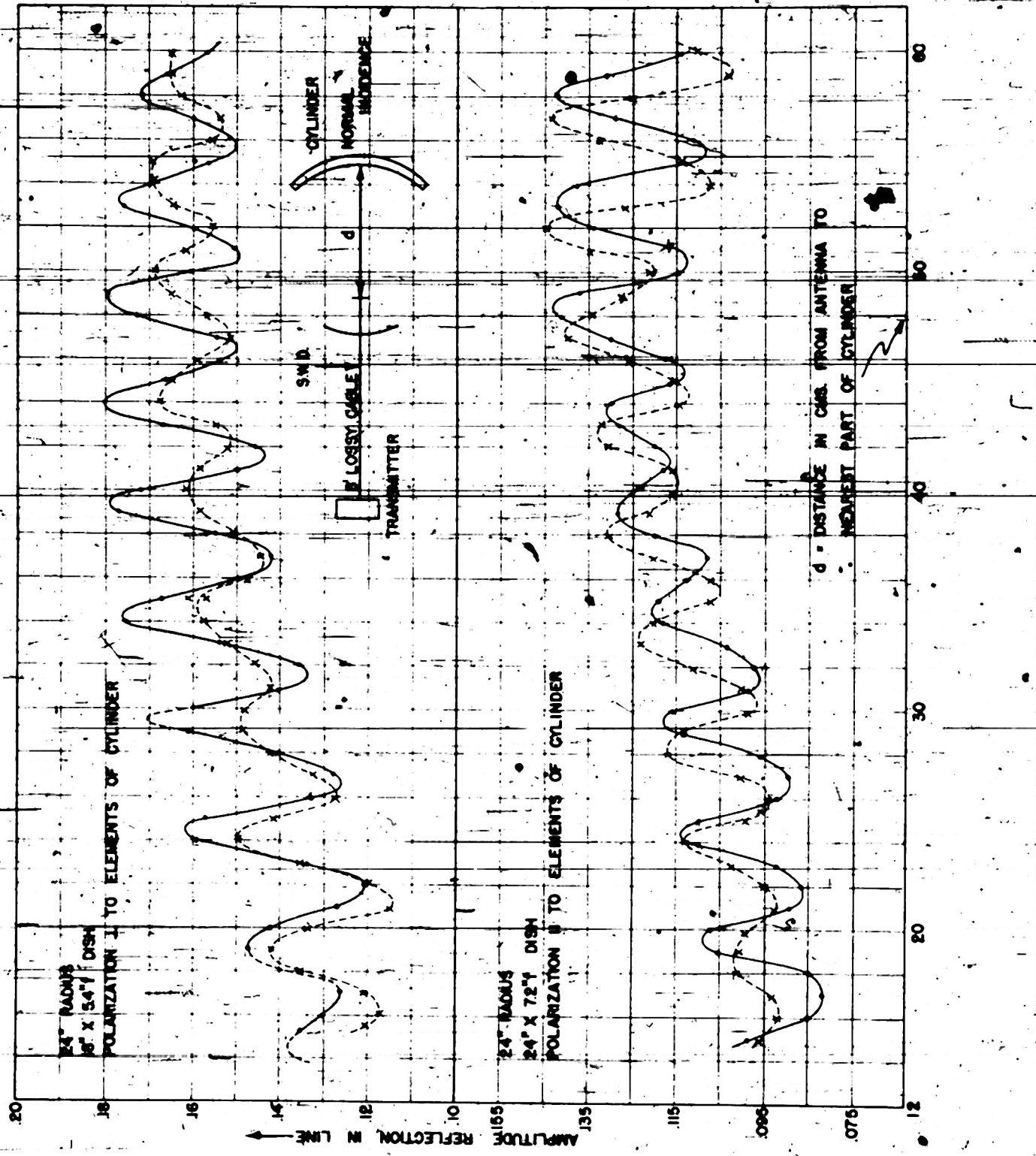


FIG. 62--EXAMPLES OF REFLECTION VERSUS DISTANCE TO ANTENNA FOR CIRCULAR CYLINDERS, SHOWING REPRODUCIBILITY OF DATA

483-18

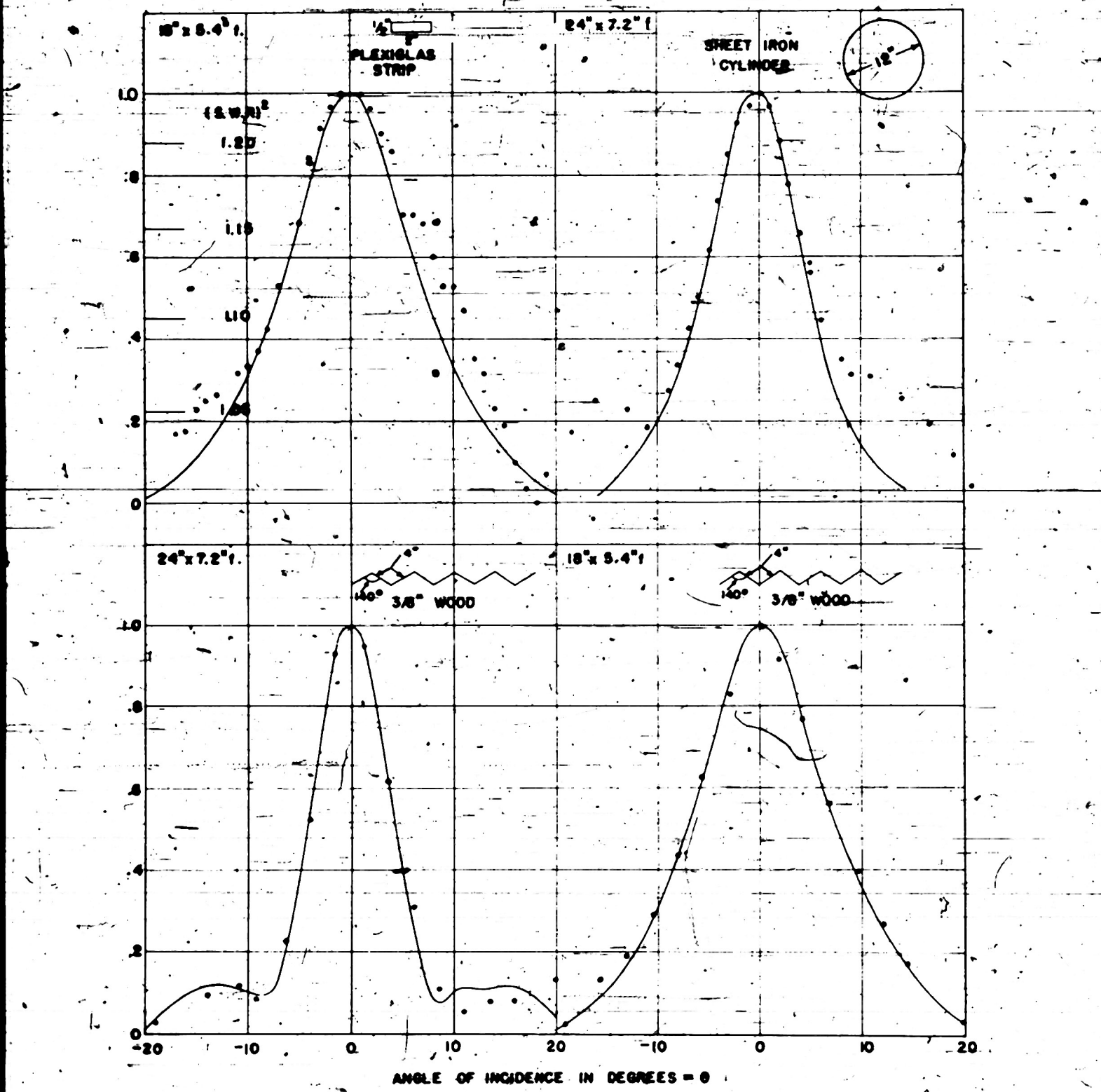


FIG. 61--SAME FOR PARABOLOIDAL ANTENNAS AND MISCELLANEOUS CYLINDRICAL SURFACES

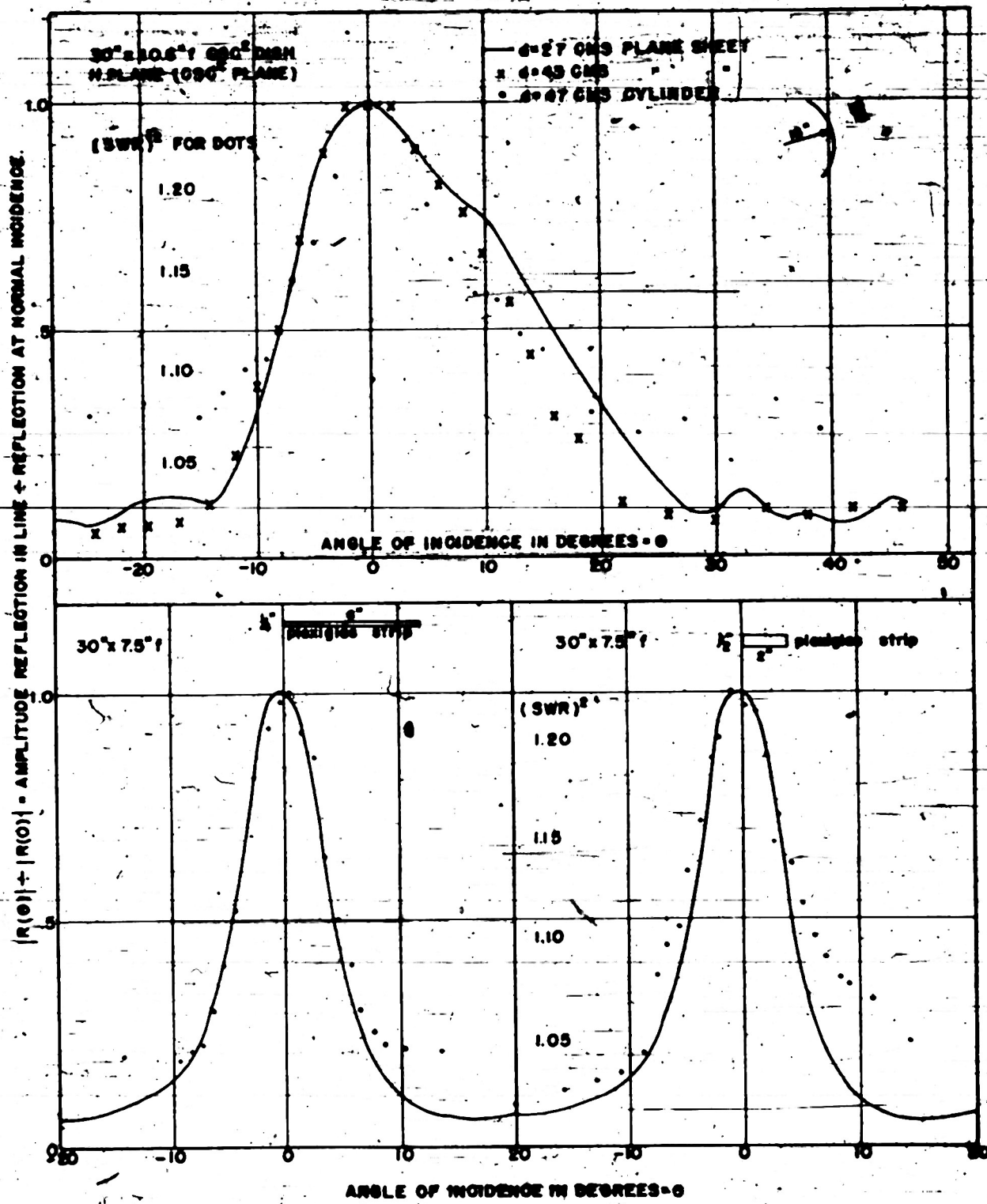


FIG. 60--SAME, FOR NON-PARABOLOIDAL ANTENNA OR FOR NON-CIRCULAR CYLINDERS,

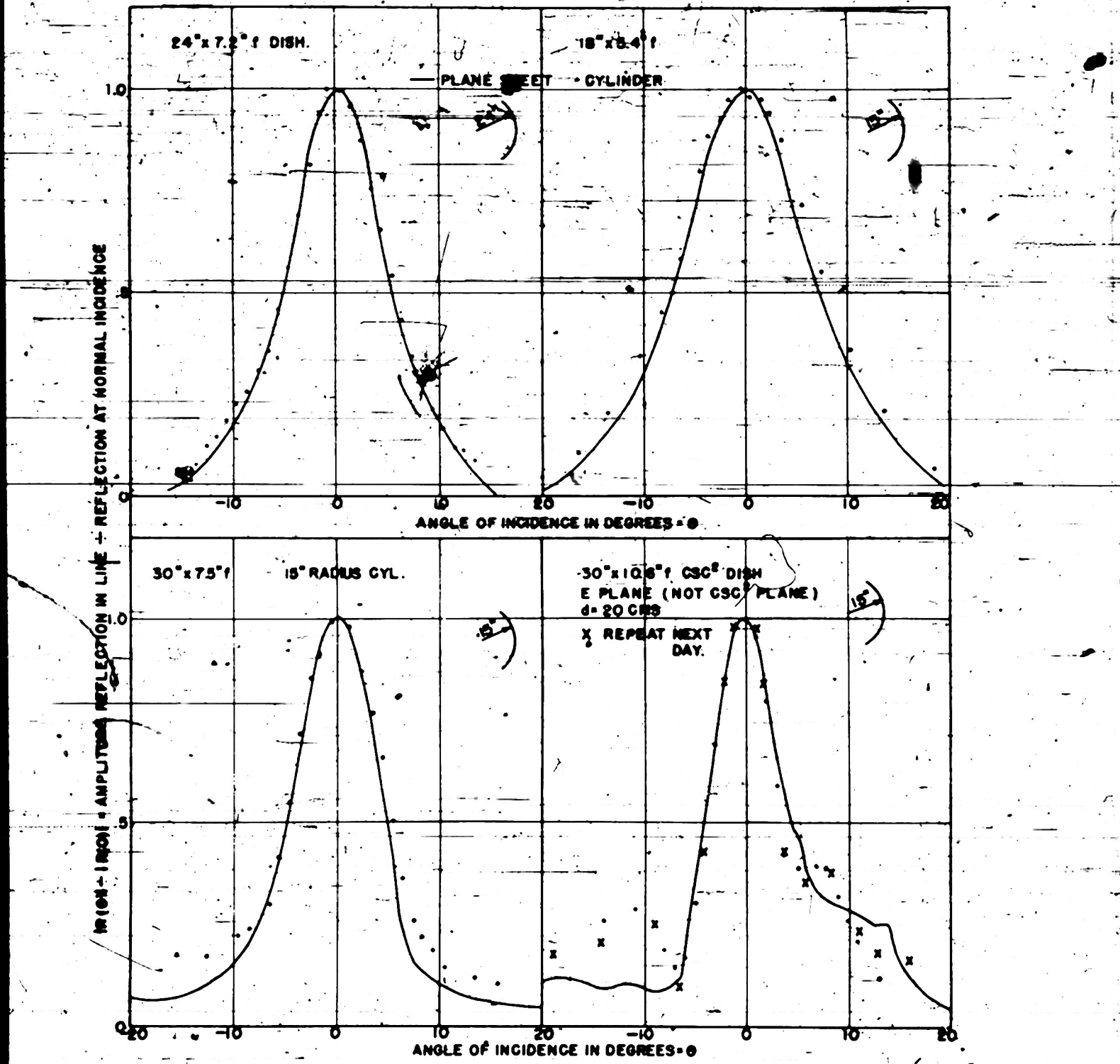


FIG. 59.—VERIFICATION THAT REFLECTION VERSUS ANGLE FOR A CIRCULAR CYLINDER IS PROPORTIONAL TO THE SAME FOR A PLANE SHEET.

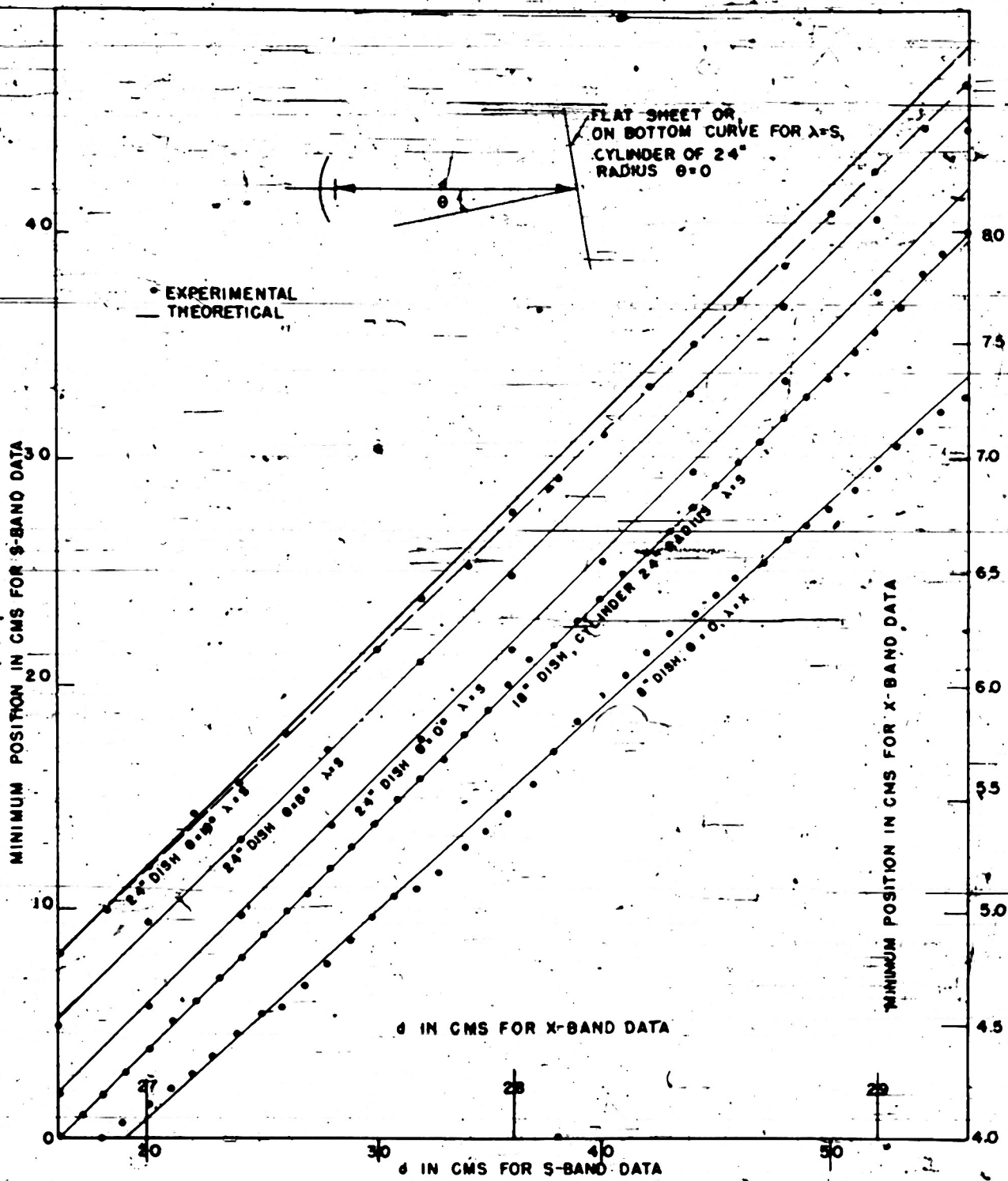


FIG. 58--VERIFICATION THAT MINIMUM POSITION MOVES WITH REFLECTING SURFACE,  
THE RATIO OF THE TWO MOTIONS BEING EQUAL TO THE RATIO OF AIR AND  
GUIDE WAVELENGTHS

POSITION OF MINIMUM MINUS POSITION AT NORMAL INCIDENCE IN MILLIMETERS

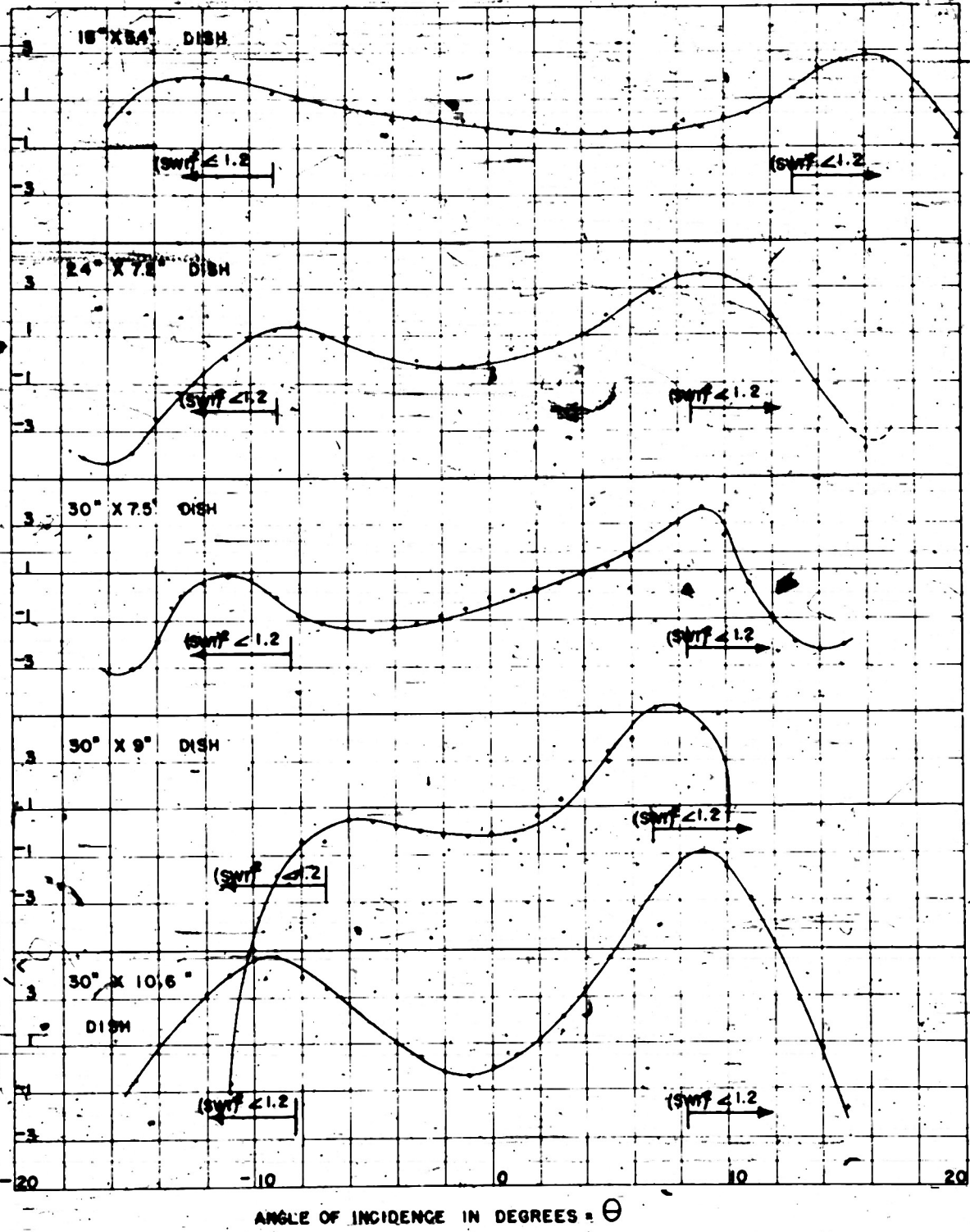


FIG. 57--VERIFICATION THAT PHASE IS NEARLY INDEPENDENT OF ANGLE OF INCIDENCE

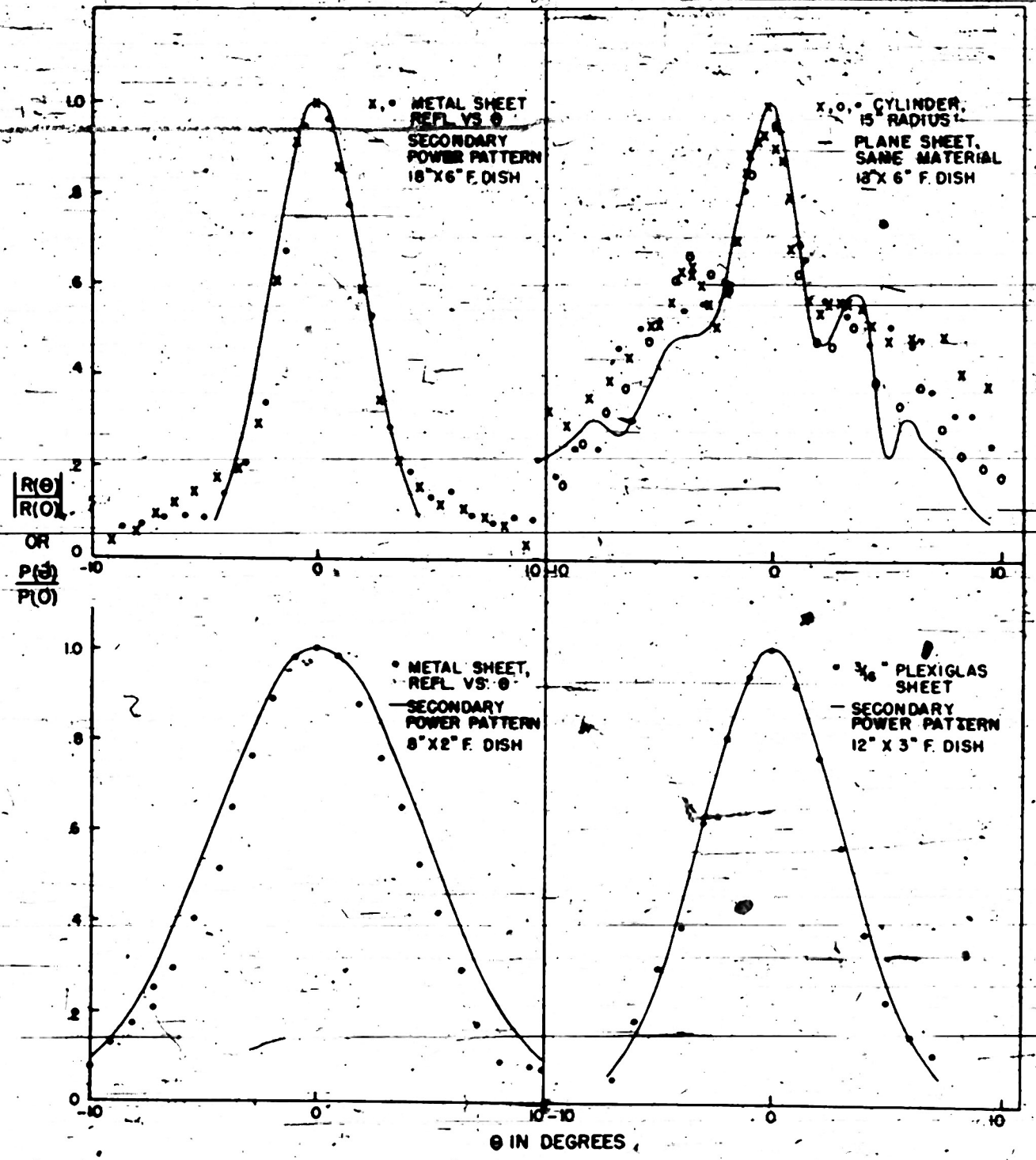


FIG. 56--COMPARISON OF AMPLITUDE REFLECTION VERSUS ANGLE WITH SECONDARY POWER PATTERN AT X-BAND

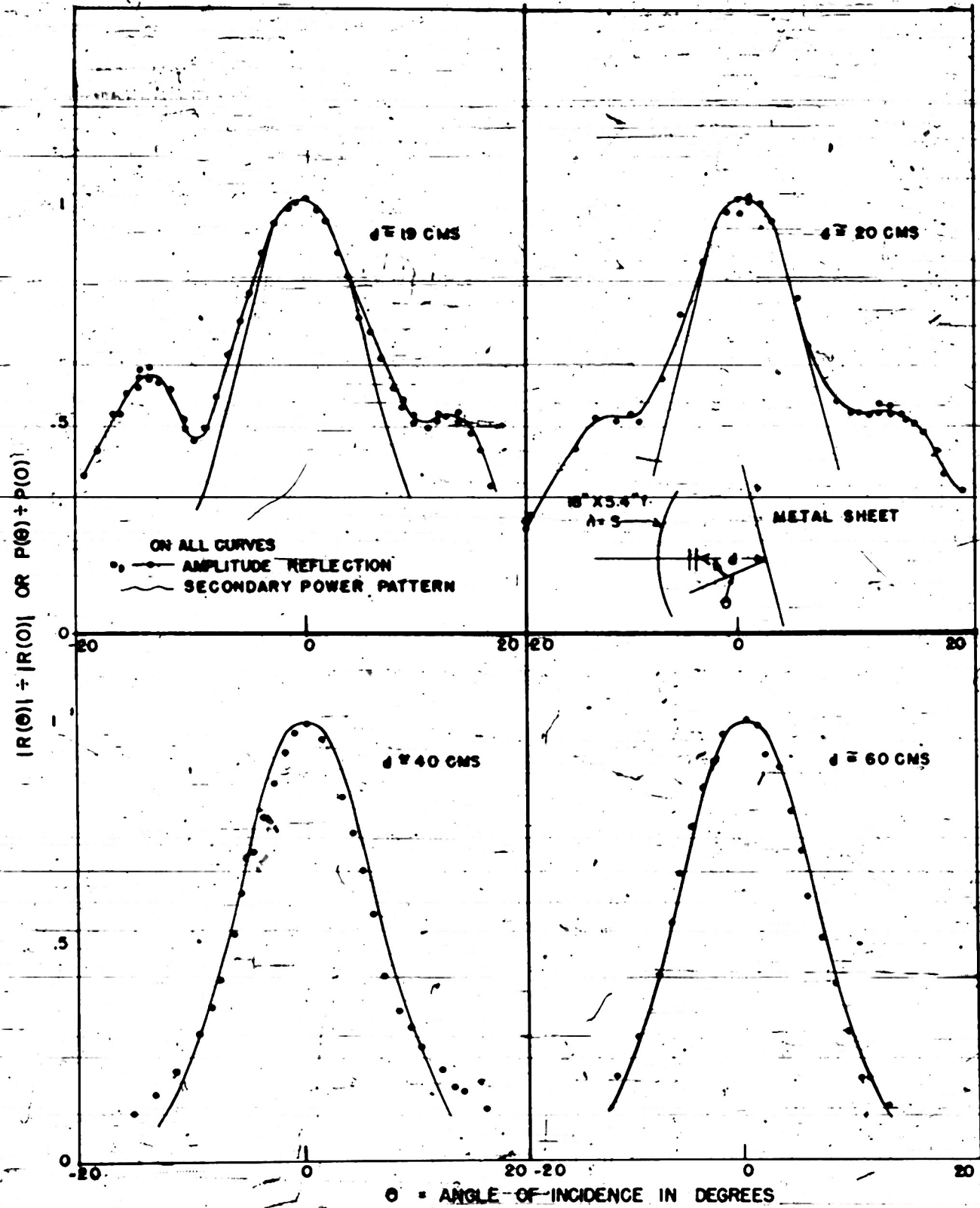


FIG. 55. SAME. ANAMOLOUS EFFECTS NOTED WHEN METAL SHEET IS CLOSE TO ANTENNA

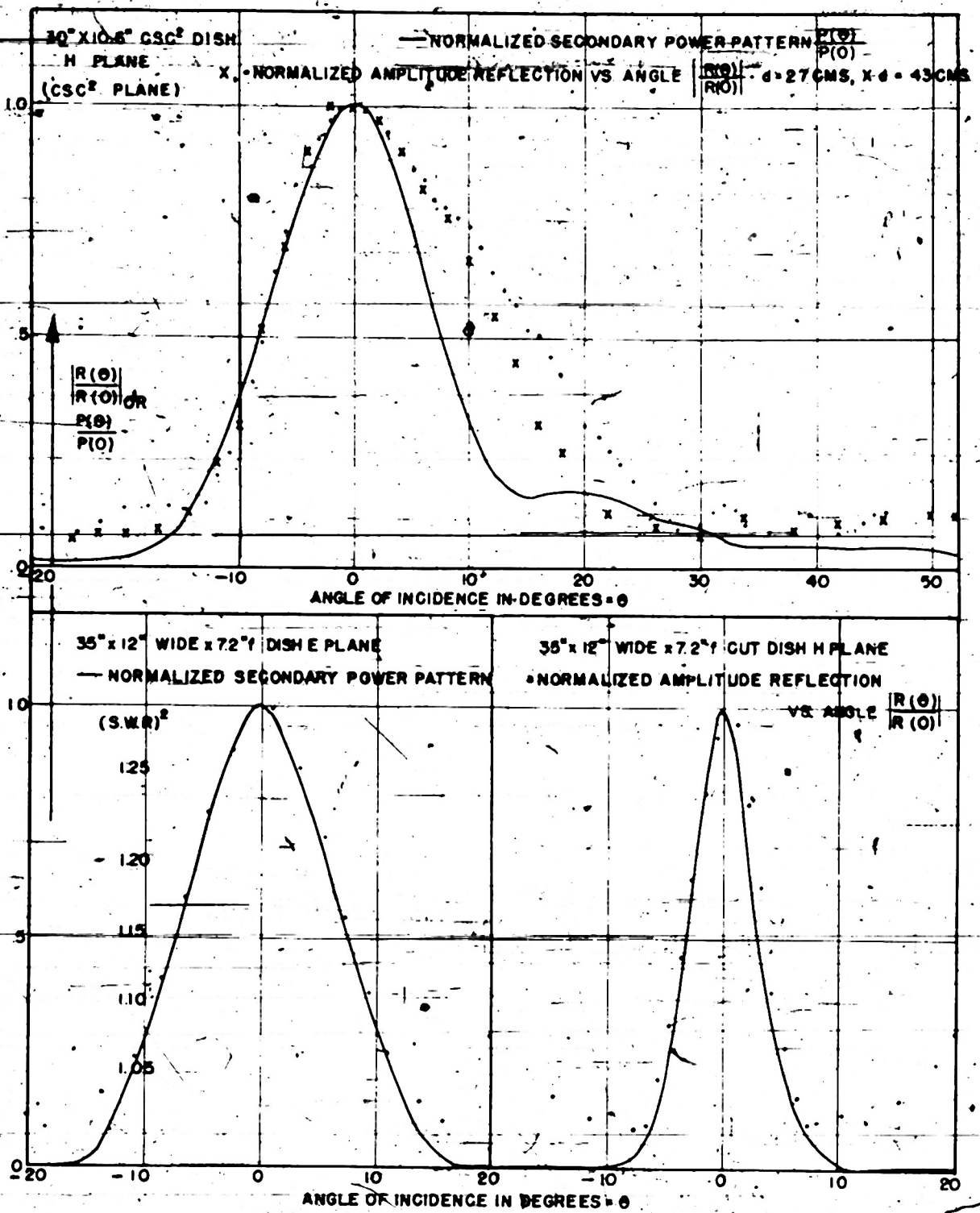


FIG. 54—SOME FOR NON-PARABOLOIDAL ANTENNAS

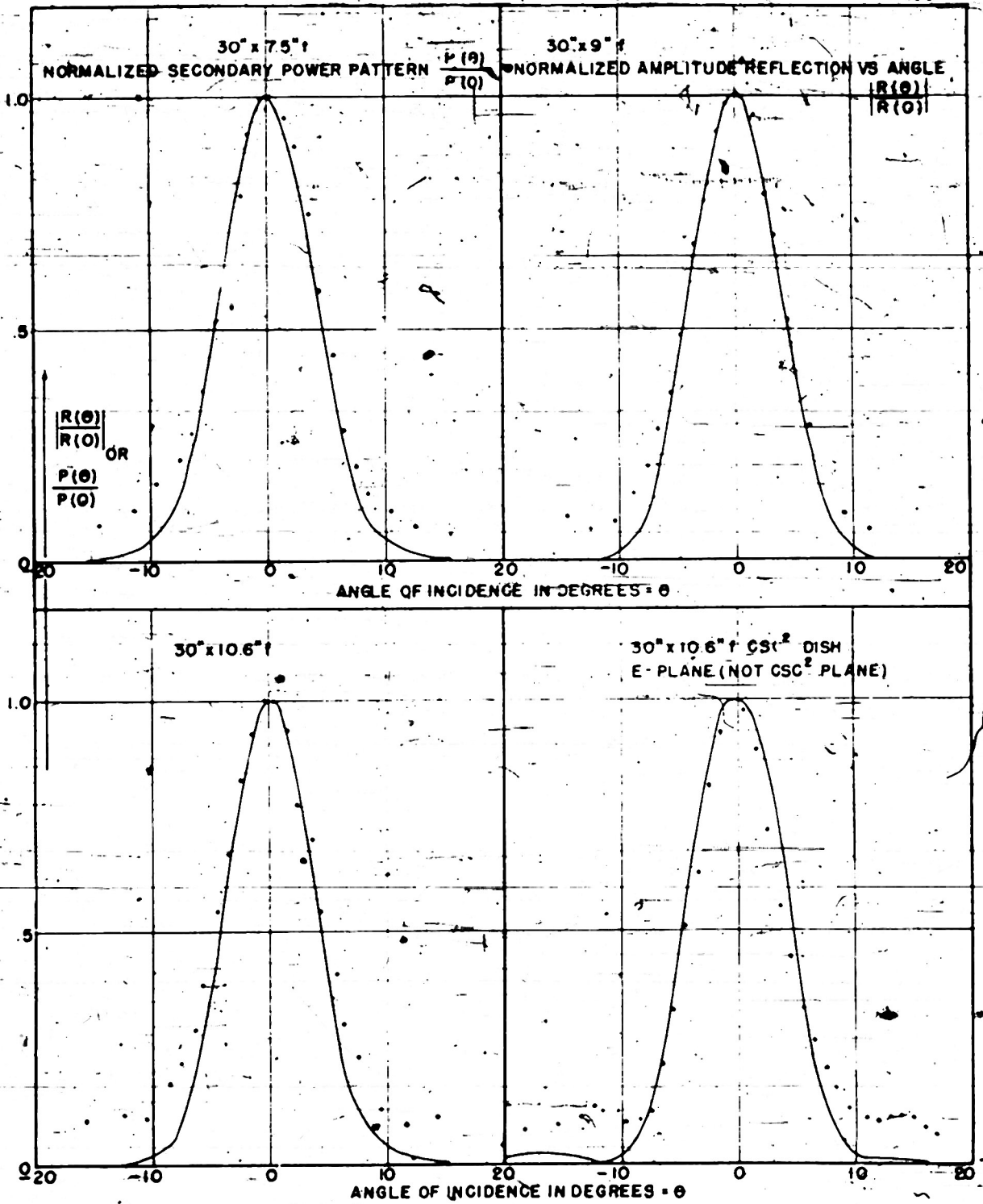


FIG. 53--SAME FOR DIFFERENT ANTENNA SHAPES

483-18

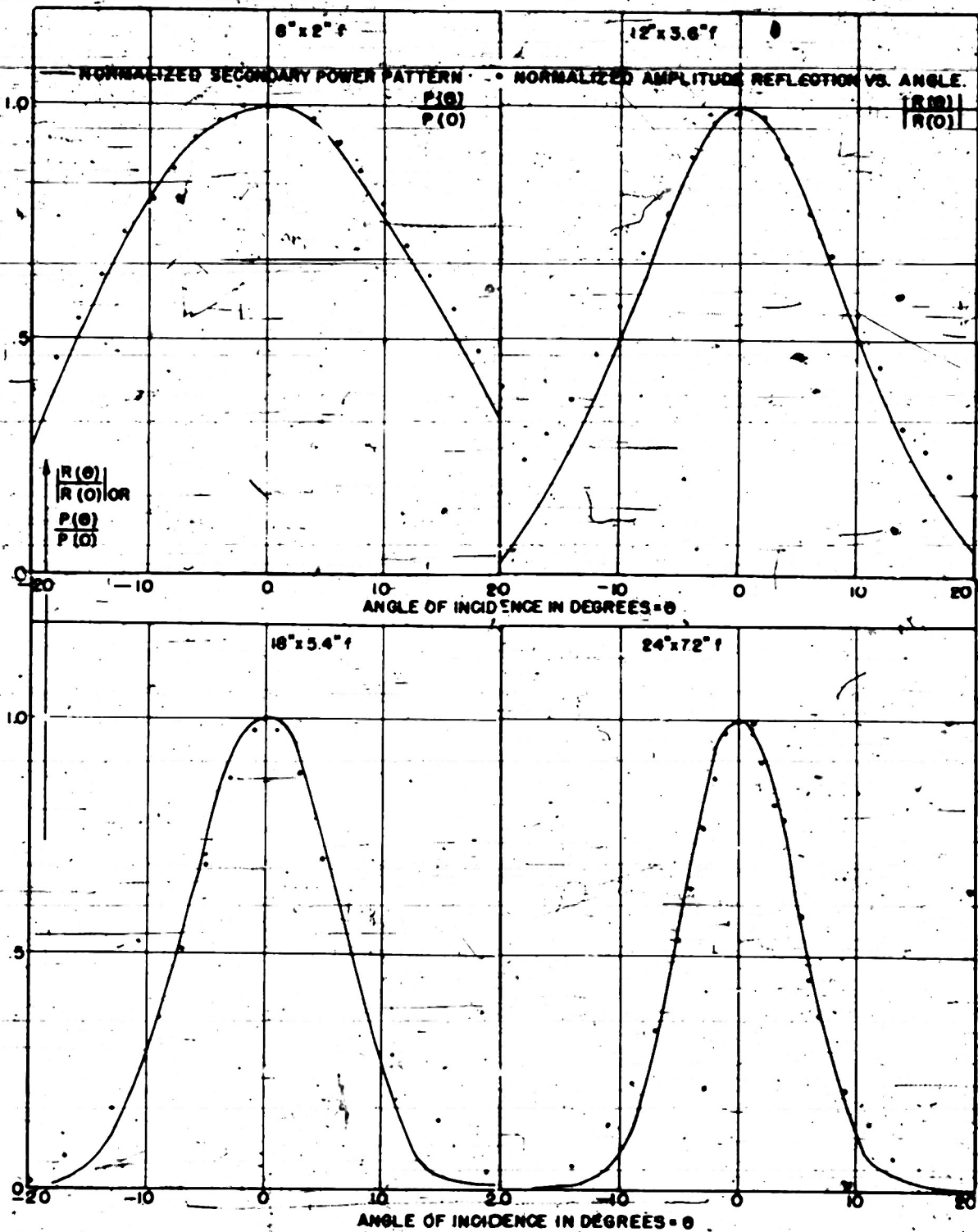


FIG. 52-COMPARISON OF AMPLITUDE REFLECTION VERSUS ANGLE WITH SECONDARY POWER PATTERN FOR SEVERAL ANTENNA SIZES

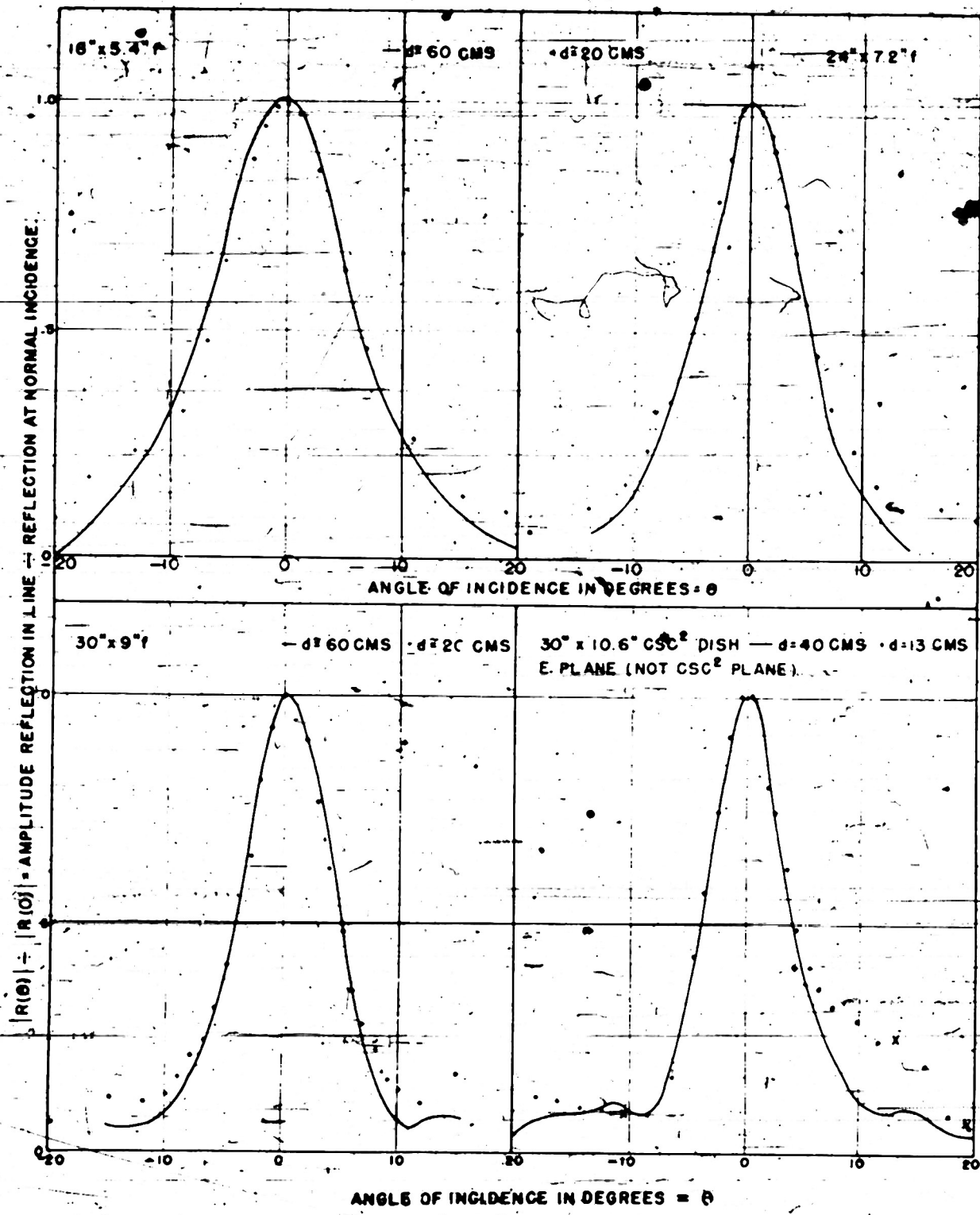


FIG. 51--VERIFICATION THAT REFLECTION VERSUS ANGLE IS INDEPENDENT OF DISTANCE IN THE FRESNEL REGION

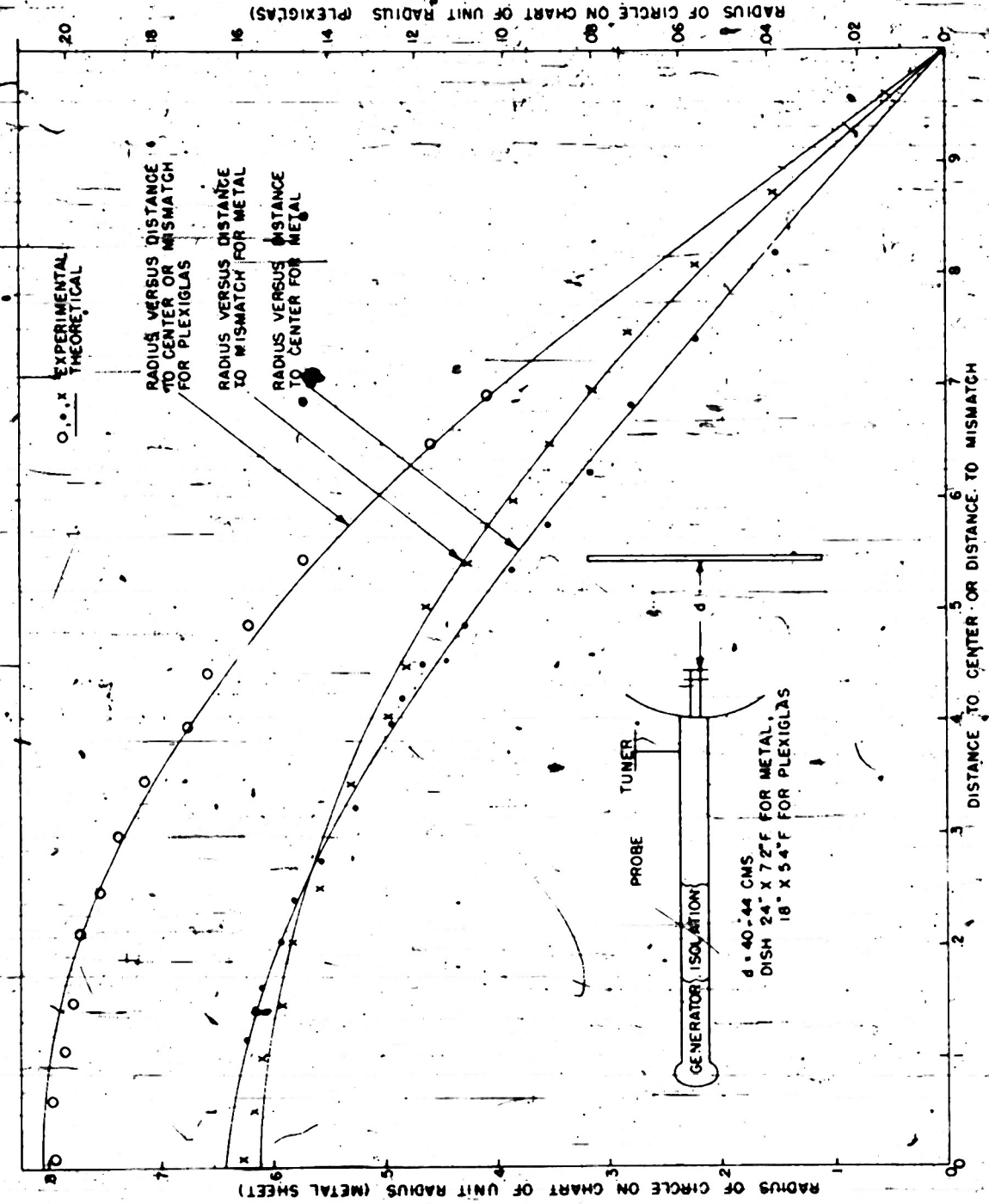


FIG. 50--EXPERIMENTAL CURVES OF RADIUS VERSUS DISTANCE TO CENTER OR MISMATCH FOR METAL AND DIELECTRIC SHEETS

INITIAL RADIUS OF  
CIRCLE (MATCHED LINE)

RADIUS OF CHART

Q31

EDGE OF CHART - (SWR = 00 CIRCLE)

Q32

Q33

Q34

Q35

Q36

Q37

Q38

Q39

Q40

Q41

Q42

Q43

Q44

Q45

Q46

Q47

Q48

Q49

Q50

Q51

Q52

Q53

Q54

Q55

Q56

Q57

Q58

Q59

Q60

Q61

Q62

Q63

Q64

Q65

Q66

Q67

Q68

Q69

Q70

Q71

Q72

Q73

Q74

Q75

Q76

Q77

Q78

Q79

Q80

Q81

Q82

Q83

Q84

Q85

Q86

Q87

Q88

Q89

Q90

Q91

Q92

Q93

Q94

Q95

Q96

Q97

Q98

Q99

Q100

Q101

Q102

Q103

Q104

Q105

Q106

Q107

Q108

Q109

Q110

Q111

Q112

Q113

Q114

Q115

Q116

Q117

Q118

Q119

Q120

Q121

Q122

Q123

Q124

Q125

Q126

Q127

Q128

Q129

Q130

Q131

Q132

Q133

Q134

Q135

Q136

Q137

Q138

Q139

Q140

Q141

Q142

Q143

Q144

Q145

Q146

Q147

Q148

Q149

Q150

Q151

Q152

Q153

Q154

Q155

Q156

Q157

Q158

Q159

Q160

Q161

Q162

Q163

Q164

Q165

Q166

Q167

Q168

Q169

Q170

Q171

Q172

Q173

Q174

Q175

Q176

Q177

Q178

Q179

Q180

Q181

Q182

Q183

Q184

Q185

Q186

Q187

Q188

Q189

Q190

Q191

Q192

Q193

Q194

Q195

Q196

Q197

Q198

Q199

Q200

483-18

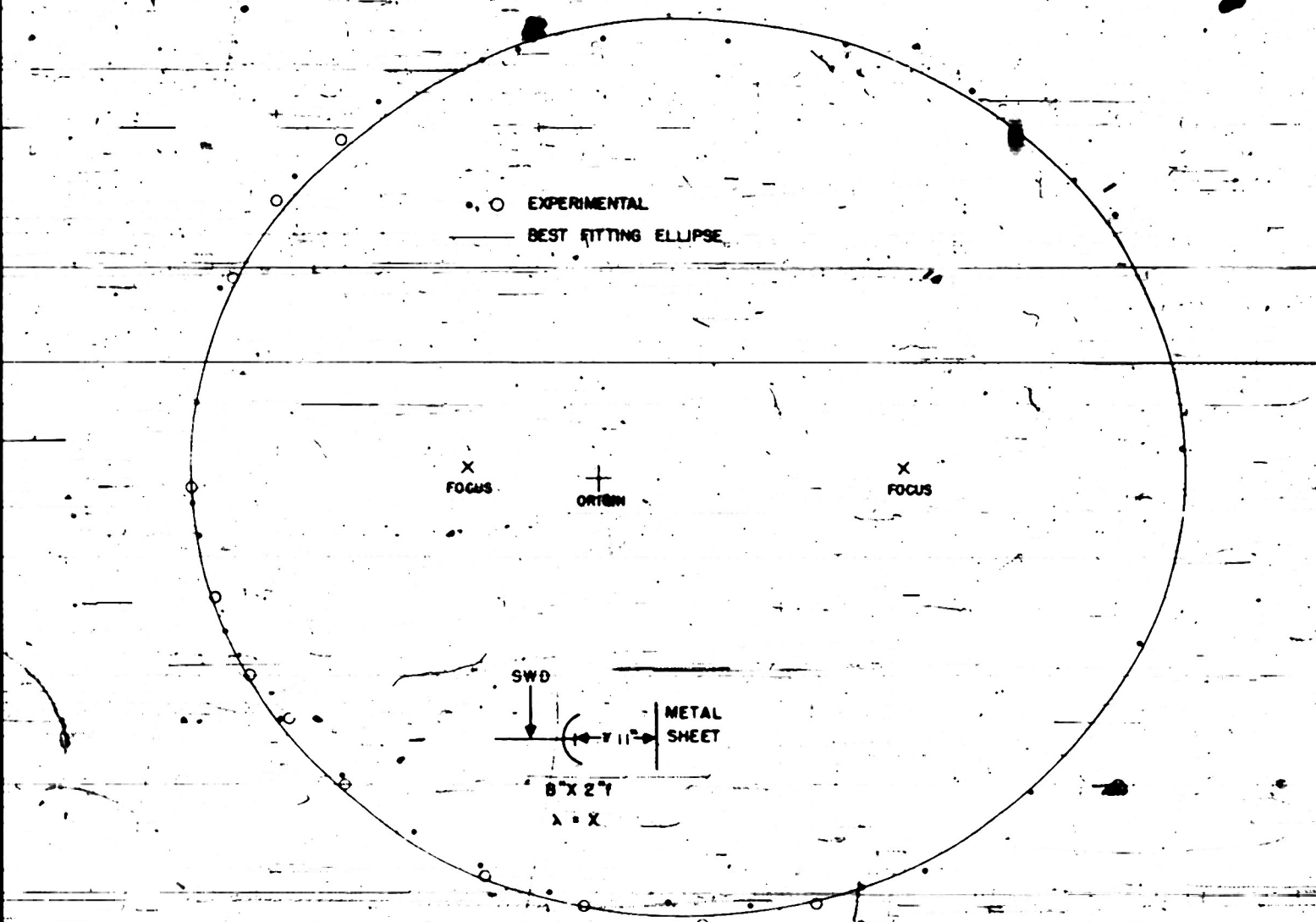


FIG. 48--EXAMPLE OF COMPLEX REFLECTION CURVE OBTAINED WITH A METAL SHEET  
AT X-BAND

● EXPERIMENTAL POINTS  
◆ REPEAT  
X CENTERS OF CIRCLES  
▲ INITIAL MISMATCHES

THEORETICAL CIRCLE  
THROUGH MISMATCHES

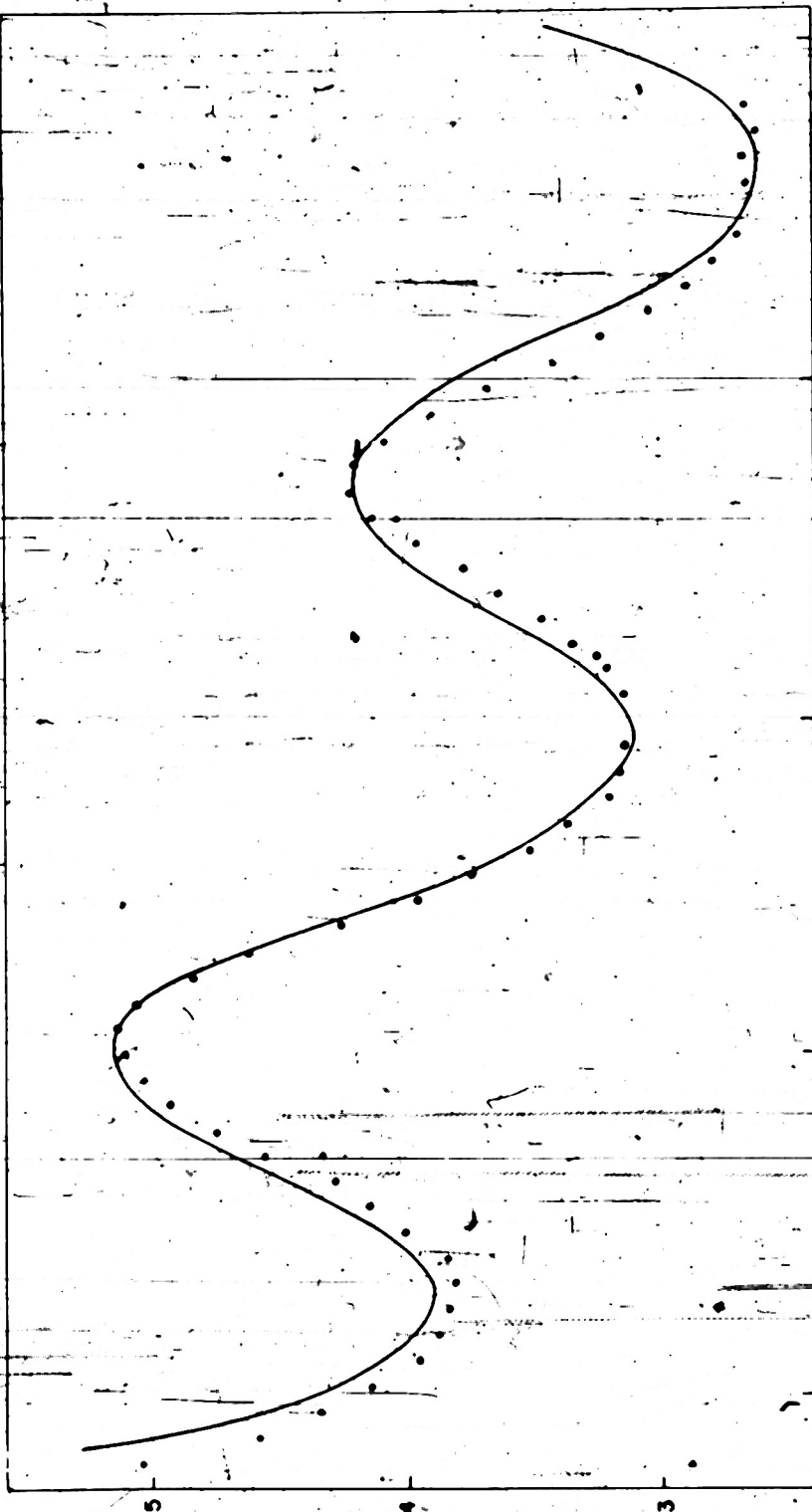
0.1 MM ERROR

0.15 MM ERROR

THEORETICAL ELLIPSE  
THROUGH CENTERS

0.1 MM ERROR

FIG. 47--COMPLEX REFLECTION AS A FUNCTION OF DISTANCE FOR VARIOUS MISMATCHES



$|C|$  = AMPLITUDE REFLECTION IN LINE

FIG. 46 - REFLECTION VERSUS DISTANCE IN FRAUNHOFER REGION, SHOWING DETAILED COMPARISON WITH THEORY

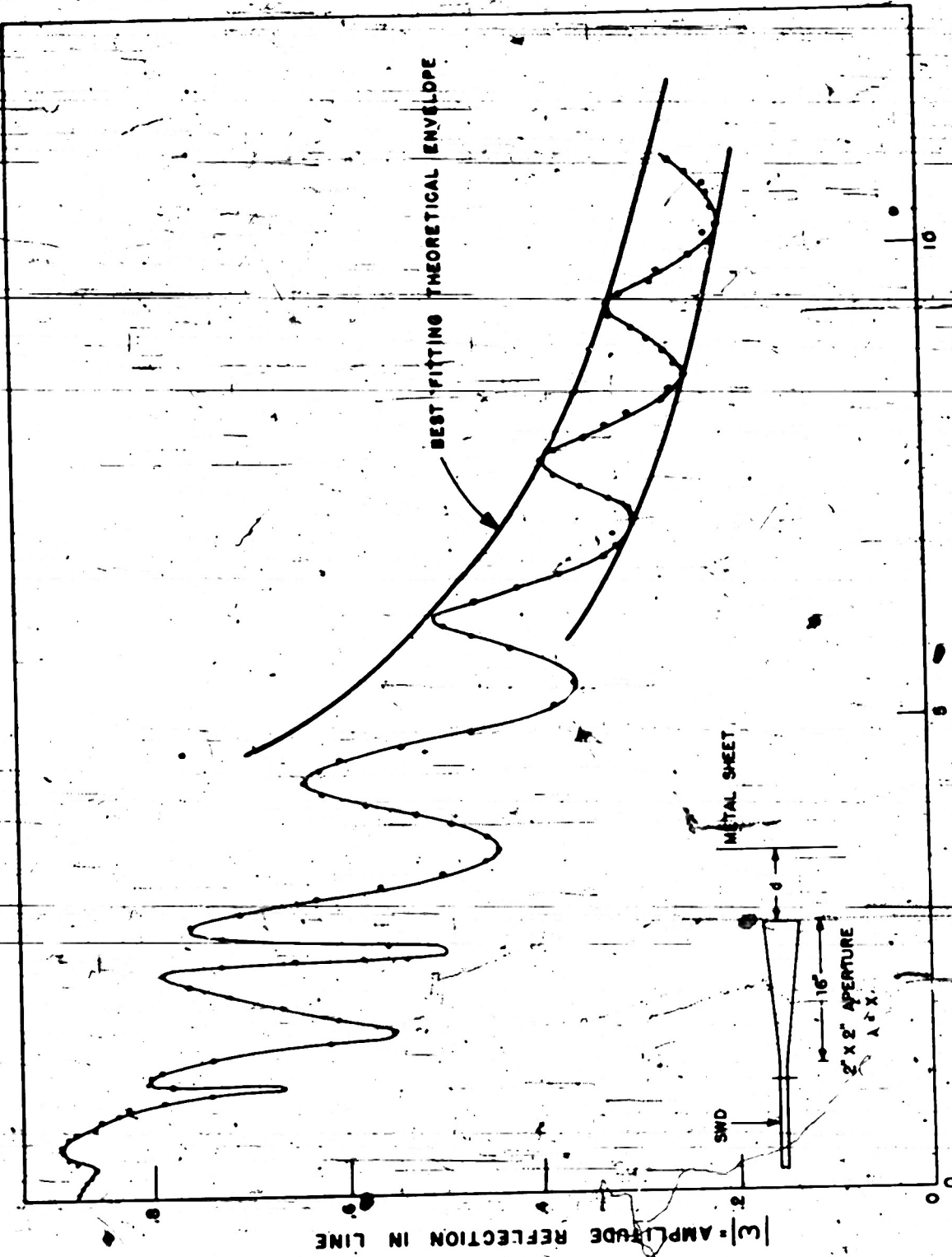


FIG. 45 - SAME F.T. HORN

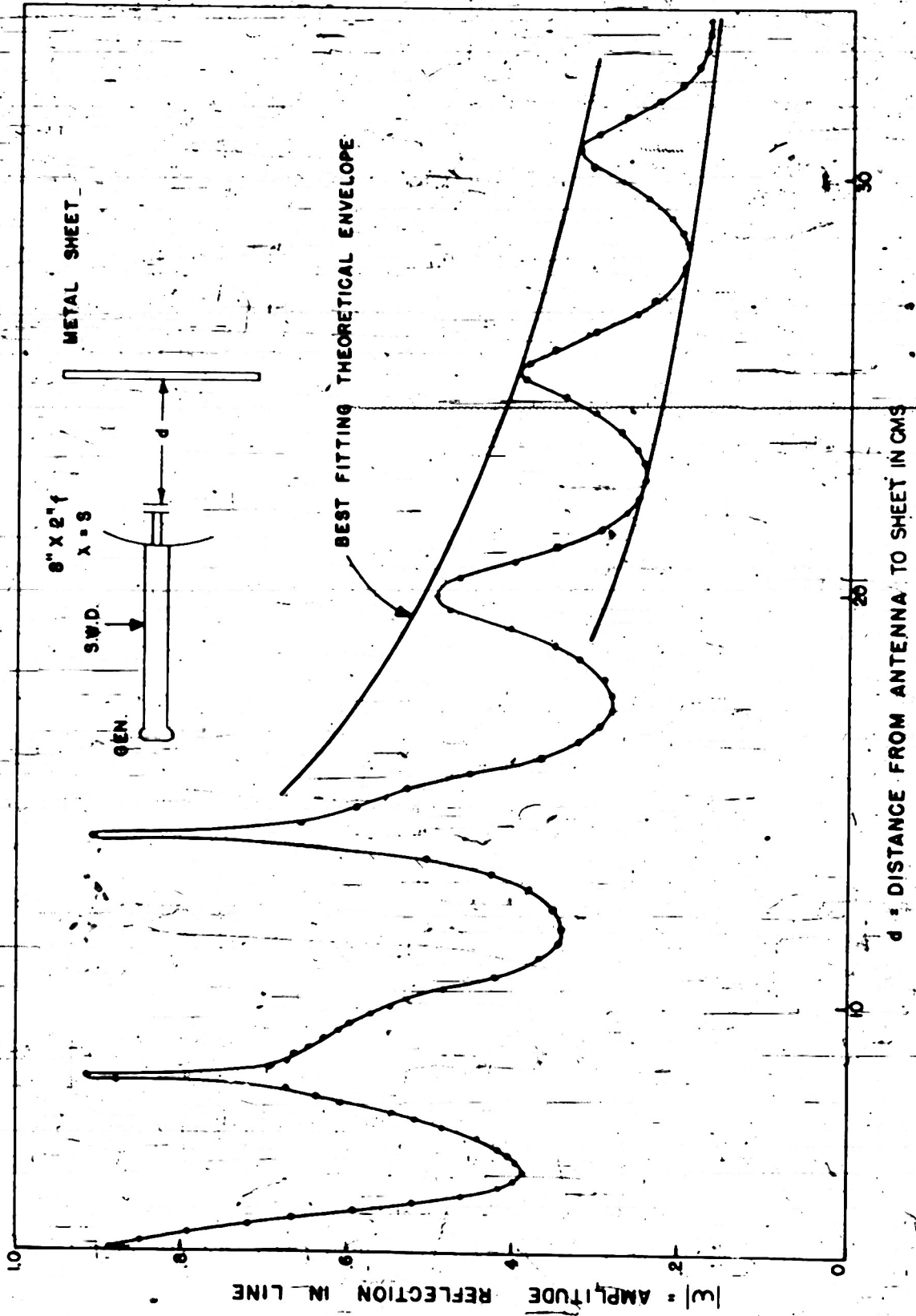


FIG. 44 - REFLECTION VERSUS DISTANCE FOR PARABOLOID / $\lambda$ / BAND, SHOWING TRANSITION FROM FRESNEL TO FRAUNHOFER REGION

483-18

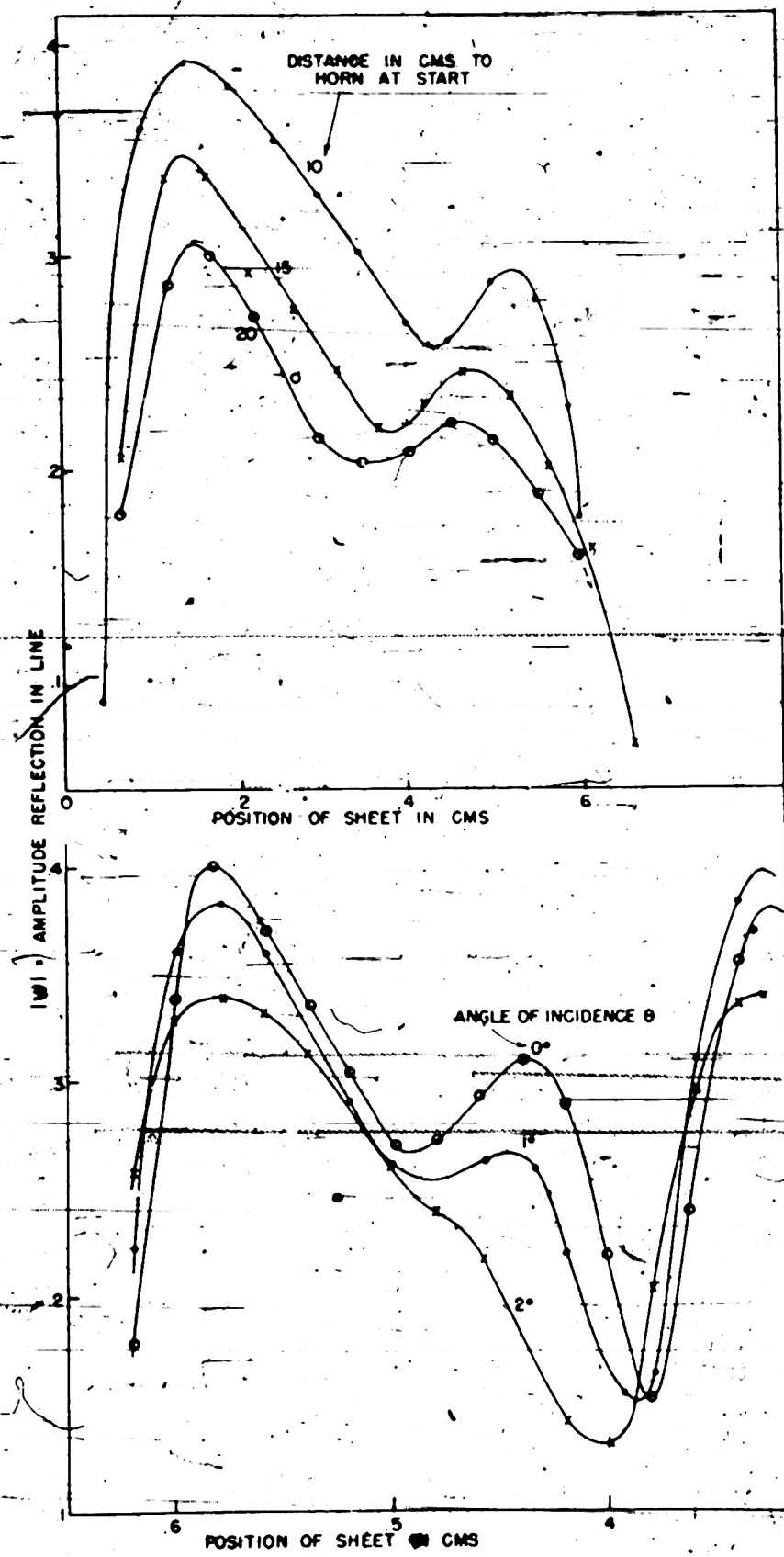


FIG. 43.—RELATIVE IMPORTANCE OF DISTANCE AND ANGLE IN DETERMINING  
CURVE SHAPE FOR REFLECTION OF METAL SHEET AT K-BAND

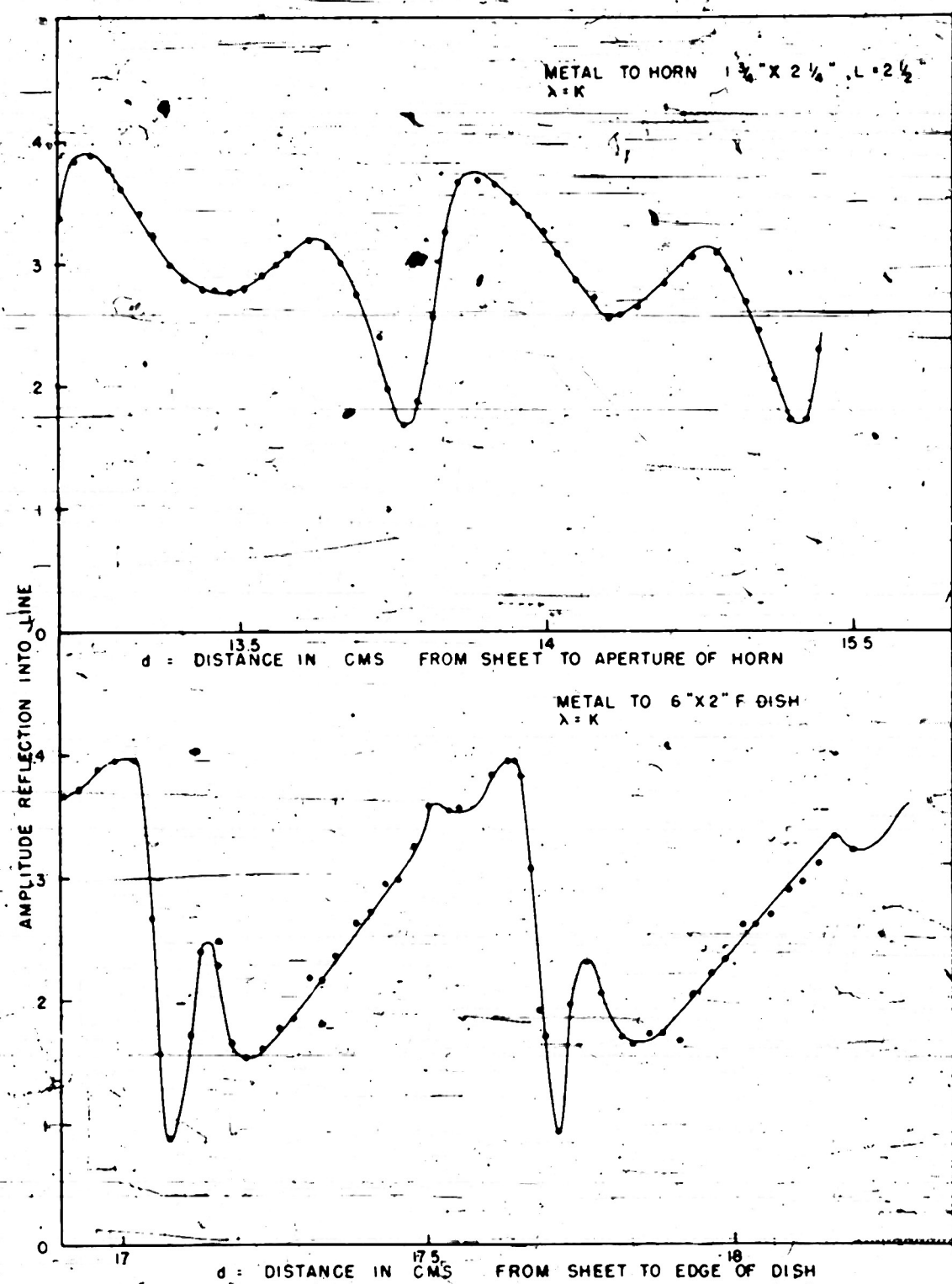


FIG. 42--SAME AT K-BAND

483-18

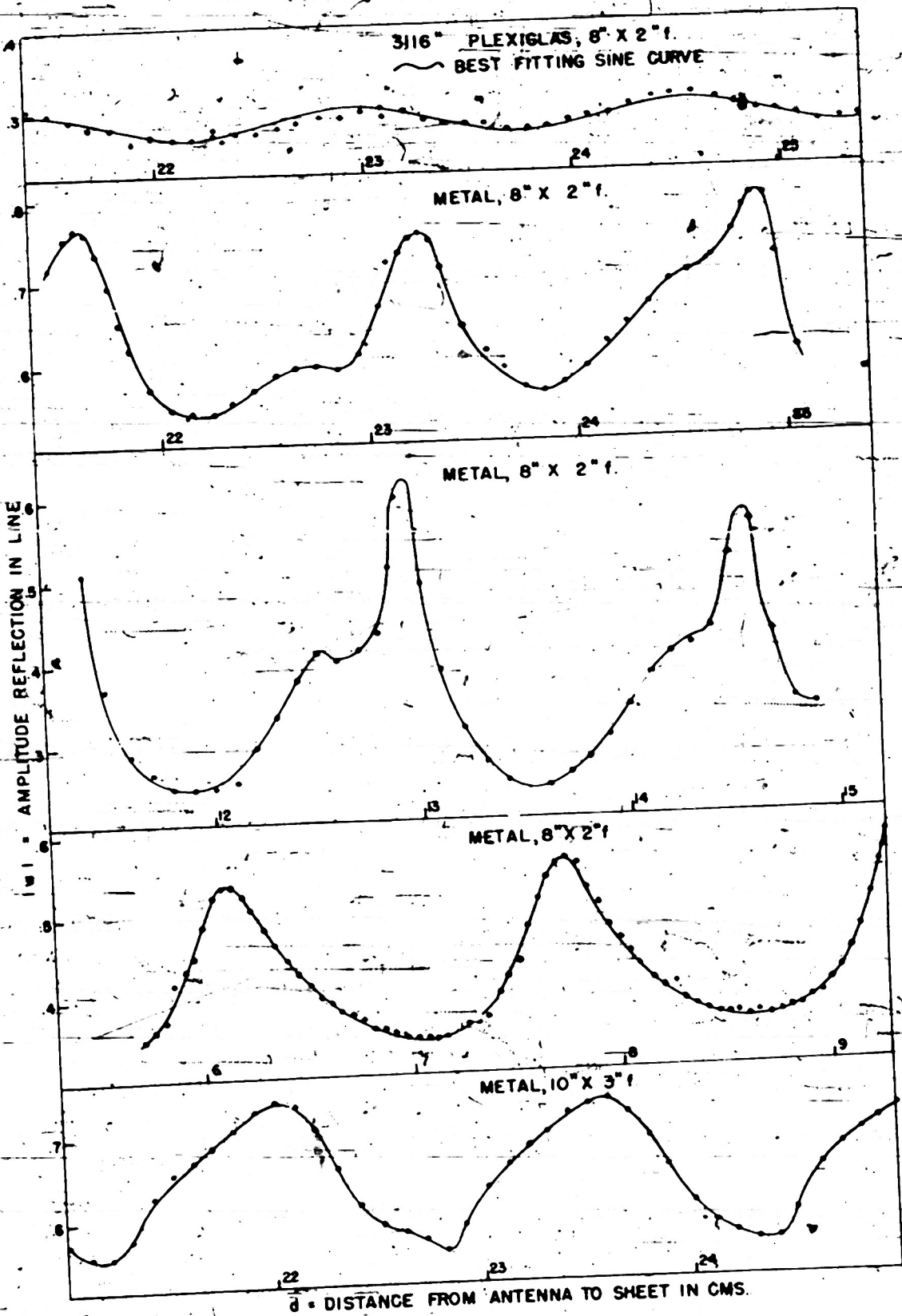
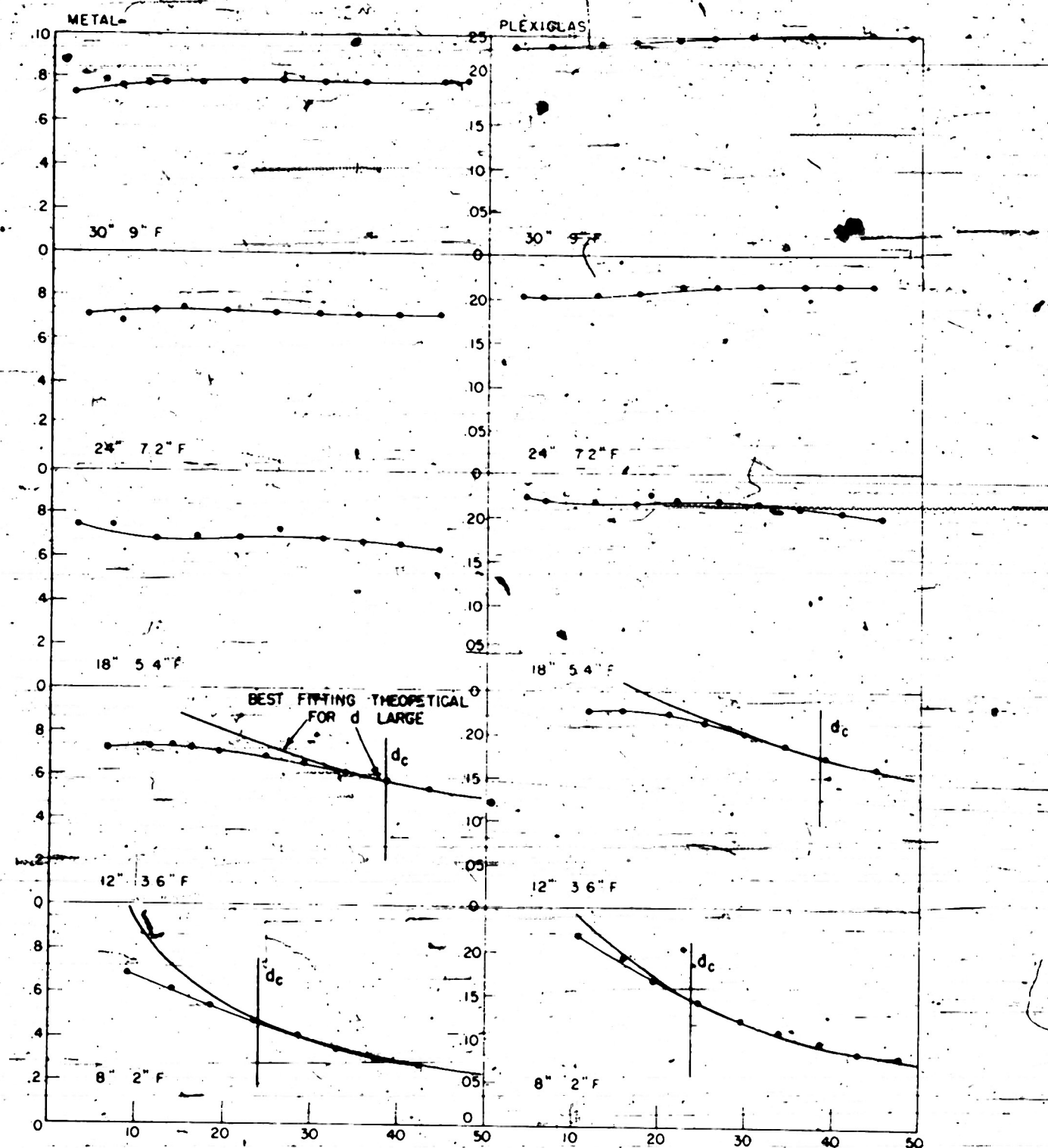


FIG. 41 REFLECTION VERSUS DISTANCE AT X-BAND, SHOWING ANOMALOUS EFFECTS WITH METAL SHEET



d : DISTANCE IN CMS FROM ANTENNA TO SHEET

G. 40 - REFLECTION VERSUS DISTANCE AT S-BAND, CONDENSED BY PLOTTING AVERAGE VALUE FOR 10-CM. INTERVALS

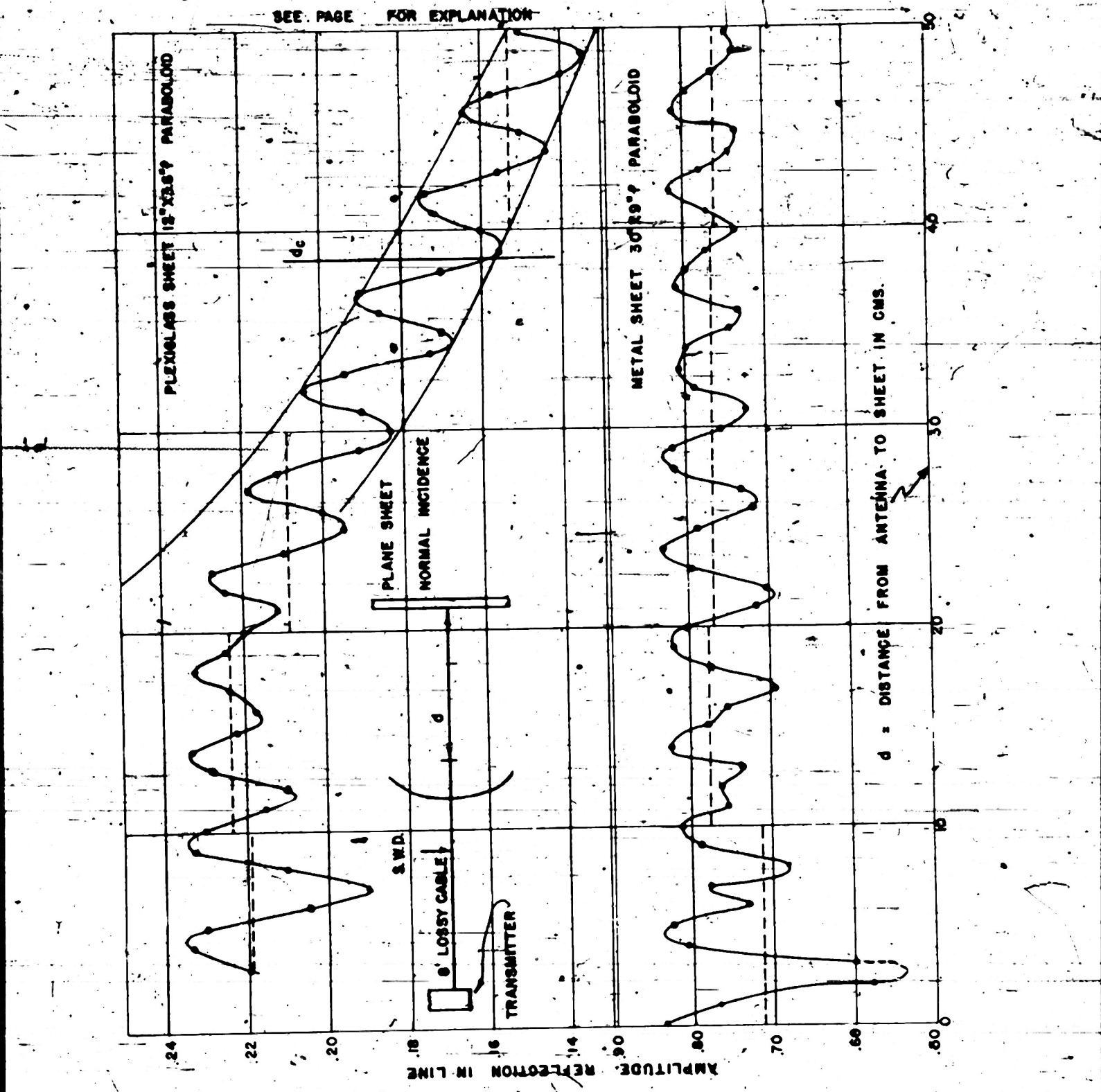


FIG. 39--TYPICAL CURVES OF REFLECTION VERSUS DISTANCE AT S-BAND

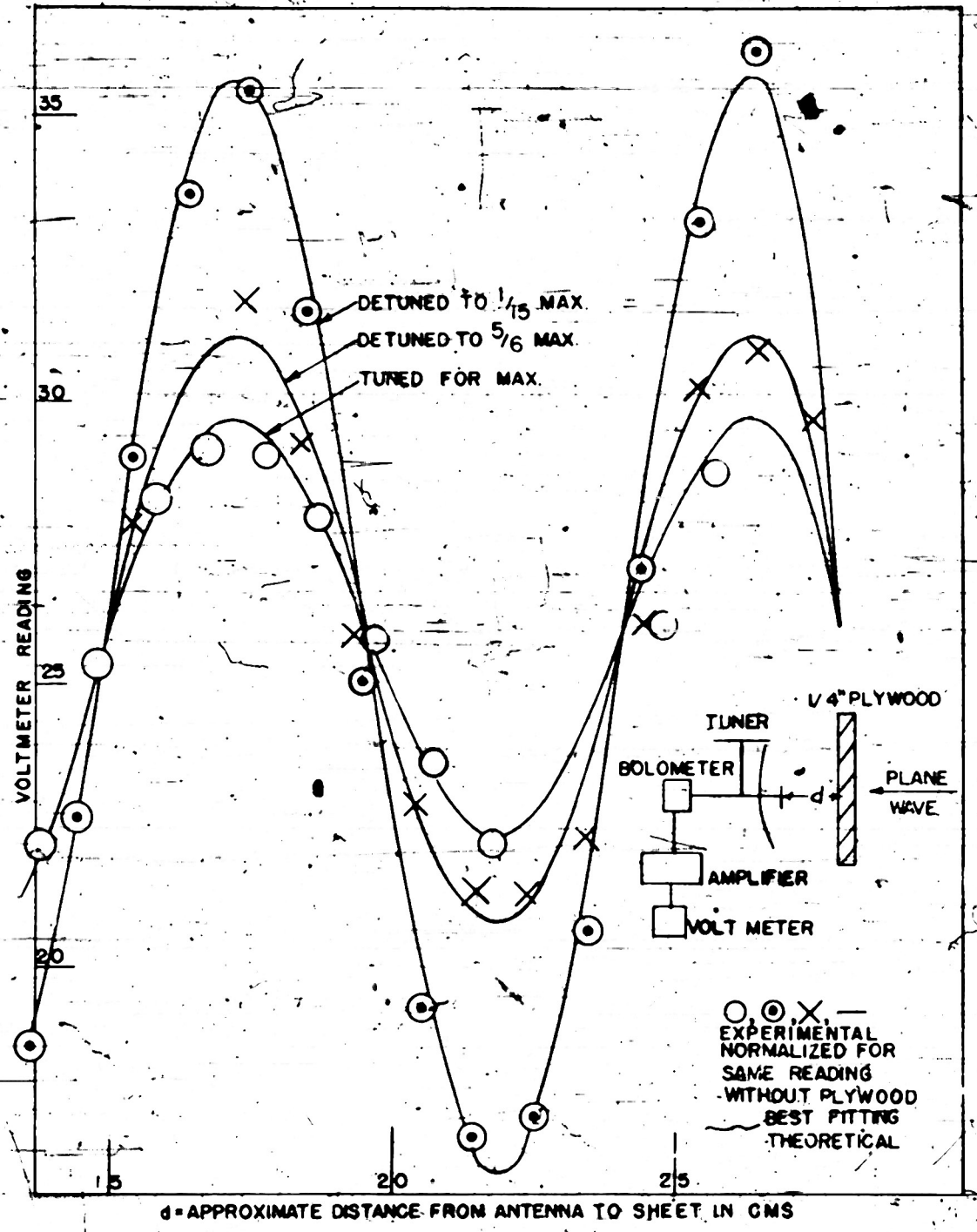


FIG. 38--TRANSMISSION AS A FUNCTION OF DISTANCE FOR VARIOUS MISMATCHES

Acknowledgment

The data of Fig. 33 were taken by S. J. Mason and C. G. Lincoln; that of 34 is due to Lincoln. The author is indebted to Steele, Winkler and Lincoln for the data of Fig. 41; to Winkler for that of 42, 43, 91. The author wishes to thank J. Ellis for his assistance in the theory and graphs for elliptical polarization, for the data of Figs. 45, 46, 48, 56, part of 65 and for help in proofreading the text. The data for Figs. 44, 86, 87 were obtained by Steele, who also supplied Fig. 80 in cooperation with T. J. Keary. The bottom curves of Fig. 88 were computed by Y. N. Cowker; the data were taken by Ellis. The author is indebted to M. Furey for the data of Figs. 78, 89, 90, and to B. Luz, M. Furey and M. Hegarty for much of the work of computation. The inked drawings were supplied by the NC Drafting Department.

R. H. Redheffer  
December 10, 1943

Bibliography

1. Redheffer, R.M.-----Radomes and Systems Performance,  
Report 483-6, November 17, 1944.
2. Redheffer, R. M.-----Electrical Properties of Double Wall  
and Sandwich Radomes, Report 483-11,  
February 1, 1945.
3. Redheffer, R. M.-----Transmission and Reflection of Parallel  
Plane Sheets, Report 483-12, January 26,  
1945.
4. Hegarty, M., Dowker, Y. -----Current Progress on RF Research,  
Redheffer, R.M.,  
Winkler, E. D.  
Report 483-17, May 10, 1945.
5. Redheffer, R.M.-----The Measurement of Dielectric Constants  
in the One Centimeter Band, Report 483-15,  
Winkler, E. D.  
May 11, 1945.
6. Mason, S. J.-----45° Microwave Reflector. Report 54-19,  
November 19, 1943.
7. Redheffer, R. M.-----An Investigation of RF Probes,  
Report 483-14.
8. Spencer, R. C.-----Paraboloid Diffraction Patterns from  
Standpoint of Physical Optics,  
Report 17, October 21, 1942.
9. Redheffer, R. M.-----Transmission and Reflection of Single  
Plane Sheets, Report 483-4, July 12, 1944.
10. Mason, S. J.-----General Design Procedure for Pencil-Beam  
Paraboloid Antennas, Report 690,  
December 1945.
11. Redheffer, R.M.-----Measurement of Small Reflections,  
Report 483-10, February 6, 1945.
12. Dowker, Yael-----Transmission of Lossy Sandwiches,  
Report 483-22, November 30, 1945.
13. Redheffer, R.M.-----Elliptical Polarization, Report 483-13,  
February 12, 1945.

by

$T_1$  = power transmission with polarization perpendicular to the plane of incidence

$T_{||}$  = power transmission with polarization parallel to the plane of incidence

$\psi$  = angle between actual polarization and perpendicular polarization

$P$  = received power with sheet in place

$P_0$  = received power without sheet in place

$\delta$  = difference in phase for transmission parallel and perpendicular to plane of incidence,  
 $\delta = T_{||} - T_1$ .

W. Ellis has shown that (73), as a function of  $\psi$ , will have an extreme at points other than  $0, \pi/2$  if and only if

$$K > \cos \delta \Rightarrow 2 \cos \delta - 1/K \quad (74)$$

in which case the intermediate value is found to be (see Fig. 97)

$$\frac{P}{P_0 T_{||}} = \frac{k^2 \sin^2 \delta}{1 - 2k \cos \delta + k^2} \quad (75)$$

For almost all work with radomes, then, it suffices to measure transmission with polarization perpendicular and parallel to the plane of incidence only; and intermediate polarizations will give intermediate values for the transmission. In the few cases for which this is not the case, the result may be obtained from the curves of Figs. 93-96 or it may be measured experimentally. We note, incidentally, that the graphs of Figs. 93-97 cover the entire range of physically possible values of the variables, because of the symmetry of the equation. Thus, if  $k > 1$ , the solution may be obtained by interchanging  $T_{||}$  and  $T_1$  wherever they occur, and using  $90^\circ - \psi$  in place of  $\psi$ .

angle of polarization, when an elliptically polarized wave is incident on an ordinary linearly polarized antenna, will be an ellipse similar to the one in the incident wave. This latter result and the methods used to derive it are of particular interest in the present discussion, and the experimental verification presented in Ref. 13 is therefore repeated here (Fig. 92). Unfortunately, the precise problem encountered in transmission measurement was not investigated in Ref. 13, and we present a brief summary of the results in the present report. In the situation of Fig. 37, the two dipoles are always parallel to each other, as is usual in transmission measurements, but each one makes an angle  $\psi$  with the normal to the plane of incidence of the dielectric sample. The question is to find, first, the manner in which the received power will depend on  $\psi$ , and second, to find the condition that the result for intermediate values of  $\psi$  shall be between the values obtained when  $\psi = 0$  or  $\pi/2$ . This latter inquiry gives the conditions under which a measurement of transmission with parallel and perpendicular polarizations will suffice, without intermediate values.

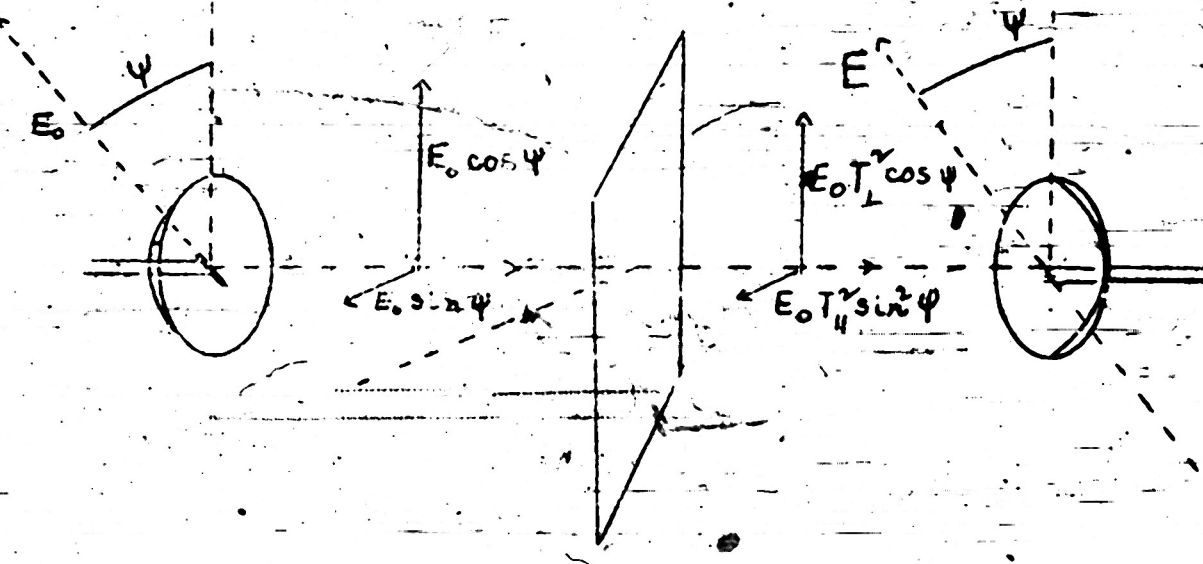


Fig. 37. Variables for Elliptical Polarization

By the method used in Ref. 13 one readily obtains

$$\frac{P}{P_0} = T_1^2 \cos^2 \psi + 2T_1 T_{\parallel} \cos^2 \psi \sin^2 \psi \cos \delta + T_{\parallel}^2 \sin^2 \psi \quad (73)$$

which is plotted in Figs. 93-96. In the equations, the variables are defined

Independent measurement of all parameters, and the loss tangents of both skin and core were included in the calculation, which was made by Y. N. Dowker, using the procedure of Ref. 12. For the plywood curves it was considered best to determine the constants for optimum fit, as the material is of rather non-uniform composition and cannot be accurately evaluated on the basis of a small sample. Thus, in the upper curve of Fig. 88 both  $\epsilon/\epsilon_0$  and  $\tan\delta$  are adjusted to give the best fit, and the value of  $\tan\delta$  so obtained was used in all other curves involving plywood. For the lower curves the reflection of the particular sheets used had been measured and was found to give a dielectric constant of 2.5 rather than the value 2 found as an average for all the sheets of the upper curve. Thus  $\tan\delta$  is the same on all curves involving plywood; the dielectric constant is the same for the two sheets used in Figs. 88, 91, but different for the group of sheets at the top of Fig. 88. The agreement is again within a few per cent in all cases. Proceeding now to reflection-measurement, we note from the curves of Fig. 99 that there is quite good agreement in amplitude, though the base measurement, made as described above, is not particularly accurate. The theoretical curves in this case were computed from independent measurement of the parameters, with no attempt to 'fit' the data. In Fig. 90 we give a curve of reflection versus core thickness for a sandwich and a curve of reflection versus spacing of two sheets. As before, the theoretical curves were obtained independently of the experiment, and as before the agreement is good enough for most applications. A final example is given in Fig. 91, where the method of Fig. 36 is used to obtain reflection versus spacing at arbitrary incidence, while that of Fig. 3C is used to obtain reflection versus spacing at K-band. In the case of the plywood the dielectric constant was adjusted for optimum fit, this time with being used, however, in the curves for transmission. In the case of the K-band curve, the anomalous effect obtained with the metal sheet introduced a fairly large error (about 10%), and the curve was therefore normalized to the reflection at the peak. A good fit is again obtained, if we take account of the difficulty of maintaining the spacing with accuracy, and hence the reflection is linearly proportional to the reflection coefficient for all values not too near unity. We remark in passing that an error of 0.01" in spacing may lead to a vertical deviation of about an inch in these curves, so that the experimental difficulties are not all contained in the microwave measurement procedure. Similar consideration accounts for much of the error in the upper curves, it is believed; for although the wavelength is longer, there is an added error in that the spacing was done with screws in this case while large brass rings were used on spacers in the K-band curves. On the whole, however, it is believed that the data of Figs. 88-91 plus that of Tables II, III would indicate that transmission and reflection coefficients may be accurately measured in free space, and that the method is both consistent and reliable when properly used.

It has been assumed hitherto that the polarization is either in the plane of incidence or perpendicular to it. When this is not the case the transmitted wave is elliptically polarized, in general, a phenomena which was briefly considered in Ref. 13. It was there shown that the sum of the squares of the axes in the ellipse represents the power in the wave, and that a plot of the reciprocal of the received amplitude versus the

Table II - Reflection Coefficient of Plexiglas as  
Measured in Free Space at S-Band

Antenna Dimensions	Distance in cms.					Average Deviation for that Antenna from Theoretical
	0-10	10-20	20-30	30-40	40-50	
8"x2 "f	0.334	0.329	0.320	0.325	0.340	0.330 +2.5%
12"x3.6"f	.306	.321	.301	.320	.311	.316 -1.5
18"x5.4"f	.309	.326	.327	.321	.326	.322 +0.1
24"x7.2"f	.294	.304	.324	.330	.328	.316 -1.7
30"x9 "f	.333	.312	.320	.324	.328	.324 +0.7
Overall av.	---	---	---	---	---	.3215 +0.8
Same with omissions	---	---	---	---	---	.3220 +0.9
Av. deviation for all 25 measurements	---	---	---	---	---	---
Same with omissions	---	---	---	---	---	+1.3
	---	---	---	---	---	+0.5

To have a second check, this time for transmission, we compare the results obtained on actual radomes by the method of Fig. 36 b with those obtained by the method of Fig. 36 a.

Table III - Transmission of SO-11 Radomes by Two Methods

Radome Number	Transmission by Method of Fig. 36a	Transmission by Method of Fig. 36 b
Radome Number		
1	0.77	0.76
2	.93	.91
3	.91	.95
4	.93	.92
5	.92	.94
6	.81	.78
7	.92	.94
8	.87	.89

Maximum error = 4.3%; average error = 2.4%

As a third check on the reliability of the free space methods we present the data of Figs. 87-89, in which theoretical curves of reflection versus various parameters are compared with the experimental values. The transmission curves of Figs. 86, 87 are computed from independent measurement of the dielectric constant and thickness of the dielectric sheet, and the agreement is sufficiently good for most practical applications. Similarly, the theoretical curves for the sandwich at the bottom of Fig. 88 was also computed from

errors on reflection measurement, though the limit is considerably lower than is the case for transmission (see Fig. 73). Besides this error and that due to initial mismatch, considerable inaccuracy may be introduced by a failure to have the sample perpendicular to the electrical axis of the antenna. A rather detailed investigation of the dependence on angle was given in Part III above; for our present purposes it suffices to note that the error can be estimated from the secondary pattern of the antenna, and decreases with antenna size. In practice, the angle is adjusted by giving a value to  $d$  which maximizes the reflection, and then adjusting  $\theta$  to maximize this maximum. Another source of error is introduced by the necessity of measuring a metal sheet, which has been seen to introduce certain anomalous effects. In practice, this difficulty is found only at the shorter wavelengths, and may be avoided by using a standard sample of known reflection coefficient in place of the metal sheet. As usual, the reflection in the line for each sheet is proportional to its free space reflection coefficient, so that the unknown reflection is readily obtained from an experiment of this type. The errors in Fig. 36b are similar to those just described, as are those in Fig. 36d, where there is an added difficulty, however, from direct reception between the two antennas.

Perhaps the most obvious method of checking the accuracy of the procedures described is to compare theoretical with measured coefficients, a comparison which is in fact made, by measuring a 'standard' sheet of known reflection, at the beginning and end of all Radiation Laboratory production tests. For more systematic investigation, the dielectric constant of a sheet of plexiglas was measured accurately, and the reflection coefficient computed by the usual methods. The thickness was chosen near a quarter wave, since the derivative of reflection with respect to thickness is zero for that value; and thus, small variations in thickness would introduce negligible error. Next, complete curves of reflection versus distance of the type shown in Fig. 39 were obtained for the plexiglas sheet and for a metal sheet with five different antennas, the variation being fifty centimeters in steps of one centimeter. The average value of each curve was then found, by integration with a planimeter, for the ranges  $d = 0-10$  cms.,  $d = 10-20$  cms., etc., whereupon the average for a given interval and a given antenna with the dielectric was divided by that obtained with the metal sheet, and the result taken as the reflection coefficient. Thus, each entry in the following table involves twenty separate measurements of reflection, and ought to give an accurate result if no systematic errors are inherent in the method. Values omitted were those in the 0-10 cm. range, for which there are anomalous effects with the metal sheet, and two of the 40-50 cm. values, for which the reflection in the line was too small to be accurately measured. From the table it appears that the method is sufficiently accurate for most applications, and in particular that it is as accurate as conventional measurement in guide.

In Fig. 36 b is given a method that is sometimes helpful as a check for internal consistency, and to verify that two-way transmission may be obtained from one-way measurements only. The procedure is to measure the reflection of the metal sheet alone, then of sheet and sample, with due care that the sample shall not be curved, or at an angle, so that multiple reflections between sample and sheet may be neglected. Except as a test of the theory, or as a temporary method for carrying out measurements in limited space, the procedure of Fig. 36 b is of course inferior to that of 36 a.

A method for obtaining reflection at incidence other than normal is illustrated in Fig. 36 d, in which we adjust all variables for maximum received power, first with a metal sheet and then with the sample, and take the ratio of the two results to be the power reflection coefficient. Phase measurement for transmission is described in Ref. 5; for reflection one can obtain approximate results by comparing the minimum position when the metal sheet is in place with that found for the sample in the same position.

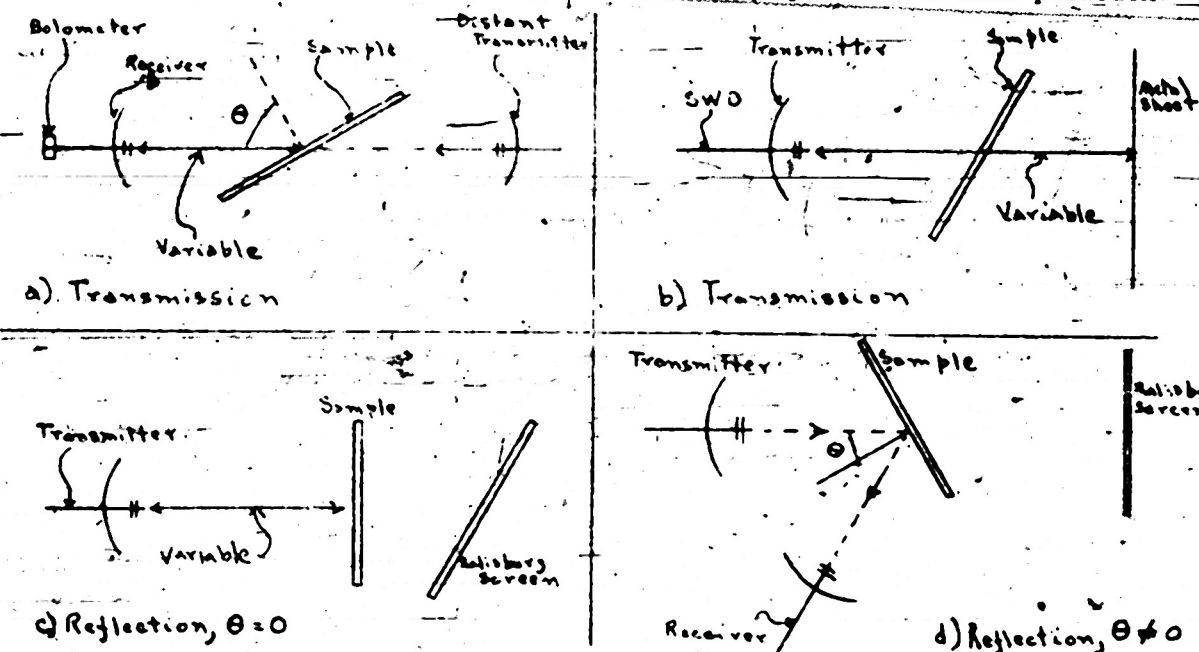


Fig. 36 Equipment for Measurement in Free Space

The sources of error are likewise evident from the foregoing discussion; for transmission, the transmitter must be sufficiently steady or else monitored, and the sample must be large enough to obviate diffraction around its edges. This last effect, in particular, can introduce large errors; transmissions as large as 300% have been observed with samples of suitable size and location. The theory, which is the conventional Fresnel theory of physical optics, need not be repeated here; in practice, the proper size is readily found by exploring the beam with a metal strip. Similarly, too small a size introduces

problem of matching the loads; for example, nor is there any effect analogous to the error introduced by a difference in probe depth for transmission. Still another difficulty is that, for the multiple layer radomes so frequently used, very little information is obtained by the guide measurement; e.g., the manufacturing error in wall spacing for double wall samples cannot be investigated at all, while for sandwiches, the preparation of the sample often causes the skins to peal away from the core or otherwise alter the sandwich dimensions. Similar improvement in accuracy is also found for measurement of the phase on transmission, as we see by Ref. 5.

The general tenor of the above comments is that free space measurement leads to results more accurate, for radome work, than can be found in guide. Even if this improvement in accuracy were not obtained, however, the free space method would still be desirable in most cases. Thus, because of the difficulty of preparing samples, it is found that complete curve of transmission versus angle requires fifty to one-hundred times as many man-hours, by the wave-guide procedure, as it requires in free space. Because of this consumption of time, this method is prohibitive for production testing, quite apart from its accuracy. The technique to make measurements in free space, then, is not a haphazard choice; on the contrary, we are well aware of the existence and techniques of wave-guide measurements, and we turn to the free space method only because of its demonstrated superiority for the problem at hand.

Methods of free space measurement are suggested in Fig. 36, the procedure for transmission being given in 36 a, b while those for reflection are shown in 36 c, d. From the discussion of Parts II, III above, the experimental manipulations are doubtless apparent; for transmission, one may change  $d$  until both a maximum and minimum are obtained, which values are then substituted in (3). This equation is plotted in Fig. 85, together with a number of other formulas of similar character. The curve labeled 'transmission formula, complete series' is the one in question; the curve labeled 'first two terms of series' represents the result obtained by taking only the first two terms of the geometric series found by the multiple-reflection method of deriving Eq. (1). From the other curves, which are self-explanatory, it is seen that the geometric mean, readily computed on a slide rule, is sufficiently close to Eq. (3) to be used in most practical applications. In fact, if the ratio of maximum to minimum is so large that this approximation is not permissible, the theory itself is of doubtful reliability.

Turning now to reflection, we note that it usually suffices to obtain two measurements with a quarter wave displacement of the sample, as described above, and average the results. The ratio of this average to the corresponding quantity found with the dielectric replaced by a metal sheet is the desired reflection coefficient  $R$ . In case difficulty is experienced in obtaining a sufficiently good match to free space, the procedure of Ref. 11 may be used.

Since the load is never exactly matched, one may reduce the error by taking both maximum and minimum readings for probe #2; but it must be emphasized that the error is not entirely eliminated by this procedure, or indeed by any procedure-alecting phase, and that the load must therefore be matched for transmission measurements as well as for those of reflection.

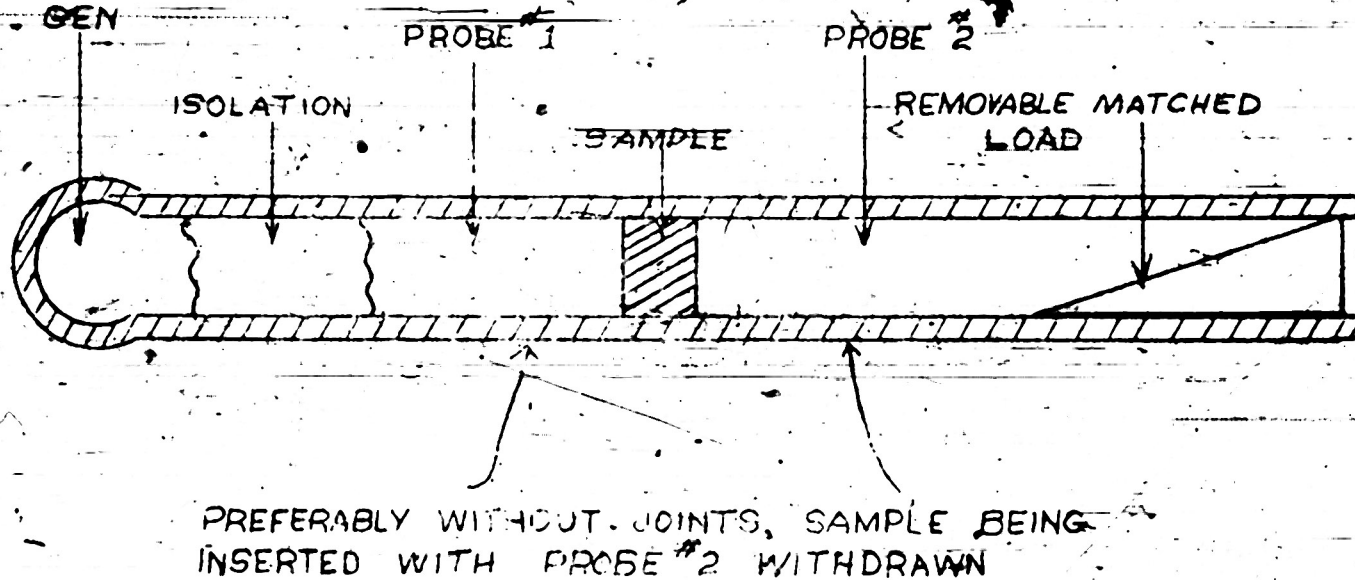


Fig. 35 Measurement of Transmission and Reflection in Guide

In view of the equivalence noted above for measurements in free space in guide, it is relevant to inquire whether free space measurements are necessary at all. This question is particularly natural inasmuch as the theory for guide measurements is exact, and the measurement techniques are standard procedure, while on the contrary the theory for free space measurements is approximate, and the techniques are comparatively little known outside of the few laboratories specializing in radomes. Upon closer examination it is found, nevertheless, that many of these advantages are only apparent, and that free space measurement is frequently far preferable to measurement in guide. Besides the obvious fact that no information as to the effect of curvature is found by guide measurements, there is the further advantage that one obtains an average determination over the whole sheet, of precisely the type desired in radome work, rather than a result based only on a small portion of the sheet. Many of the sources of error are automatically obviated in the free space measurement; there is no

of Fraunhofer attenuation" (Part III above); it is for this reason that the effective reflection must not be assumed independent of position. We remark in passing that the pressurizing cup itself has negligible effect on the antenna pattern, the change being in fact not measurable when the strip is interior to the guido. On the other hand the flange, which affects the match only slightly, may influence the pattern to a considerable extent. Clearly, the proper procedure is to adjust the flange for optimum pattern, and then, with the flange soldered in place, to adjust the cup for optimum match. (cf. Ref. 10)

3. Measurement of Transmission and Reflection Coefficients—Before considering the problem of measurements in free space, we briefly discuss the theoretically simpler problem of measurement in guide. The relevance of this to the present investigation is shown in the following result, which was suggested by the plane wave resolution for the TE modes and which may be rigorously proved by reference to the boundary conditions:

Given any pile of plates, lossy or not, in a wave-guide propagating only the fundamental mode. The reflection and transmission coefficients, as measured at normal incidence in guide, will be the same both in amplitude and phase as those found for the same pile of plates in free space, at an angle of incidence  $\theta = \sin^{-1} k_0 n_{\text{air}}$ . If the field in the guide was TE, the equivalence is found for polarization perpendicular to the plane of incidence in free space; but if the field was TM, the polarization for free space must be parallel.

In particular, the reflection and transmission of any pile of plates in a co-axial line will be the same as for free space. Unlike most of the other results given in this report the one just stated follows without approximation from Maxwell's equations. The actual technique of measurement is sufficiently evident from Fig. 35, though there are a few minor details perhaps worth mentioning. Thus, in making either reflection or transmission measurements, probe errors should be eliminated (cf. Ref. 7) as should errors from a failure to have the load matched. This latter error can be reduced to second order terms by taking an average of two measurements with a quarter wave displacement of the sample; cf., in the case of reflection, one may use the procedure of Ref. 11 where accuracies of the order of  $\pm 0.004$  are consistently obtained. Error in transmission measurement is due chiefly to the difficulty of giving equal depths to the two probes, and may be eliminated in principle by repeating the measurement with the wave traveling in the opposite direction. A much simpler procedure, however, is merely to note the probe readings with the empty line, and make appropriate corrections on subsequent values obtained with the sample in place. For the sake of completeness we give the well-known relations for transmission coefficient and reflection coefficient in terms of the maximum and minimum probe readings  $M_{\text{max}}$  as the probes are moved down the line.

$$T^2 = \sqrt{M_{\text{min}}} \text{ for probe } \#2 / \sqrt{M_{\text{max}}} \text{ for probe } \#1$$

$$R = (\sqrt{M_{\text{min}}} - 1) / (\sqrt{M_{\text{max}}} - 1) \text{ for probe } \#1$$

(72)

relative contribution from center, sides and ends, an estimate which shows that the reflection  $a_s$  is indeed equal to that from the front part of the cylinder, with sides and ends excluded.

Complete curves of complex reflection versus position and dielectric thickness are given in Fig. 34. For the strip inside the guide it has been verified that the curves have the same average diameter, and the same ratio of maximum to minimum diameter, as is predicted by the theory; and hence the fact of agreement was believed to be sufficiently established without further computation.

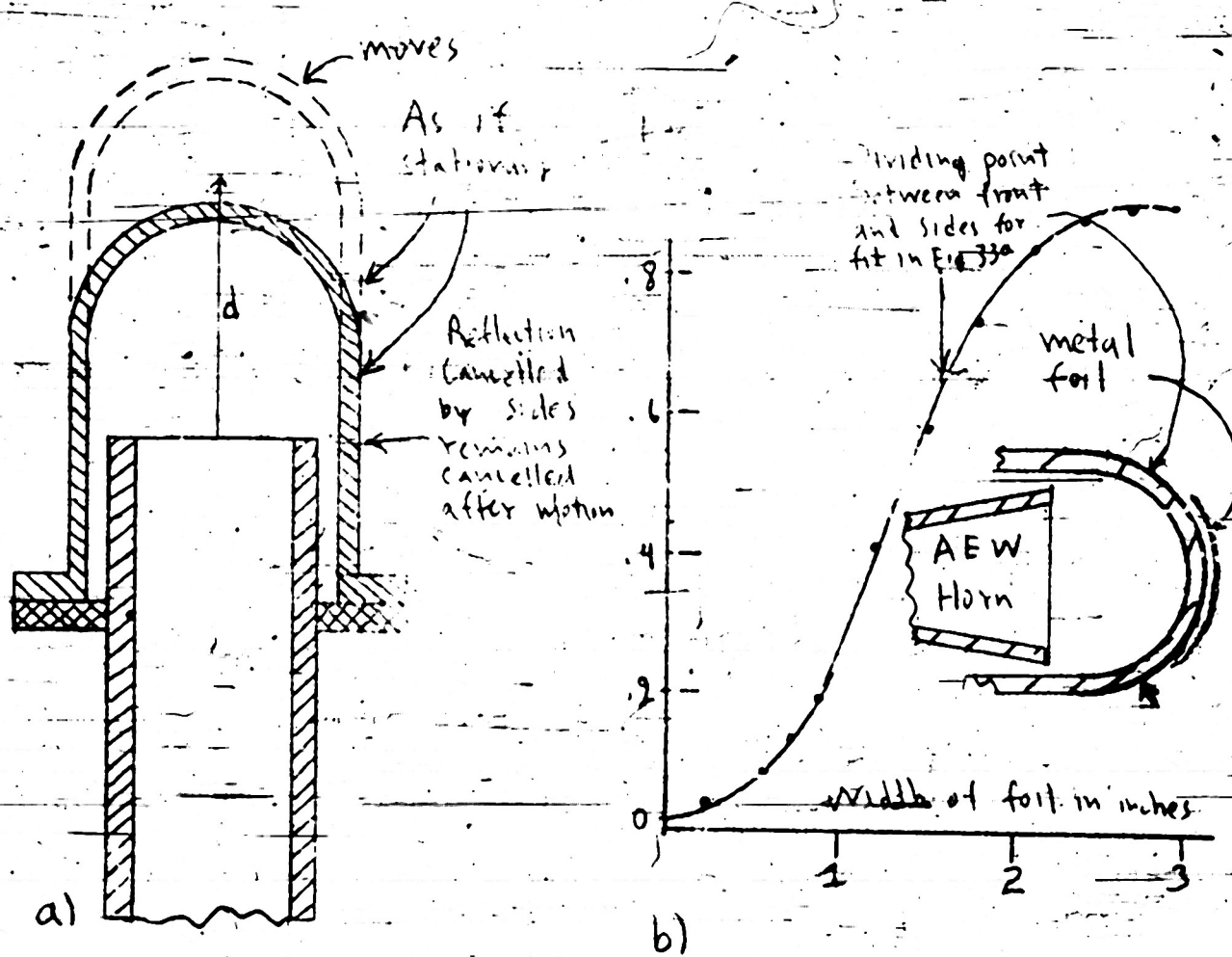


Fig. 34 Relative Importance of Front and Sides of Pressurizing Cup

We remark in passing that these curves would have been circles, according to the theory, if the phase had been measured from a point moving with the sheet rather than from a point fixed with respect to the guide. For our present purposes, however, such representation would be somewhat misleading and is therefore omitted. We note that the curves for dielectric outside of the antenna are spirals, as would be expected from the foregoing discussion.

normal incidence basis; we must have in fact

$$\text{change in } d = (\text{change in phase shift at surface}) (2\sqrt{4\pi}) \quad (71)$$

an equation that is accurately verified in Fig. 32 b

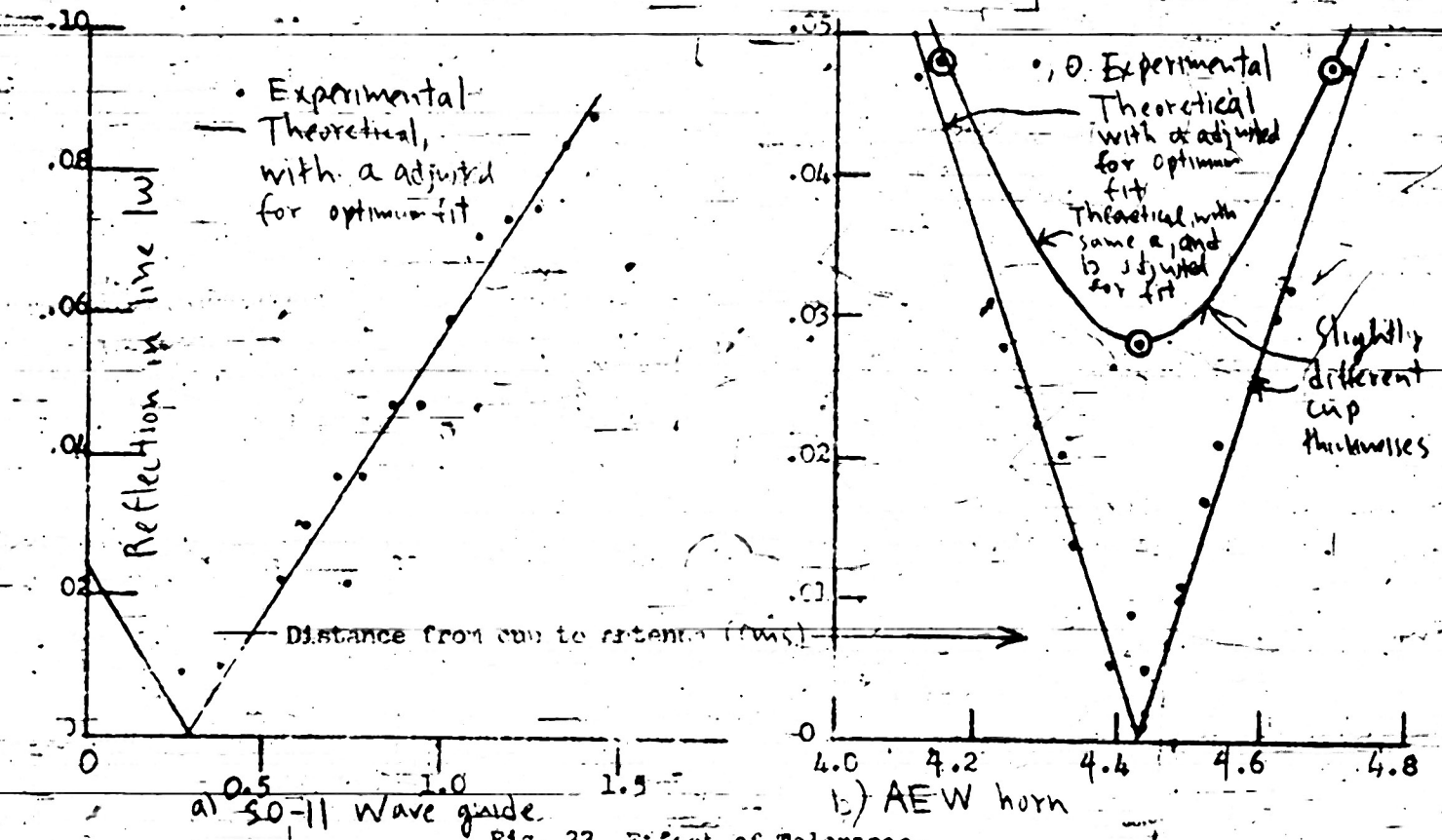


FIG. 33. Effect of Tolerances.

A third experimental check is given for the tolerances, where we compare Eq. (70) with reflection versus position (Fig. 33). Here too the agreement is well within the experimental error, with an independent of cup thickness, as it should be; but the value of  $a$  for optimum fit is considerably less than the initial mismatch prevailing before the cup was added. That such behavior should in fact be found is suggested by Fig. 34a, where we see that any part of the mismatch canceled by the sides of the pressurizing cup will continue to be canceled after the cup is moved. Thus, the reflection that changes phase with position is only that coming from the front surface of the cup, which is presumably less than the total reflection obtained. This explanation is verified by the data of Fig. 34b, where we give reflection versus the width of a metal strip placed over the central portion of the cup. In this way it is possible to estimate the

as empirical equations for reflection versus position, size, or wavelength, as the case may be, in terms of the constants  $a, b$ , depending on the cup under consideration.

Besides the fact that these methods have been successful in designing a number of pressurized antennas, verification is given by a few experiments explicitly directed to that end. In the first place, that the effective reflection is indeed proportional to the reflection coefficient  $R$  is verified in Fig. 32a, where we plot effective reflection versus  $R$  for a plane sheet inside the guide, for a plane sheet outside, and for a pressurizing cup. The proportionality is found, within the experimental error, in each case; and when the sheet is inside the guide, there is not only proportionality but equality, as predicted above. Moreover, the effective reflection is less than the coefficient for the sheet outside, still less for the cylinder, which results are again in accord with the theory of the foregoing pages.

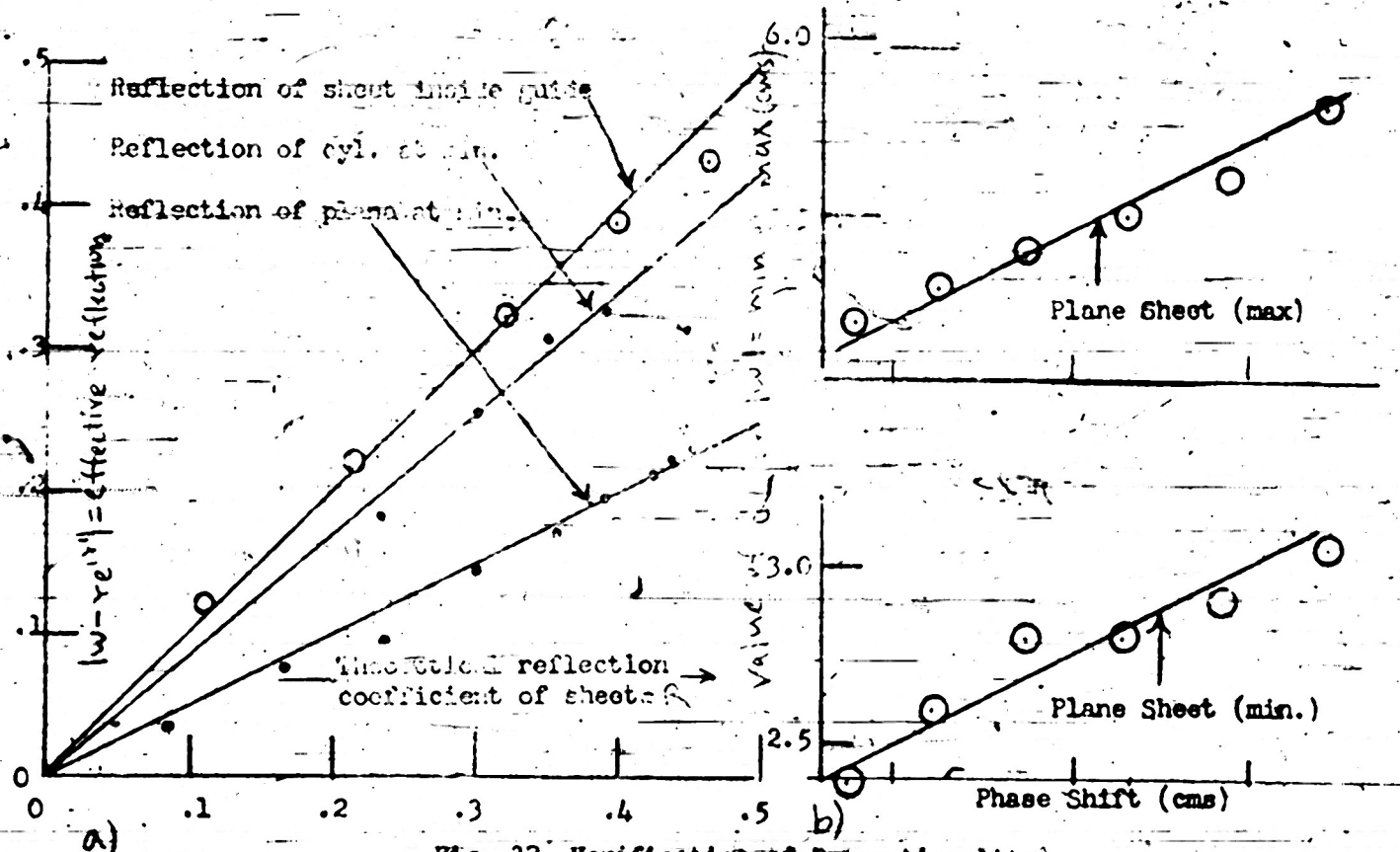


Fig. 32 Verification of Proportionality

A second result is that the position of the sheet for maximum or minimum should be proportional to the phase shift on reflection at the surface, which phase shift is to be computed on the usual plane sheet.

computed on the usual plane-sheet basis; and the phase of the effective reflection is nearly equal to a constant plus the electrical distance from antenna to pressurizer. The design procedure is accordingly to make a pressurizing cup similar in shape to the one desired, but of any material that may be easily molded (e.g., plexiglas). The position of the cup is then adjusted for minimum reflection, whereupon the effective reflection is computed as the difference between the  $|W|$  obtained before and after the cup was added. The reflection coefficient of the material used in this trial cup is computed in the usual manner, and finally the reflection coefficient necessary to achieve a match is found from the proportion

$$\frac{\text{desired reflection coefficient } R}{\text{actual reflection coefficient } R} = \frac{\text{reflection from antenna alone}}{\text{effective reflection of pressurizer}} \quad (69)$$

Once this desired reflection coefficient has been found, the thickness of the final pressurizing cup, which need not be of the same material as the trial cup used in the experiment, may be computed by the usual methods. For completeness a set of curves of reflection versus thickness are included here (Fig. 83).

In the situation of Fig. 3lc, the method must be modified in that one cannot adjust the 'position' (i.e., the size) of the cup for minimum reflection. The procedure now is to make a trial cup near the required size, use the effective reflection in (64) without adjusting for minimum, and compute the new radius in accordance with the principle noted above. This done, a second trial cup may be made with the new radius and reflection coefficient, and the whole process repeated. A single repetition of this type, which indeed is not always necessary in the first place, practically invariably leads to near-optimum design. The necessity for repetition is due to the fact that the effective reflection depends, in general, on the position or size of the cup as well as on its reflection coefficient; and thus, if the effective reflection equals the mismatch due to the antenna for one position, this equality will not be exactly preserved when the position is adjusted for minimum.

Turning now to the question of tolerance, we note that the tolerance in position will be larger, while that in thickness will be slightly smaller, in the situation of Fig. 3lc than in that of 3lb, c. The tolerances in both cases are sufficiently large, it turns out, to lead to only slight manufacturing difficulty; and hence the frequency sensitivity, which was discussed above, should usually be given the more weight in deciding between the two constructions. For quantitative investigation, let us note that the effective reflection may be assumed independent of position or size, and indeed independent of wavelength, over the small variation encountered in questions of tolerance or frequency sensitivity. With this assumption one readily obtains

$$|W| = \sqrt{-2ab \cos(2\pi d/\lambda) + b^2} \quad (\text{in general})$$

$$= 2a |\sin(2\pi d/\lambda)| \quad (\text{optimum effective reflection})$$

(d = error in position)

(70)

of design is very simple, as exact theoretical formulas are available for the reflection of a dielectric sheet in guide and for the reflection versus spacing of any two objects in a line permitting only one mode of propagation (Ref. 9, 2). It suffices, therefore, to measure the mismatch of the antenna alone and to adjust the thickness of the dielectric for this same reflection, an adjustment which is readily made by the curves of Ref. 9. If the dielectric is lossless, there exists a position of the strip in guide for which the combined reflection of strip and antenna will be exactly equal to zero. This position may be predicted in advance from a measurement of the phase of the mismatch due to antenna alone, or found by trial and error. The latter procedure is usually the more rapid in practice, and the former is therefore not discussed here (see Ref. 3).

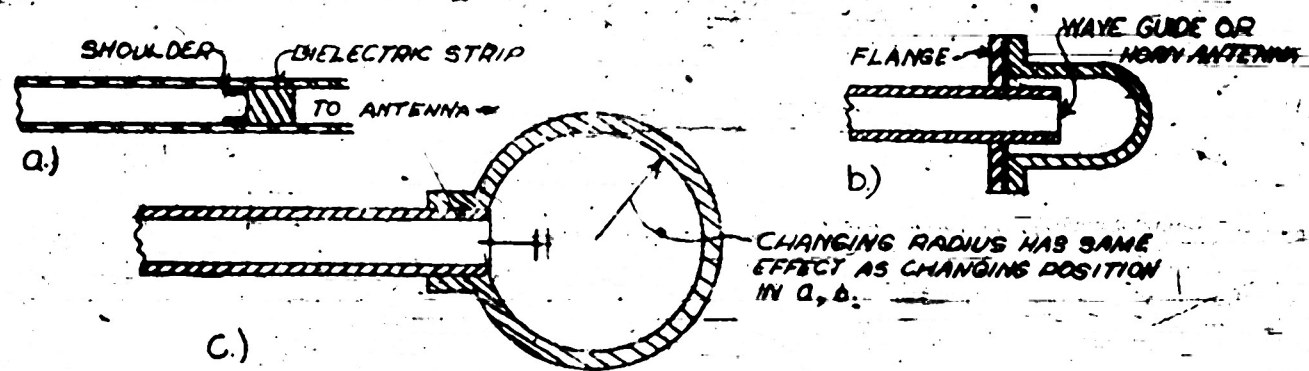


Fig. 31 Methods of Pressurizing

The foregoing procedure is exact in the sense that it follows without approximation from Maxwell's equations, and the problem of a strip inside the line is therefore believed to be completely solved. Turning now to the situations of Fig. 31b,c, we find that an exact solution of this sort is almost impossible to obtain; and in any case it would doubtless be too complicated for use in practice. The situations of Fig. 31b,c must nevertheless be investigated, as they are in several respects superior to that of Fig. 31a; in particular, the power carrying capacity is evidently greater, and the frequency sensitivity is in general decreased. This latter statement, which is true only for wave-guides as opposed to co-axial lines, is indicated theoretically by the fact that the derivative of guide wavelength is greater than that of free space wavelength whenever  $\lambda_c < \infty$ ; and it has been verified experimentally on several occasions. Since the situations of Fig. 31b, c are frequently superior, as we have just noted, investigation of some sort is clearly desirable. To this end, we introduce the notion of 'effective reflection', defined as the difference between the complex reflection of antenna alone and that noted when both antenna and pressurizing device are present (cf. Eq. 16 and Fig. 11). The effective reflection then represents that part of the observed mismatch which is due to the pressurizing device itself. To obtain a match, it evidently suffices first, that the effective reflection be equal in magnitude to that of the antenna alone; and second, that it be directly opposite in phase. The utility of this notion of effective reflection, which is also helpful in work with radomes, rests upon the following empirical observations: For a given position of the pressurizing device, the effective reflection is very nearly proportional to its reflection coefficient.

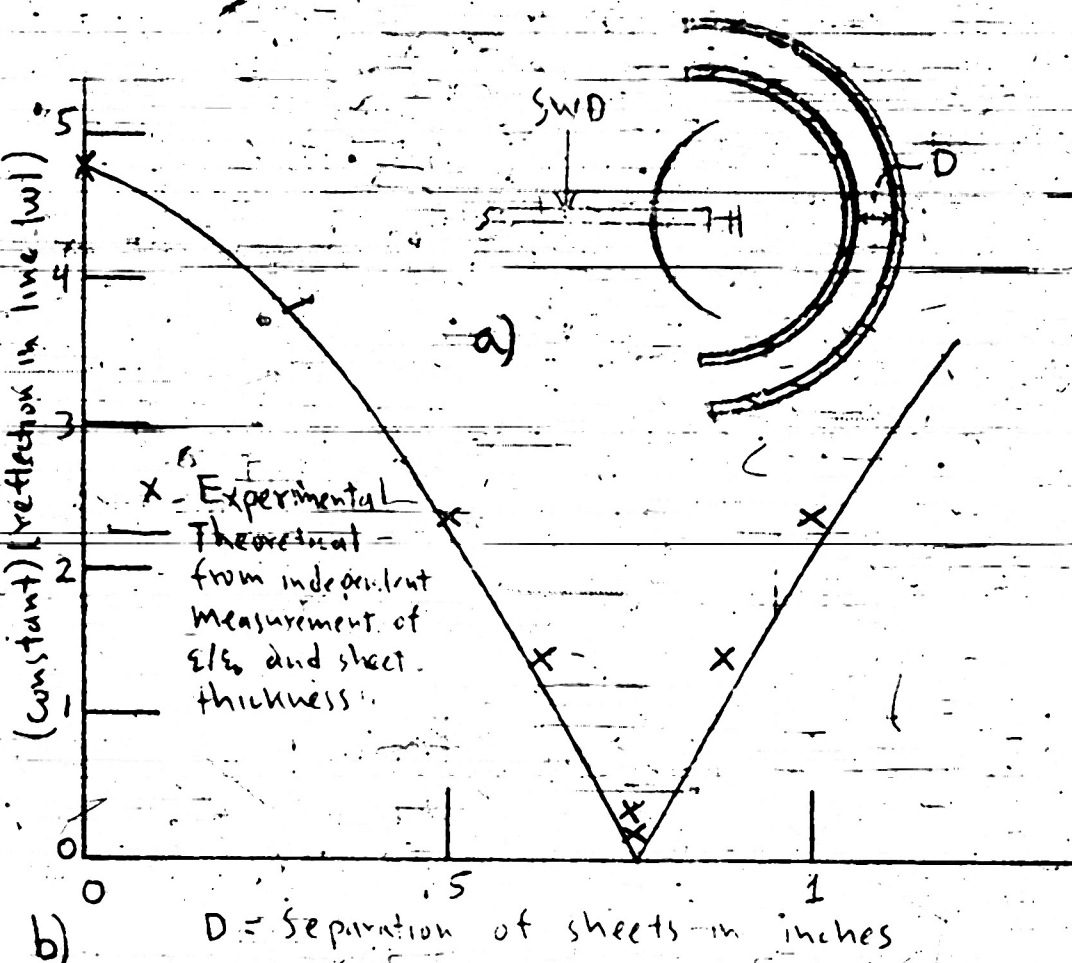


Fig. 30 Verification that Reflection in the Line Is Proportional to Reflection Coefficient for Surfaces Which Both Are Multi-Layered and Curved

2. Pressurizing--Besides its utility in the study of radomes, the methods here used are helpful in the problem of antenna pressurizing. In this case, as we noted in the introduction, one wishes to cancel the reflection due to the antenna with a second reflection introduced by the pressurizing seal. The advantages of this procedure over the more obvious method of using an iris to match out the combined reflection of antenna and seal are threefold, viz., the power carrying capacity of the system is not impaired; the fabrication is simpler, once the basic design is obtained; and the frequency sensitivity is considerably reduced. It is therefore worthwhile to have some systematic method of designing a pressurizing cup or other seal in such a way as to lead to a matched line, without additional tuning devices.

The chief types of construction used in pressurizing are shown in Fig. 31, where we see that the sealing device may consist of a strip inside the waveguide or of a cup surrounding the antenna. In the former case the procedure

for surfaces consisting of a single sheet is shown theoretically by the relative insensitivity of both reflection and transmission coefficients to angle of incidence at incidence near normal (Ref. 9); and it has been repeatedly verified experimentally. For surfaces consisting of several layers of sheets, on the other hand, the question perhaps requires further investigation, which we present here. In the first place, if the first derivative of the reflection or transmission with respect to  $\theta$  exists at all, when  $\theta = 0$ , then it must be equal to zero at that point. This result, which follows rigorously from the obvious fact that the coefficients have the same value for positive as for negative values of  $\theta$ , shows that any deviation from the normal incidence value will necessarily be of the order of  $\theta^2$ , when  $\theta$  is small, if the function admits a Taylor series expansion about the origin. It was proved in Ref. 3, however, that both the reflection and the transmission coefficients of any pile of plates are analytic functions of all the variables concerned; and hence the absolute values, though of course not analytic, will have derivatives of all orders in the real-variable sense, at every point for which the function is not zero. It follows that above conditions of the existence of the first derivative and of a Taylor's series expansion are indeed satisfied by any pile of plates at any point for which the coefficient in question is not zero; and we thus conclude, finally, that the change in reflection for small deviations from normal incidence will be proportional to the square of this deviation in practically all cases. There is every reason to believe, incidentally, that the same result is true when the coefficient is zero, as indeed has been proved for single wall (Ref. 9), double wall and sandwich constructions; but a rigorous proof in general seems hardly worthwhile for the present discussion.

When combined with the fact previously established, that reflection at angles appreciably different from zero does not enter the line, the result just obtained suggests strongly that reflection in the line for a curved surface will be nearly proportional to its reflection coefficient regarded as a plane sheet, even when the surface consists of multiple layers. Proceeding now to the question of experimental verification, we note that the error due to curvature should increase as the thickness of the surface grows larger in comparison to its radius; and hence the maximum error likely to occur in practice will be found for fairly small antennas at S-band with surfaces of maximum overall thickness. An experiment was accordingly set up as in Fig. 30a, where we use double-wall construction as an example of a multiple layer surface partly because of the ease of changing its reflection, and partly because it leads to a greater overall thickness in practice than is usually found with sandwiches. The experimental procedure was to take a curve of measured reflection versus separation in the usual manner, whereupon, the theoretical reflection versus spacing was computed, from independent determination of the thickness and dielectric constants of the individual sheets, for the unrolled (plane) sheets at normal incidence. Upon choosing the best constant for the proportionality, we obtained the fit shown in Fig. 30b, which is well within the experimental error.

for surfaces consisting of a single sheet is shown theoretically by the relative insensitivity of both reflection and transmission coefficients to angle of incidence at incidence near normal (Ref. 9); and it has been repeatedly verified experimentally. For surfaces consisting of several layers of sheets, on the other hand, the question perhaps requires further investigation, which we present here. In the first place, if the first derivative of the reflection or transmission with respect to  $\theta$  exists at all, when  $\theta = 0$ , then it must be equal to zero at that point. This result, which follows rigorously from the obvious fact that the coefficients have the same value for positive as for negative values of  $\theta$ , shows that any deviation from the normal incidence value will necessarily be of the order of  $\theta^2$ , when  $\theta$  is small, if the function admits a Taylor series expansion about the origin. It was proved in Ref. 3, however, that both the reflection and the transmission coefficients of any pile of plates are analytic functions of all the variables concerned; and hence the absolute values, though of course not analytic, will have derivatives of all orders in the real-variable sense, at every point for which the function is not zero. It follows that above conditions of the existence of the first derivative and of a Taylor's series expansion are indeed satisfied by any pile of plates at any point for which the coefficient in question is not zero; and we thus conclude, finally, that the change in reflection for small deviations from normal incidence will be proportional to the square of this deviation in practically all cases. There is every reason to believe, incidentally, that the same result is true when the coefficient is zero, as indeed has been proved for single wall (Ref. 9), double wall and sandwich constructions; but a rigorous proof in general seems hardly worthwhile for the present discussion.

When combined with the fact previously established, that reflection at angles appreciably different from zero does not enter the line, the result just obtained suggests strongly that reflection in the line for a curved surface will be nearly proportional to its reflection coefficient regarded as a plane sheet, even when the surface consists of multiple layers. Proceeding now to the question of experimental verification, we note that the error due to curvature should increase as the thickness of the surface grows larger in comparison to its radius; and hence the maximum error likely to occur in practice will be found for fairly small antennas at S-band with surfaces of maximum overall thickness. An experiment was accordingly set up as in Fig. 30a, where we use double-wall construction as an example of a multiple layer surface partly because of the ease of changing its reflection, and partly because it leads to a greater overall thickness in practice than is usually found with sandwiches. The experimental procedure was to take a curve of measured reflection versus separation in the usual manner, whereupon, the theoretical reflection versus spacing was computed, from independent determination of the thickness and dielectric constants of the individual sheets, for the unrolled (plane) sheets at normal incidence. Upon choosing the best constant for the proportionality, we obtained the fit shown in Fig. 30b, which is well within the experimental error.

reflection phenomena. In particular, there is no measurable increase of power as the antenna passes through the 'focal point' of the spherical portion of a radome; as was the case for the cylindrical surfaces discussed above, the reflection is practically independent of distance over the range which one is concerned in radome work. This absence of a focussing effect is the sine is due no doubt to the low gain, directivity of the antenna back-lobe; that some power is actually focussed in space has been verified by a small exploring antenna, and by certain detrimental effects noted for the true antenna pattern (See Ref. 1). We remark in passing that the data of Fig. 29 were taken with considerably less care than that used for most of the results hitherto described; in particular, the voltmeter was read with the unaided eye rather than with the 6x magnification eyepiece employed. Because of the large number of radomes tested, especially accurate measurement is quite uneconomical, nor is it necessary in view of the fairly large manufacturing tolerances and of the rather quantitative nature of the results desired.

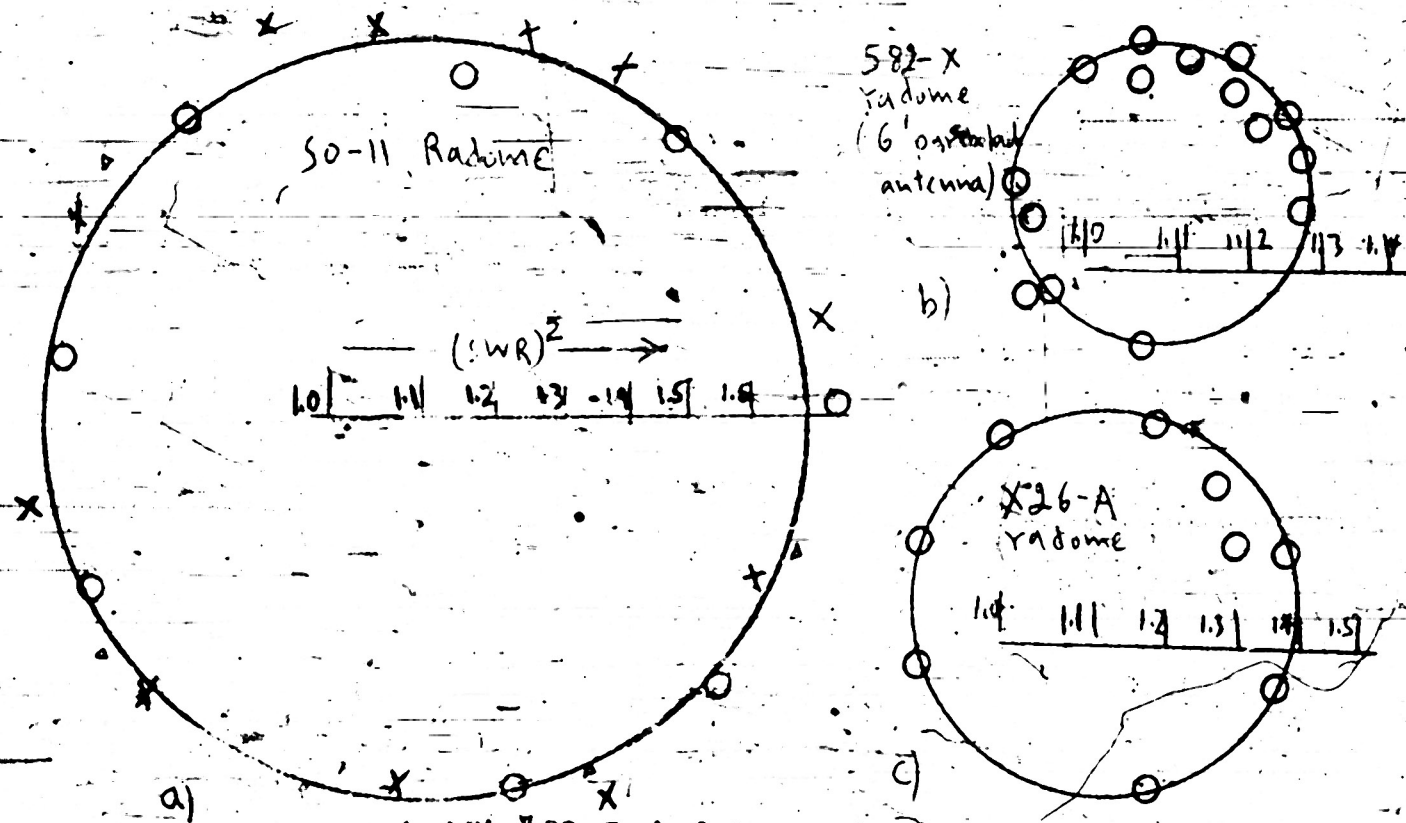


Fig. 29 Typical Curves of Complex Reflection Versus Distance with Actual Radomes

We have briefly noted two questions not explicitly considered in the theoretical discussion of Parts II-IV above, viz., whether certain of the results can be extrapolated to very large antennas, and whether the presence of compound curvature introduces any noteworthy phenomena. One other question encountered in the application of theory to actual radomes concerns our assumption that the measured reflection, (or more properly the 'effective' reflection in the sense used below) is very nearly proportional to the reflection coefficient of the surface, which coefficient is to be computed as though the surface were a plane sheet. That this assumption is satisfied

By Eq. (57), the pulling  $p(\theta)$  is found to be

$$p(\theta) = PR/\lambda P(\theta-\frac{\pi}{4})/a \quad (68)$$

and hence for the same special case as that considered above, the apparent pattern  $P(\theta)[2-2.25P(\theta-\frac{\pi}{4})]$  when  $2.25P(\theta-\frac{\pi}{4}) > 1$  unchanged when  $2.25P(\theta-\frac{\pi}{4}) < 1$  (Fig. 82). It was found experimentally that the phase is constant when the rotation is about an axis through the cylinder, rather than through the vertex of the antenna; and therefore, the discussion of phase given above in connection with the strip above is valid for this case also, with the same error term  $a(\sec\theta-1)$ .

It must be emphasized that the effect just described for the apparent pattern is quite distinct from the change in actual pattern, which of course may also be affected by the radome. In the present discussion, the true antenna pattern was assumed to be the same with radome as it was without; and even in this case, it was found that signal strength versus angle, the apparent pattern, would be greatly modified. To this modification must be added that in the true pattern, though it is not considered in the present report. It is worth noting, however, that the presence of the overlap, which produced only slight change in apparent pattern by pulling, may often produce a large change in the true antenna pattern by diffraction effects. On the other hand the uniform dome leads to only minor modification of the true pattern, in general, whereas its effect on the apparent pattern, due to pulling, was quite appreciable (Fig. 82).

Similar methods allow computation of the change in apparent cross-over point due to pulling for lobe-switching or gun-laying systems (Fig. 28d). The general procedure is to compute the pattern for each lobe in the same manner as for the single lobe in the above examples. With narrow beams, however, the procedure may be considerably simplified in that one may then take the pulling as being more or less independent of angle in a given lobe, which is merely reduced by a constant factor. This simplified procedure is frequently applicable in practice, with the result that the estimation of apparent cross-over for systems of the type shown in Fig. 28d is often simpler than finding the apparent pattern in ordinary systems.

In applying the above theory to radomes, it is desirable to have direct verification that the phenomena are essentially the same in practice as in the ideal cases here considered. We therefore present the data of Fig. 29, which is representative of the much larger background of data on actual radomes that has been obtained by the author and others in the Radiation Laboratory.

Fig. 29a shows a plot of complex reflection versus distance for a cylindrical radome, the distance extending over a range sufficient to give several revolutions of the completed curve. That the salient features of the above discussion are valid for very large radomes is illustrated in Fig. 29b where a similar curve is given for a radome over ten feet high. This radome was not cylindrical, but had considerable curvature in both directions, as does that of Fig. 29c; and it appears that such compound curvature introduces no unusual

the antenna, Eqs. (64), (66), finally lead to

$$p(\theta) = \pm 2.5 \text{ MHz} [1 - \tan^2(\theta - \psi)]^4 \quad (67)$$

for the pulling as a function of scan angle  $\theta$ , with  $\psi$  as the fixed angle between the direction of the overlap and that of the target (Fig. 28b). It has been assumed that the contours on the Rieke diagram are equally spaced and that the complex reflection moves perpendicular to these contours. This latter condition is satisfied, or will be satisfied for certain values of the distance to the overlap, if the phase is constant as the angle is changed. Experimentally we found above, however, that the phase is constant if  $q'$  is changed, instead of  $\theta$ ; and the error is a  $(\sec \theta - 1)$  in the case assumed here. This error, which is not always negligible, will cause the impedance to move in a spiral on the Rieke diagram, instead of a straight line; and the resulting deviation in apparent beam shape will be less than that indicated by the present formulas at most points, equal to it twice in every turn of the spiral. In other words, as the quantity  $a(\cos \theta - 1)$  takes the values (constant plus 0,  $\lambda/8$ ,  $\lambda/4$ ,  $3\lambda/8$ , ...), the deviation will be the above value, then zero, then the above value, then zero, etc. The change in beam shape is found by substituting for  $p(\theta)$  in the relation found in the first part of this discussion.

For example, we may take the band width  $B$  as 2 mc., the distance  $Q$  as 2 mc., the pulling figure of the magnetron as 12 mc., the reflection coefficient  $R$  as 0.30, the strip width as 3", and the antenna radius  $a$  as 12". These values lead to  $1.35 [1 - \tan^2(\theta - \psi)]^4$  for the pulling  $p(\theta)$ , so that the apparent pattern is  $P(\theta)$  when  $p(\theta) < 1$  and it is  $P(\theta) \{2 - 1.35 [1 - \tan^2(\theta - \psi)]^4\}$  when  $p(\theta) > 1$ . At S-band, the secondary pattern of a  $2\frac{1}{2}$ " paraboloid can be fitted within a few per cent to the curve  $\exp(-0.025\theta^2)$  over the first 20db, and this value for  $P(\theta)$  is taken in the curves of Fig. 81.

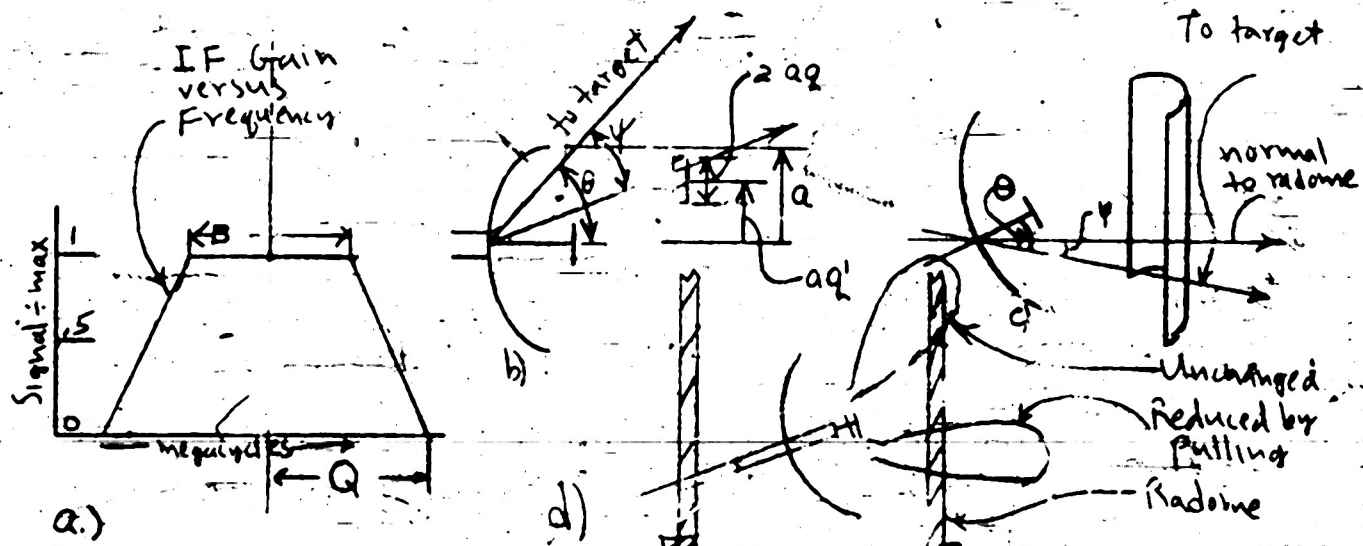


Fig. 28 Variables for Apparent Pattern

In a similar manner, one can evaluate the apparent pattern produced by a uniform dome, without overlaps, when the scan is in elevation (Fig. 28c).

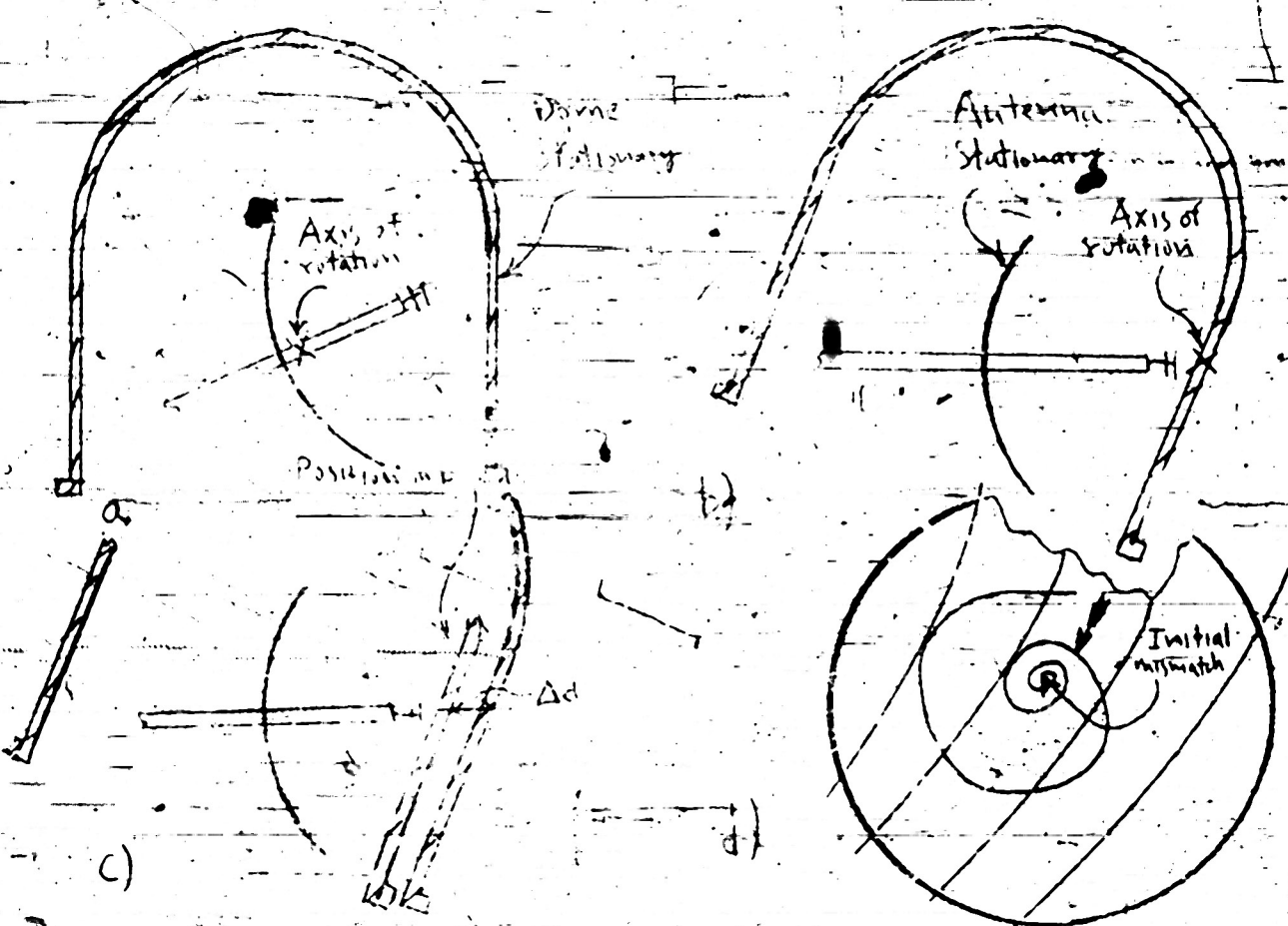


Fig. 2. Scan in elevation

Thus, the true pattern is obtained by taking received RF power versus antenna position, whereas the apparent pattern would be determined, in principle by blanking all but one signal off the scope, and using a photo-electric cell to measure the intensity of this one signal as the scanner position is changed. It is clear that one is really concerned with this apparent pattern, rather than with the true pattern in radar systems; and it is likewise easy to see that the apparent pattern will depend on the magnetron pulling whenever this varies with antenna position.

For quantitative investigation let us note that the signal is proportional to the output of the IF receiver, which output has approximately the form shown in Fig. 9g(a), as a function of frequency. Thus the normalized signal is 1 if the pulling is less than  $B/2$ , and it is  $(Q \cdot P)/(Q \cdot B/2)$  if the pulling is greater than  $B/2$ . Suppose that the secondary pattern of the dish is  $P(\theta)$  and that the pulling, as a function of angle, is  $p(\theta)$ . The apparent pattern, that is, the signal strength versus angle, will then be  $P(\theta)$  when  $p(\theta) < B/2$  and  $P(\theta)[Q-p(\theta)]/(Q-B/2)$  when  $p(\theta) > B/2$ . When the characteristics of the IF amplifier,  $B$  and  $Q$ , are known, and the pulling versus angle of scan is also known, we can predict the apparent beam shape as given by signal strength versus angle in terms of the true beam shape as given by the secondary pattern.

As an example of the procedure, we may estimate the apparent pattern noted when one has an overlap in a radome of otherwise negligible reflection (or, more generally, in a radome which is otherwise uniform). If we take the distance to the overlap as being approximately equal to the radius of

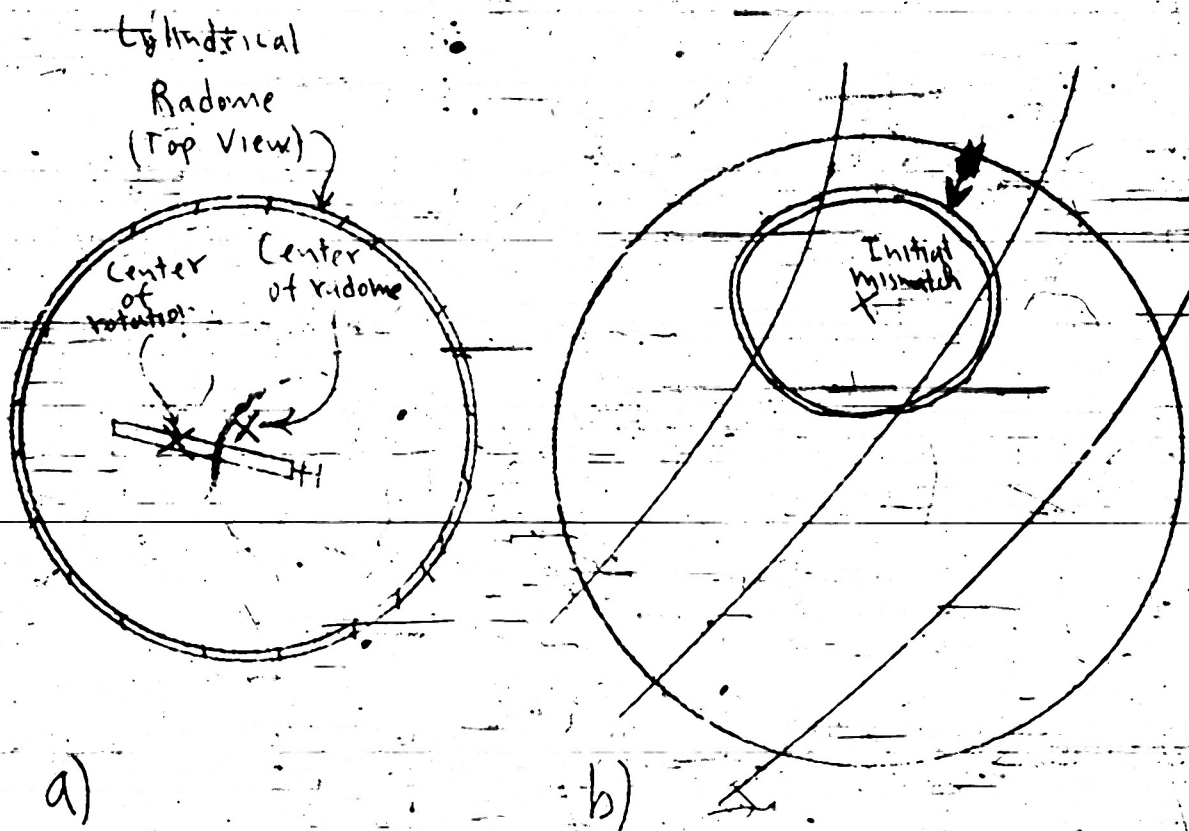


Fig. 26. Spinner Off Center

rotation about an axis through the cylinder, plus a translation away from the antenna; and both these situations have been considered in some detail above. The amplitude, which has been shown to be substantially independent of distance, is given by (5); and on the other hand the phase, which is independent of angle for the first choice of axis, is given by the change in distance,  $\Delta d$ , shown in Fig. 27c. The corresponding curve for application to the Rieke diagram, then, will have the general shape illustrated in Fig. 27d, with quantitative computation possible, as before, whenever the radome reflection coefficient, wavelength, and antenna dimensions are known. With procedures of the type suggested in Figs. 27b,c, the theory of the present report may be applied to a large variety of radome problems; and one obtains quantitative results, to the required degree of accuracy, in each case.

Before leaving the subject of magnetron pulling, we mention an effect which is fairly obvious in the case of lobe-switching antennas, but which is likely to be overlooked with a single beam. Suppose we define the apparent pattern to be a curve of signal intensity, as seen on the scope, versus scanner position. This differs from the ordinary antenna pattern in that here we are concerned essentially with the output, rather than with the input, to the receiving system.

a large phase change coupled with a decreasing amplitude. If the system is not equipped with AFC the two situations are practically equivalent, since the same total pulling is obtained in both cases. With AFC, on the other hand, Fig. 25b is considerably less desirable than 25a because of the increased rate of change of frequency for a given scanning speed.

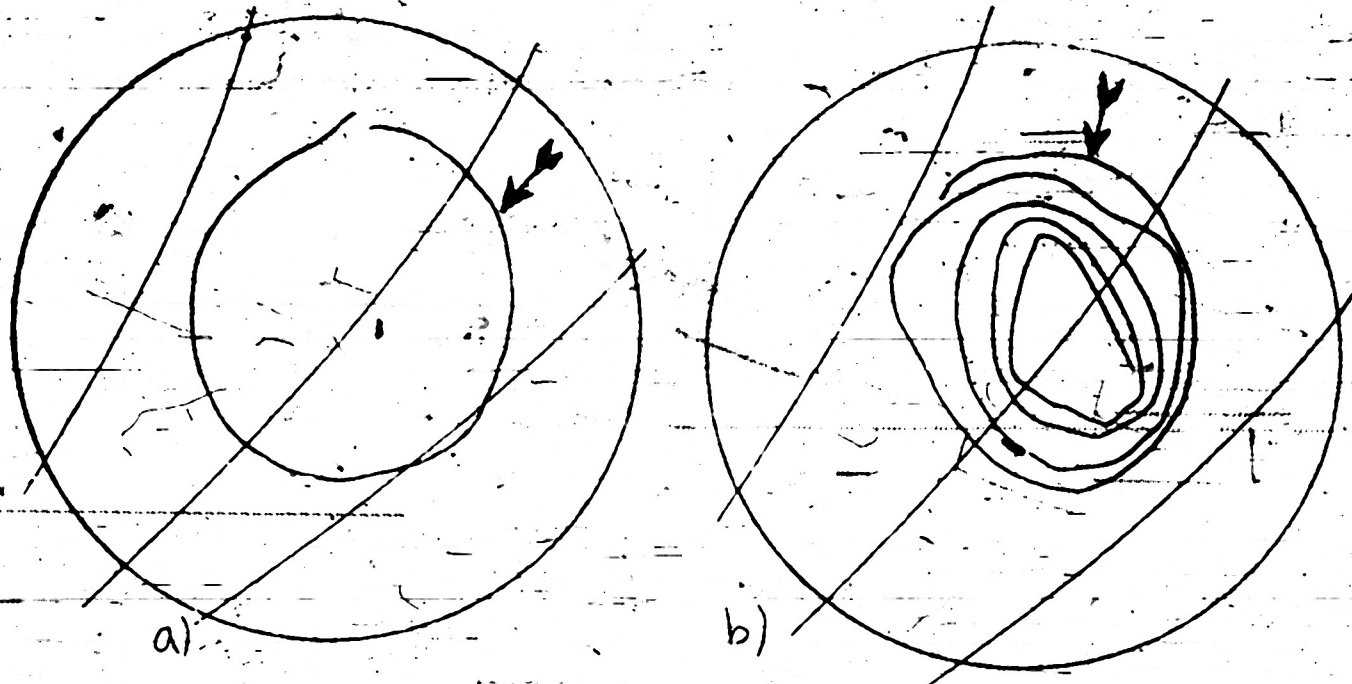


Fig. 25 Two Situations Which are Equivalent Without AFC, but Different When It Is Present.

Having indicated the use of the Rieke diagram to estimate pulling, and the difference between systems with and without AFC, we proceed to the question of determining reflection from the geometry of antenna and radome. Let us suppose, for example, that the spinner is at least a quarter wave off center in the system of Fig. 26a. To estimate the maximum pulling, we allow the elevation scan to assume the position for which the incidence is approximately normal, whereupon the reflection in the line is computed by the methods here described for that case (See IV, 2, a above). Since the spinner is at least a quarter wave off center -- which is very often the case in practice -- the complex reflection curve has the general form given in Fig. 26b, a result that is intuitively evident, or may be probed by the curves of Figs 47, 62. Upon taking account of the non-uniform rate of change of distance with angle, moreover, one obtains the information needed in systems with AFC, as well as that for the simpler case.

One other example is given in Fig. 27, where the scan this time is in elevation. Although the data and theory here given assumes an axis of rotation through the radome rather than through the antenna, it may be applied by the procedure suggested in Figs. 27b, c. Thus, the end result is equivalent to a

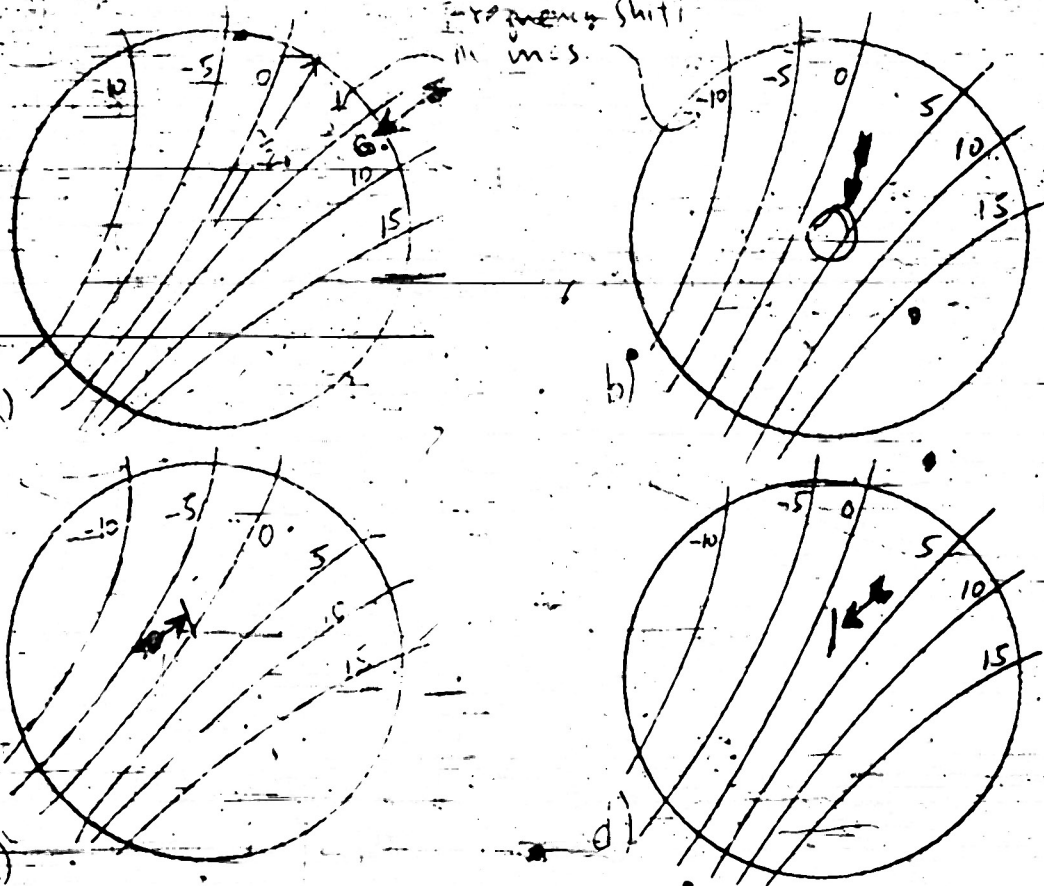


Fig. 24. Examples of Complex Reflection Curves  
on Rieke Diagram

Fig. 24b is the one most often obtained in practice. Upon combining these properties we see that the pulling should be approximately proportional to the diameter of the circle traced out by the reflection; and if the circle is centered sufficiently near the origin, the proportionality constant will depend only on the Rieke diagram. It is customary to define this constant in terms of the result obtained for a circle whose radius is 0.2 ((SWR)=1.5) the constant so obtained being termed the pulling figure of the magnetron.

pulling figure  $F = \text{pulling in mcs. for } (\text{SWR}) = 1.5, \text{ phase variable}$  (66)

For example, the pulling figures for Figs. 24a-d are respectively 8, 7, 7, and 7 while that for the magnetron of Fig. 80 is 17.

In the foregoing it was assumed that the system is not equipped with automatic frequency control, AFC, so that the actual magnitude of the frequency change was the relevant consideration in estimating system performance. When AFC is present, on the other hand, the magnitude of the frequency shift becomes relatively unimportant, since the equipment continues to function for reflections considerably higher than those produced by most radomes. In this case, the rate of change of the frequency must not be too large, for reasons mentioned in Ref. 1. To clarify the difference between the two cases, we consider the situations of Fig. 25. In the first, the phase change as the antenna scans is only about a half wave, while in the second, we assume

$$|\omega| \propto (\text{const}) \sin[(2\pi d/\lambda) \sin \theta] \quad (66)$$

an equation which is verified in Fig. 79d. From the excellance of this agreement, it appears that the step function approximation for  $f(x)$  -- a necessary procedure in the derivation of (66) -- is fairly well justified in practice. Similarly, Eq. (62) for the location of the maxima is verified within a few degrees, so that the data could hardly fail to satisfy the general equation (45) within the experimental error. We remark in passing that all experimental points of Figs. 77-79, like those of Figs. 69-75, represent the average of two measurements of reflection with a quarter-wave change in  $d$ .

#### V-- Applications

1. Radomes--The obvious application of the present theory to questions of radome transmission are discussed below; for the present, we consider only the problem of magnetron pulling. For almost all magnetrons used in systems there is available the so-called 'Rieke diagram', an experimental set of curves which give, among other things, the contours of constant frequency on a Smith chart -- the W-plane of the present report. Upon plotting complex reflection versus scanner position on such a chart, one obtains all relevant information for magnetron pulling. That this procedure is reliable in practice is verified in Fig. 80, where magnetron pulling as computed from the reflection and Rieke diagram is compared with that determined directly on the system by tuning the local oscillator dial for maximum response. A detailed description of the procedure used in obtaining Fig. 80 is given in Ref. 1; for our present purposes, it suffices to note that a curve of complex reflection, of the type here described, permits accurate evaluation of the magnetron pulling in a given system.

It must be emphasized that the change in reflection rather than its actual value, is the significant factor in producing pulling; and that there is no advantage in having the amplitude constant if the phase varies. For example, Fig. 24a represents a high reflection,  $(S.R)^2 = 9$ , which remains practically constant during the scan. In this case the pulling, as obtained from the curves of constant frequency, is only about 1/2 megacycle. In Fig. 24b, on the contrary, the reflection is very low, its maximum value being only 0.05, which corresponds to an  $(S.R)^2$  of 1.2; but the variation of phase is large, and hence the pulling now turns out to be about 4 mcs. A third example is given in Fig. 24c, where the phase is constant but the amplitude varies. The curve is here a straight line which happens to be perpendicular to the contours of constant frequency. The pulling is again high, being about 3 mcs.; but when the line is oriented parallel to the contours, as shown in Fig. 24d, the pulling is only 1 mc. From considerations of this type it is clear that no reliable criterion can be given which includes only the magnitude of the reflection, but that on the contrary one must consider both the phase and the orientation with respect to the Rieke diagram.

In spite of this complication, which must be kept in mind whenever one is investigating questions of magnetron pulling, there is a simplified procedure that may be used in certain cases. This simplification is based on two empirical observations, viz., that the contours of the Rieke diagram are approximately equally spaced; and that the phase variation in the course of the scan is usually at least a half wave, so that the general type of curve shown in

of data included in the present report, it appears that these methods all give essentially the same result. Similarly, the distance  $d_c$  at which the beam appears to diverge may be found in two ways by the methods here described, and there is also consistency in this case.

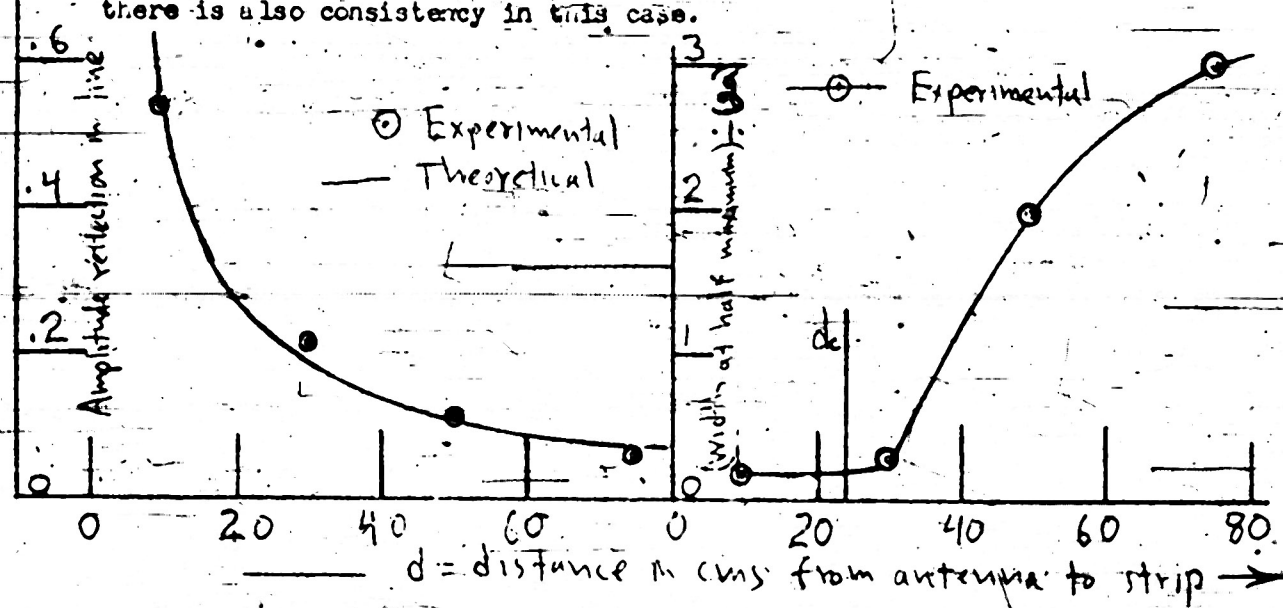


Fig. 23 Dielectric Strip in the Fraunhofer Region

Proceeding now to the case of several strips, we find that the theory is merely a simplification of that already given for corrugations, and it therefore need not be repeated in detail here. Whenever the strips are sufficiently narrow and closely spaced, the step function approximation leads to

$$|\omega| = \frac{(\text{reflection of solid sheet})(\text{area occupied by strips})}{\text{total area of sheet, including air spaces}} \quad (65)$$

for normal incidence, a result which is verified in Figs. 78, 79. Here too we see that the edge effect is apparently more pronounced, and the reflection is higher, when the polarization is perpendicular to the strips, an effect which is as before in marked contrast to the corresponding result for conductors. The deviation from (65) evidently should depend upon the character of the center of the sample, a strip in the center leading to higher values, an air gap to lower values, than are predicted by this equation. In both cases, however, the limiting values anticipated on the basis of theory for one strip are approached as the separation becomes large.

For variation of incidence, one result is given by the general theory of IV, 1, and verified in Figs. 60, 61, while variation of the other angle introduces effects which may be evaluated by the same method as that above for corrugations. In the present case, the envelope is merely the diffraction pattern of a single strip.

$$|F(\theta)| = Rq \left[ 1 - (q^*)^2 \right]^4 / \exp(4\theta^2 \ln 2 / \pi) \quad (64)$$

is an approximate solution of the problem suggested in Fig. 22c. In this equation,  $q^*$  stands for (distance from axis to center of strip)  $\div$  (radius of antenna) and the other variables are as above defined. We remark in passing that the phase associated with  $|F(\theta)|$  should be substantially independent of  $\theta$ ,  $q$  and  $q^*$ , with the simple theory here used whenever the antenna is paraboloidal and the strip is in the Fresnel region. Its independence of  $\theta$  follows from the corresponding result for infinite sheets, which was verified above; and independence of  $q^*$ , which implies independence of  $q$  as well, is verified in Fig. 76, where we see that the curves are practically constant.

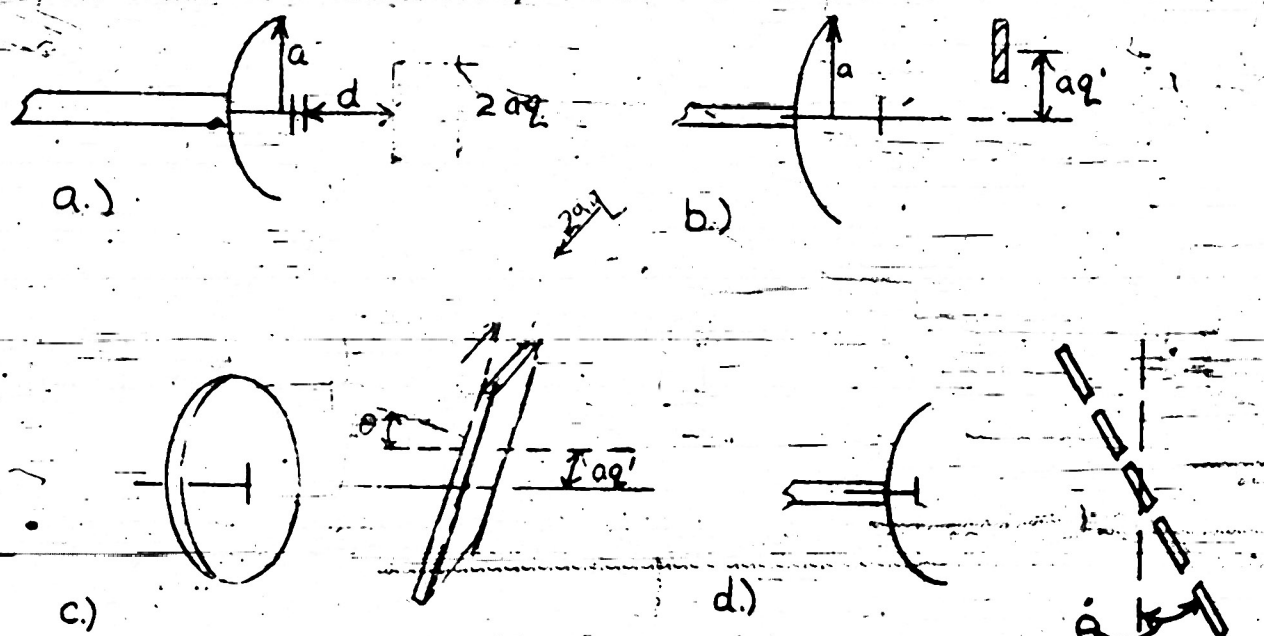


Fig. 22 Dielectric Strips

In the foregoing discussion the strip has been assumed to be in the Fresnel region of the antenna. When this is not the case, curves of  $|F(\theta)|$  versus  $q^*$  are not independent of  $d$ , but on the contrary they increase in width, decrease in height, as  $d$  decreases. The variation in amplitude is theoretically of the inverse-distance type described above, a conclusion which is verified by Fig. 23a. The theoretical curve was computed with the same effective center for the antenna as that used in Part III, Sec. 1, so that only one variable,  $a$  of Eq. (11), was adjusted to obtain the fit in Fig. 23a. Similarly, the point at which the width starts to increase with  $d$  is given approximately by the  $d_c$  of the foregoing pages, as we see in Fig. 23b, where the width of half-amplitude of the curves in Fig. 77 are plotted versus the distance  $d$  from antenna to strip. Still further verification of the theory for the Fraunhofer region is given in the upper right-hand corner of Fig. 76, where the phase is found to be that for a point source located at the previously found 'effective center' of the antenna. In that case, the curve is entirely theoretical, with no variable left free to improve the fit. To summarize, we may say that the effective center of an antenna may be determined by the properties of dielectric sheets or strips, as well as by the conventional procedure used in primary pattern measurements; and, on the basis

In addition to the normal incidence curves of Fig. 68 for checking the actual value of  $|\omega|$ , we give a number of curves of  $|\omega|$  versus  $\theta$  to check the theoretical location of the maxima, Eq. (59). The strips used in forming the corrugated surface, which were of wood, were  $1/4"$  thick, and the period  $L$  was accordingly somewhat different from  $2d \sin(\theta/2)$ . Upon taking account of this change in period due to thickness, using the true value of  $L$  as actually measured, we obtained the theoretical locations of the maxima indicated by the short vertical lines at the bottom of the curves of Figs. 69-72. The agreement is within a few degrees in most cases, a deviation which is not in excess of the experimental error; and the agreement persists even when the strip widths are considerably less than a wavelength. From these experiments on corrugations one concludes that the general equation (59), and the approximate theory which replaces  $f(x)$  by an appropriate step-function, are sufficiently accurate, in the case of paraboloidal antennas, for all applications with which we shall be concerned. Additional corroboration of the result on cylindrical surfaces, Part IV sec. 1, is also given by the properties of corrugations (Fig. 61), which likewise have been shown to have the theoretically expected dependence on  $d$  and  $r$ .

(c) Dielectric strips--If a plane sheet of insufficient width to cover the antenna aperture be substituted for the infinite plane sheet of Part III, the only significant change in the theory is to replace the limits of the integrals by values appropriate to this case. In particular one obtains, if  $q =$  (strip width) / (antenna diameter),

$$|\omega| = (q/8)(15 - 10q^2 + 3q^4)(\omega_0 \text{ for infinite sheet}) \quad (63)$$

$$\approx 1q (\omega_0 \text{ for infinite sheet}) \quad (q/15 \ll q^2 \ll 1)$$

for a paraboloidal antenna with illumination  $f(x)$  given by (52). This result, which follows readily from (59) and Fig. 22a, is experimentally verified in Fig. 73, where we note that the agreement is considerable better for polarization parallel to the strips than for perpendicular polarization. The disagreement may be due to the increased edge-effect found from the presence of more numerous discontinuities perpendicular to the  $E$ -vector, a surmise which is made more plausible by the fact that, in contrast to the behavior of metal strips, the reflection is somewhat higher in this case. The result is independent of distance, incidentally, as we see by the circles on the lower left-hand curve of Fig. 73.

If a sufficiently narrow strip be moved across the aperture of the antenna, as shown in Fig. 22b, its illumination and hence its reflection should be approximately proportional to the primary illumination  $f(x)$ , and will be constant over the strip to the extent that  $f(x)$  admits an appropriate step-function approximation. Upon re-entering the line this reflected wave experiences a further reduction of approximately  $f(x)$ , so that  $|\omega|$  is approximately proportional to  $[f(x)]$ . That this predicted dependence is verified in practice is shown by Fig. 74, which also indicates that the result is independent of distance in the Fresnel region (upper right-hand curve). Examples for more general antennas are given in Fig. 75, where no comparison is made, however, with the primary illumination.

The dependence upon angle is given by the theory of IV, 1 and is verified in Figs. 60, 61. Upon combining this result with (58) and the foregoing equation for strips at normal incidence, we obtain finally

where  $a, b$  may of course be expressed in terms of  $d'$ ,  $d''$ , and  $\theta$ . If the incidence is normal,  $\theta=0$ , one obtains only slight simplification, unless  $d'=d''$ , in which case  $p=q=(n-1)/2$ , and  $|w|=2A$  (see Fig. 67). The condition for minimum reflection, which minimum is zero for the assumed step-function illumination, takes the form

$$\theta = 2 \cos^{-1} [n\lambda/(2d)] \quad (\theta=0, d'=d'') \quad (62)$$

and is represented by the dotted curves of Fig. 65, when used in conjunction with the upper scale,  $\theta$ .

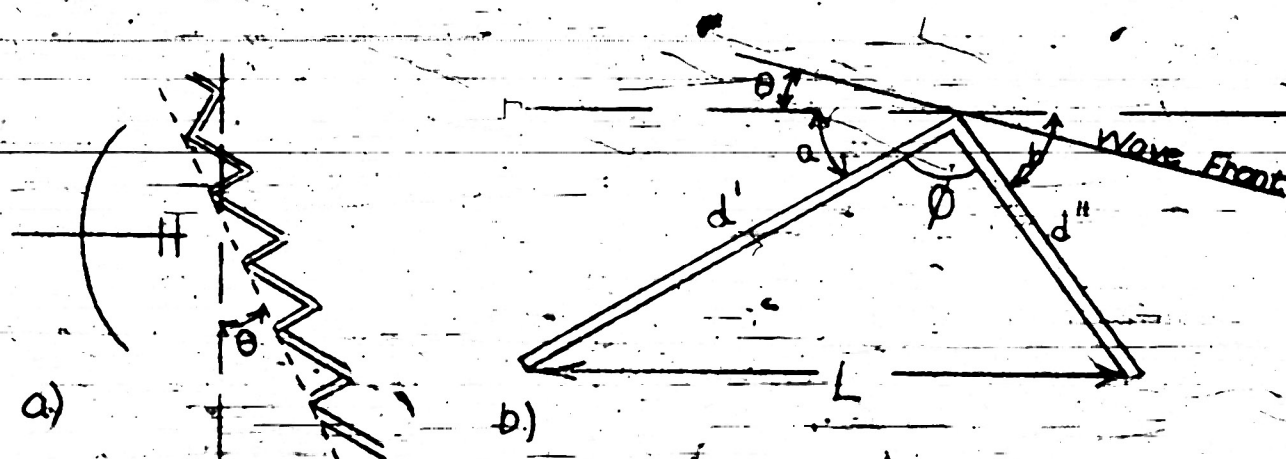


Fig. 21 Corrugated Surface

While sufficient time was not available to compute the envelope curves, experimental verification of the theory for normal incidence and of the location of maxima at arbitrary incidence is given in Figs. 68-72. The data were taken with  $f$  cancelled as usual by quarter-wave motion of the surface, so that each point represents the average of two measurements of reflection. To check for reproducibility certain curves were repeated several weeks after the initial data had been taken, a procedure which involved the complete dismantling and re-assembly of both antenna and corrugated surface. This precaution was also used in the case of the cylinder, the repeated points being represented by crosses in each case (see Figs. 62 and 70-72).

By comparing theory with experiment one can make some estimate as to the lower limit of dimensions at which ordinary diffraction theory may still be applied. Thus, we have assumed that the illumination may be found by using the ordinary reflection coefficient, defined for an infinite sheet, so that edge effects are neglected. When Huygen's principle is used in this way highly accurate results should be expected only when the sample dimensions are large compared to the wavelength. On the other hand the conventional theory may be used when the dimensions are only of the order of a half wave, as we see by the curves of Fig. 68 for  $d=1"$  and  $2"$ , provided merely qualitative accuracy is desired. For the  $4"$  strips, which have widths of the order of a wavelength, the agreement is in fact already within the experimental error as the measured reflection in these curves is too small to be found with great precision.

Experimental verification of these results on cylinders is given in the curves of Figs. 62-65. Each point of Figs. 63, 64, 65 is the integrated average of a complete curve of reflection versus distance, the points for small  $d$  being plotted independently of those for  $d$  large. From these complete curves of reflection versus distance, each of which had the same number of points and the same general shape as the examples given in Fig. 62, it was repeatedly verified that  $|w|$  is substantially independent of distance. Besides this result, which is in agreement with theory, we have further verification in that there is only slight dependence on the antenna focal length or polarization. To check the remainder of the theory, the points of Figs. 63, 64 were supplemented by additional data at X and K bands, whereupon each point was plotted versus  $a/\rho\lambda$  (see Fig. 65). Here too the agreement is believed to be as good as could be expected, in view of the experimental difficulties and the approximate character of the theory. That the dependence on  $\theta$  is correctly stated by (57) was verified in the foregoing discussion.

(b) Corrugated Surface--By approximating the paraboloid illumination with a step function, as shown in Fig. 19d, we found that the pattern of a periodic surface could be computed in terms of that for a single period uniformly illuminated and that for a series of narrow slits non-uniformly illuminated. In case the antenna is paraboloidal, as we shall assume here, it suffices to consider only the reflected wave moving directly back along the axis; and thus, the envelope of  $|w|$  versus  $\theta$  will be, very nearly, the diffraction pattern of a single period. The maxima of the curve itself, as opposed to the envelope, will occur at values of  $\theta$  given by the curves of Fig. 65, or by the equation

$$\theta = \sin^{-1} [n\lambda/(2L)] \quad (n = 0, 1, 2, \dots) \quad (59)$$

as we see upon applying (48) to the case in hand.  $A'' = -(2nL/\lambda) \sin\theta$ , phase front of a paraboloid is practically uniform. The minima are at points about half way between the maxima, and will approach zero as the change in  $f(x)$  from one period to its neighbor approaches zero. When added to the equation of the envelope, Eq. (59) adequately specifies the complete pattern,  $|w|$  versus  $\theta$ , of the non-uniformly illuminated surface except for a proportionality constant; and thus, to the extent that the step-function approximation is valid, the primary illumination  $f(x)$  cancels out of the equations and need not be considered at all.

Proceeding now to the computation for the special surface of Fig. 21a, we use standard diffraction theory to obtain

$$|w| \propto \lambda^2 + 2AB \cos[(2\pi/\lambda)(d' \sin\theta - d'' \sin\theta)] + B^2 \quad (60)$$

giving the reflection at incidence  $\theta$  of a single period, Fig. 21b. The variables A, B,  $\rho q$  in (60) are defined by

$$\begin{aligned} p &= a+\theta, \quad q = b-\theta. \\ A &= (\sqrt{2}\pi d'^2) R \cdot (b) (\cot p) \sin(2\pi d'/\lambda) \sin p \\ B &= \text{same, } p \text{ replaced by } q, \quad d' \text{ by } d'' \end{aligned} \quad (61)$$

which Mr. Ellis has derived by letting  $a/\lambda F \rightarrow \infty$  in (53). From Fig. 65 we see that the three equations are substantially equivalent in the region with which we are concerned for application to radomes; in particular, (54) and the approximation based on (55) agree over the entire range with a maximum error of only about 3%. This result is especially gratifying in that the error in (55) is maximum when  $p = a$ ; for the error clearly increases as  $p$  decreases, and on the other hand  $p$  is never less than  $a$  in radome work.

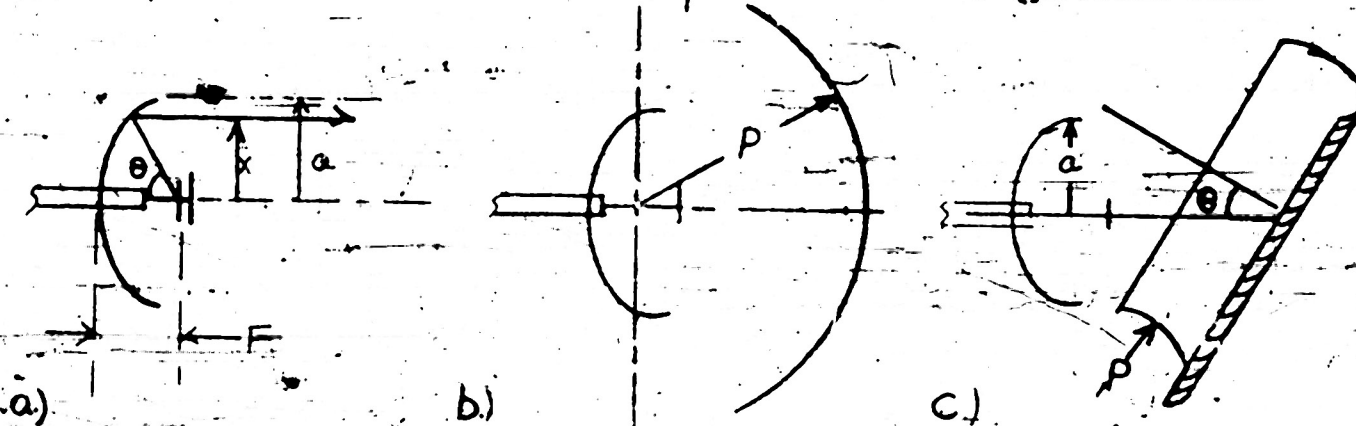


Fig. 20. Antenna and Circular Cylinder

Upon combining (56) with the general theory of section 1 above, we approximately solve the more difficult situation of Fig. 20c, obtaining

$$|w| = 7R\sqrt{p}/[19.6 \exp(40^2 \ln 2/\pi^2)] \quad (57)$$

for the reflection produced by a circular cylinder of radius  $p$  into the line of a paraboloidal antenna of radius  $a$ . In this equation  $w$  is the full-width of the antenna's secondary power pattern at half power,  $\theta$  is the angle of inclination of the cylinder elements with the antenna axis,  $\lambda$  is the free space wavelength, and  $R$  is the reflection coefficient the cylinder would have if deformed into a plane sheet. The true secondary pattern corresponding to the illumination chosen here has a rather complicated but elementary equation; it is essentially the second order spherical Bessel function as we see by direct integration or by Ref. 8. For our present purposes, however, this function may be approximated with negligible error by a Gauss error curve, a simplification which was made in (52).

The approximation (56), which was used in the derivation of (57), is valid for all values of  $p$  encountered in work with cylindrical radomes. The only other case of importance is that for a plane sheet,  $p=\infty$ , which gives

$$|w| = 5R/[9 \exp(40^2 \ln 2/\pi^2)] \quad (58)$$

on the basis of the 'exact' equation, Eq. (53). We have thus obtained simple approximations whenever  $p$  is very large or fairly small; and the intermediate case, which involves non-elementary functions, is seldom found in practice.

(a) Circular Cylinders--In the typical paraboloidal antenna of Fig. 20a, the pattern of the feed may be taken as

$$\cos \theta \cos [(\pi/2) \sin^2 (\theta/2)] \quad (49)$$

which leads to

$$f(x) = \frac{x^2 - 4F^2}{(x^2 + 4F^2)^2} \cos \frac{\pi x^2}{8F^2 + 2x^2} \quad (50)$$

for the illumination across the aperture when one takes account of inverse-distance attenuation from feed to paraboloid. For our present purposes, we require accuracy only near the peak of this primary illumination, in which case (50) takes the simpler form

$$f(x) = 1 - 3x^2/(4F^2) + O(x/F)^4 \quad (51)$$

For most antennas, including all those used here, the diameter is adjusted in such a way as to give low illumination at the edge of the paraboloid, the value of  $x/F$  usually lying between 1.4 and 2. If we take  $\sqrt{8}/3 = 1.63$  as an average figure for this dimension, the illumination is exactly zero at the edge and (51) becomes, except for terms of the fourth-degree,

$$f(x) = [1 - (x/a)^2]^2 \quad (52)$$

an equation which has been shown by R. C. Spencer (Ref. 8), to lead to antenna gain, half widths and side lobes of the order of magnitude of those actually found in practice. While these quantities depend critically on  $f(x)$ , moreover the reflection in the line is relatively insensitive; for our present purposes, a large per cent error in  $f(x)$  is permissible provided only that the general shape near the peak is correct. Using this value for  $f(x)$  we obtain from Eq. (42) and Fig. 20b

$$|W| = [25R/(48a)] \left| \int_a^\infty [1 - (x/a)^2]^2 \exp(4\pi i \sqrt{p^2 - x^2}/\lambda) dx \right|^2 \quad (\text{in general}) \quad (53)$$

$$= [25R/(24a)] \left| \int_0^{4a} \cos(\xi) \exp(4\pi i p/\lambda) \cos \xi d\xi \right|^2 \quad (a=p) \quad (54)$$

where we assume  $\cos \theta \approx R(\theta) = R$ , a procedure which is justified near the center because of the near-normal incidence, while it is justified near the edge because of the small value of  $f(x)$  in this region (cf. above). For similar reason the approximation

$$S(x) = \sqrt{p^2 - x^2} = \text{const.} - x^2/(2p) + O(x^4/p^3) \quad (55)$$

is usually justified in practice, the deviation being large only in areas of low illumination. W. Ellis has expressed (54) in terms of Bessel functions, and (53), with approximation (55), in terms of Fresnel integrals. Since these functions are tabulated, the equations may readily be plotted and compared with the asymptotic formula

$$|W| \sim 25\sqrt{p}/(48\sqrt{2}a) = 25\sqrt{p}/(198) \quad (56)$$

centers being  $L$ , say, if the constants  $A, B, C$ ... wave arbitrary absolute values, as before, but linear variation of phase -

$$\begin{aligned} A &= A' \exp(i\lambda x) \\ B &= B' \exp(2i\lambda x) \\ C &= C' \exp(3i\lambda x) \end{aligned} \quad (47)$$

then the secondary pattern of the surface  $s(x)$  illuminated by  $f(x)$  will have maxima at values  $\theta$  given by

$$\theta = \sin^{-1} n\lambda x / (2\pi R) \quad (48)$$

and the only other minima are those of  $G(\theta)$ . This result is experimentally verified in the ensuing discussion.

A third general property, this time of somewhat different nature, is that the reflection into the line should be substantially independent of distance in the Fresnel region, while it should decrease as  $1/(d+b)$  in the Fraunhofer region, both properties being independent of the nature of the surface. Thus, all the results of Part III, Sections 1, 2 are valid for arbitrary surfaces; and indeed they may be used in the Fraunhofer region if the variation of  $d$  is not too large. Although one really obtains a spiral in this case, the pitch is rather small, so that the curve obtained for, say, a half-wave change in  $d$  is practically a circle. In any case, the mean diameter of the spiral quite accurately obeys the equations for diameter versus mismatch obtained on the basis of a constant reflection. This useful property, that many results on plane sheets at normal incidence may be extrapolated to arbitrary surfaces, is a consequence of the similarity of the aperture illuminations for different values of  $d$ , and has been repeatedly observed in practice. If is of particular significance in the sequel because it permits the elimination of two variables,  $r$  and  $\rho$ ; as in the case of the plane sheet at arbitrary incidence, III, 3, we may take  $r=0$  and cancel  $\rho$  by averaging the results for quarter-wave displacement.

2. Specific Examples--By the general methods described above one can estimate the reflection produced by several of the surfaces commonly encountered in practice. Most of these surfaces are cylindrical in the general sense, so that an approximate solution for the three-dimensional problem may be found with the two-dimensional treatment used here; and thus, there is no question of multiple integration. This depends upon the fact that the primary illumination of most antennas, in the region with which we are concerned, may be represented as the product of two functions, one of  $x$  alone and one of  $y$  alone, so that there is a property analogous to cylindrical symmetry for the antenna also. Though it involves the neglect of all plane waves whose wave-fronts are not parallel to the axis of symmetry, this reduction of the number of dimensions has led to agreement with experiment in the foregoing sections, and it may therefore be assumed to be more or less accurate in the general case. We remark in passing that the case of circular symmetry, which is found, for example, with the spherical portion of a radome, may also be expressed in terms of only one variable, though it will not be considered here. With these preliminaries, we proceed to a discussion of three surfaces which are of considerable importance in the theory of radomes, viz., circular cylinders; corrugated surfaces; and parallel strips.

where  $F(x)$  is any complex function,  $A, B, C, \dots$  any complex constants, then the diffraction pattern of the surface illuminated in this way will be given by

$$g(\theta) = G(\theta) \cdot H(\theta) \quad (45)$$

where  $G(\theta)$  is the diffraction pattern for a surface  $s(x)$  illuminated by  $F(x)$ , while  $H(\theta)$  is the diffraction pattern for the function  $h(x)$ . (Fig. 19c).

$$\begin{aligned} \Delta x \cdot n(x) &= A && \text{(for the least } x \text{ in } s) \\ &= B && \text{(for the least } x \text{ in } b) \\ \dots & \dots & & \dots \\ \Delta x \cdot h(x) &= C && \text{(elsewhere)} \end{aligned} \quad (46)$$

The proof of this is the same as that for the ordinary convolution theorem, to which the present result in fact reduces whenever the intervals  $a, b, c, \dots$  are equally spaced, the constants  $A, B, C, \dots$  are all equal, and either  $s(x)$  or  $f(x)$  is constant. It is believed truly no theorem of just this type is true, for functions more general than those here considered, which must of course satisfy the usual requirements for Fraunhofer theory in addition to the ones explicitly stated.

The relevance of this result to the present discussion is indicated in Fig. 19d, where the illumination across the aperture is approximated by a step function. The approximation may be made in the manner indicated, with  $f(x)$  constant over a period of  $s(x)$ . Whenever this period is not too large compared to the diameter of the antenna; and with such an illumination, it is clear that all the conditions leading to (45) are fulfilled. Thus, for periodic surfaces, the function  $G(\xi)$  of page 29 may be approximately computed as the product of the antenna pattern,  $g(\sin \theta)$ , by the diffraction pattern of a single (period) of the surface uniformly illuminated; and such a computation is considerably simpler than direct integration of  $f(x) s(x)$ .

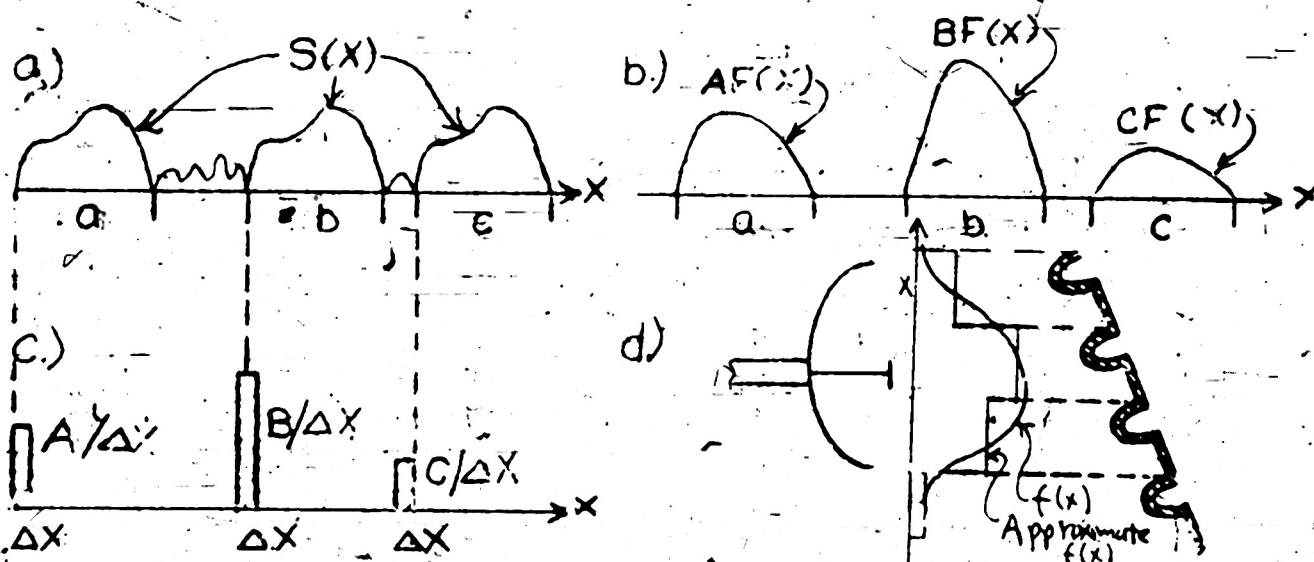


Fig. 19 Special Illuminations and Surfaces

Another result of this nature is the following, which is also a generalization of a well-known theorem and proved by the same method: Suppose the intervals  $a, b, c, \dots$  of the foregoing discussion are equally spaced, the distance between



Fig. 19 - Reflection versus angle for a cylindrical surface.

In the derivation it was not assumed that the antenna is paraboloidal or that it has an especially narrow pattern; and that such restrictions are in fact unnecessary is indicated by Fig. 19a - where the result is found to persist in the case of a csc<sup>2</sup> antenna. We remark in passing that the measured (S/R)<sup>1</sup> decreased rapidly from a maximum of only about 1.2, in several cases, and the experimental errors are correspondingly large. Whenever the reflection is this small, this is indicated on the curves.

A second result is that the well-known convolution theorem of optics is also valid for a certain type of non-uniform illumination, which frequently approximates the general illuminations actually occurring in practice. Suppose the equation of the surface,  $s(x)$ , is identical in the intervals a, b, c, ... as shown in Fig. 19b, so that we have

$$s(x) = S(x) \quad (x \text{ in } a, b, c, \dots) \quad (43)$$

$$= \text{anything} \quad (\text{elsewhere})$$

where  $S(x)$  is any function. If the illumination of the surface  $f(x)$  satisfies the similar condition (Fig. 19b)

$$\begin{aligned} f(x) &= A F(x) && (x \text{ in } a) \\ &= B F(x) && (x \text{ in } b) \\ &= C F(x) && (x \text{ in } c) \\ f(x) &= 0 && (\text{elsewhere}) \end{aligned} \quad (44)$$

discussed above and in Ref. 4. Lead to;

$$|w| = \left\{ \int_{-ay_2}^{ay_2} f(x) R [\tan^{-1} s'(x)] \exp(4\pi i s(x)/\lambda) dx \right\} \div \left[ a \int_{-ay_2}^{ay_2} |f(x)|^2 dx \right]^{1/2} \left\{ \frac{\left| \int_{-ay_2}^{ay_2} f(x) dx \right|}{\left[ a \int_{-ay_2}^{ay_2} |f(x)|^2 dx \right]^{1/2}} \right\}$$

for reflected amplitude in terms of the primary illumination  $f(x)$ , the equation of the surface  $s(x)$ , and  $R(\theta)$ , the reflection coefficient of the sheet at incidence  $\theta$ . The first factor gives the amplitude of the plane wave moving directly back toward the antenna along the axis; the second gives the fraction of this plane wave which is actually received and carried down the line; and the integral in the denominator gives the total incident power, as before. This expression differs from the more elaborate equations obtained above in that here we assume only one wave to be of importance, viz., that traveling straight back along the axis, whereas, in (34), (36), (40) and (41) we took account of all waves, allowing each one to enter the line with due regard for the variable receiver sensitivity. It is necessary, therefore, that the receiver sensitivity decrease very rapidly with angle, before (42) may be used with any confidence; the antenna must have a sharp pattern, or, which is essentially the same thing for our present purposes, it must act as a lens does, in an optical system, when it moves the image to infinity. In fact, the antenna pattern must not only be sharp, but it must be sharp compared to that of the surface itself; for otherwise the effect of decreased receiver sensitivity would sometimes be more than offset by the increase in reflected power. In this case the contribution of the plane wave which we retained might easily be less than that of those which we neglected, and the invalidity of the theory for such circumstances is apparent. An example of this is found for the simple case of a plane sheet, in which the reflected pattern is just as sharp as that of the antenna. Eq. (42) indicates that the reflected amplitude will be proportional to  $\sqrt{P(\theta)}$ , in this case, whereas both theoretically and experimentally we have found the correct result approximately equal to  $P(\theta)$ . For this reason (42) must be used with a certain diffidence, though it was suggested by methods that are frequently found in optics.

Before proceeding to specific surfaces, we mention a few rather general results which will be found useful in the subsequent discussion. In the first place, if  $f(x,y)$  is the complex illumination of the antenna aperture, now assumed two-dimensional as shown in Fig. 18a, then this illumination may sometimes be expressed as the product of a function of  $x$  alone and a function of  $y$  alone. Now, whenever this is the case, a graph of reflection versus angle for a cylindrical surface will be approximately proportional to the same for a plane sheet, provided the angle is small and provided the axis of rotation is chosen as indicated in Fig. 18c. To see this, we write Eq. (34) for the two-dimensional case, which involves an integration with respect to  $y$ . With the assumed character of  $f(x,y)$ , however, the double integral becomes the product of two integrals, so that the final result is essentially equivalent to (34), except for a constant factor. Similarly, for the cylindrical surface the two integrals may again be separated, though the constant unfortunately involves  $\theta$ . This dependence on  $\theta$  may be neglected, however, whenever the product  $(1-\cos\theta)$  (maximum deviation of surface from a plane sheet) may be neglected, which is practically always the case in practice. Thus, the deviation from a plane sheet becomes large only near the edges of the aperture, for which the illumination is small; and moreover,  $\theta$  is assumed only slightly different from zero. Verification of this theoretical result is given in Figs. 54-61, where we see that it is fairly accurate for a wide variety of cylindrical surfaces, the cross-section of which is indicated in each case.

In the case of the  $\csc^2$  antenna, for which the theory is clearly invalid, we obtain a large discrepancy; but in most of the other cases there is agreement within ten or twenty per cent. The gain factors  $f$  were determined in cooperation with R. Hiatt.  $f_1$ , having been measured in a different location from and independently of  $f_2$ . The product  $t\bar{t}$  was obtained by the equation

$$t\bar{t} = \frac{\text{average reflection in line with } \theta=0}{\text{reflection coefficient of material}} \quad (39)$$

which follows without further approximation from (8) and (37).  $(t\bar{t})_1$  was found with a metal sheet,  $R=1$ , while  $(t\bar{t})_2$  is given by a similar measurement with plexiglass, the reflection  $R$  being computed theoretically from independent measurement of the constants of the material. For determining the reflection in the line, the precautions described for the above experiment on mismatch were observed, whereupon a complete curve of reflection versus  $d$  was taken for a range of about forty centimeters in steps of one centimeter (cf. Fig. 39). The average of the curve was then found by integration, omitting the portion affected by inverse-distance attenuation; and this average was substituted in (39).

#### IV--Arbitrary Reflecting Surface

1. General Theory--Methods similar to the foregoing, which were helpful in the case of a plane sheet, may be used to estimate the reflection of an arbitrary surface into an antenna of known characteristics. Thus, if  $G(\xi)$  represents the amplitude of the wave reflected in direction  $\xi$  when the surface has the illumination produced by the antenna, we may write

$$|w| = \int_{-\pi/2}^{\pi/2} g(\xi) g(\sin \xi) (1+\cos \xi) d\xi + \int_{-\pi/2}^{\pi/2} |f(x)|^2 dx \quad (40)$$

In analogy to the result obtained above by the procedure suggested in Fig. 17c. The function  $G(\xi)$  may be computed by the usual methods for Fraunhofer diffraction. Similarly, the procedure suggested in 17d leads to

$$|w| = \int_{-\pi/2}^{\pi/2} \int_{-\pi/2}^{\pi/2} g(\sin \theta) G(\theta, \xi) g(\sin \xi) (1+\cos \theta) (1+\cos \xi) d\theta d\xi + \text{same} \quad (41)$$

where  $G(\theta, \xi)$  is the plane-wave development of the reflected field when the surface is illuminated not by  $f(x)$ , but by a plane wave of amplitude unity, traveling in direction  $\theta$ . In this case the initial integration for  $G$  is usually simpler, while the final integration is more complicated, than was the case for (40). In expressions of this type we have considered only the two-dimensional case, the extension to three dimensions being made, essentially, by using double instead of single integrals.

The foregoing equations are not only of doubtful accuracy, as are many in this section, but they lead to integrals that can rarely be expressed in terms of elementary functions. In case the antenna is a paraboloid, however, one may sometimes use the procedure suggested in Ref. 4. The illumination across the surface is taken as equivalent to that across the antenna aperture except for phase, and it is assumed that the paraboloid is large enough to permit the approximations of Fraunhofer theory. These assumptions, which are

the apparent value of  $\tau$  decreases as the secondary power pattern of the antenna for small angles of incidence. This conclusion, which follows from the theory of this section, is experimentally verified in Fig. 4 for the case of a transmitting paraboloid. Since the variation is sinusoidal, and since the period is  $\lambda/2$ , the effect may be cancelled by taking the average of two measured reflections for which  $\tau$  differs by  $\lambda/4$ . In this way one obtains the result that would have been found with  $\tau = 0$ . The dependence on  $r$  is likewise the same as for the case of normal incidence; not only does one obtain a circle, but the radius varies as predicted by Eqs. (22), (25). In the Fraunhofer region, the effect is still similar to that for  $\tau = 0$ . It suffices, then, to consider only the case of a matched line,  $\tau = 0$ , and to eliminate the effect of  $\tau$  by quarter wave displacement as described above.

Turning now from theoretical to experimental results, we note from Figs. 51-56 that the amplitude reflection ~~versus~~ angle indeed approximates the secondary power pattern near the peak of the curve for a wide variety of radiating systems. That the result is substantially independent of distance to the antenna is verified in Fig. 51, while the behavior of antennas other than paraboloids is illustrated in Fig. 54. The data for these figures were taken as described above, viz., for a given angle of incidence two measurements of the standing wave ratio were made with a quarter wave displacement of the sheet and each plotted point represents the average of these two measurements. The precautions for initial mismatch, pulling, and reflection from the surroundings were similar to those described in connection with Fig. 47. To complete the experiment, the secondary pattern was found by the usual methods, three curves having been taken in two different locations for one antenna to check the reproducibility of the measurement. The anomalous effects noted when a metal sheet is placed near an antenna are illustrated in Fig. 55; and even here there is agreement with theory in the region for which the theory is supposed to be valid, viz., near the peak.

Proceeding to the question of phase, we find by methods similar to those used above that the phase should be substantially constant as the angle is varied, a conclusion which is corroborated by the curves of Fig. 57. Similarly, the phase should theoretically be a linear function of distance, a displacement of the sheet equal to one wavelength in air leading to a displacement of the minimum position which is equal to one wavelength in guide; and this conclusion too is confirmed by experiment (Fig. 58). A final result which may be compared with experiment is that for the  $\tau$ -factor, Eq. (38). Here too the experimental agreement is reasonably good, for orders of magnitude, as we see by the following table:

Table 1 - Comparison of Antenna  $\tau$ -Factor with Reflection into the Line at Normal Incidence

Antenna	$f_1$	$f_2$	$(t\tau)_1$	$(t\tau)_2$	% Error
8"x 2 "f	0.69	0.73	0.67	0.70	3.6
12"x 3.6"f	.65	.65	.70	.69	6.5
18"x 5.4"f	.55	.55	.65	.66	1.8
24"x 7.2"f	.58	.60	.69	.68	1.4
30"x 7.5"f	.49	.50	---	.70	29
30"x 9 "f	.58	.58	.76	.77	2.6
30"x10.6"f	.57	.57	---	.76	25
30"x10.6" f $\csc^2$	.22	---	---	.50	56
cut paraboloid					
35"x13" aperture	.61	.60	---	.64	5.5

so that amplitude reflection versus  $\theta$  is given by the convolution of the secondary amplitude  $f(\theta)$  with its complex conjugate.

Eq. (35) may also be derived as follows: The plane wave leaving the antenna in direction  $\xi$  is reflected from the sheet at an angle  $\theta - \xi$  (Fig. 17a). The amplitude of this wave is (33) with  $\theta$  replaced by  $\xi$ , and the receiving sensitivity of the antenna for a wave traveling in any direction is given, as above, by the conjugate of the transmitting pattern. Hence, the net contribution to the line from this single wave is

$$(\text{const}) \cos(\xi - \theta) g(\sin\xi) [1 + \cos(\theta - \xi)] R(\xi - \theta) g(\cos\xi) \quad (36)$$

while the total received power is the integral of this from  $-\pi/2$  to  $\pi/2$ . Whenever  $\theta$  and  $\xi$  are sufficiently small, the expression reduces to the conjugate of the integral in (35), so that the absolute values are equal.

Upon applying a well-known relation for the convolution in terms of Fourier transforms, we obtain

$$|W|^2 R \left| \int_{-\pi/2}^{\pi/2} [f(x)]^2 \exp(4\pi i x/\lambda) dx \right|^2 \quad (\text{same}) \quad (37)$$

as an alternative form of (35). Thus, if we compute the secondary pattern  $P(\theta)$  for an amplitude illumination equal to the original intensity illumination then  $|P(\theta)|^2$  gives reflection versus  $\theta$  for a plane sheet whenever  $\theta$  is sufficiently small. Hence, reflection versus  $\theta$  should be symmetrical. Whenever incidence is normal one obtains

$$|W|^2 = (\text{const}) R \quad (38)$$

so that the reflection is proportional to  $|W|$ , as it must be with our assumptions. For the case of a paraboloidal antenna there is reason to suppose that the constant in (38) is approximately equal to the  $f$ -factor of the antenna, that is, to its actual gain divided by that for uniform illumination, and this conclusion is briefly investigated below. It is clear, incidentally, that this constant is identical with the product of  $t^2$  of the foregoing pages.

The results just obtained appear to be in contradiction to those noted above for the case of a paraboloid, since the integral (35), or its equivalent (37), is not in general equal to  $P(\theta)$ . If the secondary pattern is narrow, however, it may be approximated near the peak by a Gauss error curve, the deviation being completely negligible for the first one or two decades. Now the Gauss error curve,  $\exp(-ax^2)$ , does lead to  $P(\theta)$  for infinite limits of integration, as may be readily proved by either (37) or (35). If the pattern is even moderately narrow, as we assume, the integral converges rapidly, so that approximate equality persists for quite moderate values of the limits. From this we obtain the general conclusion that any antenna whose primary or secondary pattern fits a Gauss error curve near the peak will satisfy the condition first derived, viz., a plot of amplitude reflection versus angle will be proportional to the secondary power pattern.

Because of the highly approximate character of the theory, much of which amounts to little more than conjecture, it is clear that adequate experimental confirmation must be obtained before any of these results may be regarded as reliably established. In conducting such an investigation, however, we must briefly consider the effect of  $r$  and  $R$ , which have been neglected up to now but which may introduce large experimental errors none the less. The effect of  $r$  is to produce a sinusoidal variation similar to that noted above at normal incidence, though in general the amplitude is considerably reduced; indeed,

Having briefly considered the case of a paraboloidal antenna, we pass to the general case in which the antenna is unrestricted. By the reasoning suggested in Ref. 4 we find that the amplitude illumination of the plane sheet is approximately equal to that of the antenna aperture, provided it is in the Fresnel region and provided also that there are no large discontinuities in the illumination at the edges. Under the same conditions, there is a linear phase difference between the two illuminations, given by the distance from the sheet to a plane perpendicular to the axis (Fig. 17c), so that one may write

$$\text{illumination of sheet} = f(y \cos\theta) \exp(-i(2\pi y/k) \sin\theta) R(\theta) \quad (20)$$

where the complex function  $f(x)$  is the illumination across the antenna aperture and  $R(\theta)$  is the reflection coefficient of the sheet at incidence  $\theta$ . Upon taking the Fourier integral, as usual, and substituting some variable of integration  $\xi$  for  $y \cos\theta$ , we may express the plane wave traveling toward the antenna in direction  $\xi$  as

$$(\text{const}) R(\theta) [1 + \cos(\xi - \theta) \sec\theta] e^{i[\sin\theta \sin(\xi - \theta)] \sec\theta} \quad (31)$$

If  $g(u)$  is defined by

$$g(u) = \int_{-\infty}^{\infty} f(x) \exp(2\pi i u x/k) dx \quad (32)$$

The secondary pattern of the antenna is, in amplitude,

$$(\text{const})(1 + \cos\theta) g(\sin\theta) + \left[ \int_{-\infty}^{\infty} |f(x)|^2 dx \right]^{1/2} \quad (33)$$

when it is transmitting, the conjugate of this when it is receiving. Thus, upon returning into the line, the plane wave (31) is reduced by the conjugate of (33), so that the total contribution of all waves reflected back into the line from the sheet takes the form

$$(44) = \frac{R(\theta) \int_{-\infty}^{\infty} f(x) \exp[i(2\pi x/k) \cos(\xi - \theta)] (1 + \cos(\xi - \theta) e^{i[\sin\theta \sin(\xi - \theta)] \sec\theta}) g(\sin\theta) dx}{(\text{const}) \int_{-\infty}^{\infty} |f(x)|^2 dx} \quad (34)$$

when divided by the amplitude of the incident wave. It is clear that this result cannot be legitimately applied to antennas with very wide beams, or to sheets making a large angle with the system axis; and on the other hand when  $\xi, \theta$  are small there is considerable simplification, in that the reflection  $R$  may be taken as constant, and the obliquity factors may be omitted. The latter error is always, the former usually, of the order of  $\xi^2, \theta^2$ . We assume a pattern so narrow that  $P(\xi)$  is negligible for  $\xi$  differing appreciably from zero with the result that the limits of the integral may be assumed much smaller than  $\pm \pi/2$ ; and we further assume  $\theta$  to be small, which is not only necessary for the validity of the theory, but corresponds to the case of the greatest practical importance (cf. above). With these assumptions (34) takes the simple form

$$|\omega| = R \left| \int_{-\pi/2}^{\pi/2} g(2\theta - \xi) g(\xi) d\xi \right| \frac{1}{(\text{const}) \int_{-\infty}^{\infty} |f(x)|^2 dx} \quad (\xi \neq 0) \quad (35)$$

where it was found that Fraunhofer theory may sometimes be used even when close to the antenna, the procedure being closely analogous to the use of Fraunhofer diffraction in the optical problem of the spectroscope, for which one is really working in the Fresnel region of both lens and grating. The validity of such an approach depends on the selective action of the lens, which emphasizes parallel rays in much the same way as they are emphasized when image and object are far apart; in other words, the lens moves the image to infinity. It is clear, then, that the proposed extension of such a procedure to the problem at hand will be valid only for a paraboloidal antenna, and that it may be unjustified even in that case unless the antenna is large compared to the wavelength. To the extent that this type of reasoning is valid, however, one may say that the conclusion suggested by Fig. 16 is correct for any paraboloidal antenna (i. e., any antenna giving a plane phase front) whether or not the sheet is in the Fraunhofer region as there assumed.

Besides this direct application of the method of images, it is possible to reason as follows. The electric field across the aperture may be developed in a series of plane waves, the amplitude of the wave traveling in direction  $\theta$  perpendicular to the sheet being proportional to  $\sqrt{P(\theta)}$ , the amplitude of the secondary pattern in that direction. This wave is then reflected back toward the antenna, as shown in Fig. 17a, still traveling perpendicular to the sheet. Upon entering the line it experiences a reduction proportional to the antenna sensitivity for receiving a plane wave from that direction; and by the reciprocity theorem, this sensitivity is again proportional to  $\sqrt{P(\theta)}$ . The net result is that the received amplitude is proportional to  $\sqrt{P(\theta)} \cdot \sqrt{P(\theta)}$  which equals  $P(\theta)$  as before. Although somewhat more cumbersome than the original derivation, these two methods lend themselves more readily to generalization, and also suggest the probable nature of the discrepancy between exact theory and the result just described. Thus, since the paraboloid has only a finite aperture the received pattern will not be infinitely narrow; and hence the plane waves making a slight angle with the one directly reflected will also contribute somewhat to the received power. (Fig. 17b). Since all functions involved are assumed continuous, these neighboring waves will presumably differ only slightly in phase, so that they reinforce one another. We thus conclude that the observed reflection should be somewhat larger than predicted above, and that sharp minima in the secondary pattern will not be clearly reproduced in the reflection curve.

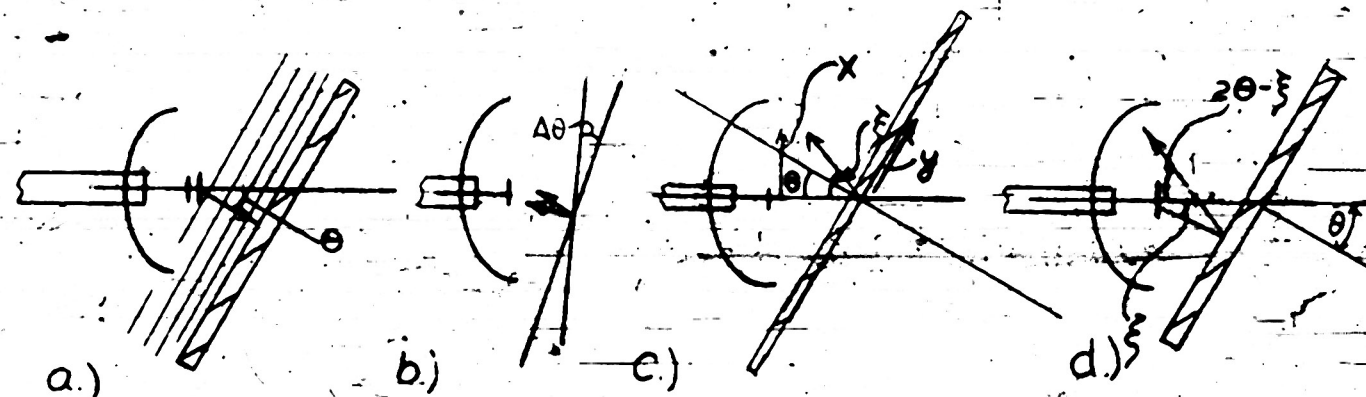


Fig. 17 Plane Wave Development

satisfied in practice. This type of argument is quite ridiculous, in the author's opinion, if the sheet is sufficiently far away; and the predicted variation should be found not only for the peak but also for the side lobes and other details of the pattern. Experimentally, however, any effects other than those in the immediate vicinity of the peak are quite unimportant, and indeed they are almost impossible to measure with accuracy. To see this, let us suppose that the reflection into the line for normal incidence has a typical value of, say, 0.2 in amplitude. If the angle of incidence be now changed to a value corresponding to the one-tenth power points of the secondary pattern, the measured reflection in amplitude will be only 0.02, which corresponds to a power standing wave ratio of 1.08. Similarly, a side lobe of 0.16 in the power pattern would be quite indistinguishable from one of, say, 2%; the former leads to a theoretical (SNR)<sup>2</sup> of 1/0008, while the latter gives 1.016. Thus, while details of the power pattern itself at a low energy level are both important and relatively easy to measure, such details are insignificant and difficult to measure in the corresponding case for reflection. To summarize, one may say that only those characteristics of the secondary pattern which are readily seen in linear, rather than logarithmic, representation are significant for the case of reflection; and henceforth the phrase secondary pattern will be used only in that special sense, which makes side lobes of say 5% practically equivalent to those of 0.01%. This difference between logarithmic and linear accuracy must be well understood, if the ensuing discussion is not to be seriously misinterpreted.

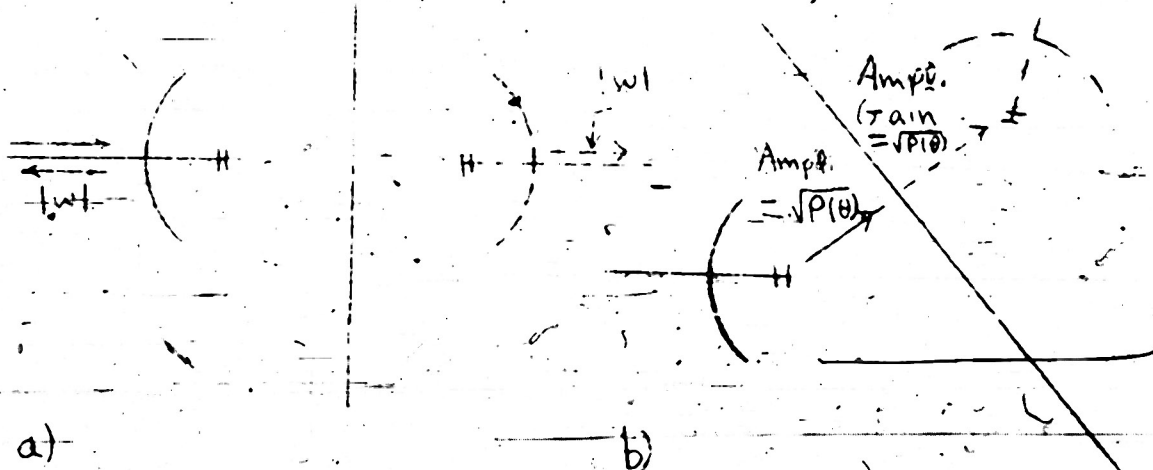


Fig. 16 The Effect of Non-normal Incidence  
for Fraunhofer Region

With these preliminaries we may consider whether the conclusion reached by inspection of Fig. 16 for the Fraunhofer region may also be applied to the Fresnel region, and if not, we may investigate the expressions appropriate to that case. To this end we use the reasoning described in detail in Ref. 4.

The antenna was then changed, so that the results should not be too specialized, and the whole experiment was repeated, this time with a metal sheet instead of a dielectric, and with nineteen complete curves instead of fourteen. The data were plotted in polar co-ordinates, as usual, the scale being so large that an angular accuracy of about  $\pm 0.05$  degrees could be obtained, together with negligible error in the plotted radius.

From these thirty-three curves one obtains verification of the more important aspect of the foregoing theory. In the first place, each one was quite accurately a circle, the deviation being well within the rather small experimental errors. Four of the circles obtained with the plastic sheet are shown in Fig. 47, for which the accuracy of the circularity is typical of that of the other curves. A second prediction is that the centers of the circles move along an ellipse with the prescribed focal points and shape, in the case of the plastic sheet, while the mismatch moves along a circle in either case (see Fig. 12 b). Unlike the other results derived on the basis  $\rho = 0$ , this one becomes inaccurate whenever  $\rho R$  is appreciable; the error introduced by  $\rho$  is not then absorbed by the equation as was the case for (22) and (25). This result, which agrees with the exact theory, would indicate that an ellipse should be found for the plastic sheet, but not for the metal; and experimentally, the centers behave as predicted. Still another theoretical conclusion checked by the present experiment is that radius versus distance to center should obey Eq. (22), a result which is confirmed by the curves of Fig. 50. We note that the scale of that figure is very large for the case of the dielectric sheet; the radii of the circles have the same length, with the scale used, as would be found on a Smith chart over six feet in diameter. The average deviation for the plastic sheet is 1.2%, while that for the metal is 1.8%, with maximum deviations of 2.3% and 6.2% respectively. These errors are well within the experimental accuracy, if we note that a small absolute deviation leads to a large percent error whenever the radius of the circle being considered is small. Further verification of the theory is given when we plot radius versus mismatch (Fig. 50). For the case of the plastic sheet both theoretical and experimental curves are practically indistinguishable from the curves for radius versus distance to center, and are therefore not shown; but for the metal sheet there is considerable difference between the two cases, as predicted by the theory, the agreement being again within the experimental error. We remark in passing that, though it does not impair the agreement between theory and experiment, the presence of  $\rho$  leads to a different theoretical radius for the case of a matched line from that obtained for the circle centered at the origin. This behavior is quite correct, since the two cases coincide, it has been rigorously proved, if and only if  $\rho R$  is negligible; that is, unless this condition is fulfilled, the circle will never be centered at the origin when the line is matched. This characteristic of the curves is therefore not a theoretical inconsistency and it leads to no difficulty in practice.

3. Arbitrary Incidence--In case the sheet is not perpendicular to the electrical axis of the antenna, as hitherto assumed, the theory must be somewhat modified. Temporarily assuming a matched line and a negligible value for  $\rho$ , we note by the method of images that a plot of amplitude reflection versus angle should be the same as the secondary power pattern of the antenna, whenever the sheet is far enough away for the image to be in the Fraunhofer region of the object (Fig. 16). It is also necessary that  $\theta$  be so small that the reflection coefficient of the sheet is essentially constant, a condition which is usually

Proceeding now to experimental verification, we note that considerable accuracy may be expected, as the phenomena at present under consideration lead to none of that magnification of error which has been so troublesome elsewhere. Thus, instead of examining the variation of measured transmission or reflection, we are now interested primarily in the quantity itself. With the experimental arrangement of Fig. 15a, the following procedure was adopted: First, the linearity of the amplifying system, including voltmeter, was checked independently with two different microvolters, the accuracy in both cases being within that of the microvolters. From the fact that the deviations from linearity did not occur at the same points in the two cases, it was concluded that the errors of the equipment itself are somewhat less than the errors observed, and therefore negligible in the proposed experiment. Next, the inner conductor of the standing wave detector was centered so accurately that the variation of the voltmeter reading, as the probe experienced its entire travel with a matched line, was less than  $\pm 0.2\%$ . The method of centering was that suggested in Fig. 15b, where we make use of that fact that a sidewise displacement of say,  $0.005"$  produces no measurable effect; i.e., the whole of the error is produced by the change in distance from probe to center conductor (cf. Ref. 7). Having considered the errors in the detecting system, we next verified that the lossy cable supplied sufficient isolation to lead to negligible pulling, the change in wavelength being less than  $\pm 1/4\%$  when the standing wave ratio was increased from 1.005 to about 3000 with several phases. Finally it was proved, by taking a curve of standing wave ratio versus transmitter position, that the net reflection into the line, from the screen and the rest of the room could not exceed 0.005% in power.

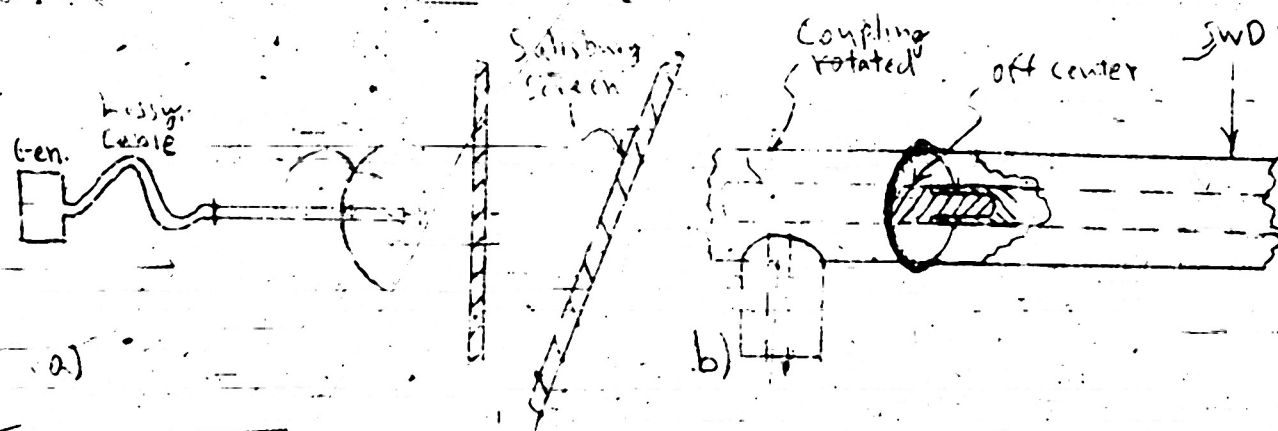


Fig. 15 Equipment for Investigating the Effect of Mismatch

With these preliminaries completed, the line was carefully matched and the standing wave ratio together with the minimum position was taken for nine equally-spaced positions of the sheet, the total travel being approximately a half-wave. Due care was exercised in adjusting the angle of incidence for maximum reflection, and in arranging that this angle would be accurately maintained throughout the experiment. With the sheet removed, the initial mismatch was again measured, to insure that it had not changed, and the line was detuned, by varying one stub only to give a fixed mismatch which was accurately determined both in phase and amplitude. The procedure just described for a matched line was then repeated in its entirety whereupon the mismatch was again increased, and the whole process repeated until a total of fourteen complete curves, amplitude and phase versus distance, had been taken with different initial mismatches.

an exact instead of an approximate portrayal of the function. An extension of this type may be made in another way, viz.: instead of retaining the property that the real and imaginary parts of  $\omega$  shall be represented explicitly, we may insist that the angle  $\theta$  of Fig. 11c shall remain equal to  $2\pi d/\lambda$ . In other words, the line drawn from mismatch to a given point on the 'circle' will be the same, but the angle determining the position of this line will be proportional to the distance  $d$  between antenna and sheet, with due regard to the requirement of periodicity. The curve so obtained is given in polar co-ordinates by Eq. (16), if we take our origin at the point  $r \exp(i\pi)$ , and this curve has a few rather interesting properties of its own. In the first place, there is an axis of symmetry, though the curve is not an ellipse; and the width, as shown in Fig. 14a, is not only independent of  $f$ , but it is exactly equal to the diameter of the circle in the approximate vector diagram.

$$\text{width of curve} = 2Rt^2 \quad (27)$$

This width will vary according to Eq. (21) or (25), irrespective of the value of  $\rho$ . If we now replace the radius of the polar plot by its square, as in Fig. 14b, we find that the curve so obtained is an ellipse with the mismatch at one focus and with eccentricity  $2fR/(1+\rho^2 R^2)$ . The ratio of its axes is given by

$$(\text{major})/(\text{minor}) = (1+\rho^2 R^2)/(1-\rho^2 R^2) \quad (28)$$

while the ratio of maximum to minimum distance from fixed mismatch to curve is equal to

$$(\text{max. dist.})/(\text{min. dist.}) = (1+\rho R)^2/(1-\rho R)^2 \quad (29)$$

Thus the ratio of the axes is equal to the voltage standing wave ratio for a power reflection  $\rho^2 R^2$ , while the ratio of maximum to minimum distance is equal to the power standing wave ratio for an amplitude reflection  $\rho R$ . These properties are incidentally all applicable to the theory of transmission, by virtue of (17).

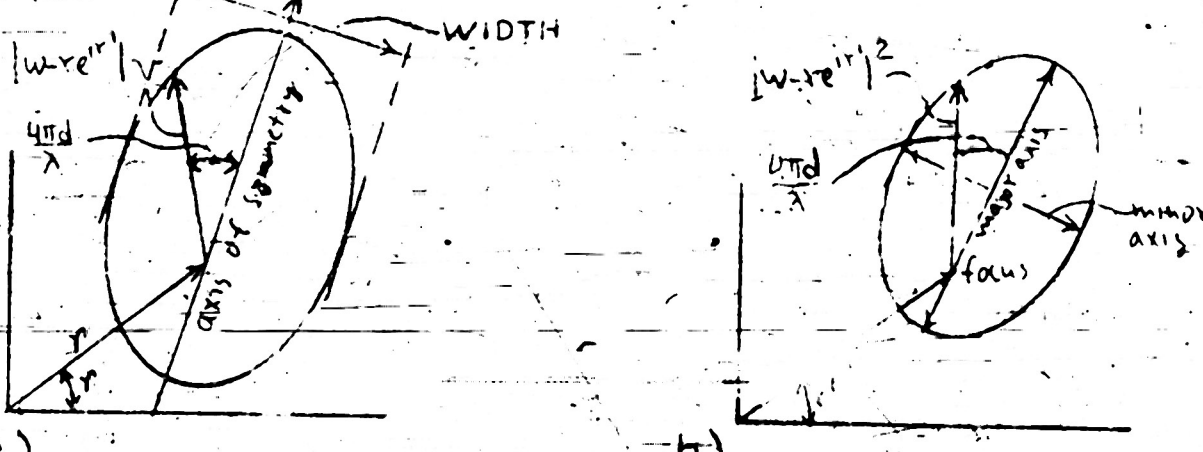


Fig. 14 Distance to Mismatch, or its Square, in Polar Co-ordinates

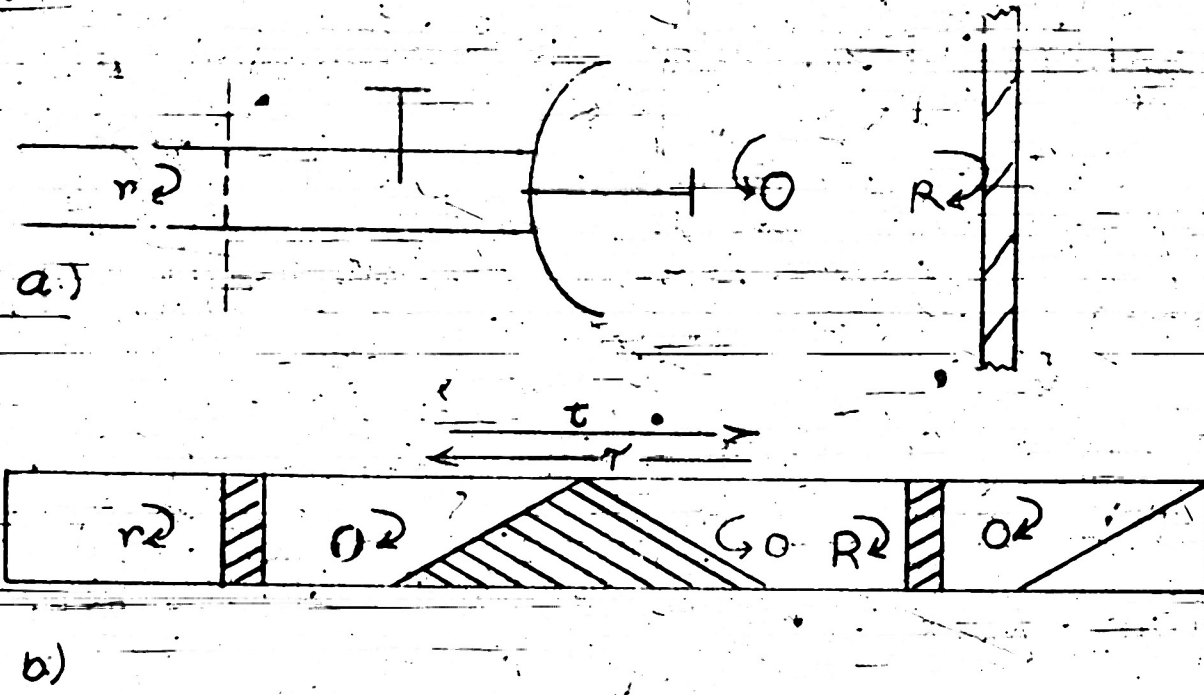


Fig. 13 Equivalent Construction when  $\rho = 0$

Having obtained the dependence of radius on distance to center, we proceed to estimate its dependence on distance mismatch. At first one would expect that the result should be given by (23), with a lossless tuner or other lossless source of reflection for  $r$ ; but this would be incorrect, as it implies, not that  $\rho \approx 0$ , but that  $\rho = r$ , an approximation which is quite unsatisfactory for our present purposes. We therefore assume  $f = 0$ , as before, and use Fig. 13 to obtain, by inspection,

$$a = a_0 (1 - r^2) \quad (25)$$

which result is again a rigorous consequence of our fundamental assumptions with no further approximations. As before, the fact that  $\rho$  is actually somewhat greater than zero leads to errors that are within the experimental error, the effect of  $\rho$  being quite negligible, as far as the radius  $a$  is concerned, if the mismatch  $r$  is held constant. That this should be the case is verified by the exact theory given above.

Upon combining (22) with (25) we obtain, after a considerable amount of algebra,

$$\frac{\text{initial radius } a \text{ for one sheet}}{\text{initial radius } a \text{ for another sheet}} = \frac{\text{final radius } a \text{ for first sheet}}{\text{final radius } a \text{ for second sheet}} \quad (26)$$

and thus, if the circles obtained with two different sheets have a certain ratio of radii for one mismatch  $r$ , then they will have the same ratio for any other mismatch.

Up to this point we have assumed that the complex reflection coefficient has been plotted in the Argand diagram or Smith chart so that the variable  $d$  is only implicitly represented. This procedure may be regarded as a sort of extension of the well-known vector diagram for small reflections, Fig. 11c, to give

which may also be obtained from the construction shown in Fig. 12c. Fig. 12b was suggested to the author by S. Silver while Fig. 12c is due to Rieke. It is easy to prove directly from the definition that the center of the circle in Fig. 12b moves along an ellipse whose focal points are at  $p$ ,  $q$  of the figure while the axes are equal to  $\sqrt{1-a_0^2}$  and 1, this being in marked contrast to the behavior of the mismatch point, which moves along a circle. As one would surmise from the assumptions, the present theory is considerably more accurate than the simple theory obtained above for small reflections, and experimental verification will be given in the ensuing discussion.

Eq. (22) was derived only for the special mismatch produced by varying one stub of a tuner, whereas in general the mismatch may be due to any arbitrary source of reflection. From the well-known properties of the reflection chart, however, one would surmise that the new radius should depend only on the distance to the center, the effect of variations in the phase  $r'$  being merely to move the circle around the origin. This conjecture, which would indicate that (22) is true in general, may be readily verified by the theory of Ref. 4, where we showed that (13), (14) take the forms

$$a = R \cdot \frac{1-r^2}{1-r^2 R^2} \quad (23)$$

$$c = r \cdot \frac{1-R^2}{1-r^2 R^2} \quad (24)$$

whenever the reflecting object leading to the fixed mismatch has zero loss. To apply this result to the case at hand, it is of course improper to assume that the antenna itself is lossless; and we therefore proceed as suggested in Fig. 13. Since the circle for a matched line is assumed to be centered about the origin, the situation of (13a) is precisely analogous to that of (13b) which in turn is equivalent to a lossless source of reflection corresponding to the tuner, or other device producing a mismatch, backed by a moving object whose reflection coefficient is  $Rt^2$ . This analogy, which is not an approximation for the assumed case  $\rho = 0$ , leads to (22) if we eliminate  $r$  from Eqs. (23), (24), using the fact that  $a_0 = Rt^2$ , and hence (22) is valid whenever the initial circle is centered at the origin. This condition amounts to assuming that  $\rho = 0$  independently of the tuner setting, and one would at first think, from Eq. (19), that the error is of the order of  $Rt^2 a$ . More careful investigation shows, however, that the error is considerably less than this, being completely negligible in practice; and indeed we have been unable to measure it experimentally. This reduction of the error is found because, with the result expressed in terms of distance to the center, the equation does not distinguish whether the displacement  $c$  is due entirely to  $r$ , or partly to  $r$  and partly to  $\rho$ ; in other words, a circle with given radius  $a$  and distance to center  $c$ , for  $\rho = 0$ , is practically unchanged if we set  $\rho > 0$  and readjust the initial mismatch  $r$  in such a way as to have the distance to the center again equal to  $c$ .

In practical work one is usually given the radius of the circle for matched line,  $a_0$ , together with the distance to the center point,  $r$ , or the distance to the center of the new circle  $c$ ; and it is required that the radius  $a$  be expressed in terms of these quantities alone. This requirement may be met with the aid of the foregoing theory but the expressions always involve  $\phi$ , which is an unknown function of the initial mismatch  $r$ . We therefore obtain approximate results by more elementary methods, using the exact theory to estimate the error. In the first place, the conventional vector diagram leads to the result shown in Fig. 11c, and, to the extent that this is valid, the center of the circle will coincide with the initial mismatch, while the radius will be the same as for a matched line. The error in this first result is of the order of  $r^2/R^2$  as we see by (18) while investigation of the type considered below shows that the error in the second result,  $a=a_0$ , is of the order of  $r^2$ . There is, incidentally, a further error in that equal increments of  $\theta$  are assumed to correspond to equal increments of  $\Delta n/\lambda$  whereas the true relation is given in (20); Here the error is of the order of  $r^2/R$ , and we thus obtain the general conclusion that the vector addition of reflections is valid if and only if  $r^2/R$  can both be neglected.

Having considered the case in which the reflections involved are very small, we proceed to a specialization of quite a different sort, viz., we assume that the mismatch  $r$  is obtained by varying the stub of a lossless tuner, the line having been matched to free space,  $r=0$ , for the initial position of the stub. We assume that the circle of radius  $a_0$ , obtained for a matched line, was centered around the origin; and we note that this circle will be translated directly upward, on an impedance diagram, as the stub setting is varied (Fig. 12a). To transfer this result from the impedance chart to the reflection chart used here, we use the facts that the transformation relating the two charts is analytic; so that tangent curves go into tangent curves; and that it is bilinear, so that circles go into circles. Upon adding other well-known properties of the transformation, we thus obtain the diagram of Fig. 12b for the new circle, with mismatched line, in terms of the original circle found when the line was matched. By elementary plane geometry we see that the new radius is given by the equation plotted in Fig. 49:

$$a = \sqrt{[1+a_0^2 - (1-a_0)^2 + 4a_0^2 c^2]/2a} \quad (22)$$

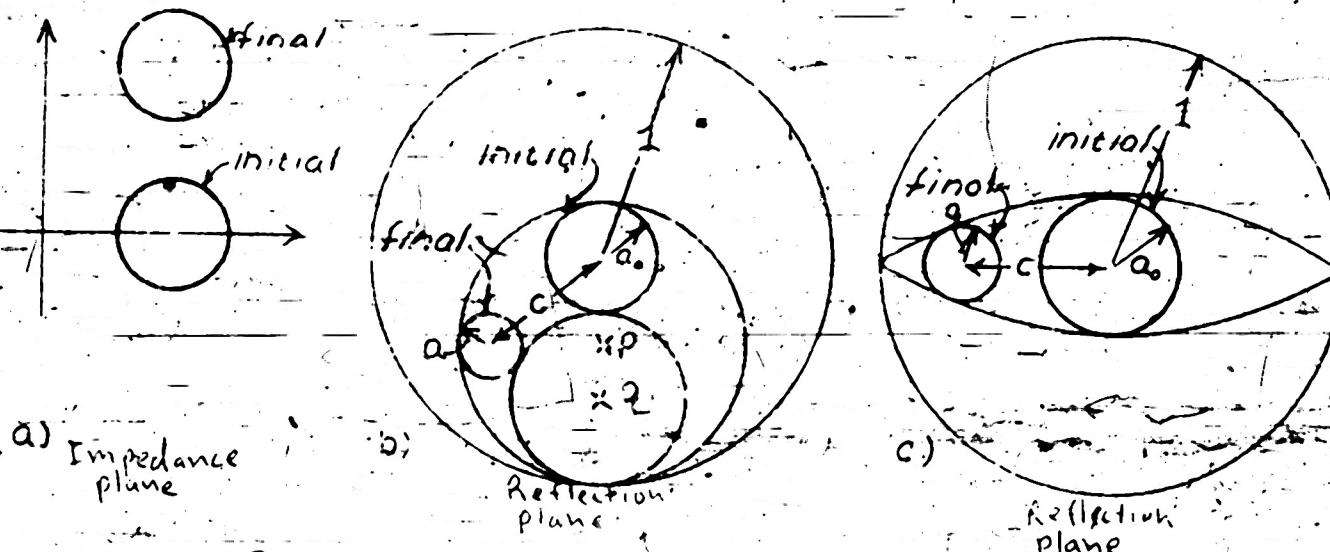


Fig. 12 Construction for Circle with Mismatched Line  
in Terms of Circle when Line is Matched

center to mismatch (Fig. 10) we have, independently of  $t, \gamma, t', \gamma', r, \rho$ ,

$$\sin \theta = \frac{(1-R^2) \sin(4\pi d/\lambda)}{1-2PR \cos(4\pi d/\lambda) + R^2} \quad (20)$$

which becomes

$$\frac{\sin \theta}{\sin(4\pi d/\lambda)} = \frac{(\text{distance from point to mismatch})^2}{(\text{distance from mismatch to center})^2} \quad (21)$$

$\frac{1}{RtY}$  same  
RtY radius

in terms of the geometrical quantities of the figure. Thus, if we take equal increments of  $d$  the experimental points will not be quite equally spaced on the circle, though the difference is negligible, as we shall see below, for ordinary practice. A final property is that the angle  $A = t' + \gamma' - r' - \rho'$  is equal to the angle between the line from mismatch to origin and that from mismatch to center, as shown in Fig. 11.

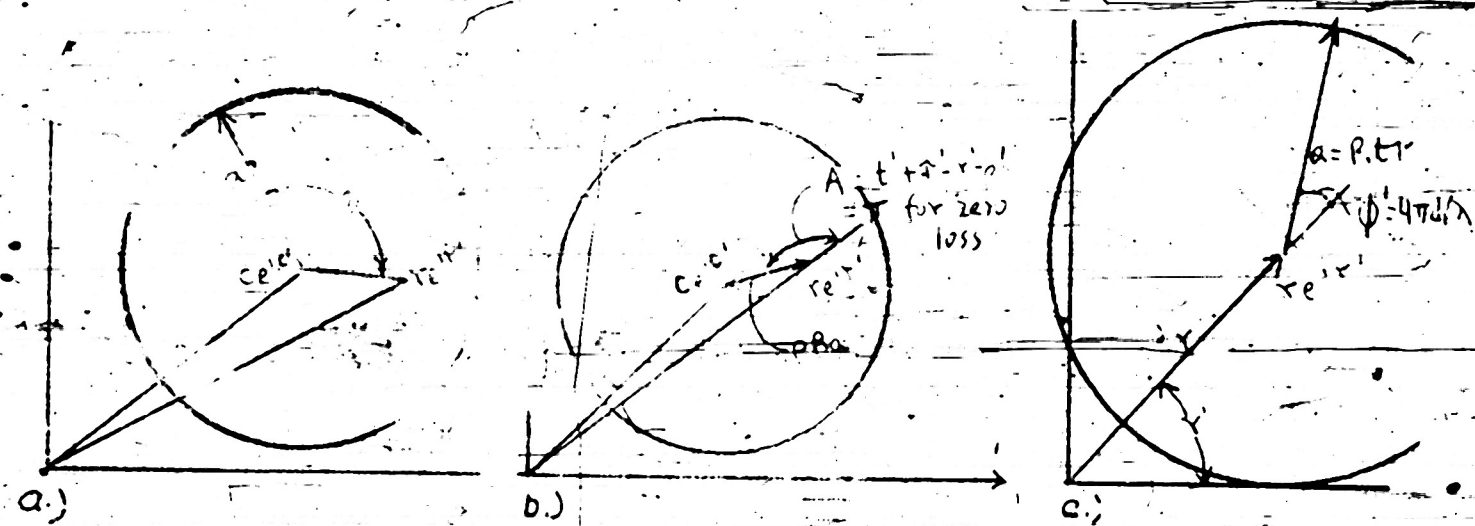


Fig. 11 Fundamental Angles, and Comparison with Conventional Vector Diagram

We remark in passing that the foregoing discussion does not assume the antenna to be a passive network; that is, besides being non-bilateral it may contain sources of EMF, provided only that the coefficients  $t, \gamma, t', \gamma', r, \rho$  exist and have values independent of  $d$  over the range considered. By making use of the fact that it is indeed passive, we obtain a number of general properties of the antenna itself, which properties are summarized in Ref. 4 and need not be repeated here.

and center

$$a = R\pi/(1-\rho^2) \quad (13)$$

where

$$c \exp(i\phi') = \exp(ir') [r - R \cos(i\Delta')] / (1 - \rho^2 R^2) \quad (14)$$

$$\Delta \exp(i\Delta') = \rho - t^2 \exp(i(t\pi + \Delta' - \phi)) = \rho - t^2 \exp(i\Delta) \quad (15)$$

Like most of the others given above, this result follows rigorously from our fundamental assumptions; in particular it is valid for a non-bilateral network, viz. that a circle is actually obtained has been abundantly verified in practice, the only exceptions occurring, as above, when we use a metal sheet very close to the antenna. A complete curve for this anomalous case is given in Fig. 48, in which it happens that an ellipse fits the data within the experimental error; but no general theory has been obtained. The more common situations of a dielectric sheet, or metal not too close to the antenna, are described in detail below; in particular, the accuracy with which the curve is a circle is illustrated by Fig. 67, where the maximum deviation corresponds to an error of only about 0.1mm. in estimating the minimum position. We note in passing that, if a plunger be moved in space, as in Fig. 67, the reflection in antenna II will move on a circle; and this result, unlike that just described, is a rigorous consequence of Maxwell's equations with no approximations whatever. The difference between the two cases is analogous to the situation noted above for reciprocity.

Besides this general property that the curve is a circle, a number of other results are derived in Ref. 4, which we re-state without repeating the proof. The notation there given is substantially the same as that used here, the only differences being that  $\beta$ ,  $x$  and  $c$  of Ref. 4 stand respectively for  $\Delta$ ,  $4\pi d/\lambda$  and  $c \exp(ic')$  of the present text.

In the first place, the circle will contain the origin if and only if  $r/R < \Delta$ , the case  $r=R\Delta$  corresponding to the case in which the circumference passes exactly through the origin. As a second general property we find that the distance from the fixed mismatch  $r \exp(ir')$  to the point on the circle obtained for a given  $d$  is equal to

$$|\omega - r \exp(ir')| = R t^2 / [1 - 2 R \cos(4\pi d/R) + R^2] \quad (16)$$

which is proportional to the total amplitude transmitted through the sheet, for that value of  $d$ :

$$|\omega - r \exp(ir')| = (\text{total transmitted power})^{1/2} R \sqrt{t} \quad (17)$$

The distance from the center of the circle to the fixed mismatch is given by

$$|\tau(\exp(i\phi) - r \exp(ir'))|^2 = R^2 t^2 / (1 - \rho^2 R^2) \quad (18)$$

or, in terms of the radius of the circle,

$$|c \exp(ic') - r \exp(ir')| = \rho R \sqrt{t} \quad (19)$$

Another property of the curve is found when we investigate the details of its dependence on  $d$ , viz., if  $\theta$  is the angle between the radius to the point and the line joining

(12), the constants being adjusted to give an exact fit at four values of  $d$ . In view of the experimental difficulties and the approximate character of the theory, the agreement is believed to be quite satisfactory and both the assumption as to attenuation and that concerning  $\lambda/2$  periodicity are adequately confirmed.

We remark in passing that there is a rather well-defined point at which the Fraunhofer theory, as opposed to the Fresnel theory, begins to agree with experiment. In connection with a different problem from that considered here, an approximate formula was derived by S. J. Mason for the distance  $d_c$  at which this transition is observed, viz.,  $d_c = A/\lambda$  if  $A$  is the aperture area and  $\lambda$  the wavelength. This result, derived in Ref. 6 for the case of uniform illumination, has been tentatively extended by Mr. Mason to the case of non-uniform illumination, for which the equation becomes  $d_c = fA/\lambda$ , where  $f$  is the factor of the antenna; i.e.,  $f$  is the ratio of its actual gain to the gain of a uniformly illuminated aperture of the same size. In applying this result to the case in hand, there is difficulty in deciding just what value of  $d$  shall be taken as zero, that is, in deciding on the precise location of the antenna aperture. This difficulty was met by taking the apparent origin of the rays as the point from which the distance should be measured, which apparent origin is given by the constant  $b$  of Eq. (11). With this understanding, the value of  $d_c$  is given by  $fA/\lambda - b$ , a result which agrees fairly well with experiment, as we see by the vertical lines drawn in Figs. 34, 40, 44, 45.

**2. General Case, Normal Incidence**--Proceeding now to the case in which the antenna need not be matched to free space, as assumed above, we find that the absolute value of  $\omega$  is considerably more complicated. If we retain the complex form, however, the theory can be expressed in comparatively simple terms; and the effect of  $r$  is readily separated from that of  $P$ , a distinction which is almost impossible to make if we use the absolute value alone.

With this complex representation the data take the form shown in Fig. 10, in which we plot amplitude of the measured reflection versus its phase in polar co-ordinates, the variable  $d$  not appearing explicitly on the curve. If the coefficients  $P, t, \tau$  are independent of distance over the range considered, it was proved by the theory of conformal transformations in Ref. 4 that the curve will always be a circle with radius

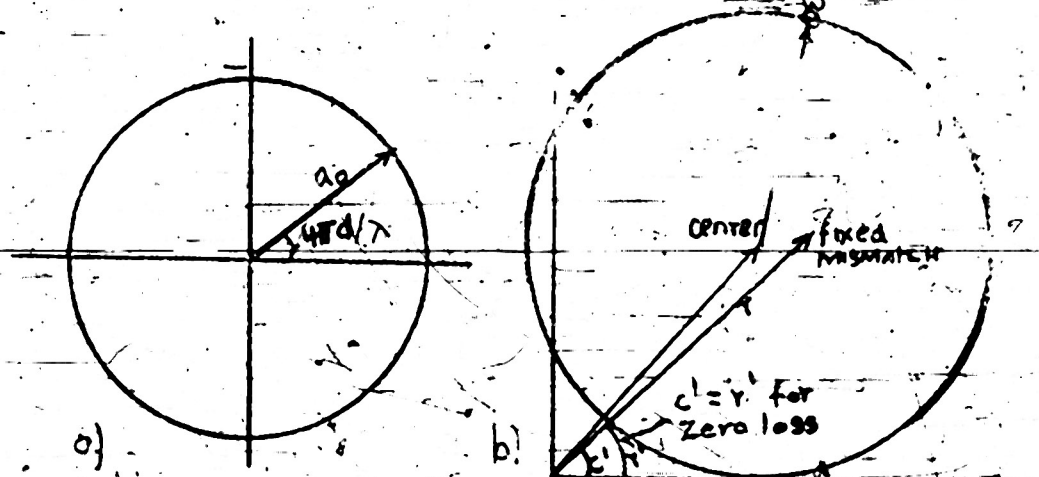


FIG. 10 Reflection in the Complex Plane

It has been assumed heretofore that the sheet is in the Fresnel region of the antenna, so that the transmission coefficients  $t, T$  are substantially independent of the distance  $d$  from antenna to sheet. In case this condition is not satisfied, the theory of images suggests that the reflection will be inversely proportional to  $d$ , measured from some suitable point, if  $d$  is sufficiently large. (See Fig. 3a). Thus, the reflection should be constant while the sheet is in the Fresnel region, and it should decrease as  $1/d$  when it is in the Fraunhofer region; a conclusion which is verified by the curves of Figs. 39, 40, 41, 45. Except for these curves were obtained in the usual manner; that is, a fixed value was given to  $d$ , whereupon the reflection was measured by an ordinary standing wave detector, the process being repeated with new values of  $d$  until the desired variation had been obtained. Fig. 40, however, was obtained as follows: After taking a complete curve of the type shown in 39, each group of points including both a maximum and a minimum was replaced by the average value of these extremes, the maximum or minimum of the curve itself being used whether or not it happened to coincide exactly with one of the points. The average so obtained was plotted as one point on Fig. 40; and thus, Fig. 40 gives a condensed version of ten curves similar to those of Fig. 39. In their original form, which took too much space for inclusion here, these complete curves all had the same general appearance as those of Fig. 39, and agreed equally well with the theory.

We have just seen that the curve does in fact decrease and that the distance for which this decrease first becomes apparent increases, as it should, with antenna size. For quantitative investigation, the theoretical curve for Fig. 46 and the envelope curves for the other figures were obtained from the equation,

$$\text{envelope} = a/(b+d) \quad (d \text{ large}) \quad (11)$$

where  $a, b$  are constants adjusted to give optimum fit. The constant  $b$  gives the effective center of the feed, that is, the point from which the rays appear to diverge; and hence it must be the same for both the upper and the lower envelope. This condition was satisfied in the curves in question, so that only one parameter,  $a$ , was adjusted to obtain a fit with the lower curve once the upper one had been found. Besides this agreement of the envelope, which corroborates our surmise that the reflection is inversely proportional to distance, we may obtain a more detailed theory by combining inverse-distance attenuation with the results of the foregoing pages. Thus, the apparent value of  $\rho$  for the Fraunhofer region, which is only a second-order effect in any case, may be assumed to decrease as  $1/d$  with the same effective center as that found by the above operation on  $|w|$ , an assumption which leads to the modified form of (7)

$$|w| = a[1+c \sin(4\pi d/\lambda + \phi)]/(b+d) \quad (d \text{ large}) \quad (12)$$

If we note that, for the Fraunhofer case,  $R$  is always small enough for the validity of (8). In this equation the constants  $a, b$  play the same role as in (11), while  $c$  accounts for the phases  $R, \phi$  and  $c$  is the effective antenna reflection appropriate to the Fraunhofer case. The sine term still has period  $\lambda/2$ , according to the simple theory here used, so that the distance between successive maxima or successive minima ought to be very nearly equal to a half-wave, even though the curve itself is not periodic. To verify these conclusions the data of Fig. 46 were obtained, in which the points are measured reflection versus distance in the Fraunhofer region of a horn, while the curve is theoretically computed from

As was the case for transmission, here too the predicted half-wave periodicity has been repeatedly noted in practice, the only exceptions occurring when a metal sheet is placed very close to the antenna, or when the sheet is in the Fraunhofer region, so that there is inverse-distance attenuation. In the former case the simple theory here developed could hardly be expected to apply; and in the latter, a modified theory which takes account of attenuation but still assumes a kind of half-wave periodicity leads to excellent agreement with experiment, as we shall see below.

Similarly, the variation is accurately sinusoidal if the reflection coefficient  $R$  is not too large; indeed, such variation has been observed in our work without exception whenever the reflecting sheet is a dielectric. For the case of a metal sheet, on the other hand, the predicted behavior is found only when there is a reasonable distance between sheet and antenna, the required distance becoming larger as the wavelength decreases. From the fact that such non-sinusoidal variation is quite accurately periodic, one would conclude that it is not due to the back lobe of the feed; and this conclusion has been proved by the use of a horn-antenna, for which no 'feed', or source of radiation other than the aperture, is present (See Fig. 45). Typical examples of sinusoidal variation are given in the top curves of Figs. 39 and 41 while the anomalous behavior noted with a metal sheet, especially at the shorter wavelengths, is illustrated in Figs. 41, 42. Similar examples are given, when  $d$  is small, in Fig. 39 and in 44, 45. From Fig. 43 it is clear that the slightest variation in the angle of incidence  $\theta$  produces a large change in the shape of the curve; and for that reason it is to be expected that the theory taking account of non-sinusoidal variation would be quite complicated. This critical dependence on angle is in marked contrast to the periodicity with distance, as we see by Figs. 41, 44 and more particularly by 43. We note in passing that the greater emphasis here given to the anomalous case is due to its greater interest; while only a few examples of sinusoidal variation are included, this is the case which is by far the most common in practice.

There are several other properties which may be readily checked by experiment, one of the most important being the fact that the average height of the curve should be proportional to  $R$  for a given antenna (Eq. (10)). Because of its particular relevance to reflection measurement, a special investigation of this property is made in Part V below, where we find it to be accurately verified in practically all situations of practical importance. It is analogous to the fact that average received power should be proportional to  $T^2$  for the case of a transmitting sheet (Part II above), and the verification of this property has likewise been deferred to the section on measurement, Part V. As for the other tests made above in connection with a transmitting sheet, it is clear that they too have their analogues; for the most part, in the case of reflection; but the sources of error are much more troublesome, so that the corresponding tests for this case would not be very reliable. Not only is there a large error due to the initial mismatch  $r$ , which cannot be reduced exactly to zero, but reflection measurement is more difficult than merely taking a receiver reading; and in addition, many results which were formerly of the first order in  $R$  become of the second order when we deal with reflection. This latter difficulty is obviated if we use a metal sheet, but then the theory does not always apply with accuracy; and on the other hand, the use of a dielectric sheet requires measurement of small variations in a reflection which is itself small. This difference between detailed reflection and detailed transmission phenomena is analogous to the difference between Fig. 5 and the other figures in the text of Part II. For these reasons we rely exclusively on transmission rather than reflection measurements, for details of the behavior of  $P$ .

Up to this point we have suggested an explanation for the observed dependence of received power on distance, and then tested the validity of the explanation by a number of experiments specifically directed to that end. Because the sheet is in the Fresnel region of the antenna, and because of the superficial similarity of the observed results to the well-known 'ripples' of diffraction phenomena, it would be natural to assume that the effects here considered are due to ordinary Fresnel interference, that is, to the interception of a varying number of zones on sheet or antenna as the distance is varied. Such a conclusion would be particularly natural because, in taking transmission versus sample size, one encounters effects that are unquestionably due to diffraction of the usual type; and in certain experiments involving metal sheets, one notes irregular effects which suggest Fresnel interference. Nevertheless, it is the author's opinion that the existence of an equivalent reflection coefficient for the antenna, as assumed above, represents a more accurate approximation to the actual mechanism; not only is this assumption fairly consistent with experiment, but it has been considerably more fruitful in predicting simple results. Moreover, no explanation based on ordinary interference has been obtained which agrees with the half-wave periodicity so consistently observed, with the dependence on tuning, or indeed with most of the other experiments just described. Since additional verification is found in many of the results obtained below, much of the following discussion will be written as though the existence of  $\rho$  has been definitely established.

### III--Reflecting Plane Sheet

1. Matched Line, Normal Incidence--For the overall reflection into the line of antenna and sheet arranged as in Fig. 1a, the methods used to derive (1) lead to

$$W = r \exp(ir') + \frac{Rt'}{1-R\exp(i4\pi d/\lambda)} \quad (6)$$

which is also a rigorous consequence of our fundamental assumption concerning  $t, T, \rho$ , without additional approximations. When  $r > 0$  it is more convenient to use the complex value, interpreting (6) as a conformal transformation; and this is the procedure followed for that case in Part III, 2, below. When  $r=0$ , however, the absolute value takes the simple form

$$|w| = R t' / [1 - 2R \cos(4\pi d/\lambda) + R^2]^{1/2} \quad (r=0) \quad (7)$$

which gives the amplitude reflection directly for the case in which the antenna is matched to free space. We see that the curve should be periodic with period  $\lambda/2$ , that it is sinusoidal whenever  $R$  is small,

$$|w| \approx R t' [1 + R \cos(4\pi d/\lambda)] \quad (\rho \approx 0) \quad (8)$$

and that in the whole it is closely analogous to the transmission variation, Eq. (1). If  $M, m$  are the maximum values of the reflection, Eq. (7) gives a result for  $\rho R$  which is identical with Eq. (5).

$$\rho R = -(M-m)/(M+m) \quad (9)$$

and the reflection  $\rho$  may be eliminated as in (3):

$$R t' = 2Mm/(M+m) \quad (10)$$

Besides their utility in other investigations to be considered later on, these relations can be used to give additional verification of our fundamental assumptions.

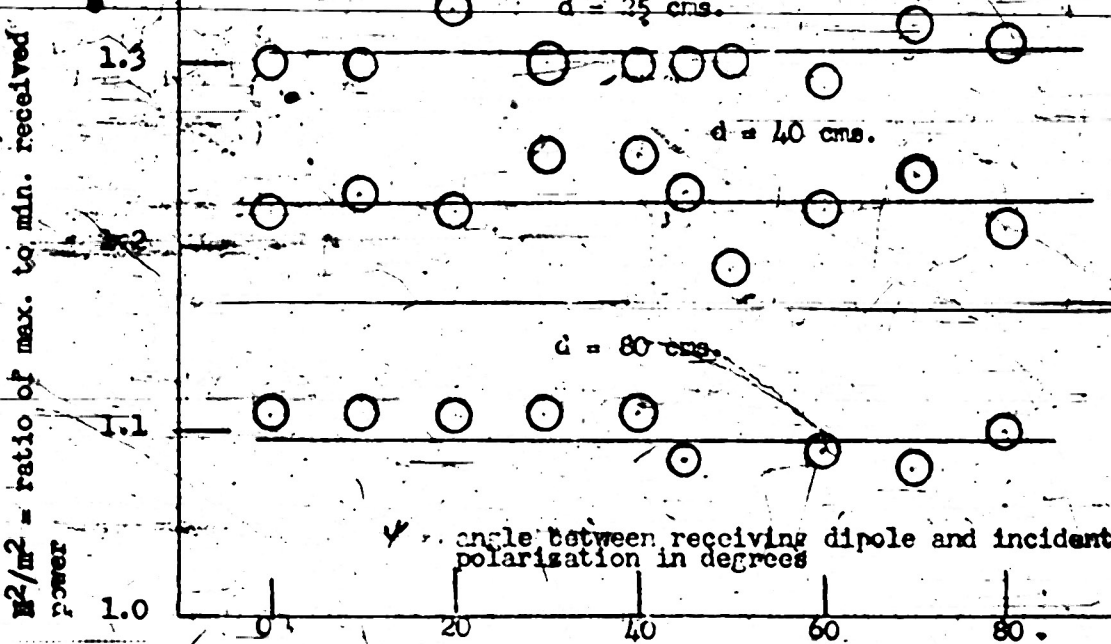
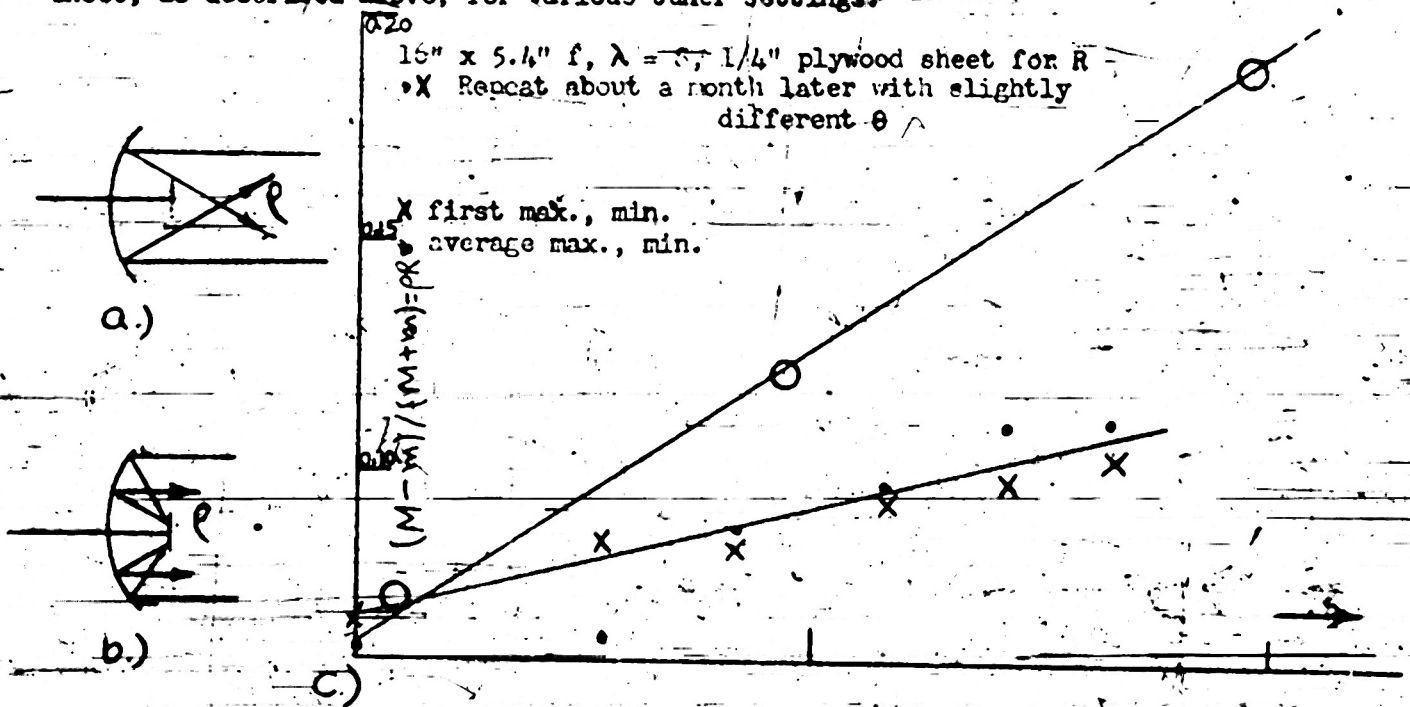


Fig. 8. Verification that the Effective Reflection is Substantially Independent of Polarization

A final experiment, which tends to distinguish between the possible mechanisms suggested in Figs. 9a, 9b, is to take  $\rho$ —versus-mismatch. Thus, if 9a represents the true state of affairs, the value of  $\rho$  should be independent of tuner setting, whereas if 9b is correct, then  $\rho$  may be expected to vary linearly with  $r$ . From the fact that  $\rho$  is approximately independent of distance, in the Fresnel region, it appears that Fig. 9b is the more plausible; and further verification is given by the following curves, in which  $\rho$  was measured by means of a reflecting sheet, as described above, for various tuner settings:



large experimental errors the variation is linear, as it should be, and the values for  $\phi$  obtained from the slopes are consistent with the other experimental results obtained above (e.g., with Fig. 5).

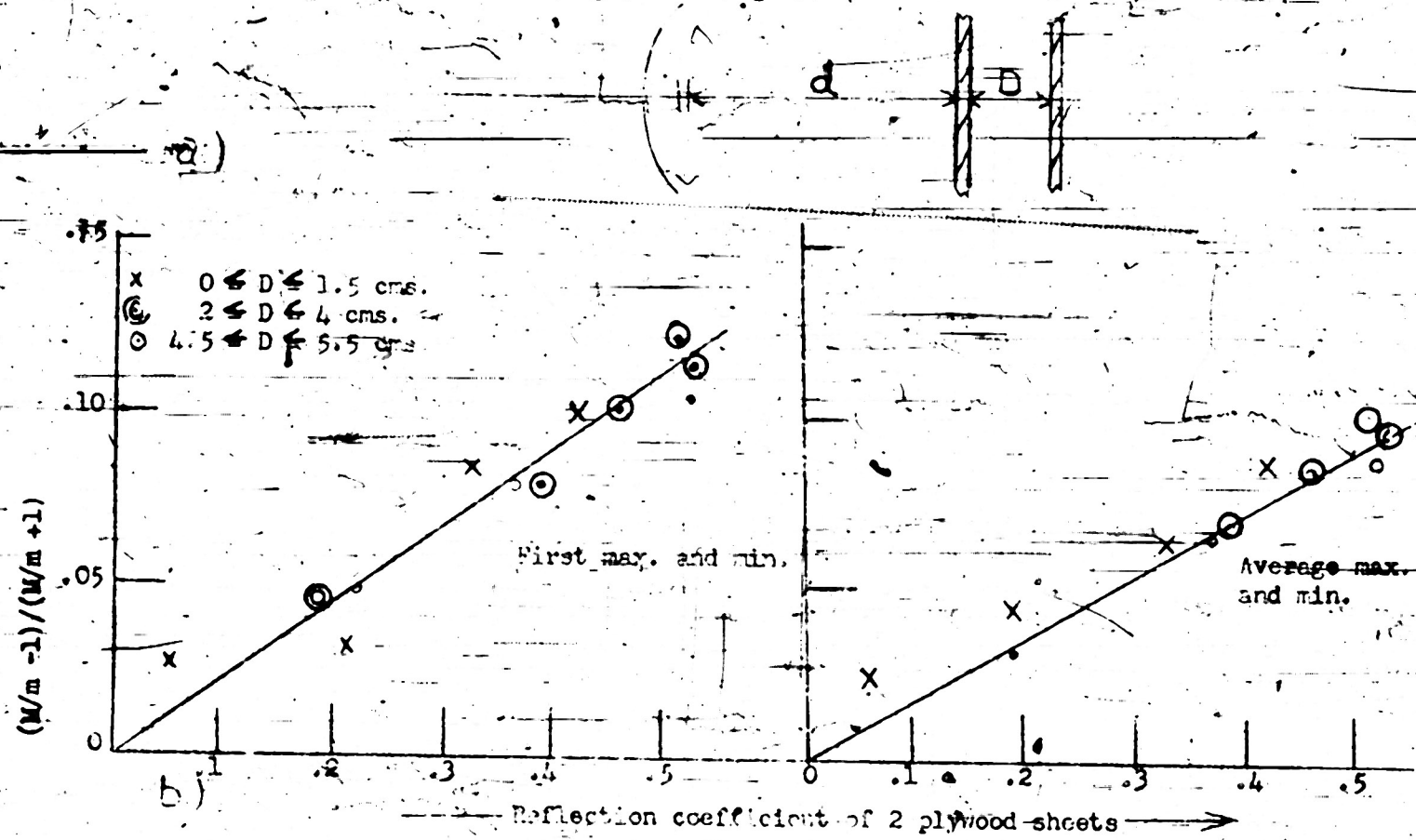


Fig. 7 Verification that  $(W/m^{-1}) / (W/m^{+1})$  is Proportional to  $R$

In the experiments described hitherto, the receiving antenna has been polarized in the same direction as the incident wave. If this is not the case, and the sheets are isotropic, then we may resolve the incident wave into two components, one parallel and one perpendicular to the direction of the receiving dipole. If the perpendicular component retains its direction of polarization after successive reflections between antenna and sheet, then it may be neglected altogether as it cannot enter the line and contribute to receiver reading at any stage of its career. Thus the component parallel to the receiving dipole is the only one that need be considered, whence we conclude that the net result is the same as it would be with a transmitter, of lower power, polarized in the same way as the receiver. Specifically, the ratio of maximum to minimum received power, as the sheet is moved, should not depend upon the angle  $\psi$  between the receiving dipole and the incident polarization, a conclusion which is verified within a few per cent by the following experimental curve. The procedure was similar to that already described.

From the above rather elaborate experiment one obtains another check on the simple theory heretofore used, which check has the two advantages that no error should be introduced by a transition into the Fraunhofer region -- a source of error in the above experiment -- and that the measured quantity will be of the first order in  $R$ , rather than of the second order, as was the case above. By virtue of (3), which may be applied here if we think of the antenna-plus-sheet assembly as being itself an antenna, we see that the harmonic mean of maximum and minimum received amplitude, as  $d$  is changed in 5b, should give the transmission of the arrangement of Fig. 5a. In other words, the harmonic mean for two sheets should give, essentially, received power versus distance for one sheet. Like the other results here given, this one follows rigorously from our fundamental assumption concerning  $\rho$ ,  $\tau$ ,  $\gamma$ , with no additional approximations; that it agrees with experiment is verified in Fig. 6.

26

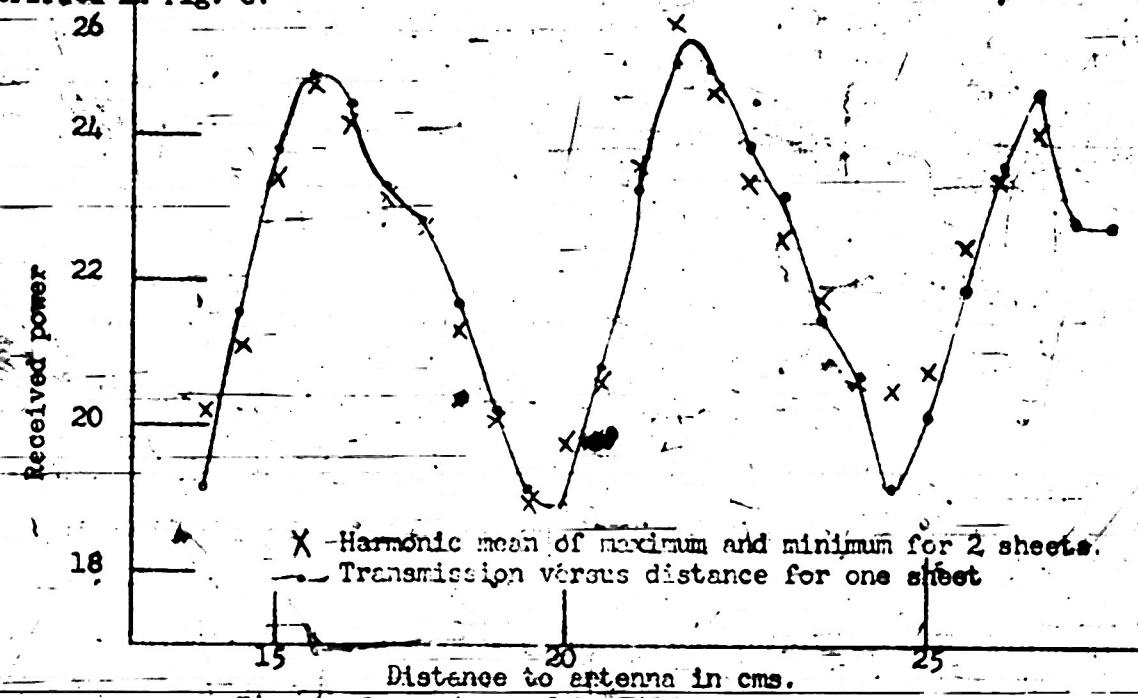


Fig. 6 Comparison of Power Versus Distance for One Sheet, With Harmonic Mean of Maximum and Minimum for Two Sheets

The use of two sheets permits a test of quite another sort from those just described. To the extent that the theory is valid, the quantity  $(M/m-1)/(k/m+1)$  must be proportional to  $R$ ; for a given antenna; by Eq. (5) it is in fact equal to  $\rho R$  so that  $(M/m-1)/(M/m+1)$  versus  $R$  will not only be a straight line, but its slope ought to be equal to  $\rho$ . To check this consequence of the theory, an experiment was performed as suggested in Fig. 7a. Specifically, a fixed value was given to  $D$  of that figure whereupon a complete curve of received power was found versus the distance  $d$  between antenna and sheets. The experimental points, which were taken every em., extended over a range of 12 cms. so that several maxima and minima would be obtained; and thus the variation of  $\rho$  with distance could also be investigated by using either the first maximum and minimum or the average of all maxima and minima. After repeating the curve, as usual, to check for transmitter variations, the entire process was performed over again with a new value for  $D$ , until  $D$  had been changed from 0 to 5.5 cms. in steps of 1/2 cm. For each value of  $D$  the reflection of the two sheets was next measured as in Part III below, and finally  $(M/m-1)/(M/m+1)$  was plotted versus the value of  $R$  thus obtained (Fig. 7b). Within the rather

The condition of perpendicularity is rather critical, as we shall see below in connection with reflection measurements, and in the early experiments here described the adjustment was not made as carefully as was found necessary, by later experiments, for optimum results. In view of this qualification, it is believed that the data of Fig. 3B corroborate, while data of the type shown in Fig. 6 do not contradict, our fundamental assumption as to the nature of  $\rho$ . For measurements of phase, on the other hand, the expected sinusoidal variation, which again depends on  $\rho$ , has been very accurately verified by more recent data taken at K-band. Not only is a sine curve the one that gives optimum fit, but the fit itself is well within the experimental error of the measurement, and the period has its predicted value of precisely  $\lambda/2$  (see Fig. 13 of Ref. 5').

Besides the apparent decrease of  $\rho$  with angle, and the sinusoidal variation with distance, a third check on the nature of  $\rho$  may be found by the use of a second sheet. Thus, if the antenna truly has an equivalent reflection coefficient, then the overall reflection  $R$  of sheet-plus-antenna, arranged as in Fig. 5a, should obey the usual equation for reflection versus separation as the distance is changed. We accordingly add a second sheet, as in Fig. 5b, and proceed to evaluate the reflection of the antenna-plus-sheet combination by the method described above. It is important that the roles of the two sheets be clearly understood: Sheet No. 1 represents part of the antenna, that is to say, part of the system being measured, whereas sheet No. 2 is used to determine  $R$ , and thus it represents part of the measuring equipment. With a given value for  $R$ , the voltmeter-reading was taken versus  $d$  for a total range of about 6 cms. in steps of 1/2 cm., whereupon the experiment was repeated as described above, because the transmitters at that time (1942) were not particularly steady. Next the distance  $D$  was increased by 1/2 cm., the entire operation being continued until  $D$  had experienced a total variation of 5.5 cms. The value of  $\rho$  for the antenna alone was found from Fig. 7 of the text, and finally the reflection coefficient  $R$  of each sheet was determined by the procedure of Part II. Knowing  $\rho$  together with  $R$  one can predict the variation of  $M/m$ , with  $D$  or, which is the same thing, the effective reflection  $\rho$  for antenna-plus-plywood as  $D$  is varied. This predicted result is given by the solid curve of Fig. 5c while the experimental points, obtained for 1/2 cm. intervals, are represented by the circles. The agreement is believed to be as good as could be expected in view of the many sources of experimental error.

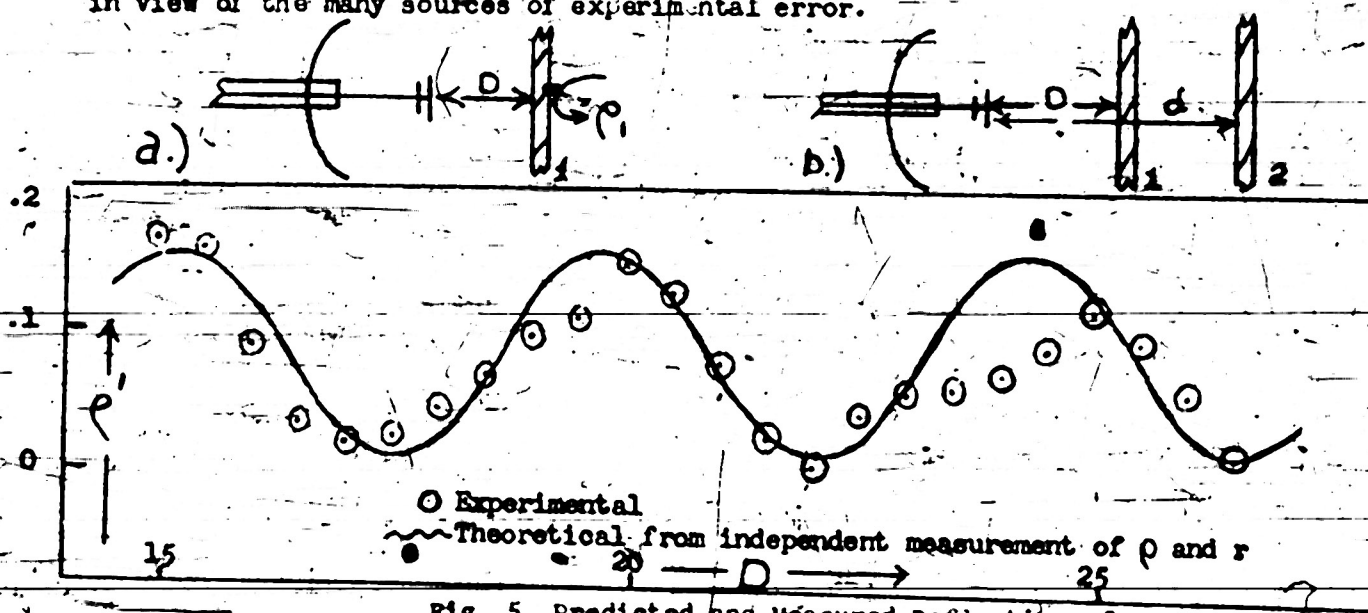


Fig. 5 - Predicted and Measured Reflection of  
Antenna-Plus-Sheet Assembly

each point of Fig 4c is obtained from approximately 30 voltmeter readings. It is seen that the ratio of maximum to minimum does in fact decrease, and that the shape of the curve near the peak agrees with the result predicted for that case, on the basis of simple theory described below, from the secondary power pattern of the antenna.

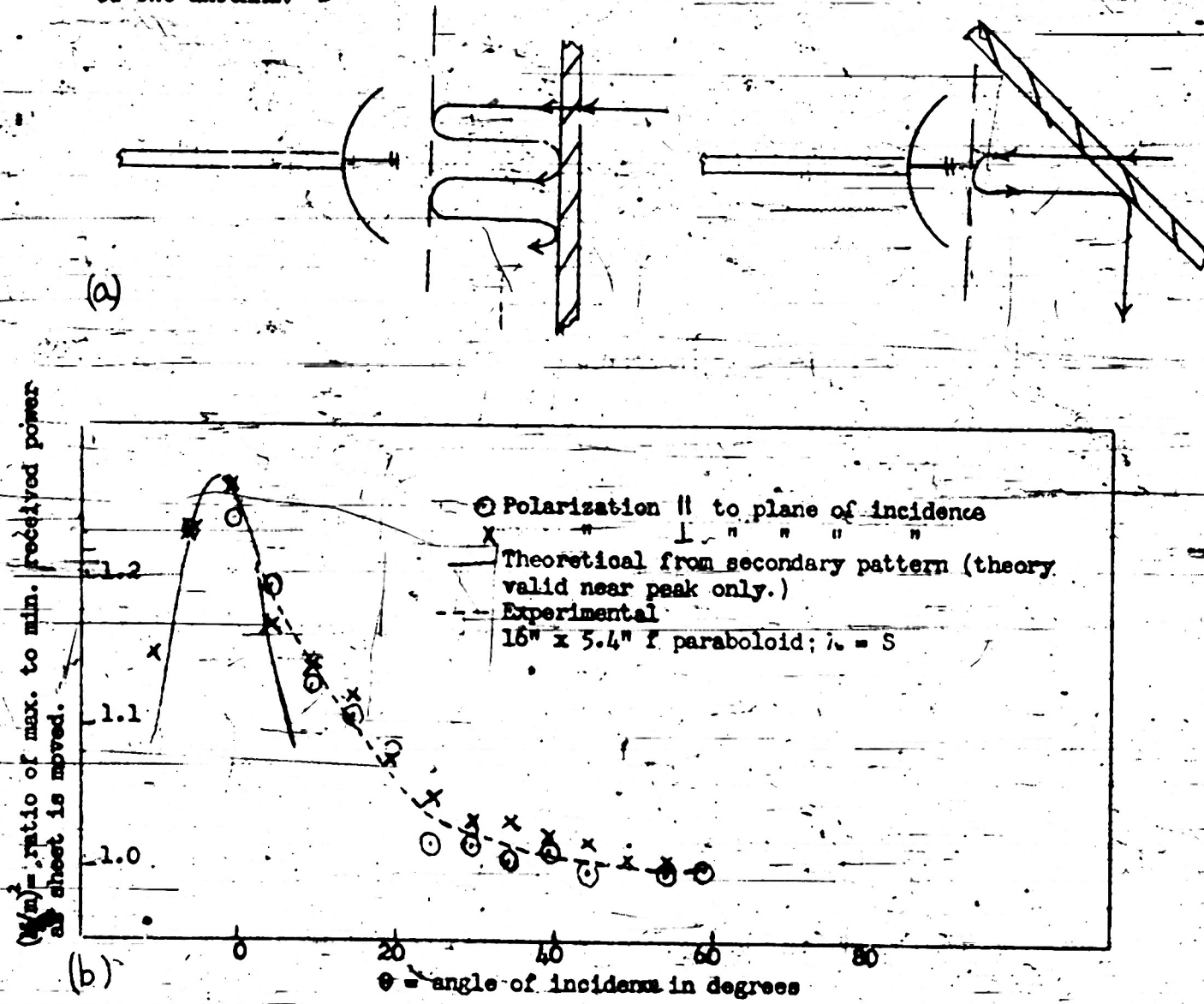


Fig. 4. Effect of Non-normal Incidence

A second check on the existence of an equivalent reflection coefficient is that the variation with distance is approximately sinusoidal. In the case of amplitude measurements, which are the ones that we have considered thus far, the verification is only fair in general; while no marked deviation from sinusoidal variation has ever been observed in practice, the best fitting curve is not always as accurately a sine curve as was the case, for example, in Fig. 3g. This discrepancy, which is illustrated by Fig. 6, is believed to be caused by a failure to have the sheet exactly perpendicular to the electrical axis of the antenna.

since the reading is determined essentially by the resultant field at that point. In the case of the plane sheet, on the other hand, there is a strong selective action; not only does one obtain an average over the whole aperture but plane waves making an angle with the axis are reflected back into the receiver at twice this angle; so that, as we shall see below, their net effect is considerably reduced in most cases. A similar difference between the two methods of measuring  $\rho$  is found when we consider the back lobe of the feed in the receiving antenna. In the case of the dipole probe, this back lobe frequently contributes a large share of the received power; for the dipole intercepts only a small part of the wave reflected from the dish, while it intercepts practically all of the power in the back lobe when close to the antenna. In the case of the sheet, on the contrary, the whole of the wave reflected from the dish is intercepted, while the effect of the back lobe is made negligible by inverse-distance attenuation (see Figs. 3b, 3c). That these difficulties are actually encountered in practice has been verified in a number of experiments: the measured reflection coefficient, with the procedure of Fig. 3a, is found to vary over an extremely wide range as the distance to the exploring dipole is changed. The results are difficult to duplicate, as the slightest alteration in the position or geometry of the reflecting antenna produces large changes in the final result. That much of the difficulty is due to the back lobe of the feed has been verified by curves in which the receiver antenna is polarized at right angles to the direction of polarization of the incident wave, so that the chief contribution to the dipole reading is due to the wave reflected from the dish directly, rather than to the wave re-radiated from the feed.

In this case, the variation with distance is greatly reduced, though it is still considerable; but the information so obtained is of course not applicable to the normal situation which is the one in which we are interested. Throughout the following discussion we shall accordingly determine  $\rho$  by means of a plane sheet, as suggested in Fig. 1a, the fundamental equation now being

$$\rho R = (M-m)/(M+m) \quad (5)$$

for  $\rho$  in terms of  $M^2, m^2$  the maximum and minimum received power as the sheet is moved and  $R$ , the reflection coefficient of the sheet. With this procedure a number of separate checks on the existence of the equivalent reflection  $\rho$  have been found, and it has also been possible to decide tentatively whether the reflected power is re-radiated from the dish, as in Fig. 8a, or from the feed as in 8b.

In the first place, if the observed variation is due to a plane wave re-radiated essentially along the axis, as we assume, then the dependence of received power on distance should decrease as the angle between the dielectric sheet and the axis increases (Figs. 4a, 4b). That such behavior is actually found has been repeatedly verified in the course of routine transmission measurements; and for quantitative investigation we also give the curve of Fig. 4c for which the data were taken as follows: With a given value for  $\theta$ , a complete curve of transmission versus distance was taken for variation somewhat exceeding a half wave, the points being close enough to insure that no unexpected maximum or minimum would be overlooked. To check for transmitter variation the curve was immediately repeated, so that

$$T = 2\pi m / (M+m)$$

(3)

Besides the data given in Part V below, this prediction is verified by Fig. 38, in which complete curves of transmission versus distance are taken for various values of  $\rho$ . In each case the curves are normalized to give the same reading without the dielectric sheet, and the best-fitting theoretical curves, based on Eq. (2), are found quite accurately to have the same average values. This figure also shows the expected sinusoidal variation, incidentally, and the period is  $\lambda/2$ . To check for transmitter unsturdiness, all experimental points were repeated three times, only the average of the three values for a given distance being plotted in Fig. 38.

2. The Equivalent Reflection Coefficient of the Antenna—While the foregoing checks several aspects of the theory, the effective reflection  $\rho$  is of sufficient importance to warrant separate consideration, and a number of tests for its validity have accordingly been devised. Perhaps the most obvious procedure would be to use an exploring dipole in somewhat the same manner as a probe is used for conventional standing wave measurements (Fig. 3). If the dipole is symmetric, so that the same weight is given to signals from the transmitter as to those reflected from the receiver, then the ratio of reflected to incident wave,  $\rho$ , would be given by the usual equation

$$\rho = (M-m) / (M+m)$$

(4)

where  $M, m^2$  in this case stand for the maximum and minimum power received by the dipole as its distance to the receiver is varied. Symmetry of the dipole may be verified by repeating the experiment with the dipole turned around, so that the side formerly facing the receiver now faces the transmitter and conversely.

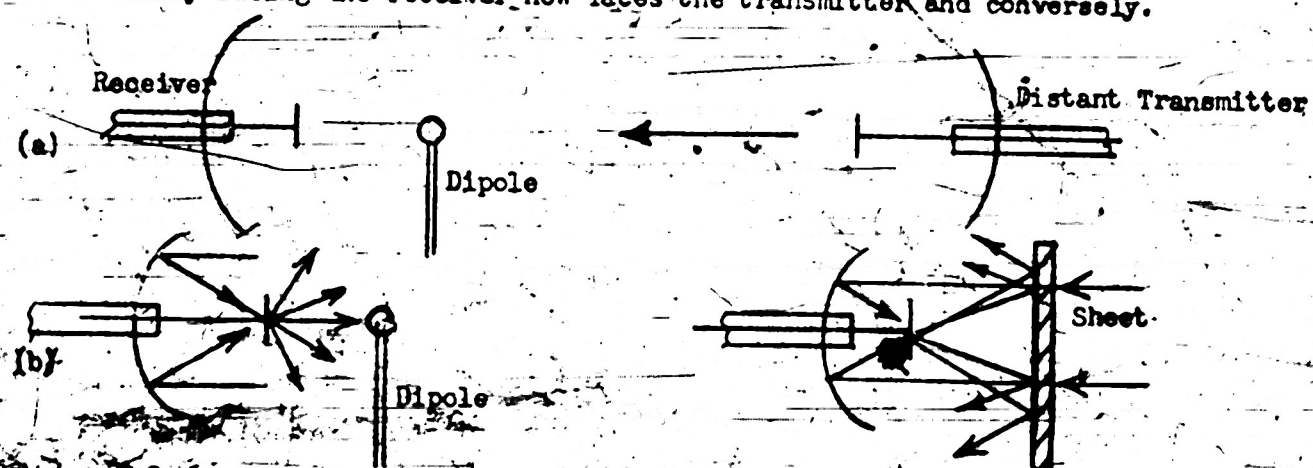


Fig. 3 Measurement of  $\rho$  by an Exploring Dipole

This procedure is apparently straight forward and direct; but more careful investigation indicates that the value of  $\rho$  so obtained would be quite different from the  $\rho$  of Eq. (1). The difficulty is that the dipole responds more or less with equal sensitivity to all plane waves, whatever their direction or source,

axis. The validity of thus assigning an equivalent reflection coefficient for the antenna is investigated in some detail below and also in Part III, where we find that the predicted results agree with experiment whenever the sheet has a moderate reflection coefficient, but there is considerable disagreement in certain cases when the reflection becomes near to unity. Further investigation of this and the coefficients  $t$ ,  $\gamma$  will be given at several points in the course of the ensuing discussion.

With these preliminaries we may write down the received power in the form

$$P = P_0 T^2 / [1 - 2\alpha R \cos(4\pi d/\lambda) + \rho^2 R^2] \quad (1)$$

where the distance  $d$  from antenna to sheet is measured in such a way as to cancel the phase shifts  $r$ ,  $R$ , and  $P$ .  $P_0$  stand respectively for the received power with and without the dielectric sheet. This equation, which may be obtained as in Refs. 2 or more concisely as in 4, is a rigorous consequence of our fundamental assumptions on the existence and nature of  $t$ ,  $\gamma$ ,  $\rho$  and no further approximations are made in its derivation. Whenever  $\rho R$  is small, which is frequently the case in normal practice, (1) becomes

$$P = P_0 [T^2 + 2\alpha R \cos(4\pi d/\lambda) - (\rho^2 R^2)] \quad (2)$$

These equations, which are a direct consequence of our fundamental assumptions, lead to results that may be readily compared with experiment; and such a comparison will in turn yield information as to their validity and that of the underlying theory.

In the first place, the equation predicts that the variation will be periodic with period  $\lambda/2$ , a property found in all the experimental curves hitherto obtained for the Fresnel region. When the sheet is sufficiently far from the antenna, however, the amplitude is found to decrease; and this too is predicted from the modified theory appropriate to that case (see below). Periodicity of this kind indicates that the observed variation with distance is not due to Fresnel interference in the ordinary sense, that is, it is not due to the successive contributions of zones on antenna or sheet. Indeed, this notion of conventional interference is repeatedly disproved, in the author's opinion, by a large variety of experimental results, but the present one, which has been observed without exception, is particularly convincing. Even in the Fraunhofer case, for which the curve is no longer periodic, the distance between successive maxima or minima is still equal to a half wave. We remark incidentally that half-wave variation of this type, which is also found below for the case of reflection, indicates on the basis of the present theory that the predominant mode in the region between antenna and sheet is the plane wave traveling along the axis; for the predominance of any other mode would be expected to lead to an equivalent guide wavelength for this region which would either be undefined or else different from the free space wavelength.

In addition to this half-wave periodicity, which tends to corroborate our basic assumptions, we have further verification in the behavior of the transmission coefficients. Thus, according to Eq. (1) the transmission  $T$  should be given by the harmonic mean of the maximum and minimum received amplitudes independently of the antenna reflection.

have the well-known properties of ordinary coefficients. The chief difference between the two cases is that the part of the line between  $\tau$  and  $R$  in (a), i.e., the free space, permits propagation of higher modes, while it is tacitly assumed that only one mode is propagated in the line of Fig. 1b. Thus, the postulate of  $t, t', r, \rho$ , as they will be used here, amounts to assuming that only the fundamental mode of the free-space line need be considered. The same idea may be expressed by saying that the field between antenna and sheet can be resolved into an infinite set of plane waves, making various angles with the axis, and that our assumption is essentially to replace this infinite set by only two waves, one traveling toward and one away from the antenna. It is of interest briefly to investigate the validity of this hypothesis, and to find in what sense 1a should be regarded as equivalent to 1b.

From linearity of the field equations, which for ordinary antennas and ordinary sheets is to be anticipated even in the complicated situation of Fig. 1a, we find that the coefficients  $t, t', r, \rho$ , like any other amplitude ratios, will be independent of field strength. In particular the equivalent reflection coefficient  $r$  and the overall reflection  $w$  may quite properly be introduced and treated as ordinary coefficients since both incident and reflected waves are in a line permitting only one mode of propagation.

Turning now to  $t'$ , we remark that the above neglect of higher modes (or, alternatively, of plane waves making an angle with the axis) is a restriction which makes  $t, t'$  quite different from the ordinary coefficients of Fig. 1b. Specifically, we have no assurance that the reciprocity theorem will be satisfied in their case, so that it is improper to take  $t = t'$  with  $t, t'$  defined in this way. To clarify this consideration we compare Fig. 1a with Fig. 2. In the latter case it has been proved by R. Dicke that  $t$  necessarily equals  $t'$  whenever the coefficients exist if the field equations are linear throughout the enclosed volume; and thus we have a rigorous proof of the reciprocity theorem for antennas as well as a number of other general results. Nevertheless, the situation of Fig. 2, which leads to reciprocity, is not to be confused with 1a, for which no such result has been proved. In the ensuing discussion, where  $t, t'$  are defined in the special sense mentioned above, we treat the antenna as a non-bilateral network; and with this qualification, it is believed that the introduction of  $t, t'$  represents a fair approximation to the true state of affairs.



Fig. 2 Typical Situation in which the Reciprocity Theorem May Be Applied

The coefficient  $\rho$  is more difficult to justify, as the re-radiation of the antenna is certainly not confined to a plane wave traveling along the antenna.

two to the angle between sheet and dish axis.

A final question involving geometry in the present sense of the word is the relation of pattern to random shape, or, in the case of a beacon, to the beacon housing. Unfortunately the theory for such effects, which is itself highly approximate, leads to expressions that cannot be readily evaluated, and our investigation has accordingly best of an empirical nature only. In the present report questions concerning the relation of geometry to antenna pattern have been omitted altogether. This omission should not, however, be taken as proof that such effects are negligible. Rather, the material available, which shows the great importance of these questions, is not sufficiently well correlated with theory to warrant publication.

Most of the experimental results here included are taken at S-band, with only occasional verification at the shorter wavelengths. This policy is due partly to the greater significance of magnetron pulling at S-band, and partly to the fact that the results were obtained, for the most part, before X and E-bands had assumed their present importance. Indeed, the great majority of the experimental results here described were found in 1942 or 1943, at which time practically all operating systems used the longer wavelengths. Sufficient data at the shorter wavelengths are obtained, however, to permit extrapolation of the general results more systematically investigated at S.

## II - Transmitting Plane Sheet

1. General Theory--In the arrangement of Fig. 1 it is found experimentally that the received power depends on the distance to the sheet, as shown in Figs. 6, 38. Although the effect is rather small, it is not negligible for ordinary practice; and in any case it must be investigated before we can proceed to the more complicated situations investigated below. To explain the observed variation with distance, T. J. Keary suggested that the antenna itself has an equivalent reflection coefficient of its own, which we shall denote by  $\rho$ , so that the arrangement of Fig. 1 (a) is regarded as analogous to that of Fig. 1 (b).

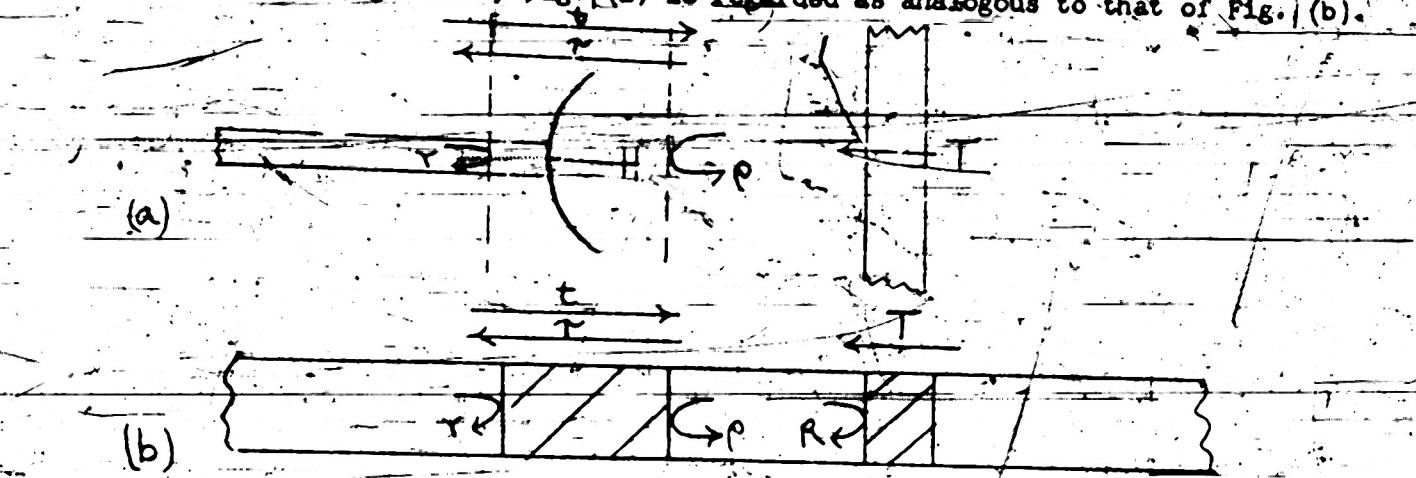


Fig. 1 Definition of Equivalent Coefficients

It is clear that this is a rather far-reaching assumption, and that these equivalent coefficients, if they exist at all, could hardly be expected to

## THE INTERACTION OF MICROWAVE ANTENNAS WITH DIELECTRIC SHEETS

### I--Introduction

The interaction of antennas with dielectric sheets is a problem which assumes particular importance in the microwave region, as the thickness of sheets which are mechanically suitable is then comparable to the wavelength. Though the effect on the field cannot be neglected, it is still necessary to use dielectric sheets in connection with such antennas; and the present report represents a summary of the more important geometrical effects encountered in these applications. The term geometry, as here used, refers to the general disposition of the dielectric sheet with respect to the antenna, rather than to the reflection coefficient or other properties depending chiefly on the thickness of the sheet. Thus, the properties of dielectric sheets per se are described in some detail in Refs. 2, 3; the present report, confined to geometrical effects almost exclusively, is intended to supplement the results there obtained.

Perhaps the most important use of a dielectric sheet near an antenna is the radome, which may introduce any or all of the effects mentioned in Ref. 1. In particular, the transmission is reduced, and the amount of this reduction depends on the geometry of the system as well as on the transmission properties of the radome itself.

This dependence on geometry, noted for the case of transmission, is far more significant for reflection, the importance of which is clear from the other reports of this series. In fact, the reflection entering the line, and thus contributing to magnetron pulling, is more dependent upon radome shape and orientation than upon radome reflection coefficient, and the need for investigation is apparent.

Similarly, the pulling introduced by ribs, overlaps, or other deviations from a simple surface must also be considered, as such design features, if permissible, materially reduce the cost of the radome. This too is a question of geometry, and is here considered in sufficient detail to allow prediction of the pulling introduced by such obstacles in most systems.

Besides the use of radomes, a similar application of dielectric surfaces is found in the closely related theory of pressurizing. In this case, we seek not to minimize the reflection, but to design the housing or pressurizing cup in such a way as to cancel the initial mismatch due to the antenna alone. Because of the difficulty of obtaining trial cups, which must be made by hand, it is desirable to have some systematic procedure of design; and such a procedure is readily found in terms of the results here described.

Still another application of the theory of dielectric sheets and antennas is the measurement of free space transmission or reflection coefficients, which are repeatedly required in radome work. Here too the effect of geometry plays an important role; the apparent transmission coefficient depends on the distance to the antenna in most cases, and on the sample size if it is too small. For reflection, the effect is much more noticeable, as above; an error of 5% in the reflection coefficient can sometimes be introduced by adding a degree or

MRC

11/14/64

OEM - 262

Radiation Laboratory

Report No. 10 March 1965

Radome Bulletin Number 18

THE INTERACTION OF MICROWAVE ANTENNAS  
WITH DIELECTRIC SHEETS

By the authority of OERD  
this report has been downgraded  
for security reasons

The general theory of a plane sheet in the Fresnel region, where the receiving antenna is briefly investigated, with a discussion of the scattered radiation when the antenna is transmitting, experimental and theoretical results are given for the reflection of a plane sheet as a function of distance, initial misalignment angle, and for both the Fresnel and Fraunhofer regions. It is shown that amplitude reflection versus angle should approximate the secondary, over, pattern of the antenna, and that the result for any cylindrical surface should approximate that for a plane sheet. These and other general experiments are investigated for special surfaces consisting of circular rings, corrugated surfaces, and strips. The results are applied to the theory of magnetron pulsing, pressurizing, and measurement of coefficients.

R. H. McGehee

Approved by